The genetics and association of photosynthesis parameters and flag leaf morphology in barley and their use for breeding

Inaugural dissertation

for the attainment of the title of doctor
in the Faculty of Mathematics and Natural Sciences
at the Heinrich Heine University Düsseldorf

presented by

Yanrong Gao

From Ningxia, China

Düsseldorf, December 2025

From the institute for Quantitative Genetics and Genomics of Plants at the Heinrich Heine University Düsseldorf

Published by the permission of the

Faculty of Mathematics and Natural Sciences at

Heinrich Heine University Düsseldorf

Supervisor: Prof. Dr. Benjamin Stich

Mentor: PD Dr. Shizue Matsubara

Date of the oral examination:

Declaration of the Doctoral Dissertation

I herewith declare under oath that this dissertation was the result of my own work without any unauthorized help in compliance with the “Principles for the Safeguarding of Good Scientific Practice at Heinrich Heine University Düsseldorf”. This dissertation has never been submitted in this or similar format to any other institution. I have not previously failed a doctoral examination procedure.

Düsseldorf,

Contents

Summary

To meet a growing global population requires substantial increases in crop yield, optimizing photosynthesis recognized as one of the most promising strategies. Although photosynthesis is central to plant growth and productivity, the natural genetic variation in photosynthesis is still underexplored. Similarly, leaf morphology, particularly flag leaf size, is a key determinant of photosynthesis capacity and assimilate supply to grains. The genetic architecture of flag leaf size in barley is still not well explored. The integration of photosynthesis into plant breeding has been limited by three main factors: 1) difficulties in high-throughput phenotyping under field conditions, 2) high sensitivity of photosynthesis to short- and long-term environmental fluctuations, and 3) the complexity of the genetic basis for photosynthesis.

This thesis addressed these challenges by combining physiological phenotyping, quantitative genetics and genomic prediction to estimate the potential of incorporating photosynthesis parameters into crop yield breeding programs, using barley as a model crop. First, we compared gas exchange-based techniques and chlorophyll fluorescence-based techniques, and we confirmed that chlorophyll fluorescence-based measurements can reliably detect genetic variation in Photosystem II (PSII) related parameters in barley under climate chamber conditions. Extending these analyses to the field, chlorophyll fluorescence measurements of barley inbred lines largely reflected variation in carbon assimilation properties measured in climate chamber, confirming chlorophyll fluorescence as a reliable proxy to explore genetic variation under field conditions. Importantly, the significant genotype x environment interactions and developmental stage effects demonstrated that single time-point measurements are insufficient to fully explore the genetic variation in photosynthesis under field conditions. Therefore, time-series and high-throughput phenotyping strategies, which are more likely to be possible with chlorophyll fluorescence-based techniques, are required for robust characterization of photosynthesis under field conditions (**Chapter 2**).

Building on this phenotyping framework, this thesis then assessed the correlation between photosynthesis parameters and yield-related traits by exploring both a germplasm panel of diverse barley inbred lines (natural variation) and a segregating recombinant inbred line (RIL) population. By exploring 23 barley inbred lines, we observed the significant correlation between Fv′/Fm′ and

NPQt with yield-related traits such as above ground dry matter and straw weight at final developmental stage (**Chapter 2**). Furthermore, by analyzing the correlation between photosynthesis-related parameters and agronomic traits in 631 recombinant inbred lines (RILs), we observed dynamic significant correlation as well (**Chapter 3**). Notably, both studies revealed that these correlations changed over plant developmental phases, highlighting the temporal dimension of the relationship between photosynthesis and yield. These results demonstrated the potential of optimizing photosynthesis-related parameters in crop yield improvement programs. These findings motivated a more detailed genetic analysis of photosynthesis-related parameters (**Chapter 3**) and of flag leaf morphology (**Chapter 4**).

Building on the observed dynamic correlations, the thesis next investigated the genetic architecture underlying photosynthesis-related parameters (**Chapter 3**) and flag leaf morphology (**Chapter 4**) in barley. By analyzing photosynthesis-related parameters of 23 barley inbred lines, we observed a wide range of heritability from 0.16 for the quantum yield of non-photochemical quenching to 0.78 for the fraction of open PSII center (**Chapter 2**). Furthermore, large-scale analyses of 631 RILs uncovered substantial genetic variation in photosynthesis-related parameters, with heritabilities ranging from 0.37 to 0.54. Dynamic QTL identified across plant development underscored the complexity of the genetic control of photosynthesis, which was also in line with the observation that the photosynthesis-related parameters changed over the plant growth and development. Importantly, genomic prediction models outperformed QTL-based approaches. These results indicated that photosynthesis-related parameters are controlled by many small-effect loci, which is consistent with a highly polygenic and complex genetic architecture of photosynthesis. More importantly, prediction ability for yield was improved by integrating photosynthesis-related parameters into the genomic prediction models. These results open up new perspectives for crop breeding via integrating photosynthesis-related parameters into genomic prediction pipelines (**Chapter 3**).

In parallel with the analysis of photosynthesis-related traits, the thesis dissected the genetic and cellular bases of flag leaf size in barley (**Chapter 4**). Using the double round-robin population (HvDRR) comprising 45 RIL sub-populations, quantified flag leaf length (FLL) and flag leaf width (FLW) and estimated their heritabilities as 0.77 and 0.58, respectively, indicating a substantial genetic variability for flag leaf size in the HvDRR population. Furthermore, 24 consensus QTL were identified, and 17 of them were novel genetic loci associated with flag leaf size. Fine mapping

of qHvDRR-FLS-8 narrowed the candidate region and demonstrated shared effects on multiple leaves, suggesting a broader role in leaf size regulation. In addition, cellular analysis confirmed that epidermal cell number is the major driver of differences in leaf size (**Chapter 4**).

Together, the results of this thesis highlighted considerable genetic variation in photosynthesis-related parameters and flag leaf morphology in barley, and the dynamic correlations across the plant growth and development. By combining high-throughput phenotyping, quantitative genetics, and genomic prediction, this thesis proposed a coherent framework for integrating photosynthesis-related parameters in crop breeding programs, offering a potential approach to contribute to food security.

Chapter 1

General introduction

1.1 Why optimize photosynthesis to improve crop yields?

1.1.1 Crop yields need to be improved

To meet the increasing demand for agricultural products while maintaining constant crop production areas, crop yields need to be increased by approximately 25%-70% from the current levels by 2050 (Hunter et al., 2017). In reality, agriculture and the environment are deeply interconnected. On one hand, agricultural activities contribute 11% -13% of the total greenhouse gas emissions (IPCC, 2014). On the other hand, climate change directly and negatively influences agricultural production (Yang et al., 2024). This dual relationship creates a pressing need for more efficient and sustainable crop production methods to improve crop yield per unit land area reducing environmental impacts.

1.1.2 Potential for crop improvement by optimizing photosynthesis

Under optimal conditions, the yield potential of a crop can simply be described by four main factors: incident solar radiation, light interception efficiency, conversion efficiency, and harvest index (Long et al., 2006a; Monteith, 1977). Among these, incident solar radiation is largely beyond agronomic control, whereas light interception efficiency, conversion efficiency, and harvest index could be improved by genetic and agronomic interventions in cereals.

Light interception efficiency reflects the canopy's ability to absorb photosynthetically active radiation (PAR) and is determined by canopy development, leaf absorptance, architecture, and longevity. Conversion efficiency is the efficiency of the plant to convert the intercepted solar energy into chemical energy via photosynthesis. Harvest index (HI) is the fraction of total biomass partitioned to the harvested product. The Green Revolution is a prime example of the successful application of genetic variation in agriculture. By identifying natural semi-dwarf rice varieties, dwarfing genes were introduced into cereal crops, and significantly increased the harvest index resulting in considerable yield improvements (Hedden, 2003). However, HI is likely approaching its theoretical limit in modern crop varieties (e.g. Zhu et al., 2010). Consequently, the remaining bottlenecks for increasing the yield potential lie in optimizing interception and conversion efficiency and offer significant potential to improve crop yields sustainably (Kromdijk and Long, 2016; Long et al., 2006a; Prado et al., 2013).

Direct selection for crop yield has probably led to some unintentional enhancement in photosynthesis performance (Richards, 2000). Nevertheless, after decades of direct selection for crop yields, photosynthesis efficiency has still not reached the theoretical maximum in C3 plants (Long et al., 2006b; Prosekov and Ivanova, 2018; Zhu et al., 2010). This suggests that the selection on yield alone is not sufficient for enhancing photosynthesis and has not fully exploited existing genetic variation in photosynthesis (Croce et al., 2024; Theeuwen et al., 2022). Therefore, meaningful progress requires direct phenotyping and selection on photosynthesis-related parameters to identify both phenotypic and genetic variation in photosynthesis of crop (Theeuwen et al., 2022). At the same time, photosynthesis is an underused parameter in crop yield breeding, not only because of the complexity of its physiological and molecular regulation, but also due to genotype x environment interactions and the inconsistent relationships between photosynthesis and crop yields (e.g. Driever et al., 2014). These limitations motivate a deeper understanding of how photosynthesis varies genetically within crops and how this variation can be harnessed in breeding.

1.1.3 Dynamic Regulation of Photosynthesis

Photosynthesis efficiency is dynamically regulated and depends on not only the molecular, structural, and physiological process of the plant itself (Eberhard et al., 2008; Foyer and Noctor, 2012; Zhu et al., 2008), but also the ambient environment conditions on a short-term as well as long-term basis (Gifford, 1995; Kono and Terashima, 2014). Internally, photosynthesis changes with the growth and development of plants and differs among leaf levels within the same plant (Bielczynski et al., 2017; Wingler et al., 2004). Externally, environmental factors shape photosynthesis at both leaf, canopy, and whole-plants levels.

For example, fluctuating light intensities, which are, e.g. caused by moving clouds or leaves (Chazdon and Pearcy, 1991), trigger rapid regulatory responses and longer-term acclimation of photosynthesis (Alter et al., 2012; Vialet-Chabrand et al., 2017). The response of photosynthesis to both external and internal factors occur at leaf, canopy, and plant levels. At the leaf level, photosynthesis efficiency responses to instantaneous light fluctuation and can acclimate to specific light regimes over time (Oguchi et al., 2003; Oguchi et al., 2005). At the canopy level, photosynthesis is affected by the distribution of leaf photosynthesis capacity, which is driven by the distribution of light energy in the canopy (Hikosaka et al., 2016). Together, these internal and

external factors make photosynthesis as a dynamic trait which is challenging to measure and interpret, especially under field conditions. Precisely because of this complexity, exploiting photosynthesis for yield improvement requires approaches that can account for its temporal and spatial dynamics, as well as its genetic basis.

1.2 Natural genetic variation in photosynthesis

1.2.1 Limitations of gene modification on photosynthetic pathways for yield improvement

Despite complexity of photosynthesis mentioned above, the core photosynthetic mechanisms are highly conserved within C3 plants (Flood et al., 2011), which are encoded by around a hundred genes (Berry et al., 2013; Tyagi and Gaur, 2003). If direct selection for crop yield has not fully improved photosynthesis, can direct selection or gene modification on photosynthesis improve crop yield? This conservation initially suggested that targeted modification of core components might be a straightforward route to enhancing photosynthesis and yield. Actually, several studies have successfully optimized photosynthesis through gene modification on the core photosynthesis apparatus or the direct pathway of photosynthesis. For instance, overexpressing the Calvin-Benson cycle enzyme Brachypodium sedoheptulose-1,7-biphosphatase (*SBPase*) in wheat increased the leaf carbon assimilation rate, which led to greater total biomass and higher dry seed yield (Driever et al., 2017). Gong et al. (2015) enhanced the mesophyll conductance and net photosynthetic rate in rice by introducing two CO_2-transporting and fixing relevant genes, which improved the tillering capacity and biomass. In addition, under fluctuating light, accelerating the engagement and relaxation of photoprotection (NPQ) increased biomass and/or yield in tobacco and soybean (De Souza et al., 2022; Kromdijk et al., 2016).

These successes demonstrate that genetically modifying photosynthetic pathways can improve photosynthetic performance and, in some cases, yield. However, this approach also has its limitations. First, modifying the common photosynthesis pathway through genetic engineering may not consistently improve the crop yield across species or environment (van Bezouw, 2022). For instance, overexpressing SBPase in rice did not improve plant growth under controlled condition (Feng et al., 2007), which is contrasting with the results observed in wheat (Driever et al., 2017). Accelerating non-photochemical quenching (NPQ) improved biomass or yield in tobacco and soybean under field-like fluctuations (De Souza et al., 2022; Kromdijk et al., 2016). In contrast, modifying photoprotective components in *Arabidopsis thaliana* can reduce growth

under fluctuating light when the balance of light harvesting and dissipation is disturbed. These examples show that pathway modifications may depend on the situation, with beneficial effects in one species or light regime and trade-offs in another.

Second, current gene modification approaches typically target a relatively small subset of core photosynthetic genes and may not fully explore and use the genetic resource of photosynthesis. More and more studies have pointed out that the variation in photosynthesis is caused by genes, which are mainly outside the above-mentioned core photosynthesis genes (Flood, 2019; Flood et al., 2011; Theeuwen et al., 2022). For example, Van Rooijen et al. (2017) reported that allelic sequence variation at the *Arabidopsis thaliana YELLOW SEEDLING1* (*YS1*) genes, which encode pentatrico-peptide-repeat (PPR) proteins involved in RNA editing of plastid-encoded genes, caused the variation in photosynthesis acclimation. Third, photosynthesis is a complex process, which is coordinated by many processes from chloroplast to whole-plant levels (reviewed by e.g. Croce et al., 2024; Ort et al., 2015; Zhu et al., 2010). Stomatal and mesophyll conductance limits e.g. the carbon assimilation, particularly under fluctuating conditions (reviewed by Flexas et al., 2012; Lawson and Blatt, 2014). In addition, source–sink dynamics affect photosynthesis. When an imbalance arises between source and sink at the whole-plant level, the expression of photosynthetic genes is down-regulated (Paul and Foyer, 2001). As a result, single or several gene(s) modification might not be sufficient to exploring the maximum potential for optimizing photosynthesis. These aspects help explain why some transgenic successes are partial or conditional, and why gains in controlled environments do not always translate to consistent yield improvements in the field.

1.2.2 Exploring natural genetic variation as an alternative route to optimizing photosynthesis for yield improvement

Because of these limitations of targeted genetic modification, conventional breeding approaches that explore natural genetic variation provide a potential alternative route to improve crop yield via optimizing photosynthesis. Natural genetic variation for photosynthesis is still underestimated and underexplored (reviewed by Flood et al., 2011; Theeuwen et al., 2022) even though such variation forms the basis for both natural and artificial selection. Gene modification approach did offer us insight about the genetics of the photosynthesis, by knocking out the genes to confirm the corresponding biochemical functions, but sometimes, the loss-of-function of the

core genes might be lethal. Meanwhile, the variation for photosynthesis is due to the variations of abundance of the core photosynthetic components in some cases (e.g. Rungrat et al., 2019; Simkin et al., 2019; Yin et al., 2010). These observations suggest that exploring natural genetic variation enhances our understanding of evolution and adaptation, provides insights into biological mechanisms, and offers the opportunities for improving crop breeding programs. However, to translate this variation into breeding progress, we need quantitative genetic approaches and phenotyping strategies that can capture the dynamic and environmentally sensitive nature of photosynthesis.

1.3 Approaches to exploring genetic and phenotypic variation in photosynthesis

1.3.1 Genetic dissection of natural variation in photosynthesis

There is already considerable evidence of genetic variations in photosynthesis parameters within and between species. The variation in photosynthesis is highly heritable in model and crop species, such as Arabidopsis, wheat, soybean, and rice (Acevedo-Siaca et al., 2021; Lopez et al., 2019; Salter et al., 2020; van Rooijen et al., 2015). Over the past decade, with the cost of genome sequencing decreasing, there has been increasing genome sequencing based studies. Larger panels and sequenced populations make it possible to connect phenotype to genotype. Quantitative trait locus (QTL) mapping and genome-wide association studies (GWAS) are now frequently used to identify loci for photosynthesis-related parameters.

As mentioned above, the variation of photosynthesis is not mainly driven by the major core genes of photosynthesis, but rather by many minor effect QTLs. This complex genetic architecture can lead to inconsistent estimated QTL effects (Bernardo, 2008). Furthermore, genome-wide association mapping is limited in its ability to dissect such complex trait, as it typically identifies only significant loci that are common within the germplasm (Bernardo, 2014). As a consequence, QTL and GWAS studies often capture only part of the genetic variance, particularly for highly polygenic traits such as photosynthesis.

Genomic prediction is a powerful approach for both enhancing our understanding of the genetics of photosynthesis and accelerating genetic gain for traits in breeding programs (Heffner et al., 2009; Meuwissen et al., 2001). By using whole genome-wide single nucleotide polymorphism (SNP) markers, genomic prediction models aim to capture all the QTL effects, not

only those that pass a significant threshold. A training population with known genotypic and phenotypic data is used to derive a genomic prediction model, which is then applied to a testing population to estimate genomic estimated breeding values (GEBVs) based on their genotypes alone. Based on their GEBVs, the superior genotypes could be preselected before field phenotyping, which can potentially shorten the breeding cycles.

As highlighted above, variation in photosynthesis appears to be driven largely by many minor-effect loci rather than a few major core genes. This polygenic architecture can lead to unstable QTL effect estimates and limited resolution from GWAS alone. Therefore, genomic prediction is a particularly suitable approach to capture all effects of QTLs for photosynthesis. Evaluating the prediction ability of photosynthesis-related parameters might not only provide a practical tool for breeding but also offer insight into the underlying genetic architecture of photosynthesis.

Many studies have reported successful prediction of the phenotypic performance in a wide range of species, including livestock and plants (reviewed by Voss-Fels et al., 2019). However, direct for photosynthesis in crop breeding is still rare, largely because of the challenge of high-throughput phenotyping for photosynthesis. Due to the complexity and the dynamic feature of photosynthesis-related parameters compared to other agronomic traits, integration of genomic prediction for photosynthesis into crop breeding programs still needs to be investigated.

1.3.2 Phenotyping photosynthesis: from leaf physiology to agronomic traits

As mentioned above, the main challenge for exploring the natural genetic variation for photosynthesis and for building genomic prediction models is on effective phenotyping. Photosynthesis consists of two main processes, light reaction and carbon assimilation. These two main processes are typically assessed by using chlorophyll fluorescence- and gas exchange-based techniques, respectively (Baker, 2008; Long et al., 1996). Chlorophyll fluorescence is a non-invasive probe of photosystem II (PSII) activity in plants. By analyzing the chlorophyll fluorescence parameters, this technique provides the information of photosystem II photochemistry, including the effective and the maximum quantum yields of PSII (Phi2 and Fv′/Fm′, respectively, for the light-adapted state) or non-photochemical quenching (NPQ), linear electro flow (LEF), and electro transport rate (ETR). Imaging systems enable high-throughput capture of chlorophyll fluorescence across large populations, and they can also quantify dynamic responses under fluctuating light (van Bezouw, 2022). In contrast, gas exchange measurements

provide direct estimates of the net CO2 assimilation rate (A) and related physiological parameters (Sharkey, 2015).

Traditionally, gas-exchange throughput has been low because the steady-state conditions are required before each measurement. Dynamic assimilation techniques (DAT) now allow measurements under non-steady-state conditions and substantially increase throughput compared to conventional gas-exchange protocols (Saathoff and Welles, 2021). Nevertheless, even with DAT, gas-exchange-based approaches remain considerably slower and more time-consuming than chlorophyll fluorescence-based approaches, especially in large field experiments.

Under specific conditions, such as low photorespiration and optimal environmental control, chlorophyll fluorescence can be used to indirectly estimate carbon assimilation through electron transport rates (ETR). However, for application in crop breeding and selection, it is essential to determine whether the genetic variation detected by chlorophyll fluorescence is comparable to that revealed by gas exchange measurements and whether chlorophyll fluorescence is a reliable proxy for photosynthetic performance and, ultimately, yield under field conditions.

1.4 Exploring the genetic architecture and cellular basis of flag leaf

While the previous section considered how optimizing photosynthesis can raise the yield potential at the physiological level, realizing this potential in the field also depends critically on the leaf canopy, which is the principal photosynthetic organ (Blum, 1985; Wang et al., 2016). Leaf number and size are major determinants of canopy photosynthesis and consequently, crop yields (Li et al., 2022; Liu et al., 2021). In cereals, the flag leaf is particularly important because of its position at the top of the plant, close to spike, where it intercepts substantial light and converts it into carbohydrates that are translocated to the developing grains (Acevedo-Siaca et al., 2021; Sanchez-Bragado et al., 2016).

Consistent with this role, the flag leaf has been reported to substantially contribute carbohydrates to the grain in different cereals. Large contributions have been reported in wheat and rice (Fan et al., 2017; Gladun, 1993; Wu et al., 2012; Yang et al., 2022). Also in barley, flag-leaf size was strongly associated with single-plant yield (Zheng, 1999). Yet, compared to other major cereals, the genetic architecture of flag-leaf morphology in barley and its relationship with photosynthesis remain less well understood.

Given the central role of photosynthesis and flag-leaf traits in determining yield, and the need to understand their natural genetic variation in a major cereal crop, I used barley (Hordeum vulgare L.) as the study species. Barley is the fourth most widely produced cereal crop worldwide and is widely used as a model for genetic and physiological studies because it is a self-pollinating diploid (2n = 14) with a relatively small genome and only seven chromosomes. In this thesis, I analyzed 23 barley inbred lines and 45 HvDRR sub-populations derived from these 23 parental lines using a doubled round-robin mating design for flag-leaf size. Because phenotyping photosynthesis is much more time-consuming and complex, a subset of eight of these 45 sub-populations was used for detailed analysis of the genetics of photosynthetic traits.

By combining phenotypic characterization with genomic analyses, I aim to assess the potential of integrating photosynthesis-related traits and flag-leaf morphology into conventional barley breeding programs to improve grain yield.

Objective of this thesis

This thesis aims to investigate the genetics of photosynthesis-related parameters and flag leaf morphology in field-grown barley and evaluate the potential of integrating photosynthesis-related parameters into crop yield breeding programs. In particular, the objectives were to:

1. investigate genetic variation of photosynthesis-related parameters in barley across different developmental stages and evaluate the interaction between genotypes and environment under field conditions;
2. compare gas exchange- and chlorophyll fluorescence-based assessments of photosynthetic traits;
3. assess correlations between photosynthesis-related and morphological and growth-related parameters;
4. explore genetic variation of photosynthesis-related parameters in barley RIL populations across different developmental phases;
5. unravel the genetic complexity of photosynthesis-related parameters in barley by using bi-parental and multi-parental QTL analyses;
6. evaluate the utilization of photosynthesis-related parameters as predictors in genomic prediction models for yield and its components;
7. characterize the genetic complexity of flag leaf size variation using a multi-parent population (MPP) resource, the double round-robin population of barley (HvDRR);
8. refine QTL for flag leaf size and identify the allelic series at each QTL and a subset of the QTLs of candidate genes by local association mapping exploiting genome-wide variant information of parental inbreds as well as classical fine-mapping;
9. assess the potential cellular cause of flag leaf size variation for a subset of the QTLs.

Reference

Acevedo-Siaca, L.G., R. Coe, W.P. Quick, and S.P. Long. 2021. Variation between rice accessions in photosynthetic induction in flag leaves and underlying mechanisms. *Journal of Experimental Botany* 72:1282-1294.

Acevedo-Siaca, L.G., R. Coe, W.P. Quick, and S.P. Long. 2021. Evaluating natural variation, heritability, and genetic advance of photosynthetic traits in rice (Oryza sativa). *Plant Breeding* 140:745-757.

Alter, P., A. Dreissen, F.L. Luo, and S. Matsubara. 2012. Acclimatory responses of Arabidopsis to fluctuating light environment: Comparison of different sunfleck regimes and accessions. *Photosynthesis research*, *113*(1), 221-237.

Baker, N.R. 2008. Chlorophyll fluorescence: a probe of photosynthesis in vivo. *Annu. Rev. Plant Biol.* 59:89-113.

Bernardo, R. 2008. Molecular markers and selection for complex traits in plants: learning from the last 20 years. *Crop science* 48:1649-1664.

Bernardo, R. 2014. Genomewide selection when major genes are known. *Crop Science* 54:68-75.

Berry, J.O., P. Yerramsetty, A.M. Zielinski, and C.M. Mure. 2013. Photosynthetic gene expression in higher plants. *Photosynthesis Research*, *117*(1), 91-120.

Bielczynski, L.W., M.K. Łączki, I. Hoefnagels, A. Gambin, and R. Croce. 2017. Leaf and plant age affects photosynthetic performance and photoprotective capacity. *Plant Physiology* 175:1634-1648.

Blum, A. 1985. Photosynthesis and transpiration in leaves and ears of wheat and barley varieties. *Journal of experimental botany* 36:432-440.

Chazdon, R.L., and R.W. Pearcy. 1991. The Importance of Sunflecks for Forest Understory Plants Photosynthetic machinery appears adapted to brief, unpredictable periods of radiation. *BioScience*, *41*(11), 760-766.

Croce, R., E. Carmo-Silva, Y.B. Cho, M. Ermakova, J. Harbinson, T. Lawson, A.J. McCormick, K.K. Niyogi, D.R. Ort, D. Patel-Tupper, P. Pesaresi, C. Raines, A.P.M. Weber, and X.-G. Zhu. 2024. Perspectives on improving photosynthesis to increase crop yield. *The plant cell, 36(10), 3944-3973.*

De Souza, A.P., S.J. Burgess, L. Doran, J. Hansen, L. Manukyan, N. Maryn, D. Gotarkar, L. Leonelli, K.K. Niyogi, and S.P. Long. 2022. Soybean photosynthesis and crop yield are improved by accelerating recovery from photoprotection. *Science* 377:851-854.

Driever, S.M., T. Lawson, P.J. Andralojc, C.A. Raines, and M.A.J. Parry. 2014. Natural variation in photosynthetic capacity, growth, and yield in 64 field-grown wheat genotypes. *Journal of Experimental Botany* 65:4959-4973.

Driever, S.M., A.J. Simkin, S. Alotaibi, S.J. Fisk, P.J. Madgwick, C.A. Sparks, H.D. Jones, T. Lawson, M.A.J. Parry, and C.A. Raines. 2017. Increased sbpase activity improves photosynthesis and grain yield in wheat grown in greenhouse conditions. *Philosophical Transactions of the Royal Society B: Biological Sciences* 372:

Eberhard, S., G. Finazzi, and F.-A. Wollman. 2008. The dynamics of photosynthesis. *Annual review of genetics* 42:463-515.

Fan, Y., Z. Tian, Y. Yan, C. Hu, M. Abid, D. Jiang, C. Ma, Z. Huang, and T. Dai. 2017. Winter night-warming improves post-anthesis physiological activities and sink strength in relation to grain filling in winter wheat (Triticum aestivum L.). *Frontiers in Plant Science* 8:992.

Feng, L., K. Wang, Y. Li, Y. Tan, J. Kong, H. Li, Y. Li, and Y. Zhu. 2007. Overexpression of SBPase enhances photosynthesis against high temperature stress in transgenic rice plants. *Plant cell reports* 26:1635-1646.

Flexas, J., M.M. Barbour, O. Brendel, H.M. Cabrera, M. Carriquí, A. Díaz-Espejo, C. Douthe, E. Dreyer, J.P. Ferrio, and J. Gago. 2012. Mesophyll diffusion conductance to CO2: an unappreciated central player in photosynthesis. *Plant Science* 193:70-84.

Flood, P.J. 2019. Using natural variation to understand the evolutionary pressures on plant photosynthesis. *Current Opinion in Plant Biology* 49:68-73.

Flood, P.J., J. Harbinson, and M.G. Aarts. 2011. Natural genetic variation in plant photosynthesis. *Trends in plant science* 16:327-335.

Foyer, C.H., and G. Noctor. 2012. Managing the cellular redox hub in photosynthetic organisms. *Plant, Cell & Environment*, *35*(2), 199-201.

Gifford, R.M. 1995. Whole plant respiration and photosynthesis of wheat under increased CO2 concentration and temperature: long‐term vs. short‐term distinctions for modelling. *Global Change Biology* 1:385-396.

Gladun, I. 1993. Distribution of assimilates from the flag leaf of rice during the reproductive period of development. *Russ. J. Plant. Physiol.* 40:215-219.

Gong, H.Y., Y. Li, G. Fang, D.H. Hu, W.B. Jin, Z.H. Wang, and Y.S. Li. 2015. Transgenic rice expressing Ictb and FBP/Sbpase derived from cyanobacteria exhibits enhanced photosynthesis and mesophyll conductance to CO2. *PLoS ONE* 10:1-23.

Hedden, P. 2003. The genes of the Green Revolution. *TRENDS in Genetics* 19:5-9.

Heffner, E.L., M.E. Sorrells, and J.L. Jannink. 2009. Genomic selection for crop improvement. *Crop Science* 49:1-12.

Hikosaka, K., T.o. Kumagai, and A. Ito. 2016. Modeling canopy photosynthesis. In Canopy photosynthesis: from basics to applications. (pp. 239-268). Dordrecht: Springer Netherlands.

Hunter, M.C., R.G. Smith, M.E. Schipanski, L.W. Atwood, and D.A. Mortensen. 2017. Agriculture in 2050: Recalibrating targets for sustainable intensification. *BioScience* 67:386-391.

Kono, M., and I. Terashima. 2014. Long-term and short-term responses of the photosynthetic electron transport to fluctuating light. *Journal of Photochemistry and Photobiology B: Biology* 137:89-99.

Kromdijk, J., K. Głowacka, L. Leonelli, S.T. Gabilly, M. Iwai, K.K. Niyogi, and S.P. Long. 2016. Improving photosynthesis and crop productivity by accelerating recovery from photoprotection. *Science* 354:857-861.

Kromdijk, J., and S.P. Long. 2016. One crop breeding cycle from starvation? How engineering crop photosynthesis for rising CO2 and temperature could be one important route to alleviation. *Proceedings of the Royal Society B: Biological Sciences* 283:

Lawson, T., and M.R. Blatt. 2014. Stomatal size, speed, and responsiveness impact on photosynthesis and water use efficiency. *Plant physiology* 164:1556-1570.

Li, H., Z. Liu, Y. Chen, X. Zhang, and D. Chen. 2022. A positive correlation between seed cotton yield and high-efficiency leaf area index in directly seeded short-season cotton after wheat. *Field Crops Research* 285:108594.

Liu, F., Q. Song, J. Zhao, L. Mao, H. Bu, Y. Hu, and X.G. Zhu. 2021. Canopy occupation volume as an indicator of canopy photosynthetic capacity. *New Phytologist* 232:941-956.

Long, S., P. Farage, and R. Garcia. 1996. Measurement of leaf and canopy photosynthetic CO2 exchange in the field. *Journal of experimental botany* 47:1629-1642.

Long, S.P., E.A. Ainsworth, A.D.B. Leakey, J. Nösbsrger, and D.R. Ort. 2006a. Food for thought: Lower-than-expected crop yield stimulation with rising CO2 concentrations. *Science* 312:1918-1921.

Long, S.P., X.G. Zhu, S.L. Naidu, and D.R. Ort. 2006b. Can improvement in photosynthesis increase crop yields? *Plant, Cell and Environment* 29:315-330.

Lopez, M.A., A. Xavier, and K.M. Rainey. 2019. Phenotypic variation and genetic architecture for photosynthesis and water use efficiency in soybean (Glycine max L. Merr). *Frontiers in plant science* 10:680.

Meuwissen, T.H.E., B.J. Hayes, and M.E. Goddard. 2001. Prediction of Total Genetic Value Using Genome-Wide Dense Marker Maps. *genetics*, *157*(4), 1819-1829.

Monteith, J.L. 1977. Climate and the efficiency of crop production in Britain. *Philosophical transactions of the royal society of London. B, Biological Sciences* 281:277-294.

Oguchi, R., K. Hikosaka, and T. Hirose. 2003. Does the photosynthetic light‐acclimation need change in leaf anatomy? *Plant, Cell & Environment* 26:505-512.

Oguchi, R., K. Hikosaka, and T. Hirose. 2005. Leaf anatomy as a constraint for photosynthetic acclimation: differential responses in leaf anatomy to increasing growth irradiance among three deciduous trees. *Plant, Cell & Environment* 28:916-927.

Ort, D.R., S.S. Merchant, J. Alric, A. Barkan, R.E. Blankenship, R. Bock, R. Croce, M.R. Hanson, J.M. Hibberd, and S.P. Long. 2015. Redesigning photosynthesis to sustainably meet global food and bioenergy demand. *Proceedings of the national academy of sciences* 112:8529-8536.

Paul, M.J., and C.H. Foyer. 2001. Sink regulation of photosynthesis. *Journal of experimental botany* 52:1383-1400.

Prado, S.A., J.M. Gallardo, R.A. Serrago, B.C. Kruk, and D.J. Miralles. 2013. Comparative behavior of wheat and barley associated with field release and grain weight determination. *Field Crops Research* 144:28-33.

Prosekov, A.Y., and S.A. Ivanova. 2018. Food security: The challenge of the present. *Geoforum* 91:73-77.

Richards, R. A. (2000). Selectable traits to increase crop photosynthesis and yield of grain crops. *Journal of experimental botany*, *51*(suppl_1), 447-458.

Rungrat, T., A.A. Almonte, R. Cheng, P.J. Gollan, T. Stuart, E.M. Aro, J.O. Borevitz, B. Pogson, and P.B. Wilson. 2019. A genome‐wide association study of non‐photochemical quenching in response to local seasonal climates in Arabidopsis thaliana. *Plant direct* 3:e00138.

Saathoff, A.J., and J. Welles. 2021. Gas exchange measurements in the unsteady state. *Plant, Cell & Environment* 44:3509-3523.

Salter, W.T., A. Merchant, R.M. Trethowan, R.A. Richards, and T.N. Buckley. 2020. Wide variation in the suboptimal distribution of photosynthetic capacity in relation to light across genotypes of wheat. *AoB Plants* 12:plaa039.

Sanchez-Bragado, R., G. Molero, M.P. Reynolds, and J.L. Araus. 2016. Photosynthetic contribution of the ear to grain filling in wheat: a comparison of different methodologies for evaluation. *Journal of experimental botany* 67:2787-2798.

Sharkey, T.D. 2015. What gas exchange data can tell us about photosynthesis. *Plant, cell & environment* 39:1161-1163.

Simkin, A.J., P.E. López-Calcagno, and C.A. Raines. 2019. Feeding the world: improving photosynthetic efficiency for sustainable crop production. *Journal of Experimental Botany* 70:1119-1140.

Theeuwen, T.P.J.M., L.L. Logie, J. Harbinson, and M.G.M. Aarts. 2022. Genetics as a key to improving crop photosynthesis. *Journal of Experimental Botany* 73:3122-3137.

Tyagi, A.K., and T. Gaur. 2003. Light Regulation of Nuclear Photosynthetic Genes in Higher Plants. *Critical Reviews in Plant Sciences*, *22*(5), 417-452.

van Bezouw, R.F.H.M. 2022. Towards breeding for improved photosynthesis traits using the Arabidopsis thaliana model. In Wageningen University and Research.

van Rooijen, R., M.G. Aarts, and J. Harbinson. 2015. Natural genetic variation for acclimation of photosynthetic light use efficiency to growth irradiance in Arabidopsis. *Plant physiology* 167:1412-1429.

Van Rooijen, R., W. Kruijer, R. Boesten, F.A. Van Eeuwijk, J. Harbinson, and M.G. Aarts. 2017. Natural variation of YELLOW SEEDLING1 affects photosynthetic acclimation of Arabidopsis thaliana. *Nature Communications* 8:1421.

Vialet-Chabrand, S., J.S.A. Matthews, A.J. Simkin, C.A. Raines, and T. Lawson. 2017. Importance of fluctuations in light on plant photosynthetic acclimation. *Plant Physiology* 173:2163-2179.

Voss-Fels, K.P., M. Cooper, and B.J. Hayes. 2019. Accelerating crop genetic gains with genomic selection. *Theoretical and Applied Genetics* 132:669-686.

Wang, H., L. Hou, M. Wang, and P. Mao. 2016. Contribution of the pod wall to seed grain filling in alfalfa. *Scientific Reports* 6:26586.

Wingler, A., M. Marès, and N. Pourtau. 2004. Spatial patterns and metabolic regulation of photosynthetic parameters during leaf senescence. *New Phytologist* 161:781-789.

Wu, X.Y., B.K. Kuai, J.Z. Jia, and H.C. Jing. 2012. Regulation of leaf senescence and crop genetic improvement F. *Journal of Integrative Plant Biology* 54:936-952.

Yang, H., C. Fang, Y. Li, Y. Wu, P. Fransson, M.C. Rillig, S. Zhai, J. Xie, Z. Tong, and Q. Zhang. 2022. Temporal complementarity between roots and mycorrhizal fungi drives wheat nitrogen use efficiency. *New Phytologist* 236:1168-1181.

Yang, Y., D. Tilman, Z. Jin, P. Smith, C.B. Barrett, Y.-G. Zhu, J. Burney, P. D'Odorico, P. Fantke, J. Fargione, and others. 2024. Climate change exacerbates the environmental impacts of agriculture. *Science* 385:eadn3747.

Yin, Z., F. Meng, H. Song, X. Wang, X. Xu, and D. Yu. 2010. Expression quantitative trait loci analysis of two genes encoding rubisco activase in soybean. *Plant physiology* 152:1625-1637.

Zheng, T. 1999. Effects of some photosynthetic organs on milking and grain yield of barley. *Barley Science* 1:21-22.

Zhu, X.-G., S.P. Long, and D.R. Ort. 2008. What is the maximum efficiency with which photosynthesis can convert solar energy into biomass? *Current opinion in biotechnology* 19:153-159.

Zhu, X.G., S.P. Long, and D.R. Ort. 2010. Improving photosynthetic efficiency for greater yield. *Annual Review of Plant Biology* 61:235-261.

Chapter 2

Exploring natural genetic variation in photosynthesis-related traits of barley in the field

Yanrong Gao[1,2], Merle Stein[1], Lilian Oshana[2], Wenxia Zhao[1,3], Shizue Matsubara[2,4], Benjamin Stich[1,4,5,*]

Published as

Gao, Y., Stein, M., Oshana, L., Zhao, W., Matsubara, S., & Stich, B. (2024). Exploring natural genetic variation in photosynthesis-related traits of barley in the field. Journal of Experimental Botany, 75(16), 4904-4925.

Own contribution: I am the first author of this paper. I completed 80% of experiments and performed all data analyses. I contributed 90% of the data interpretation. My contribution to the final writing was 90%.

Journal of Experimental Botany, Vol. 75, No. 16 pp. 4904–4925, 2024
https://doi.org/10.1093/jxb/erae198 Advance Access Publication 3 May 2024

RESEARCH PAPER

Exploring natural genetic variation in photosynthesis-related traits of barley in the field

Yanrong Gao[1,2], Merle Stein[1], Lilian Oshana[2], Wenxia Zhao[1,3], Shizue Matsubara[2,4], and Benjamin Stich[1,4,5,*]

[1] Institute of Quantitative Genetics and Genomics of Plants, Heinrich Heine University, Düsseldorf, Germany
[2] IBG-2: Plant Sciences, Forschungszentrum Jülich, Jülich, Germany
[3] Xinjiang Seed Industry Development Center of China, Urumqi, China
[4] Cluster of Excellence on Plant Sciences (CEPLAS), Heinrich Heine University, Düsseldorf, Germany
[5] Julius Kühn Institute (JKI) – Federal Research Centre for Cultivated Plants, Institute for Breeding Research on Agricultural Crops, Sanitz, Germany

* Correspondence: benjamin.stich@julius-kuehn.de

Received 4 December 2023; Editorial decision 26 April 2024; Accepted 1 May 2024

Editor: Tracy Lawson, University of Essex, UK

Abstract

Optimizing photosynthesis is considered an important strategy for improving crop yields to ensure food security. To evaluate the potential of using photosynthesis-related parameters in crop breeding programs, we measured chlorophyll fluorescence along with growth-related and morphological traits of 23 barley inbred lines across different developmental stages in field conditions. The photosynthesis-related parameters were highly variable, changing with light intensity and developmental progression of plants. Yet, the variation in photosystem II quantum yield observed among the inbred lines in the field largely reflected the variation in CO_2 assimilation properties in controlled climate chamber conditions, confirming that the chlorophyll fluorescence-based technique can provide proxy parameters of photosynthesis to explore genetic variation under field conditions. Heritability (H^2) of the photosynthesis-related parameters in the field ranged from 0.16 for the quantum yield of non-photochemical quenching to 0.78 for the fraction of open photosystem II center. Two parameters, the maximum photosystem II efficiency in the light-adapted state (H^2=0.58) and the total non-photochemical quenching (H^2=0.53), showed significant positive and negative correlations, respectively, with yield-related traits (dry weight per plant and net straw weight) in the barley inbred lines. These results indicate the possibility of improving crop yield through optimizing photosynthetic light use efficiency by conventional breeding programs.

Keywords: Barley, chlorophyll fluorescence, crop yields, development, heritability, natural genetic variation, photosynthesis.

Abbreviations: A_{sat}, carbon assimilation at saturating light intensity; ASP, anthesis and senescence phase; DMP, dry mass per plant; F_v'/F_m, maximum efficiency of PSII in light-adapted state; J_{max}, maximum rate of electron transport; LEF, linear electron flow; NPQ, non-photochemical quenching; NPQt, total non-photochemical quenching; PAR, photosynthetically active radiation; Phi2, quantum yield of PSII; PhiNO, quantum yield of non-regulated dissipation processes; PhiNPQ, quantum yield of non-photochemical quenching; PSII, photosystem II; qL, fraction of PSII open center; REP, rapid expansion phase; RGR, relative growth rate; SEP, slow expansion phase; SPAD, relative chlorophyll content; TPU, triose phosphate utilization; $V_{c,max}$, maximum rate of carboxylation.

© The Author(s) 2024. Published by Oxford University Press on behalf of the Society for Experimental Biology.
This is an Open Access article distributed under the terms of the Creative Commons Attribution-NonCommercial-NoDerivs licence (https://creativecommons.org/licenses/by-nc-nd/4.0/), which permits non-commercial reproduction and distribution of the work, in any medium, provided the original work is not altered or transformed in any way, and that the work is properly cited. For commercial re-use, please contact reprints@oup.com for reprints and translation rights for reprints. All other permissions can be obtained through our RightsLink service via the Permissions link on the article page on our site—for further information please contact journals.permissions@oup.com.

Downloaded from https://academic.oup.com/jxb/article/75/16/4904/7663878 by Bundesanstalt fuer Zuechtungsforschung an Kulturpflanzen, Hauptbibliothek user on 03 December 2025

Downloaded from https://academic.oup.com/jxb/article/75/16/4904/7663878 by Bundesanstalt fuer Zuechtungsforschung an Kulturpflanzen, Hauptbibliothek user on 03 December 2025

Introduction

To satisfy the increasing demand for agricultural products at constant crop production areas, crop yields need to be increased by the year 2050 by about 25–70% (Hunter *et al.*, 2017). The potential genetic yield under an optimal environment is the product of four main factors: incident solar radiation, light interception efficiency, conversion efficiency, and harvest index (Bonington, 1977). The green revolution led to considerable increases of light interception efficiency and harvest index by introducing dwarfing genes into cereal crops (Hedden, 2003). However, some studies suggest that these two parameters are close to their theoretical maximum in modern crop varieties (e.g. Zhu *et al.*, 2010). Accordingly, crop yield potential may be limited by the remaining bottleneck, the efficiency of light energy conversion by photosynthesis (source limitation) (Long *et al.*, 2006a; Alvarez Prado *et al.*, 2013; Kromdijk and Long, 2016). Thus, enhancing this conversion efficiency has become a breakthrough goal to improve crop yields (Zhu *et al.*, 2010).

Notably, selection of yields might have unintentionally improved the conversion efficiency, as indicated by a positive relationship between photosynthesis and crop yields (Kromdijk and Long, 2016; Theeuwen *et al.*, 2022). Still, the conversion efficiency has not reached the theoretical maximum in C_3 plants (Long *et al.*, 2006b; Zhu *et al.*, 2010; Prosekov and Ivanova, 2018) after decades of selection for crop yields. This suggests that the selection for yields is not sufficient to fully explore and make better use of natural genetic variation of photosynthesis. Direct phenotyping and selection for photosynthetic parameters are needed to identify variations in photosynthetic capacity and source limitation of crop yield (Theeuwen *et al.*, 2022).

Several studies have successfully increased yields through optimizing photosynthesis by genetic engineering (reviewed by Simkin *et al.*, 2019), such as manipulating the Calvin–Benson cycle in wheat (Driever *et al.*, 2017), carbon transport in rice (Gong *et al.*, 2015) and soybean (Hay *et al.*, 2017), and photoprotection in tobacco (Kromdijk *et al.*, 2016) and soybean (De Souza *et al.*, 2022). However, the use of genetically modified crops is restricted in some parts of the world (Turnbull *et al.*, 2021), and suggested yield improvements by genetic modification await rigorous testing in practical agricultural production conditions (Khaipho-burch *et al.*, 2023). Classical breeding can offer an alternative or additional approach. Indeed, natural variation of photosynthesis within (Wullschleger, 1993) and across species (Flood *et al.*, 2011; van Bezouw *et al.*, 2019; Garcia *et al.*, 2022) can be exploited by classical breeding.

Natural genetic diversity of photosynthesis has been studied in cereals under field conditions. Driever *et al.* (2014) reported significant variations in photosynthetic capacity, biomass and yield in 64 wheat genotypes. Acevedo-Siaca *et al.* (2021a) observed high heritabilities for carbon assimilation-related parameters in 30 accessions of rice. However, the relationships between photosynthesis and yield observed in these studies were not consistent. For example, Carmo-Silva *et al.* (2017) observed a positive correlation between carbon assimilation rate and grain yield in field-grown wheat at pre- and post-anthesis stages, while Driever *et al.* (2014) found no correlation between carbon assimilation-related parameters and grain yield in field-grown wheat in pre-anthesis stages. A possible explanation for such discrepancies may be the dependency of the photosynthetic traits on environmental conditions and/or developmental stages of the plants, although further research is needed to clarify this. Furthermore, in barley, one of the most important cereal crops as well as a model for other cereals because of its simpler genetics, natural variation of photosynthesis has not been investigated under field conditions.

High-throughput phenotyping techniques are essential for investigating the natural genetic variation in photosynthesis. Photosynthesis is divided into two main processes, the light reaction and CO_2 assimilation, which can be assessed by chlorophyll fluorescence- and gas exchange-based techniques, respectively (Long *et al.*, 1996; Baker, 2008). The analysis of chlorophyll fluorescence provides information on photosystem II (PSII) activity, such as the effective and the maximum quantum yields of PSII (Phi2 and F_v'/F_m', respectively, for the light-adapted state) or non-photochemical quenching (NPQ) (Baker, 2008). Measurement of gas exchange allows estimation of carbon assimilation rate (A) and related parameters (Sharkey, 2016). Recently, the dynamic assimilation technique was introduced to enable gas exchange measurements in non-steady state, which substantially increased the throughput compared with steady-state measurements (Saathoff and Welles, 2021) albeit still slower than chlorophyll fluorescence-based methods. For application to crop breeding and selection, it is essential to check whether the genetic variation detected by these two techniques is comparable or not.

The objectives of this study were to (i) investigate genetic variation of photosynthesis-related parameters in barley across different developmental stages and evaluate the interaction between genotypes and environment in field conditions, (ii) compare gas exchange- and chlorophyll fluorescence-based assessments of photosynthetic traits, and (iii) assess correlation between photosynthesis-related and morphological or growth-related parameters. Based on the results obtained, we will consider the potential of using photosynthesis-related parameters in crop and particularly barley breeding programs.

Materials and methods

Field experimental design

Twenty-three spring barley (*Hordeum vulgare*) inbred lines (inbreds) were selected from a worldwide collection of 224 barley landraces and cultivars based on their genetic and phenotypic diversity (Weisweiler *et al.*, 2019). These 23 barley inbreds are the parents of the double round-robin population (Casale *et al.*, 2022). All 23 inbreds were grown at three

different locations [Bonn (50°37′31.82″ N 6°59′18.508″ E), Cologne (50°57′34.345″ N 6°51′36.407″ E), and Düsseldorf (51°10′42.599″ N 6°48′8.268″ E)] in Germany in 2021. In Bonn, the experimental design was an α-design with two complete replications, where the plants were sown in 10 m^2 plots on 31 March 2021. In Düsseldorf, the experimental design was an α-design with three complete replications. The experimental units were single rows with 33 kernels per row, and six rows together were considered as one plot (replicate). The plants in Düsseldorf were sown on 31 March 2021. In Cologne, two distinct trials were performed, which are named in the following as 'mini-big plot' and 'big plot' trials. Within each of these two trials, 23 inbreds were grown as replicated checks in an augmented design. In the mini-big plot trial, each plot had a size of 2.25 m^2. The entire mini-big plot trial had 320 plots, in which the 23 inbreds were grown as replicated checks twice. The big plot trial, in which each plot had a size of 10 m^2, comprised also 320 plots and the 23 inbreds were also grown as checks but only one time. Fertilization and crop protection followed local practices. Air temperature and precipitation were recorded during the field experiments at all three locations (Supplementary Fig. S1). In Bonn, the field site has chernozem-para-brown soil, and the field sites, in Cologne and Düsseldorf, have para-brown soil (Bundesanstalt für Geowissenschaften und Rohstoffe).

Climate chamber experimental conditions and design

Based on the results of the field experiments, six representative barley inbreds (HOR1842, IG128216, IG31424, ItuNative, K10877, and W23829/803911) were selected for a climate chamber experiment. The experimental design was a randomized complete block design with three replicates/blocks. A total of 32 plants were planted for each inbred in total. The gas exchange measurements were performed 21, 24, 26, 31, 36, 39, 46, 51, 57, 74, 87, 88, 100, and 102 days after sowing (DAS). At each measurement day, three measurements were taken from three different plants of an inbred, where always one plant from each of the blocks was studied. In addition, the Zadoks score for each evaluated plant was rated. In addition, we harvested three plants per inbred (i.e. one per block) and then measured dry weight of aboveground biomass per plant 26, 36, 46, 57, 74, 102, 113, and 142 DAS. The growth conditions in the climate chamber were as follows: 14 h/10 h light/dark photoperiod, 18 °C/16 °C temperature, and 55% relative humidity. The maximal light intensity measured at 15 cm from the light panel was 750 μmol m^{-2} s^{-1}.

Assessment of photosynthesis-related parameters

In the field experiments, the top fully expanded leaves of three representative plants from each plot were measured from seedling stage (ZS13; Zadoks *et al.*, 1974) to dough development (ZS87) using a MultispeQ V2 device (Kuhlgert *et al.*, 2016). We used the measurement protocol 'Photosynthesis RIDES', by which the intensity of actinic light was automatically set to the ambient light intensity measured by the built-in light sensor. The following parameters were used for the further analyses: linear electron flow (LEF), the fraction of open PSII centers (qL), the quantum yield of PSII (Phi2), the maximum efficiency of PSII in light-adapted state (F_v'/F_m'), the total NPQ (NPQt), the quantum yield of NPQ (PhiNPQ), the quantum yield of non-regulated dissipation processes (PhiNO), and relative chlorophyll content (SPAD). In addition, the MultispeQ also recorded environmental parameters, such as the intensity of photosynthetically active radiation (PAR), ambient temperature, ambient humidity, and ambient pressure.

In the climate chamber experiment, gas exchange parameters were measured multiple times from tillering stage (ZS21) to dough development (ZS89) alongside the MultispeQ measurements. The measurements were made on the top fully expanded leaves on the main stem. Three different light intensities (PAR=400, 800, 1500 μmol m^{-2} s^{-1}) were used as simulated low-light (LL), medium-light (ML) and high-light (HL) conditions for the MultispeQ measurements. Leaf-level gas exchange measurements were performed by LI-6800 (LI-COR Biosciences Inc., Lincoln, NE, USA). Three replicates per genotype were measured from 1 h after the onset of the light period. The settings inside the LI-6800 chamber were as follows: PAR was kept at 1500 μmol m^{-2} s^{-1} (as in the simulated HL) with 50% blue and 50% red light, 400 μmol m^{-2} s^{-1} air flow rate, 10 000 rpm fan speed, 55% relative humidity, and 18 °C air temperature. The proportion of blue and red light was chosen to mimic the HL conditions in the field. The humidity and air temperature in the LI-6800 chamber were chosen to mimic the growth condition in the climate chamber and, thus, reduce the time needed for stabilization prior to the measurements. The CO_2 concentration inside the LI-6800 chamber was 400 ppm during pre-acclimation, which lasted between 10 and 15 min. After the pre-acclimation, photosynthetic CO_2 response (A–C_i) curves were measured according to the dynamic assimilation technique (Saathoff and Welles, 2021). CO_2 ramps were started from 1605 to 5 ppm with ramping rates of 200 ppm. The A–C_i curves were then analysed using the 'plantecophys' package (Duursma, 2015) in R version 4.0.3 to estimate the maximum rate of carboxylation ($V_{c,max}$), the maximum rate of electron transport (J_{max}), and triose phosphate utilization (TPU).

Assessment of morphological and growth-related traits

To determine the relative growth rate (RGR) of the 23 barley inbreds, aboveground biomass data were collected in the field experiment in Düsseldorf at six different time points during the vegetative period: at 62, 69, 76, 83, 97, and 125 DAS. Plants of one row (initially 33 kernels were sown) per plot were harvested for the 23 genotypes with three replicate plots. Wild animals visited the trails, and therefore the number of damaged plants for each row was recorded.

The dry weight per row per plot was used to estimate the dry mass per plant (DMP), which was needed for the assessment of growth curve parameters, using the following equation:

$$\mathrm{DMP} = \frac{\mathrm{DM}}{(\mathrm{TNP} - \mathrm{NDP}) + 0.8 \times \mathrm{NDP}} \quad (1)$$

where TNP was the total number of plants, NDP the number of damaged plants, 0.8 was the completeness of the damaged plants based on the observation during the harvest. DMP calculated as described above, was corrected separately for each time point for replicate and block effects. The corrected values were then used for further analyses.

In the climate chamber experiment, the total aboveground DMP was measured by weighing at eight different time points (26, 36, 46, 57, 74, 102, 113, and 142 DAS) except for the two inbreds IG31424 and HOR1842, for which only the initial and the final DMP were determined at 26 and 142 DAS. Three replicates per genotype were collected for each time point.

To assess the relationship between DMP and time, logistic (Verhulst, 1838), power-low (Paine *et al.*, 2012), and quadratic regression (Lithourgidis and Dordas, 2010) models were fitted. The quadratic regression model was used:

$$y_r = a + bt - ct^2 \quad (2)$$

where a represents the initial biomass, b and c the growth rate parameters. This model had a high coefficient of determination (R^2) and the highest heritability across all 23 barley inbreds. Thus, the quadratic regression was used for estimation of RGR. RGR_a, RGR_b, RGR_c represent the parameters in quadratic regression a, b, and c, respectively.

Morphological parameters were collected in multi-year and multi-environment field experiments that took place in the years 2017–2021

Downloaded from https://academic.oup.com/jxb/article/75/16/4904/7663878 by Bundesanstalt fuer Zuechtungsforschung an Kulturpflanzen, Hauptbibliothek user on 03 December 2025

at Düsseldorf, Cologne, Mechernich, and Quedlinburg (Shrestha *et al.*, 2022; Wu *et al.*, 2022). Not all locations were used in all years to assess all parameters. Flag leaf length (FL, cm) and width (FW, cm), plant height (PH, cm), flowering time (FT), awn length (AL, cm), spike length (EL, cm), and spikelet number in one row of the spike (SR), seed length (SL, mm), seed width (SW, mm), seed area (SA, mm^2), and thousand grain weight (TGW, g), grain weight (GW, kg per 10 m^2), and net straw weight (NSW, kg per 10 m^2) were measured as morphological parameters. FL, FW, AL, EL were measured by ruler, SL, SW, and SA were measured by MARViN seed analyser (MARViNTECH GmbH, Germany), and TGW was measured by MARViN and a balance.

The same set of morphological parameters were also measured in the climate chamber experiment. FL and FW were collected at 74 and 102 DAS with three replicates, and spike-related traits (AL, EL, SR, SL, SW SA, and TGW) were collected at 142 DAS with three replicates. Additionally, the total stem (without spike) weight per plant (SWP, g), total spike weight per plant (SKWP, g), total stem weight of main stem (TSWM, g), and spike weight of main stem (SKWM, g) were also collected in the climate chamber experiment. Harvest index (HI) was calculated using the following equation:

$$\mathrm{HI} = \frac{\mathrm{SKWP}}{\mathrm{DMP}} \tag{3}$$

In addition, harvest index of main stem (MSHI) was calculated using the following equation:

$$\mathrm{MSHI} = \frac{\mathrm{SKWM}}{\mathrm{TSWM}} \tag{4}$$

Statistical analyses

Field experiment

Due to the strong dependence of photosynthesis on light intensity (Ogren, 1993), we considered three light intensity clusters when analysing field measurements: LL, ML, and HL conditions. These light intensity clusters were identified by *K*-means clustering of PAR and LEF. In addition, we also compared three main developmental phases of barley, i.e. slow expansion phase (SEP) (ZS<30), rapid expansion phase (REP) (30≤ZS<60), and anthesis and senescence phase (ASP) (ZS≥60). These two factors, light intensity (L) and developmental phase (S), each with three levels, were considered when analysing the MultispeQ parameters from the field experiments based on the following linear model with the quantitative covariates light intensity (PAR) and developmental stage (ZS):

$$\begin{aligned}\gamma_{(p)ijklmnopqr} = \; & \mu + G_i + E_j + (G:E)_{ij} + \mathrm{ZS}_k + L_l + S_m + (G:L)_{il} \\ & + (G:S)_{im} + M_n + D_o + \mathrm{PAR}_{ijklmnor} + T_{ijklmnor} \\ & + (E:R)_{jp} + (E:R:B)_{jpq} + \epsilon_{(p)ijklmnopqr}\end{aligned} \tag{5}$$

where $\gamma_{(p)ijklmnor}$ was the observed MultispeQ parameter across all light conditions and all developmental stages, μ the general mean, G_i the effect of the ith inbred, E_j the effect of the jth environment, $(G:E)_{ij}$ the interaction between the ith inbred and the jth environment, ZS_k the effect of the kth Zadoks score of barley development, L_l the effect of the lth light intensity cluster, S_m the effect of the mth barely developmental phase, $(G:L)_{il}$ the interaction between the ith inbred and the lth light intensity cluster, $(G:S)_{im}$ the interaction between the ith inbred and the mth barley developmental phase, M_n the effect of the nth MultispeQ device, D_o the effect of measurement date, $(E:R)_{jp}$ the effect of the pth replicate nested within the jth environment, $(E:R:B)_{jpq}$ the effect of the qth block nested within the pth replicate in the jth environment, $\mathrm{PAR}_{ijklmnopqr}$ the light intensity of each measurement, $T_{ijklmnopqr}$ the ambient temperature of each measurement, and $\epsilon_{(p)ijklmnopqr}$ the random error.

To estimate adjusted entry means for MultispeQ parameters of all inbreds, G_i, E_j, $(G:E)_{ij}$, ZS_k, L_l, S_m, $(G:L)_{il}$, and $(G:S)_{im}$ were treated as fixed effects, and M_n, D_o, $(E:R)_{jp}$, $(E:R:B)_{jpq}$ as random effects, $\mathrm{PAR}_{ijklmnopqr}$ and $T_{ijklmnopqr}$ were covariates. Furthermore, we calculated adjusted entry means for all inbreds for each light intensity cluster as well as each developmental phase.

In addition, to evaluate the effect of each fixed factor and covariate, analysis of variance (ANOVA) was conducted.

To assess the heritability of each photosynthesis-related parameter at each developmental stage, which was considerably shorter than the above-mentioned three developmental phases, data were separated into eight stages from Zadoks principal growth stages. The adjusted entry means were calculated based on the following model:

$$\begin{aligned}\gamma_{(pd)ijlnopqr} = \; & \mu + G_i + E_j + M_n + D_o + \mathrm{PAR}_{ijklmnopqr} + T_{ijklmnopqr} \\ & + (E:R)_{jp} + (E:R:B)_{jpq} + \epsilon_{(p)ijklmnopqr}\end{aligned} \tag{6}$$

where, $\gamma_{(pd)ijlnopqr}$ was the photosynthesis-related parameter for each developmental stage across all other factors. Due to convergence problems, the interaction between G_i and E_j was removed from this model.

To assess the similarities among the barley genotypes with respect to their photosynthesis parameters, we performed hierarchical clustering by Ward's minimum variance theory (Ward, 1963) using the adjusted entry means of PSII parameters and SPAD at three different developmental phases. Furthermore, principal component analysis (PCA) was conducted by using the adjusted entry means calculated for each inbred in each of the developmental phases described before. In addition, a PCA was conducted by using the environmental factors (temperature and precipitation) of the inbreds at the country of origin. The relationship between photosynthesis-related parameters and morphological or growth-related parameters of the inbreds was evaluated by Pearson's correlation coefficient among adjusted entry means.

Climate chamber experiment

The adjusted entry means of carbon assimilation-related parameters from the climate chamber experiment were calculated based on the following model:

$$\begin{aligned}\gamma_{(A)ijklmr} = \; & \mu + G_i + \mathrm{ZS}_j + D_k + (D:\mathrm{TW})_{kl} \\ & + S_m + (G:S)_{im} + \epsilon_{(A)ijklmr}\end{aligned} \tag{7}$$

where $\gamma_{(A)ijklmr}$ was the carbon assimilation-related parameter, $D:\mathrm{TW}_{kl}$ the effect of the lth time window in the kth date of measurement, and $\epsilon_{(A)ijklmr}$ the random error. To estimate adjusted entry means for carbon assimilation-related parameters of six barley inbreds, G_i, ZS_j, S_m and $(G:S)_{im}$ were treated as fixed effects, as well as D_k and $D:\mathrm{TW}_{kl}$ as random effects.

The relationship between photosynthesis-related parameters and morphological or growth-related parameters of the inbreds was evaluated by Pearson's correlation coefficient between adjusted entry means.

Estimation of heritability

Broad-sense heritability (H^2) was estimated for both field and climate chamber experiments based on the following method:

$$H^2 = \sigma_G^2 / \left(\sigma_G^2 + \bar{v}_\delta^{\mathrm{BLUE}}/2\right) \tag{8}$$

Downloaded from https://academic.oup.com/jxb/article/75/16/4904/7663878 by Bundesanstalt fuer Zuechtungsforschung an Kulturpflanzen, Hauptbibliothek user on 03 December 2025

where σ^2_G was the genotypic variance calculated based on the above models with a random effect for G_i and $\bar{v}_{\delta}^{\mathrm{BLUE}}$ was the mean variance of the difference of two genotypic means (Holland *et al.*, 2003; Piepho and Möhring, 2007).

To avoid the effect of the varying number of replicates, the H^2 of photosynthesis-related parameters was estimated for each developmental stage based on the following equation:

$$H^2 = \sigma^2_G / \left(\sigma^2_G + \sigma^2_{G:E}/5 + \sigma^2_e/5\right) \quad (9)$$

where $\sigma^2_{G:E}$ was the variance of the interaction of barley inbreds and environments, and σ^2_e was the residual variance.

We used the statistical software R to perform all statistical analyses.

Results

Factors affecting photosynthesis-related parameters in the field

Parameters of PSII and SPAD were collected under field conditions with a wide range of PAR from 67 to 2172 μmol m^{-2} s^{-1}. In general, LEF increased as PAR increased, with an increasing variability among the individual observations at higher PAR (Fig. 1A). An increase of PAR was associated with a decrease of Phi2 and an increase of PhiNPQ, while PhiNO remained relatively stable (Supplementary Fig. S2A–C). Note that the sum of Phi2, PhiNPQ, and PhiNO is equal to 1. The light-dependent changes in Phi2 were accompanied by the corresponding changes in F_v'/F_m' and qL (Supplementary Fig. S2D, E). The light response of NPQt was similar to that of PhiNPQ except that it often gave extreme values (Supplementary Fig. S2F). In contrast to these PSII parameters, SPAD values were not affected by momentary PAR (Supplementary Fig. S2G).

Given the strong influence of PAR on PSII parameters, *K*-means clustering was performed to separate the observations of LEF into three groups based on the light intensity: LL, ML, and HL conditions (Fig. 1B). As expected, significant ($P<0.05$) differences in Phi2 and PhiNPQ, but not SPAD, were observed among the three light intensities (Fig. 2A; Supplementary Table S1). We then assessed the impact of developmental phase (SEP, REP, and ASP) on these parameters (Fig. 2B; Supplementary Table S2). All three parameters showed significant ($P<0.05$) differences between SEP and REP; Phi2 and SPAD increased from SEP to REP while PhiNPQ decreased (Fig. 2B). Thus, both PAR and developmental phases seem to affect Phi2 and PhiNPQ, whereas SPAD changed with plant development.

Significant ($P<0.05$) effects on PSII parameters and SPAD were observed for the interactions between genotype and environment ($\sigma^2_{G:E}$), genotype and light condition ($\sigma^2_{G:L}$) and genotype and developmental phase ($\sigma^2_{G:S}$), along with the effects of genetic variation (σ^2_G) or other variables such as the date of measurement (σ^2_D), the used MultispeQ device (σ^2_M), and the replicate ($\sigma^2_{E:R}$) (Table 1). Analysis of variance also confirmed significant ($P<0.05$) effects of PAR, light condition, developmental phase, and developmental stage (rated on the Zadoks scale) on the different PSII parameters and SPAD (Table 2). In addition, ambient temperature (T), which typically co-varies with light intensity in the field, also significantly ($P<0.05$) affected the PSII parameters except PhiNPQ in barley.

Genetic variations in photosynthesis-related traits

When data from all light conditions and all developmental stages were combined together, H^2 of the examined parameters ranged between 0.16 (PhiNPQ) and 0.78 (qL) (Table 1). Notably, when the heritability was calculated separately at different developmental stages as defined by the Zadoks growth scale, the H^2 values of these parameters were considerably lower in the seedling growth stage and significantly ($P<0.05$) higher in the dough developmental stage (Supplementary Fig. S3). In accordance, all PSII parameters and SPAD had low H^2 values in the SEP (Fig. 3). In the REP, SPAD and Phi2 had the highest H^2 while NPQt and F_v'/F_m' had the lowest. In the ASP, the H^2 of Phi2 decreased dramatically.

Hierarchical cluster analysis of the adjusted entry means of the PSII parameters and SPAD observed in each of the three developmental phases indicated the presence of four major clusters among the 23 barley inbred lines (Fig. 4A). In general, the four clusters differed in the PSII parameters but not in SPAD (Fig. 5A). All PSII parameters except NPQt showed significant ($P<0.05$) differences among the four clusters in each of the three developmental phases (Fig. 5A).

We then asked whether the four clusters also represented differences in growth-related and morphological parameters among the 23 inbred lines. Relative growth rates (RGR) were calculated from the changes in DMP in the field experiment in Düsseldorf (Supplementary Fig. S4). Based on the growth parameters alone, the inbred lines could be divided into two clusters by hierarchical cluster analysis: DMP remained at the same level after 100 days after sowing, and DMP increased throughout the entire growth season (Supplementary Fig. S4). We observed no significant difference ($P=0.3$) in flowering time between the two groups. When PCA was performed on a combination of the PSII parameters and SPAD data shown in Fig. 2 as well as the growth-related parameters derived from Supplementary Fig. S4 and morphological traits collected from multi-year and multi-environment field experiments, the analysis revealed four clusters (Fig. 4B) that were very similar to those identified based on the PSII parameters and SPAD alone (Fig. 4A). Comparing the four clusters, we found no significant difference in DMP and RGR (Fig. 5B) or the morphological traits (Supplementary Fig. S5). Moreover, no significant correlation was observed between the first two principal components and the environmental information of the country of origin of inbreds (Fig. 4C). Together, these results suggest that the clustering of the inbreds according to photosynthetic parameters primarily reflects genetic variations in photosynthetic traits among the 23 inbreds and is not confounded by differences in growth-related and morphological parameters.

Downloaded from https://academic.oup.com/jxb/article/75/16/4904/7663878 by Bundesanstalt fuer Zuechtungsforschung an Kulturpflanzen, Hauptbibliothek user on 03 December 2025

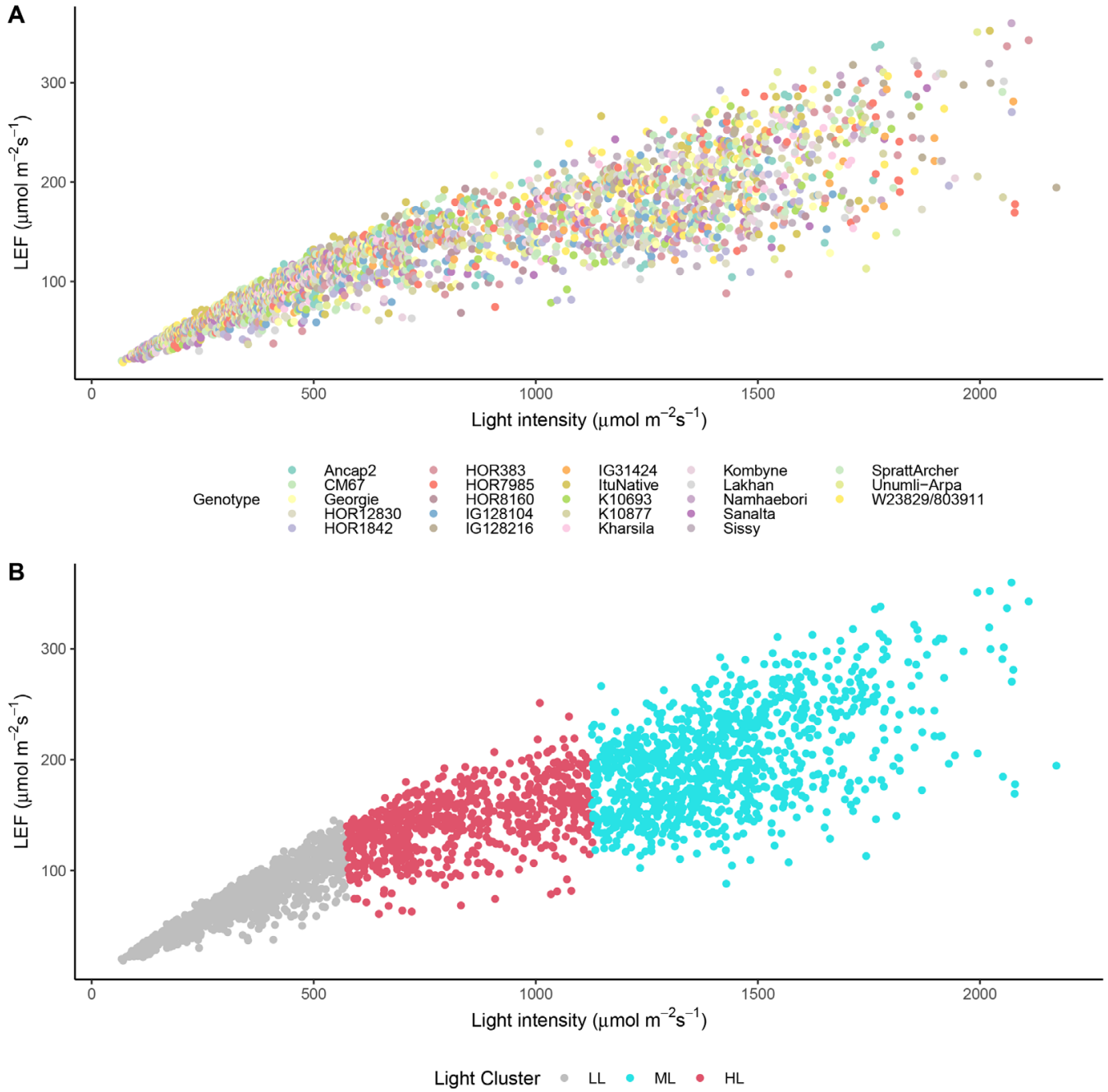

Fig. 1. Linear electron flow (LEF) for 23 barley inbred lines in the field experiment in response to changing light intensity across all environments. The different colors of the dots in (A) indicate 23 different barley inbred lines. Three different colors of the dots in (B) represent the clusters of low (LL), medium (ML), and high (HL) light condition.

Comparison of gas exchange-based parameters and PSII parameters

Of the 23 barley inbreds, six (HOR1842, IG128216, IG31424, ItuNative, K10877, and W23829/803911) were selected to assess carbon assimilation-related parameters in climate chamber conditions. These six inbreds differed in the PSII parameters and SPAD assessed in the field. HOR1842 had the lowest adjusted entry means for Phi2, qL, and SPAD; IG128216 had the highest Phi2 and LEF. IG31424 had the highest PhiNPQ and the lowest SPAD. ItuNative had the lowest SPAD with relatively high Phi2, whereas K10877 had the highest SPAD with average values of PSII parameters. W23829/803911 was characterized by the lowest PhiNPQ and NPQt.

Downloaded from https://academic.oup.com/jxb/article/75/16/4904/7663878 by Bundesanstalt fuer Zuechtungsforschung an Kulturpflanzen, Hauptbibliothek user on 03 December 2025

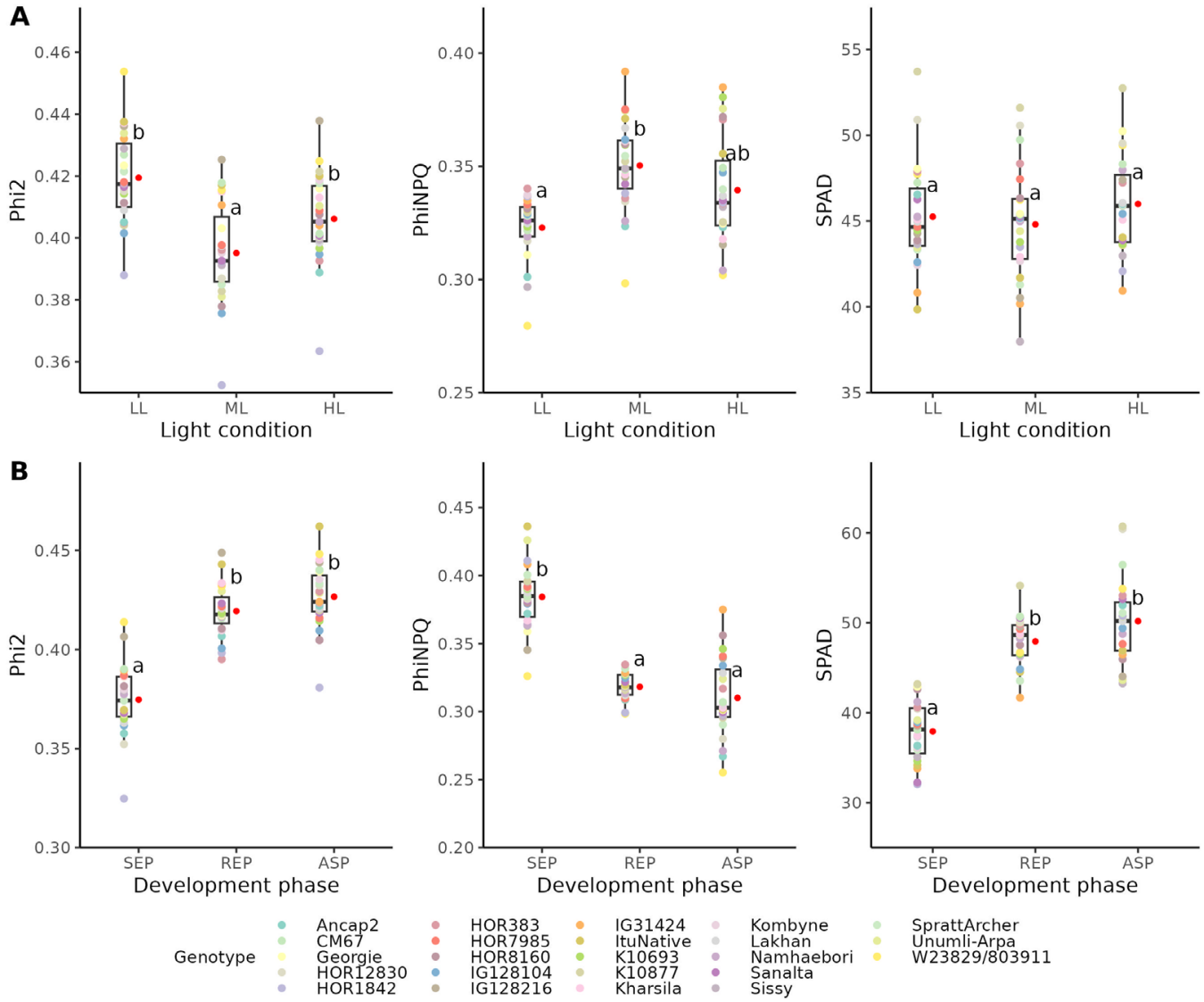

Fig. 2. Effects of light intensity and developmental phase on the quantum yield of PSII (Phi2), the quantum yield of non-photochemical quenching (PhiNPQ), and relative chlorophyll content (SPAD) of 23 barley inbred lines. (A) Comparison of three light conditions: LL (low light), ML (medium light), and HL (high light). (B) Comparison of three developmental phases: slow expansive phase [SEP; Zadoks score (ZS) from 10 to 29)], rapid expansive phase (REP; ZS from 30 to 59), and anthesis and senescence phase (ASP; ZS from 60 to 87). The colored dots represent the adjusted entry means for 23 barley inbred lines. The red point next to each box plot indicates the average across all inbreds for each light condition (A) or developmental phase (B). The letters next to each box plot indicate statistical significance. Different letters denote significant differences based on Tukey's test (P<0.05) between the means for each parameter in each condition.

The gas exchange measurements in the climate chamber resulted in high H^2 values for carbon assimilation-related parameters, ranging between 0.820 and 0.895 (Table 3). We observed a significant genetic variation (P<0.05) for carbon assimilation at saturating light intensity (A_{sat}) among the six inbreds (Fig. 6A); the adjusted entry means of (A_{sat}) were ranging from 14.7 (IG31424) to 19.7 (K10877) μmol m^{-2} s^{-1}. The differences in the maximal carboxylation ($V_{c,max}$) and electron transport rates (J_{max}) as well as triose phosphate utilization capacity (TPU) were also significant (P<0.05) among the six inbreds (Fig. 6A). Similarly, Phi2 (measured at LL, ML and HL) and SPAD showed significant (P<0.05) differences among the six inbreds (Fig. 6B). Carbon assimilation-related parameters underwent significant (P<0.05) changes across the developmental phases, all peaking in REP together with Phi2 and SPAD (Fig. 6C, D). The H^2 values for the PSII parameters and SPAD were also generally high, including 0.92 for Phi2 and 0.96 for SPAD (Table 3).

We observed significant (P<0.05) positive correlations between SPAD, Phi2, and LEF (both measured at HL) and all

Downloaded from https://academic.oup.com/jxb/article/75/16/4904/7663878 by Bundesanstalt fuer Zuechtungsforschung an Kulturpflanzen, Hauptbibliothek user on 03 December 2025

Table 1. Summary statistics of adjusted entry means, variance components, and broad-sense heritability (H^2) for PSII parameters and SPAD measured in the field experiments

Trait	Mean	Min	Max	σ^2_G	$\sigma^2_{G:E}$	$\sigma^2_{G:L}$	$\sigma^2_{G:S}$	σ^2_D	σ^2_M	$\sigma^2_{E:R}$	$\sigma^2_{E:R:B}$	σ^2_e	H^2
LEF	126.2	110.6	139	4.987		8.307**	7.497*			0.325	2.935	469.69	0.42
					23.742***			151.189***	236.731***				
Phi2	0.41	0.37	0.43	0.90***	0.84***	0.17	0.24	16.25***	12.54***	0.72**	0.1	21.29	0.74
F_v'/F_m'	0.67	0.64	0.7	0.5	0.54**	0.71***	0.87***	11.73***	2.34***	0.52**	0.03	25.52	0.58
PhiNO	0.26	0.22	0.3	1.36***	0.62**	0.65**	0.48*	6.99***	1.46***	1.29***	0.06	34.12	0.74
PhiNPQ	0.34	0.29	0.37	0.09	1.37***	0.84***	1.85***	32.62***	11.52***	0.29	0.17	32.57	0.16
NPQt	1.58	1.19	2.01	84.2	97.99***	168.23***	252.15***	1736.00***	372.24***	121.13***	7.58	5311.71	0.53
qL	0.35	0.28	0.42	4.25***	1.04*	0.96*	0	17.46***	5.51**	3.38***	0.29	83.11	0.78
SPAD	45.35	40.65	52.68	2.091	5.850***	0.544	5.309***	33.570***	31.471***	1.199*	0.983**	67.98	0.68

Note that the values of variance components of six photosynthesis-related parameters (Phi2, F_v'/F_m', PhiNO, PhiNPQ, NPQt, qL) were multiplied by 10 000. Asterisks indicate the significance of a likelihood ratio test (*P<0.05, **P<0.01, ***P<0.001). F_v'/F_m', maximum efficiency of PSII in light-adapted state; NPQt, total non-photochemical quenching; Phi2, quantum yield of PSII; PhiNO, quantum yield of non-regulated dissipation processes; PhiNPQ, quantum yield of non-photochemical quenching; qL, fraction of PSII open center; SPAD, relative chlorophyll content; σ^2_G, genotypic variance component; $\sigma^2_{G:E}$, variance component of interaction between genotype and environment; $\sigma^2_{G:L}$, variance component of interaction between genotype and light conditions; $\sigma^2_{G:S}$, variance component of interaction between genotype and developmental phase; σ^2_D, variance component of date of measurement; σ^2_M, variance component of MultispeQ device; $\sigma^2_{E:R}$, variance component of replicate in environment; $\sigma^2_{E:R:B}$, variance component of block nested within the replicate in environment.

four carbon assimilation-related parameters (determined at HL) in the climate chamber (Fig. 7). As anticipated, PhiNPQ and NPQt were negatively correlated with the four carbon assimilation-related parameters.

The adjusted entry means of the six barley inbreds showed significant (P<0.05) positive correlations between Phi2 and carbon assimilation-related parameters in the climate chamber experiment (Fig. 8). In comparison, the correlations between these parameters assessed in the climate chamber experiment and Phi2 observed in the field were lower, with the highest correlation coefficient of 0.72 found for Phi2 at HL between these experiments.

Relationship between photosynthesis-related parameters and growth or morphological parameters

Morphological parameters and DMP were determined in the climate chamber experiment to assess the relationship between the photosynthesis-related parameters and morphological or growth-related parameters. As done for the field experiments (Supplementary Fig. S4), RGR was calculated for the six inbred lines by fitting a quadratic regression to the DMP data (Supplementary Fig. S6). No significant correlation was observed between the morphological traits, DMP-based RGR and photosynthesis-related parameters among the six barley inbreds (Fig. 7).

We then made the same analysis using the data from the 23 inbred lines in the field experiments (Fig. 9; Supplementary Table S3). As expected, we found significant (P<0.05) positive or negative correlations among the PSII parameters as well as among the growth-related parameters. No significant correlation was observed between SPAD and all PSII parameters when the adjusted entry means of all developmental stages and locations were considered (Fig. 9). Comparing the PSII parameters and the growth-related parameters, the final DMP was significantly (P<0.05) positively and negatively correlated with F_v'/F_m' and NPQt, respectively. RGR_c showed a significant (P<0.05) positive correlation with NPQt (Fig. 9). Looking at the PSII parameters and morphological traits collected from multiple environments and years, significant (P<0.05) positive correlations were observed between two PSII parameters (PhiNO and F_v'/F_m') and NSW (Fig. 10). In addition, significant negative correlations were observed between three PSII parameters (qL, NPQt, PhiNPQ) and NSW. Phi2, LEF and qL were significantly (P<0.05) negatively correlated with flag leaf morphology (FL and FW) (Fig. 10).

Discussion

Comparison of chlorophyll fluorescence- and gas exchange-based techniques

In order to assess the genetic variation of photosynthesis-related parameters in breeding programs, high-throughput methods

Downloaded from https://academic.oup.com/jxb/article/75/16/4904/7663878 by Bundesanstalt fuer Zuechtungsforschung an Kulturpflanzen, Hauptbibliothek user on 03 December 2025

Table 2. Mean square values from analysis of variance for photosystem II parameters and SPAD measured in the field experiments

Trait	G	PAR	T	E	L	ZS	S
LEF	593.67	846205.72***	14345.49***	1751.45*	10979.05***	951.84	1453.20*
Phi2	0.48*	133.61***	6.99***	0.36	6.10***	0.35	1.06**
F_v'/F_m'	0.35	29.88***	2.85***	0.09	1.00*	4.74***	2.71***
PhiNO	0.73*	0.04	7.99***	0.56	0.03	9.78***	5.17***
PhiNPQ	0.31	136.65***	0.23	0.12	4.93***	6.33***	2.99***
NPQt	69.53	5967.81***	264.87*	10.22	86.6	686.60***	394.44***
qL	3.16***	74.74***	43.61***	0.91	4.01**	10.01***	10.02***
SPAD	94.54	0.19	216.02	45.77	80.4	4537.56***	932.87***

Asterisks indicate the significance of a likelihood ratio test (*P<0.05, **P<0.01, ***P<0.001). *G*, genotype; PAR; light intensity; *T*, ambient temperature; *E*, environment; *L*, light condition; ZS, Zadoks score of barley development; *S*, developmental phases. Photosynthetic parameters: F_v'/F_m', maximum efficiency of PSII in light-adapted state; LEF, linear electron flow; NPQt, total non-photochemical quenching; Phi2, quantum yield of PSII; PhiNO, quantum yield of non-regulated dissipation processes; PhiNPQ, quantum yield of non-photochemical quenching; qL, fraction of PSII open center; SPAD, relative chlorophyll content.

are needed. Chlorophyll fluorescence-based techniques and hyperspectral measurement techniques have the potential to serve as high-throughput methods to evaluate photosynthetic traits (for review see van Bezouw *et al.*, 2019). Hyperspectral sensing techniques rely on indirect correlations between features of reflectance spectra and photosynthesis. Once such correlations have been characterized, they can be used to predict photosynthesis capacity at plot level (Meacham-Hensold *et al.*, 2019) or leaf level (Serbin *et al.*, 2011; Ainsworth *et al.*, 2014; Yendrek *et al.*, 2016; Silva-Perez *et al.*, 2017). However, compared with chlorophyll fluorescence- and gas exchange-based techniques, reflectance spectra are less sensitive to short-term changes in photosynthesis. Furthermore, correlation-based prediction models cannot be readily applied to new genetic materials, especially across different years and different environmental conditions (Meacham-Hensold *et al.*, 2019). Hence, gas exchange- and chlorophyll fluorescence-based techniques, particularly the latter for high-throughput measurements, are considered more reliable and straightforward to explore genetic diversity of photosynthesis and related traits.

Positive correlations between PSII electron transport and carbon assimilation have been demonstrated under laboratory conditions, such as in *Phaseolus vulgaris* L. (Farquhar *et al.*, 1980), red campion, barley, and maize (Genty *et al.*, 1989) (for review see Bellasio *et al.*, 2016). Our climate chamber experiment also confirmed the significant positive correlation between Phi2 and carbon assimilation-related parameters (Fig. 7) across diverse inbreds of barley. In addition, significant genetic effects with high heritability were estimated for both gas exchange- and chlorophyll fluorescence-based parameters in the climate chamber (ranging from 0.76 to 0.96) (Table 3). These results show the utility of chlorophyll fluorescence-based techniques to detect genetic variation in photosynthesis under controlled conditions (Flood *et al.*, 2016).

Despite the increasing number of studies focusing on photosynthesis under dynamic conditions (Keller *et al.*, 2019; Acevedo-Siaca *et al.*, 2021c; Fu and Walker, 2023; reviewed by Long *et al.*, 2022), few studies have demonstrated that chlorophyll fluorescence-based parameters can replace carbon assimilation parameters when investigating genetic diversity of photosynthesis parameters in the field (Bucher *et al.*, 2018). Under field conditions, in which light intensity is changing dynamically, the relationship between the photosynthetic light reaction and carbon assimilation, as seen in a steady-state condition (Farquhar *et al.*, 1980; Bellasio *et al.*, 2016), may be broken (Rascher and Nedbal, 2006; Eberhard *et al.*, 2008; Long *et al.*, 2022) due to competing processes such as photorespiration in C_3 species (Pearcy, 1990; Cornic and Fresneau, 2002; Lawson *et al.*, 2012).

However, we observed a strong positive correlation of Phi2 between the dynamic conditions in the field and steady-state conditions in the climate chamber (Fig. 8). This correlation is based on the adjusted entry mean of Phi2, i.e. non-genetic variation was corrected for these means. Our results thus provide a strong support to the use of chlorophyll fluorescence-based high-throughput measurement techniques to study genetic diversity under dynamically changing, natural environmental conditions.

To use chlorophyll fluorescence-based techniques to assess highly variable photosynthesis parameters (Figs 1, 2) in breeding programs, however, it is important to consider the factors contributing to their variation.

Factors contributing to photosynthesis variability in the field

We observed a high variability in photosynthesis-related parameters among 23 barley inbreds in the field (Table 1; Fig. 2). Four main factors are potentially contributing to the high variability of photosynthesis-related parameters: (i) environmental conditions, (ii) developmental stages, (iii) genetic diversity, and (iv) interaction among genotypes, environment conditions, and developmental stages. Below we will discuss these factors one by one.

Downloaded from https://academic.oup.com/jxb/article/75/16/4904/7663878 by Bundesanstalt fuer Zuechtungsforschung an Kulturpflanzen, Hauptbibliothek user on 03 December 2025

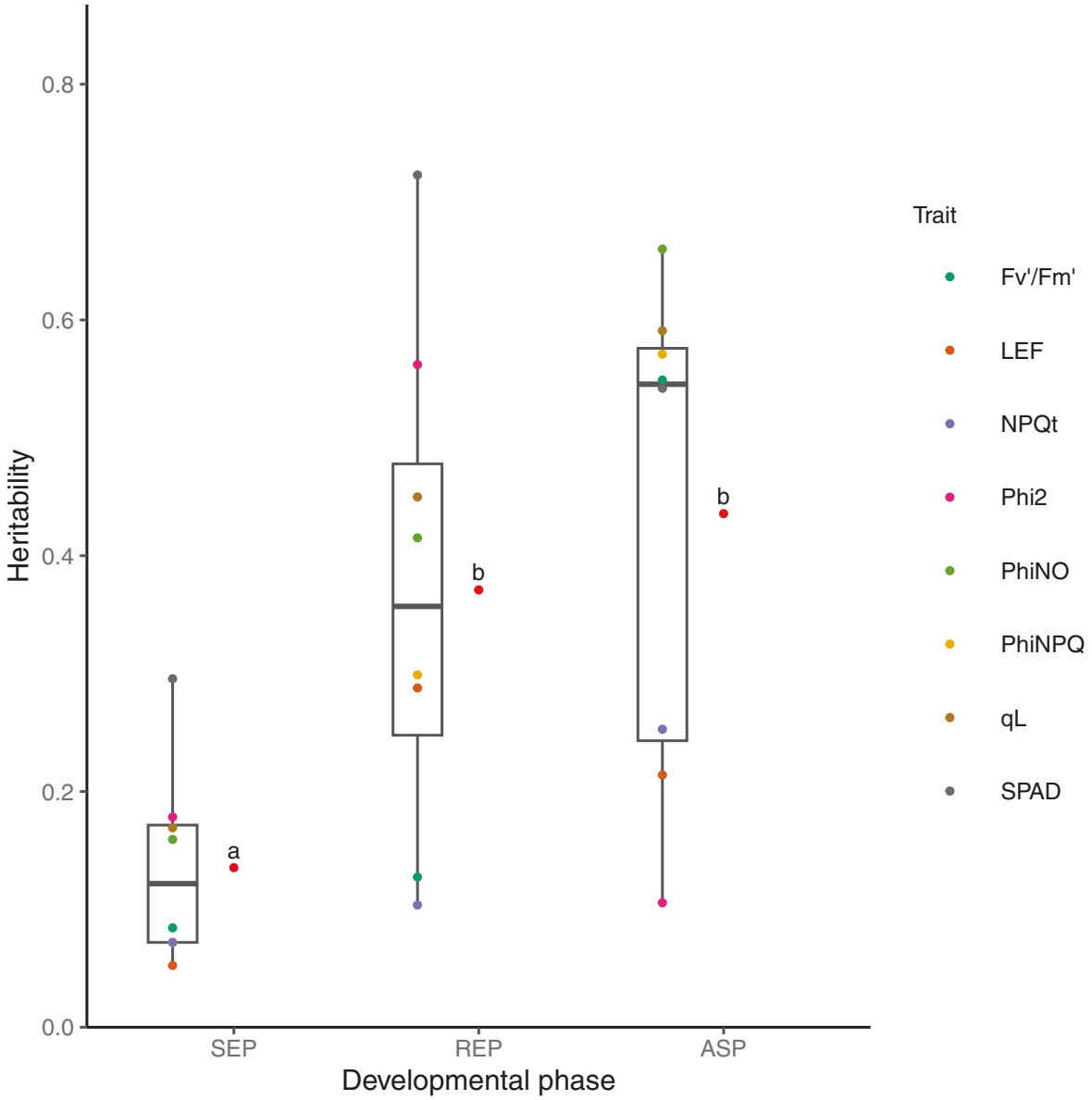

Fig. 3. Heritability of PSII parameters and SPAD in different developmental phases. SEP, slow expansive phase [Zadoks score (ZS) 10–29]; REP, rapid expansive phase (ZS 30–59); ASP, anthesis and senescence phase (ZS 60–87). The red point next to each box plot indicates the mean heritability across all traits for each developmental phase. Different letters next to each box plot indicate significant differences based on Tukey's test (P<0.05) between the mean heritability. F_v'/F_m', maximum efficiency of PSII in light-adapted state; LEF, linear electron flow; NPQt, total non-photochemical quenching; Phi2, quantum yield of PSII; PhiNO, quantum yield of non-regulated dissipation processes; PhiNPQ, quantum yield of non-photochemical quenching; qL, fraction of PSII open center; SPAD, relative chlorophyll content.

Growth environment of spring barley

We observed significant (P<0.05) effects for the design variables, namely, location of the experiment, measurement date (Table 1), as well as replicate ($\sigma^2_{E:R}$). This can be explained by the dynamic environmental conditions during the growth season of spring barley, which was from late March to the beginning of August. Daily average temperature was fluctuating with an increasing trend (Supplementary Fig. S1). Also, fluctuations in light intensity occurring within and between days must have affected photosynthesis. We observed a significant (P<0.05) effect of light intensity (PAR) and ambient temperature (T) (Table 2), which were considered as co-variants because of the variability within a day and location of the measurement. In addition, lower temperature in May (Supplementary Fig. S1) might have suppressed Phi2 in the SEP compared with the other two developmental phases (Fig. 2B) (Bagley *et al.*, 2015; Moore *et al.*, 2021).

In parallel to the erratic changes of temperature and light intensity in the field, photosynthetic efficiency typically exhibits

Downloaded from https://academic.oup.com/jxb/article/75/16/4904/7663878 by Bundesanstalt fuer Zuechtungsforschung an Kulturpflanzen, Hauptbibliothek user on 03 December 2025

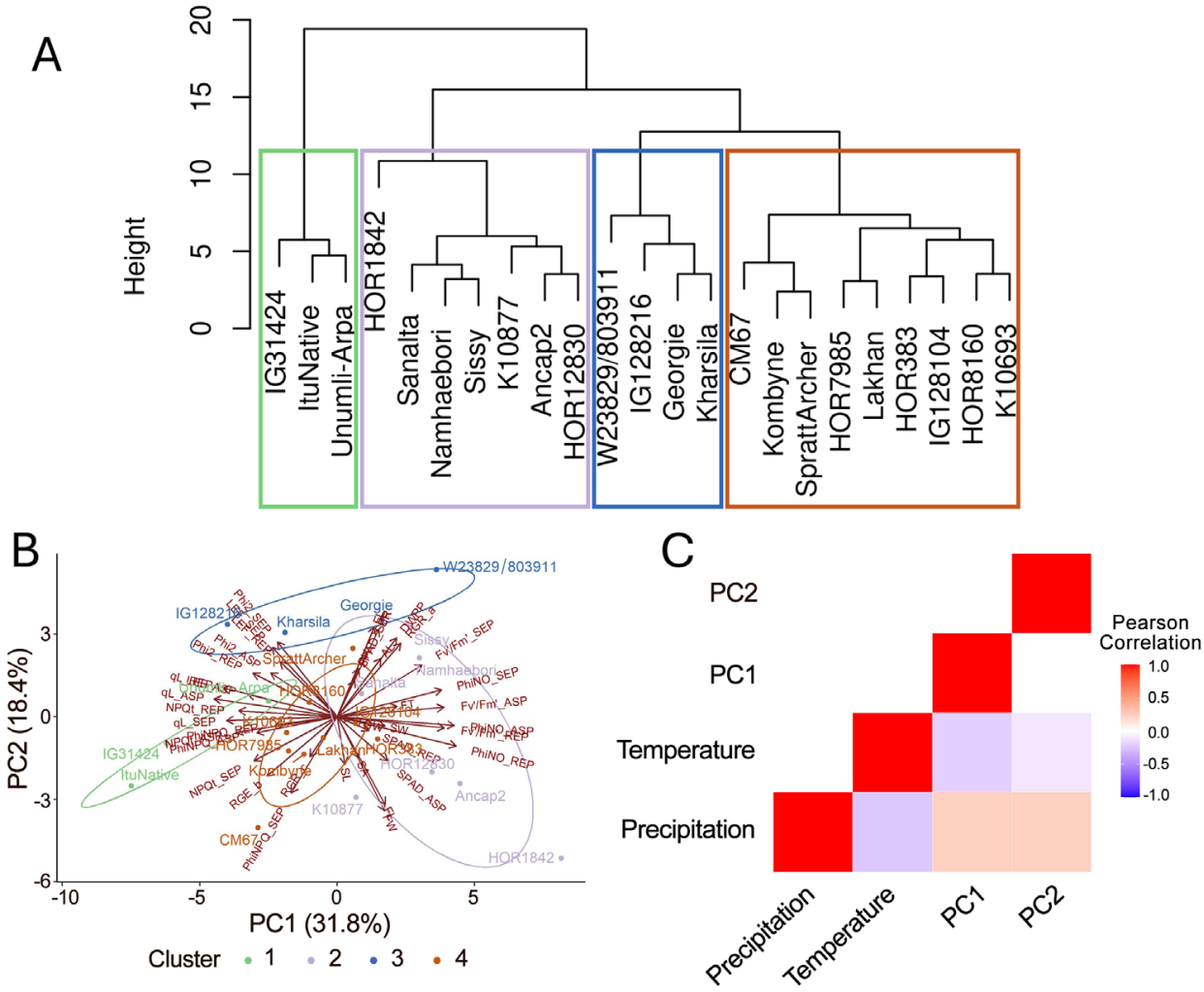

Fig. 4. Multi-variate analysis of photosynthesis related parameters. (A) Hierarchical clustering of 23 barley inbred lines based on their adjusted entry means for PSII parameters and relative chlorophyll content (SPAD) in three developmental phases. (B) Principal component analysis based on the adjusted entry means of the combination of PSII parameters and SPAD in three developmental phases, the growth-related parameters based on dry mass per plant, and the morphological traits from multi-year and multi-environment experiments. (C) Pearson's correlation coefficient calculated between pairs of PC1 and PC2 loadings of each inbred in PCA (B), precipitation and temperature of the country of the origin of each inbred.

diurnal (Flood *et al.*, 2016) and seasonal (Keller *et al.*, 2019) patterns. Leaf movement (Flood *et al.*, 2016), in interaction with dynamic environments, can also affect photosynthesis.

The significant (P<0.05) variance components observed in our study for environmental factors, namely date (D), PAR and ambient temperature (T), indicate that single time point measurements are not sufficient to draw conclusions on genetic variation in photosynthesis under field conditions.

Developmental stages

Most previous studies exploring the genetic diversity of photosynthesis in cereals focused on carbon assimilation in the flag leaf, which is the most important leaf in pre- or post- anthesis (Driever *et al.*, 2014; Carmo-Silva *et al.*, 2017; Acevedo-Siaca *et al.*, 2021b). In our study, however, significant (P<0.05) differences in photosynthesis-related parameters were observed in both the field and the climate chamber experiments at different developmental stages (Figs 2, 6C, D; Tables 1, 3). As our analysis was corrected for environmental conditions, the observed differences in developmental phases are not due to the environmental changes during the experiments but due to the development of the plant itself. This is in accordance with the earlier reports of changing heritability for photosynthesis-related parameters across the lifespan of Arabidopsis (Flood *et al.*, 2016) and changing quantitative trait loci detected for plant growth across the cultivation period under controlled conditions (Meyer *et al.*, 2021).

Photosynthesis-related parameters are linked to plant development as well as leaf development (Wingler *et al.*, 2004; Bielczynski *et al.*, 2017). At the plant level, the sink tissues in

Downloaded from https://academic.oup.com/jxb/article/75/16/4904/7663878 by Bundesanstalt fuer Zuechtungsforschung an Kulturpflanzen, Hauptbibliothek user on 03 December 2025

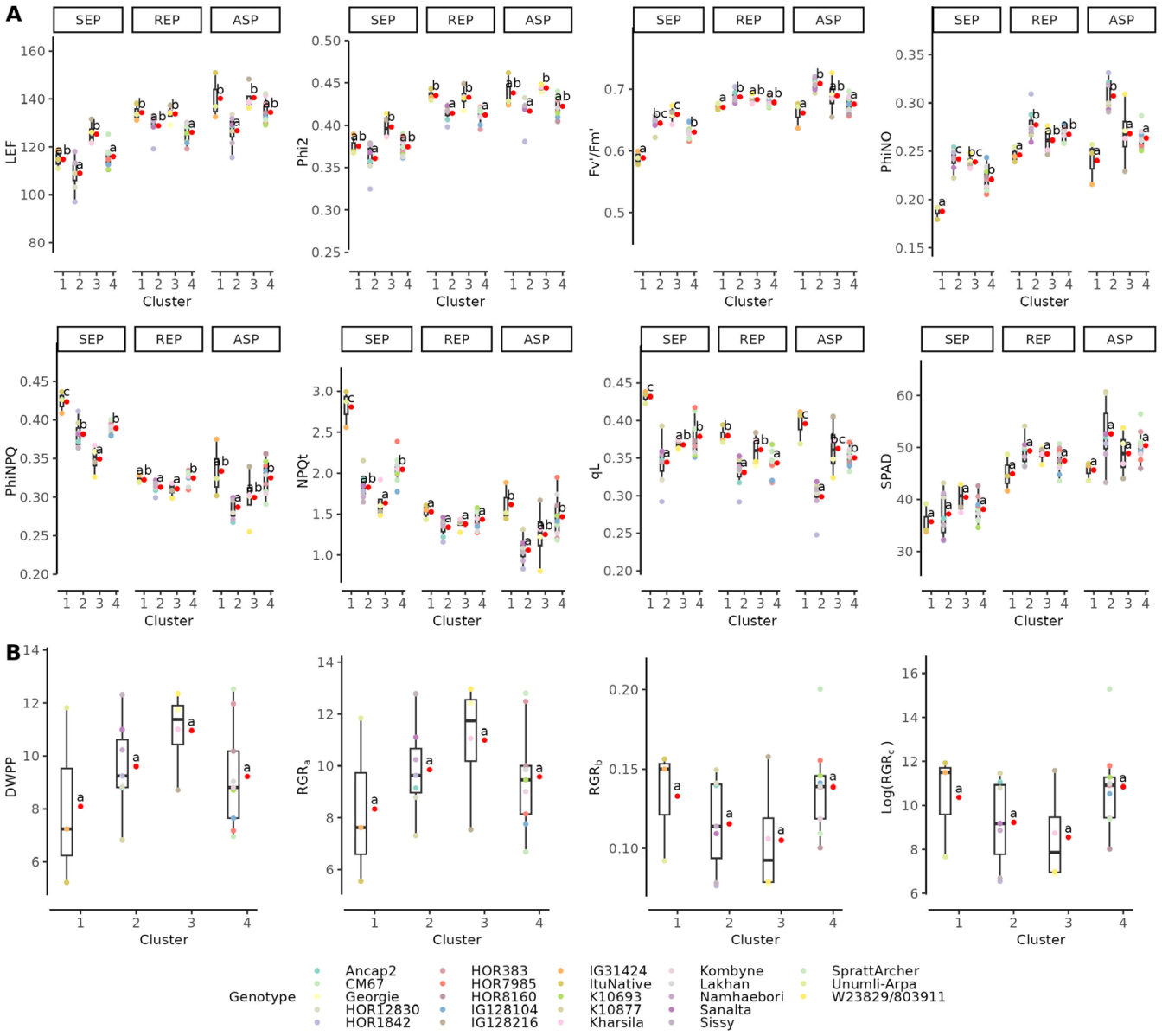

Fig. 5. Comparison of PSII parameters, relative chlorophyll content (SPAD) and growth-related parameters among the four clusters. (A) PSII parameters and SPAD in different developmental phases. (B) Dry mass per plant (DMP) and relative growth rates (RGR_a, RGR_b, RGR_c) calculated from DMP based on the quadratic regression ($y_t = a + bt - ct^2$). Due to the wide range of RGR_c, log-transformed data of RGR_c were used. The red point next to each box plot indicates the mean of the parameters in each cluster. Different letters next to each box show significant differences based on Tukey's test (P<0.05) between the clusters. SEP, slow expansive phase [Zadoks score (ZS) 10–29]; REP, rapid expansive phase (ZS 30–59); ASP, anthesis and senescence phase (ZS 60–87); F_v'/F_m', maximum efficiency of PSII in light-adapted state; LEF, linear electron flow; NPQt, total non-photochemical quenching; Phi2, quantum yield of PSII; PhiNO, quantum yield of non-regulated dissipation processes; PhiNPQ, quantum yield of non-photochemical quenching; qL, fraction of PSII open center; SPAD, relative chlorophyll content.

SEP are mainly growing leaves and roots, while new sink tissues emerged in REP, such as larger root system and formation of inflorescence (Alqudah and Schnurbusch, 2017). The increased sink activity in REP coincided with the high Phi2 (Fig. 2B). In ASP, barley went from the anthesis stage to grain filling stage, which may further increase the sink strength. However, photosynthesis-related (source) parameters did not show corresponding increases in ASP compared with REP (Fig. 2B). In fact, it has been proposed that spike photosynthesis may serve as the major photosynthate source for grain filling, as previously shown for wheat (Maydup *et al.*, 2010; Vicente *et al.*, 2018; Molero and Reynolds, 2020).

At the leaf level, photosynthetic efficiency typically increases with leaf development to reach the maximum during leaf

Downloaded from https://academic.oup.com/jxb/article/75/16/4904/7663878 by Bundesanstalt fuer Zuechtungsforschung an Kulturpflanzen, Hauptbibliothek user on 03 December 2025

Table 3. Summary statistics of adjusted entry means, variance components and broad-sense heritability (H^2) for carbon assimilation-related parameters, SPAD and photosystem II parameters under 1500 μmol m^{-2} s^{-1} assessed in the climate chamber experiment

Trait	Mean	Min	Max	σ^2_G	$\sigma^2_{G:S}$	σ^2_D	$\sigma^2_{D:TW}$	σ^2_e	H^2
$V_{c,max}$	43.3	37.5	49.8	14.9*	6.432*	21.331**	6.432*	50.886	0.848
J_{max}	111.6	94.8	132.4	141.76**	38.85	193.515***	38.85	324.241	0.895
TPU	7.61	6.37	9.13	0.717**	0.23*	0.688***	0.23	1.297	0.892
A_{sat}	17.2	14.7	19.7	2.169*	1.32*	2.544**	1.319	9.608	0.82
LEF_1500	185.18	73.39	278.13	132.69**	61.39***	197.73***	87.64***	707.85	0.92
Phi2_1500	0.27	0.11	0.41	0.03**	0.01***	0.04***	0.02***	0.16	0.92
F_v'/F_m'_1500	0.6	0.21	0.75	0.05**	0.02**	0.05**	0.02**	0.26	0.92
PhiNO_1500	0.23	0.04	0.45	0.03**	0.01	0.05***	0.02*	0.27	0.86
PhiNPQ_1500	0.49	0.24	0.79	0.08**	0.02**	0.08**	0.05***	0.39	0.93
NPQt_1500	2.33	0.64	17.89	11.70*	5.45**	11.51*	6.32**	80.99	0.9
qL_1500	0.26	0.1	0.74	0.02	0.02*	0.11***	0.02*	0.43	0.76
SPAD	44.19	6.28	75.47	36.22***	3.81*	10.45	28.91***	75.63	0.96

Note, the values of variance components of six PSII parameters (Phi2_1500, F_v'/F_m' _1500, PhiNO_1500, PhiNPQ_1500, NPQt_1500, qL_1500) were multiplied by 100. Asterisks indicate the significance of a likelihood ratio test (*P<0.05, **P<0.01, ***P<0.001). A_{sat}, carbon assimilation at saturating light intensity; F_v'/F_m', maximum efficiency of PSII in light-adapted state; J_{max}, maximum rate of electron transport; LEF, linear electron flow; NPQt, total non-photochemical quenching; Phi2, quantum yield of PSII; PhiNO, quantum yield of non-regulated dissipation processes; PhiNPQ, quantum yield of non-photochemical quenching; qL, fraction of PSII open center; SPAD, relative chlorophyll content; TPU, triose phosphate utilization; $V_{c,max}$, maximum rate of carboxylation. σ^2_G variance component of inbred; $\sigma^2_{G:S}$ variance component of interaction between inbred and developmental phase; σ^2_D variance component of date of measurement, $\sigma^2_{D:TW}$ variance component of time window nested in date of measurement.

expansion (Bielczynski *et al.*, 2017). After anthesis, declining activity of photosynthesis has been reported in many studies (Wingler *et al.*, 2004; Liu *et al.*, 2017; Miao *et al.*, 2018; Yang *et al.*, 2018). This was not the case in the present study as no significant difference in Phi2 and SPAD was found between REP and ASP (Fig. 2B). By always choosing the top fully expanded leaves for measurements throughout all developmental stages of the plant, we minimized the effect of leaf development.

Genotypic effect

To evaluate the potential of classical breeding to optimize photosynthesis, the relative importance of genotypic effects versus non-genotypic effects on photosynthesis-related parameters (i.e. heritability) needs to be considered. The broad sense heritability varied between 0.16 and 0.78 (Table 1). As homozygous genotypes were evaluated in this study, dominance variance as well as additive×dominance and dominance×dominance epistasis will not contribute to the genotypic variation. Thus, broad sense heritability can be interpreted to evaluate the potential of selection.

The relatively high heritability together with the significant (P<0.05) genetic variances found for Phi2, PhiNO, and qL suggests that these parameters could be manipulated in barley by photosynthesis-oriented breeding programs, hence making them promising targets for quantitative genetic approaches. Notably, the heritability of photosynthesis-related parameters varied in the different developmental stages of barley plants, with the lowest values in the seedling stage (Supplementary Fig. S3). This dynamic heritability suggests that the relative contributions of environment and genetics are not stable during the plant growth and development (Yang *et al.*, 2015). Similar dynamic heritability of photosynthetic traits has been observed in other species, such as in field-grown wheat, in which the heritability ranged from 0.267 to 0.764 in pre-anthesis stage and from 0.314 to 0.757 in post-anthesis stage (Carmo-Silva *et al.*, 2017). Even under controlled conditions, dynamic heritability of photosynthesis-related traits has been reported in Arabidopsis during long- and short-term response to light intensity (van Rooijen *et al.*, 2015; Flood *et al.*, 2016). Unlike in our study, however, the dynamic heritability found for short-term response of Arabidopsis under controlled conditions was mainly attributed to genetic variation and diurnal changes of photosynthesis (Flood *et al.*, 2016).

It is reasonable that the heritability of the photosynthesis-related parameters was lower in the field than that in the climate chamber (Tables 1, 3), due to variable environmental factors and interaction between genotypes and environments (Visscher *et al.*, 2008). Given the changing heritability, taking the photosynthetic measurements when the heritability is low may not be efficient to select genotypes (Visscher *et al.*, 2008). Better knowledge about the dynamic change of heritability during plant growth and development would help us identify the developmental stage(s) when genotype significantly contributes to variation of photosynthesis, thus facilitating more targeted and efficient plant breeding (Flood *et al.*, 2016).

From an evolutionary perspective, one could argue that historical (natural or artificial) selection has reduced genotypic variance of the traits, which are more tightly associated with fitness, thus leading to a lower heritability (Mousseau and Roff, 1987; Flood, 2019). In the context of variable heritability across developmental stages of barley found in this study (Fig. 3; Supplementary Fig. S3), this may imply stronger historical

Downloaded from https://academic.oup.com/jxb/article/75/16/4904/7663878 by Bundesanstalt fuer Zuechtungsforschung an Kulturpflanzen, Hauptbibliothek user on 03 December 2025

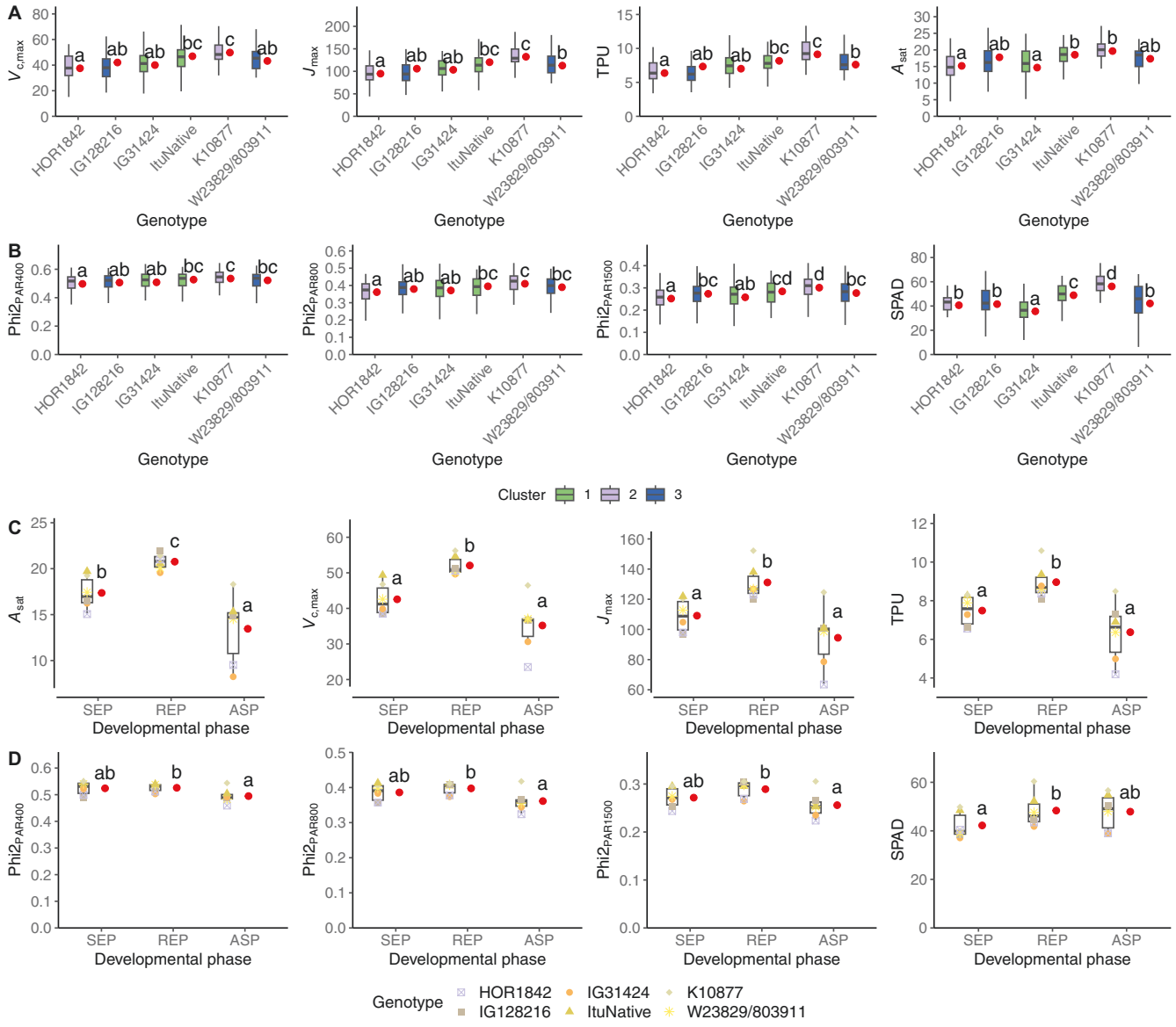

Fig. 6. Comparison of the six barley inbred lines in the climate chamber. (A) Carbon assimilation-related parameters (A_{sat}, $V_{c,max}$, J_{max}, TPU). (B) Phi2 under simulated low light (LL; PAR 400 µmol m^{-2} s^{-1}), medium light (ML; 800 µmol m^{-2} s^{-1}), and high light (HL; 1500 µmol m^{-2} s^{-1}) conditions, and SPAD. For (A, B), the colors of boxes represent the clusters determined by the hierarchical clustering in Fig. 5A. (C) Adjusted entry means of A_{sat}, $V_{c,max}$, J_{max}, TPU of the six inbred lines in SEP, REP, and ASP. (D) Adjusted entry means of Phi2 under the simulated LL, ML, and HL conditions, and SPAD of the six inbred lines in different developmental phases. The red dots next to boxes in (A, B) are the adjusted entry means of parameters of each genotype. The red dots next to boxes in (C, D) are the mean values of the six inbreds for each parameter in each developmental phase. Different letters next to each box denote significant difference based on Tukey's test (P<0.05). A_{sat}, carbon assimilation at saturating light intensity; ASP, anthesis and senescence phase; J_{max}, maximum rate of electron transport; Phi2, quantum yield of PSII; REP, rapid expansion phase; SEP, slow expansion phase; SPAD, relative chlorophyll content; TPU, triose phosphate utilization; $V_{c,max}$, maximum rate of carboxylation.

selection of photosynthesis in SEP than in REP, reflecting presumably the importance of the adaptation of photosynthesis in SEP (Ackerly *et al.*, 2000). Accordingly, investigating the genetics of photosynthesis-related parameters in SEP in old and therefore less selected genetic material of barley might help to understand the evolutionary pressure on photosynthesis.

Interactions between genotype, environment, and developmental stage

As discussed above, photosynthesis is highly responsive to environmental conditions and subject to developmental influences. Except Phi2, PhiNO, and qL, no significant genetic variation was observed for the other parameters. However, we found

Downloaded from https://academic.oup.com/jxb/article/75/16/4904/7663878 by Bundesanstalt fuer Zuechtungsforschung an Kulturpflanzen, Hauptbibliothek user on 03 December 2025

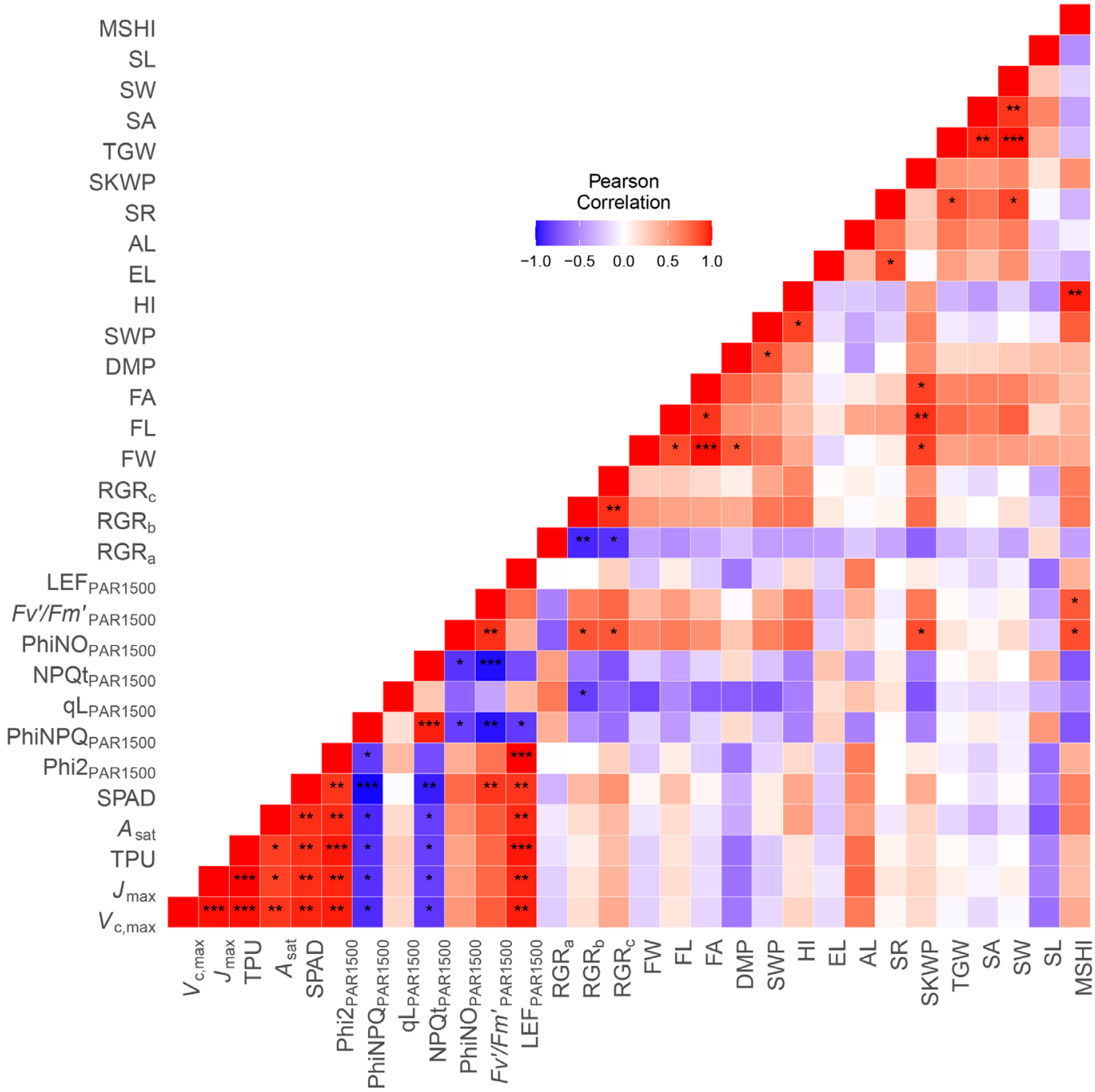

Fig. 7. Pearson's correlation coefficient calculated between pairs of adjusted entry means for six barley inbreds for photosynthesis-related parameters, dry mass per plant, flag leaf width (FW), flag leaf length (FL), flag leaf area (FA) and relative growth rate related parameters (RGR_a, RGR_b, RGR_c), awn length (AL), spike length (EL), spikelet number in one row of the spike (SR), seed length (SL), seed width (SW) seed area (SA), thousand grain weight (TGW), total aboveground dry mass (DMP), total stem weight without spike weight (SWP), harvest index (HI), spike weight per plant (SKWP), and main stem harvest index (MSHI), which were collected from the climate chamber experiments. Asterisks indicate the significance level (*P<0.05, **P<0.01, ***P<0.001). A_{sat}, carbon assimilation at saturating light intensity; F_v'/F_m', maximum efficiency of PSII in light-adapted state; J_{max}, maximum rate of electron transport; LEF, linear electron flow; NPQt, total non-photochemical quenching; Phi2, quantum yield of PSII; PhiNO, quantum yield of non-regulated dissipation processes; PhiNPQ, quantum yield of non-photochemical quenching; qL, fraction of PSII open center; SPAD, relative chlorophyll content; TPU, triose phosphate utilization; $V_{c,max}$, maximum rate of carboxylation.

Downloaded from https://academic.oup.com/jxb/article/75/16/4904/7663878 by Bundesanstalt fuer Zuechtungsforschung an Kulturpflanzen, Hauptbibliothek user on 03 December 2025

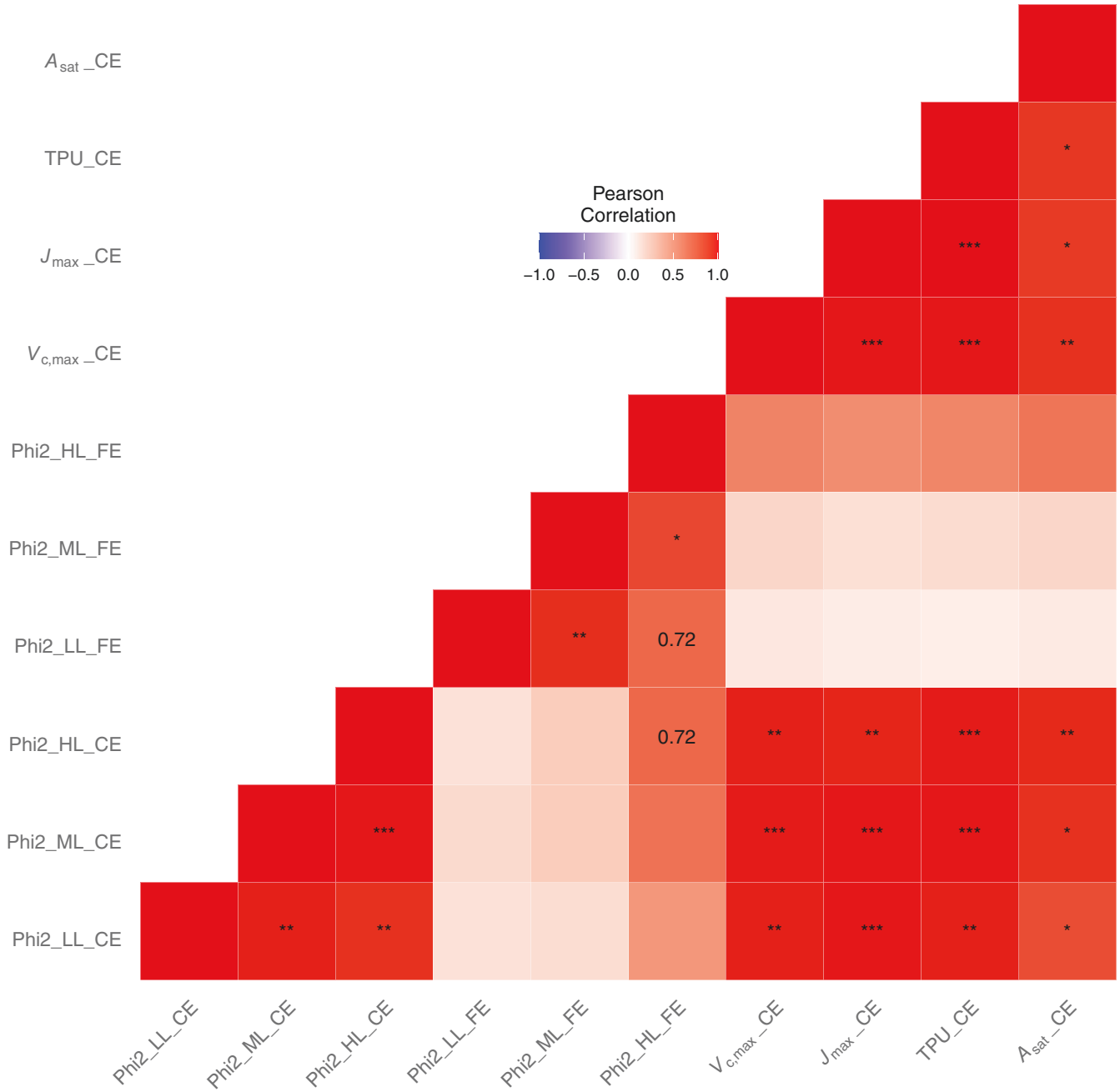

Fig. 8. Pearson's correlation coefficients calculated between pairs of adjusted entry means of six barley inbreds for Phi2 and carbon assimilation-related parameters measured in the climate chamber experiments (CE) and Phi2 measured in the field (FE). Phi2 was assessed separately for LL, ML and HL conditions. Caron assimilation was analysed at the light intensity of the HL condition. Asterisks indicate the significance level (*P<0.05, **P<0.01, ***P<0.001). A_{sat}, carbon assimilation at saturating light intensity; J_{max}, maximum rate of electron transport; Phi2, quantum yield of PSII; TPU, triose phosphate utilization; $V_{c,max}$, maximum rate of carboxylation.

significant (P<0.05) interaction effects on all photosynthesis-related parameters between genotype and environment $(G:E)$, genotype and light condition $(G:L)$ except Phi2 and SPAD, and genotype and developmental phases $(G:S)$ except Phi2 and qL (Table 1).

The significant $(G:S)$ effect suggested that the 23 inbreds showed significant different responses across the different developmental phases. This might suggest changing importance of different genes across the development phases, highlighting again the necessity to assess the genetics of photosynthesis

Downloaded from https://academic.oup.com/jxb/article/75/16/4904/7663878 by Bundesanstalt fuer Zuechtungsforschung an Kulturpflanzen, Hauptbibliothek user on 03 December 2025

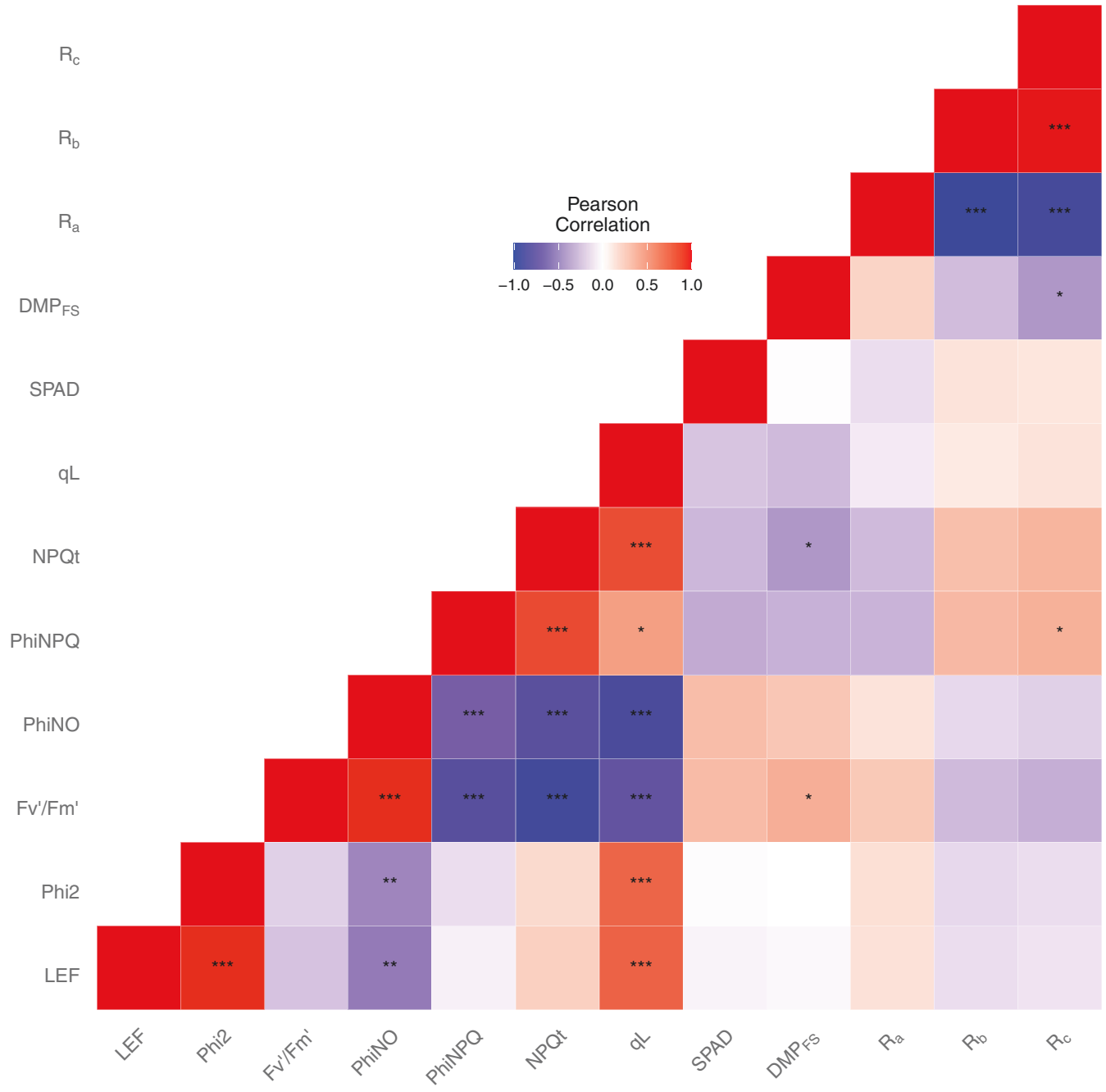

Fig. 9. Pearson's correlation coefficients calculated between pairs of adjusted entry means of 23 barley inbreds for photosynthesis- and growth-related parameters collected in the field. Asterisks indicate the significance level (*P<0.05, **P<0.01, ***P<0.001). DMP, dry mass per plant; F_v'/F_m', maximum efficiency of PSII in light-adapted state; LEF, linear electron flow; NPQt, total non-photochemical quenching; Phi2, quantum yield of PSII; PhiNO, quantum yield of non-regulated dissipation processes; PhiNPQ, quantum yield of non-photochemical quenching; qL, fraction of PSII open center; RGR, relative growth rates (RGR_a, RGR_b, RGR_c) calculated from DMP based on the quadratic regression ($y_r = a + bt - ct^2$); SPAD, relative chlorophyll content.

during plant growth and development (leaf-level and plant level). While it is still challenging to assess chlorophyll fluorescence-based parameters continuously, automatically, and in a high through-put fashion across plant developmental stages under field conditions, several indoor facilities are able to do this (for review see van Bezouw *et al.*, 2019).

The significant $(G:L)$ effect, on the other hand, indicates that different genes may gain importance in different

Downloaded from https://academic.oup.com/jxb/article/75/16/4904/7663878 by Bundesanstalt fuer Zuechtungsforschung an Kulturpflanzen, Hauptbibliothek user on 03 December 2025

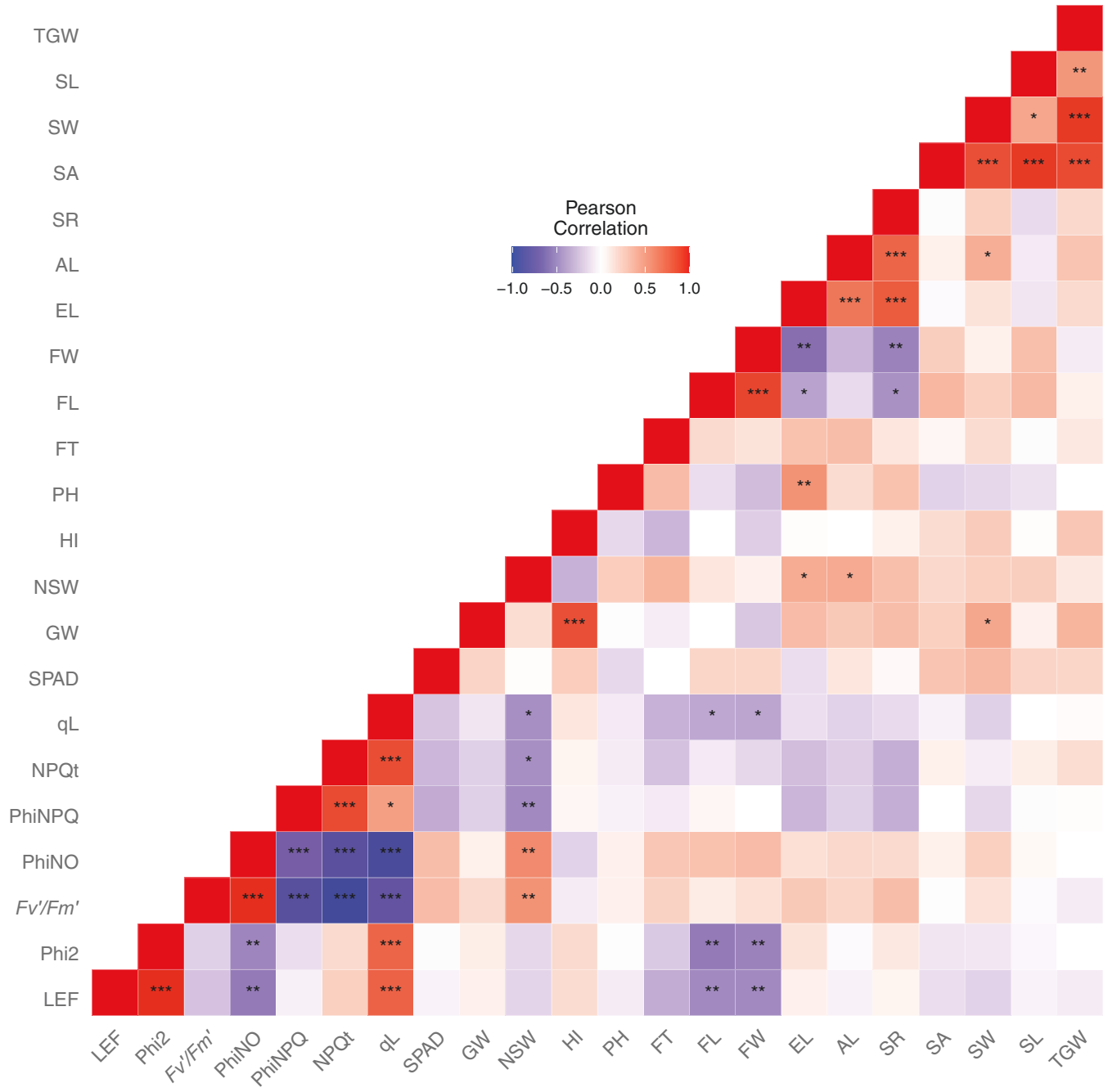

Fig. 10. Pearson's correlation coefficients calculated between pairs of adjusted entry means of 23 barley inbreds for PSII parameters, SPAD and morphological traits collected from multiple environments and years in the field conditions. Asterisks indicate the significance level (*P<0.05, **P<0.01, ***P<0.001). Morphological parameters: AL, awn length; EL, spike length; FL, flag leaf length; FT, flowering time; FW, flag leaf width; GW, grain weight; HI, harvest index; NSW, net straw weight; PH, plant height; SA, seed area; SL, seed length; SR, spikelet number in one row of the spike; SW, seed width; TGW, thousand grain weight. Photosynthetic parameters: F_v'/F_m', maximum efficiency of PSII in light-adapted state; LEF, linear electron flow; NPQt, total non-photochemical quenching; Phi2, quantum yield of PSII; PhiNO, quantum yield of non-regulated dissipation processes; PhiNPQ, quantum yield of non-photochemical quenching; qL, fraction of PSII open center; SPAD, relative chlorophyll content.

light conditions. This is in line with previous observations in Arabidopsis under controlled conditions (van Rooijen *et al.*, 2015; Meyer *et al.*, 2023). The separation of three light intensity levels (LL, ML, and HL) by *K*-means clustering (Fig. 1B), roughly corresponding to the three major phases of light response curve (Benedetti *et al.*, 2018), also underlines distinct

Downloaded from https://academic.oup.com/jxb/article/75/16/4904/7663878 by Bundesanstalt fuer Zuechtungsforschung an Kulturpflanzen, Hauptbibliothek user on 03 December 2025

responses of photosynthesis to different light intensity levels. In our field experiments, we could only assess the parameters of instantaneous photosynthesis while the light condition was fluctuating. However, especially in fluctuating light environments, an increasing number of studies have shown the importance of the speed of photosynthetic reactions to respond to changing light for crop yields (Kromdijk *et al.*, 2016; De Souza *et al.*, 2022). The relevance of natural genetic variation for such kinetic traits of photosynthesis awaits investigations.

The factors (i)–(iv) are important not only in the context of photosynthesis breeding but also for fundamental understanding of how the genetics of photosynthesis interacts with environment (*E*), light condition (*L*) and plant developmental phase (*S*). Quantitative knowledge and understanding of these factors are essential for improving photosynthesis models and crop yield prediction (for review see Yin and Struik, 2010).

Covariation between photosynthesis and yield-related traits

Having confirmed genetic variation for photosynthesis-related parameters in the 23 spring barley inbreds, we also analysed the relationship between photosynthesis- and yield-related traits. The yield-related traits were collected in multi-environment and multi-year experiments, while photosynthesis-related parameters were collected in three different locations in one year. Our results indicated significant positive or negative correlations between some of the chlorophyll fluorescence parameters and NSW, but not for others (Fig. 10). The genotype×environment interactions, which are important not only for yield but also for photosynthesis, are most likely responsible for the non-significant correlations between photosynthesis-related parameters and yield-related traits in these experiments.

Several studies did not find a significant correlation between leaf-level photosynthesis and crop yields. For instance, Acevedo-Siaca *et al.* (2021a) reported no significant correlation between photosynthesis and agronomic traits of rice in field experiments. Likewise, Driever *et al.* (2014) observed no significant correlation between photosynthesis and yield in wheat. Plant growth may respond to environmental stress and perturbations more sensitively than photosynthesis does (Körner, 2015). In this case, increase in photosynthesis does not necessarily result in increased growth. Under controlled conditions or benign environments, however, targeted engineering of photosynthesis by transgenic approaches has led to increased biomass and/or yield in a number of plant species (reviewed by Simkin *et al.*, 2019). Clearly, we need to better understand the genotype×environment interactions of complex photosynthesis-related traits on one hand, and of similarly complex traits of growth and yield on the other hand to decipher the genetic relationship between photosynthesis and yield. Exploration of system biology (for review see Yin *et al.*, 2018) and gene regulatory networks (for review see Flood *et al.*, 2011; Theeuwen *et al.*, 2022) might facilitate understanding of photosynthetic regulation, and how it responds to the ambient environments, which ultimately improves crop yield.

Interestingly, Phi2 was significantly negatively correlated with flag leaf length and width across all three developmental phases (Fig. 10). This may imply that small size of flag leaf is compensated by increased photosynthetic efficiency (Poorter and Evans, 1998; Garnier *et al.*, 1999). Similar negative correlation was also observed between leaf area and CO_2 exchange rate in peanut, soybean, and sweet potato (Bhagsari and Brown, 1986). Future studies may explore natural genetic variation in trait-trait interactions.

Conclusions

The results of this study show that a chlorophyll fluorescence-based technique is able to detect genetic variation in PSII-related parameters in barley under climate chamber conditions, and Phi2, PhiNO, and qL could be suitable parameters to detect genetic variation also under field conditions. Due to the significant effects of environmental factors and significant interactions between the genotype and environments, single time point measurements are not sufficient to draw conclusions on genetic variation in photosynthesis under field conditions but elaborated experimental designs are required.

Significant correlations observed between photosynthesis-related traits (F_v'/F_m' and NPQt) and yield-related traits (NSW and DMP at final stage) in barley under field conditions suggest the possibility of improving crop yields via optimizing photosynthesis through conventional breeding approaches. Moreover, the difference in heritability of photosynthesis, across the plant development and growth stages, could be used to explore the selection pressure on photosynthesis an evolutionary timeline.

Supplementary data

The following supplementary data are available at *JXB* online.

Fig. S1. Air temperature and precipitation recorded during the field experiments in Bonn, Cologne, Düsseldorf.

Fig. S2. Light response curves of PSII parameters and SPAD for the 23 barley inbred lines.

Fig. S3. Developmental changes in heritability.

Fig. S4. The growth trajectories for 23 barley inbred lines grown in the field.

Fig. S5. Boxplot of the adjusted entry means for 11 morphological traits of twenty-three barley inbred lines in multiple environments across multiple years experiments assigned to four clusters.

Fig. S6. The growth trajectory curves for six barley inbred lines grown in the climate chamber condition.

Table S1. The adjusted entry means of photosynthesis-related parameters of 23 barley inbreds for each light condition.

Downloaded from https://academic.oup.com/jxb/article/75/16/4904/7663878 by Bundesanstalt fuer Zuechtungsforschung an Kulturpflanzen, Hauptbibliothek user on 03 December 2025

Downloaded from https://academic.oup.com/jxb/article/75/16/4904/7663878 by Bundesanstalt fuer Zuechtungsforschung an Kulturpflanzen, Hauptbibliothek user on 03 December 2025

Table S2. The adjusted entry means of photosynthesis-related parameters of 23 barley inbreds for each developmental phase.

Table S3. The adjusted entry means of photosynthesis-related parameters of 23 barley inbreds across all developmental phases in the field experiment.

Acknowledgements

The authors would like to thank Florian Esser and George Alskief (Institute of Quantitative Genetics and Genomics of Plants, Biology Department, Heinrich Heine University, Düsseldorf, Germany) for the field management in Cologne and Düsseldorf. We also thank Onno Muller (Institut für Bio- und Geowissenschaften (IBG), Forschungszentrum Jülich, Jülich, Germany) for organization of the field trial in Bonn. We would like to thank Urte Schlüter (Institute of Plant Biochemistry, Heinrich Heine University, Düsseldorf, Germany) for support with LI-6800. We would like to thank Katharina Luhmer (Universität Bonn, Bonn, Germany) and Monika Bilstein (Landeshauptstadt Düsseldorf, Düsseldorf, Germany) for offering the weather data. WZ thanks the China Scholarship Council for a fellowship (No.202009655001). The authors thank two anonymous reviewers for helpful comments on an earlier version of the manuscript.

Author contributions

BS and SM conceptualized the study, acquired funding and supervised the work; YG, SM, and BS designed the research. YG, MS, LO, and WZ performed experiments. YG analysed the data. YG, SM, and BS interpreted the results. YG, SM, and BS wrote the manuscript.

Conflict of interest

The authors declare no conflict of interest.

Funding

The work in BS and SM labs was supported by the Deutsche Forschungsgemeinschaft (DFG, German Research Foundation) through the Cluster of Excellence on Plant Sciences (Heinrich Heine University, Düsseldorf, Germany) (CEPLAS, EXC2048).

Data availability

Data are publicly available in the manuscript and in the supplementary data.

References

Acevedo-Siaca LG, Coe R, Quick WP, Long SP. 2021a. Evaluating natural variation, heritability, and genetic advance of photosynthetic traits in rice (*Oryza sativa*). Plant Breeding **140**, 745–757.

Acevedo-Siaca LG, Coe R, Quick WP, Long SP. 2021b. Variation between rice accessions in photosynthetic induction in flag leaves and underlying mechanisms. Journal of Experimental Botany **72**, 1282–1294.

Acevedo-Siaca LG, Dionora J, Laza R, Paul Quick W, Long SP. 2021c. Dynamics of photosynthetic induction and relaxation within the canopy of rice and two wild relatives. Food and Energy Security **10**, e286.

Ackerly DD, Dudley SA, Sultan SE, *et al*. 2000. The evolution of plant ecophysiological traits: recent advances and future directions: new research addresses natural selection, genetic constraints, and the adaptive evolution of plant ecophysiological traits. Bioscience **50**, 979–995.

Ainsworth EA, Serbin SP, Skoneczka JA, Townsend PA. 2014. Using leaf optical properties to detect ozone effects on foliar biochemistry. Photosynthesis Research **119**, 65–76.

Alqudah AM, Schnurbusch T. 2017. Heading date is not flowering time in spring barley. Frontiers in Plant Science **8**, 896.

Alvarez Prado S, Gallardo JM, Serrago RA, Kruk BC, Miralles DJ. 2013. Comparative behavior of wheat and barley associated with field release and grain weight determination. Field Crops Research **144**, 28–33.

Bagley J, Rosenthal DM, Ruiz-Vera UM, Siebers MH, Kumar P, Ort DR, Bernacchi CJ. 2015. The influence of photosynthetic acclimation to rising CO_2 and warmer temperatures on leaf and canopy photosynthesis models. Global Biogeochemical Cycles **29**, 194–206.

Baker NR. 2008. Chlorophyll fluorescence: a probe of photosynthesis in vivo. Annual Review of Plant Biology **59**, 89–113.

Bellasio C, Beerling DJ, Griffiths H. 2016. An Excel tool for deriving key photosynthetic parameters from combined gas exchange and chlorophyll fluorescence: theory and practice. Plant, Cell & Environment **39**, 1180–1197.

Benedetti M, Vecchi V, Barera S, Dall'Osto L. 2018. Biomass from microalgae: the potential of domestication towards sustainable biofactories. Microbial Cell Factories **17**, 173.

Bhagsari AS, Brown R. 1986. Leaf photosynthesis and its correlation with leaf area 1. Crop Science **26**, 127–132.

Bielczynski LW, Łaçki MK, Hoefnagels I, Gambin A, Croce R. 2017. Leaf and plant age affects photosynthetic performance and photoprotective capacity. Plant Physiology **175**, 1634–1648.

Bonington S. 1977. Climate and the efficiency of crop production in Britain. Philosophical Transactions of the Royal Society of London. B. Biological Sciences **281**, 277–294.

Bucher SF, Bernhardt–Römermann M, Römermann C. 2018. Chlorophyll fluorescence and gas exchange measurements in field research: an ecological case study. Photosynthetica **56**, 1161–1170.

Carmo-Silva E, Andralojc PJ, Scales JC, Driever SM, Mead A, Lawson T, Raines CA, Parry MA. 2017. Phenotyping of field-grown wheat in the UK highlights contribution of light response of photosynthesis and flag leaf longevity to grain yield. Journal of Experimental Botany **68**, 3473–3486.

Casale F, Van Inghelandt D, Weisweiler M, Li J, Stich B. 2022. Genomic prediction of the recombination rate variation in barley – a route to highly recombinogenic genotypes. Plant Biotechnology Journal **20**, 676–690.

Cornic G, Fresneau C. 2002. Photosynthetic carbon reduction and carbon oxidation cycles are the main electron sinks for photosystem II activity during a mild drought. Annals of Botany **89**, 887–894.

De Souza AP, Burgess SJ, Doran L, Hansen J, Manukyan L, Maryn N, Gotarkar D, Leonelli L, Niyogi KK, Long SP. 2022. Soybean photosynthesis and crop yield are improved by accelerating recovery from photoprotection. Science **377**, 851–854.

Driever SM, Lawson T, Andralojc PJ, Raines CA, Parry MAJ. 2014. Natural variation in photosynthetic capacity, growth, and yield in 64 field-grown wheat genotypes. Journal of Experimental Botany **65**, 4959–4973.

Driever SM, Simkin AJ, Alotaibi S, Fisk SJ, Madgwick PJ, Sparks CA, Jones HD, Lawson T, Parry MAJ, Raines CA. 2017. Increased SBPase activity improves photosynthesis and grain yield in wheat grown in greenhouse conditions. Philosophical Transactions of the Royal Society B: Biological Sciences **372**, 20160384.

Duursma RA. 2015. Plantecophys – an R package for analysing and modelling leaf gas exchange data. PLoS One **10**, e0143346.

Eberhard S, Finazzi G, Wollman FA. 2008. The dynamics of photosynthesis. Annual Review of Genetics **42**, 463–515.

Farquhar GD, Caemmerer S, Berry JA. 1980. A biochemical model of photosynthetic CO_2 assimilation in leaves of C_3 species. Planta **149**, 78–90.

Flood PJ. 2019. Using natural variation to understand the evolutionary pressures on plant photosynthesis. Current Opinion in Plant Biology **49**, 68–73.

Flood PJ, Harbinson J, Aarts MGM. 2011. Natural genetic variation in plant photosynthesis. Trends in Plant Science **16**, 327–335.

Flood PJ, Kruijer W, Schnabel SK, Schoor R, Jalink H, Snel JFH, Harbinson J, Aarts MGM. 2016. Phenomics for photosynthesis, growth and reflectance in *Arabidopsis thaliana* reveals circadian and long-term fluctuations in heritability. Plant Methods **12**, 14.

Fu X, Walker BJ. 2023. Dynamic response of photorespiration in fluctuating light environments. Journal of Experimental Botany **74**, 600–611.

Garcia A, Gaju O, Bowerman AF, Buck SA, John R, Furbank RT, Gilliham M, Millar AH, Pogson BJ. 2022. Enhancing crop yields through improvements in the efficiency of photosynthesis and respiration. New Phytologist **237**, 60–77.

Garnier E, Salager J-L, Laurent G, Sonié L. 1999. Relationships between photosynthesis, nitrogen and leaf structure in 14 grass species and their dependence on the basis of expression. New Phytologist **143**, 119–129.

Genty B, Briantais JM, Baker NR. 1989. The relationship between the quantum yield of photosynthetic electron transport and quenching of chlorophyll fluorescence. Biochimica et Biophysica Acta **990**, 87–92.

Gong HY, Li Y, Fang G, Hu DH, Jin WB, Wang ZH, Li YS. 2015. Transgenic rice expressing *Ictb* and *FBP/Sbpase* derived from cyanobacteria exhibits enhanced photosynthesis and mesophyll conductance to CO_2. PLoS One **10**, e0140928.

Hay WT, Bihmidine S, Mutlu N, Hoang KL, Awada T, Weeks DP, Clemente TE, Long SP. 2017. Enhancing soybean photosynthetic CO_2 assimilation using a cyanobacterial membrane protein, ictB. Journal of Plant Physiology **212**, 58–68.

Hedden P. 2003. The genes of the Green Revolution. Trends in Genetics **19**, 5–9.

Holland JB, Nyquist WE, Cervantes-Martínez CT, Janick J. 2003. Estimating and interpreting heritability for plant breeding: an update. In: Janick J, ed. Plant Breeding Reviews Vol. **22**. Hoboken: John Wiley & Sons, Inc., 9–112.

Hunter MC, Smith RG, Schipanski ME, Atwood LW, Mortensen DA. 2017. Agriculture in 2050: recalibrating targets for sustainable intensification. BioScience **67**, 386–391.

Keller B, Matsubara S, Rascher U, Pieruschka R, Steier A, Kraska T, Muller O. 2019. Genotype specific photosynthesis × environment interactions captured by automated fluorescence canopy scans over two fluctuating growing seasons. Frontiers in Plant Science **10**, 1482.

Khaipho-burch M, Cooper M, Crossa J, *et al*. 2023. Scale up trials to validate modified crops' benefits. Chemical Engineering **621**, 470.

Körner C. 2015. Paradigm shift in plant growth control. Current Opinion in Plant Biology **25**, 107–114.

Kromdijk J, Głowacka K, Leonelli L, Gabilly ST, Iwai M, Niyogi KK, Long SP. 2016. Improving photosynthesis and crop productivity by accelerating recovery from photoprotection. Science **354**, 857–861.

Kromdijk J, Long SP. 2016. One crop breeding cycle from starvation? How engineering crop photosynthesis for rising CO_2 and temperature could be one important route to alleviation. Proceedings of the Royal Society B: Biological Sciences **283**, 20152578.

Kuhlgert S, Austic G, Zegarac R, *et al*. 2016. MultispeQ Beta: a tool for large-scale plant phenotyping connected to the open photosynQ network. Royal Society Open Science **3**, 160592.

Lawson T, Kramer DM, Raines CA. 2012. Improving yield by exploiting mechanisms underlying natural variation of photosynthesis. Current Opinion in Biotechnology **23**, 215–220.

Lithourgidis AS, Dordas CA. 2010. Forage yield, growth rate, and nitrogen uptake of faba bean intercrops with wheat, barley, and rye in three seeding ratios. Crop Science **50**, 2148–2158.

Liu L, Guan L, Liu X. 2017. Directly estimating diurnal changes in GPP for C3 and C4 crops using far-red sun-induced chlorophyll fluorescence. Agricultural and Forest Meteorology **232**, 1–9.

Long SP, Ainsworth EA, Leakey ADB, Nösbsrger J, Ort DR. 2006a. Food for thought: lower-than-expected crop yield stimulation with rising CO_2 concentrations. Science **312**, 1918–1921.

Long SP, Farage PK, Garcia RL. 1996. Measurement of leaf and canopy photosynthetic CO_2 exchange in the field. Journal of Experimental Botany **47**, 1629–1642.

Long SP, Taylor SH, Burgess SJ, Carmo-Silva E, Lawson T, De Souza AP, Leonelli L, Wang Y. 2022. Into the shadows and back into sunlight: photosynthesis in fluctuating light. Annual Review of Plant Biology **73**, 617–648.

Long SP, Zhu XG, Naidu SL, Ort DR. 2006b. Can improvement in photosynthesis increase crop yields? Plant, Cell and Environment **29**, 315–330.

Maydup ML, Antonietta M, Guiamet JJ, Graciano C, López JR, Tambussi EA. 2010. The contribution of ear photosynthesis to grain filling in bread wheat (*Triticum aestivum* L.). Field Crops Research **119**, 48–58.

Meacham-Hensold K, Montes CM, Wu J, *et al*. 2019. High-throughput field phenotyping using hyperspectral reflectance and partial least squares regression (PLSR) reveals genetic modifications to photosynthetic capacity. Remote Sensing of Environment **231**, 111176.

Meyer RC, Weigelt-Fischer K, Knoch D, Heuermann M, Zhao Y, Altmann T. 2021. Temporal dynamics of QTL effects on vegetative growth in *Arabidopsis thaliana*. Journal of Experimental Botany **72**, 476–490.

Meyer RC, Weigelt-Fischer K, Tschiersch H, Topali G, Altschmied L, Heuermann MC, Knoch D, Kuhlmann M, Zhao Y, Altmann T. 2023. Dynamic growth QTL action in diverse light environments: characterization of light regime-specific and stable QTL in Arabidopsis. Journal of Experimental Botany **74**, 5341–5362.

Miao G, Guan K, Yang X, *et al*. 2018. Sun-induced chlorophyll fluorescence, photosynthesis, and light use efficiency of a soybean field from seasonally continuous measurements. Journal of Geophysical Research, Biogeosciences **123**, 610–623.

Molero G, Reynolds MP. 2020. Spike photosynthesis measured at high throughput indicates genetic variation independent of flag leaf photosynthesis. Field Crops Research **255**, 107866.

Moore CE, Meacham-Hensold K, Lemonnier P, Slattery RA, Benjamin C, Bernacchi CJ, Lawson T, Cavanagh AP. 2021. The effect of increasing temperature on crop photosynthesis: from enzymes to ecosystems. Journal of Experimental Botany **72**, 2822–2844.

Mousseau TA, Roff DA. 1987. Natural selection and the heritability of fitness components. Heredity **59**, 181–197.

Ogren E. 1993. Convexity of the photosynthetic light-response curve in relation to intensity and direction of light during growth'. Plant Physiology **101**, 1013–1019.

Paine CET, Marthews TR, Vogt DR, Purves D, Rees M, Hector A, Turnbull LA. 2012. How to fit nonlinear plant growth models and calculate growth rates: an update for ecologists. Methods in Ecology and Evolution **3**, 245–256.

Pearcy RW. 1990. Sunflecks and photosynthesis in plant canopies. Annual Review of Plant Physiology and Plant Molecular Biology **41**, 421–453.

Piepho HP, Möhring J. 2007. Computing heritability and selection response from unbalanced plant breeding trials. Genetics **177**, 1881–1888.

Poorter H, Evans JR. 1998. Photosynthetic nitrogen-use efficiency of species that differ inherently in specific leaf area. Oecologia **116**, 26–37.

Prosekov AY, Ivanova SA. 2018. Food security: the challenge of the present. Geoforum **91**, 73–77.

Rascher U, Nedbal L. 2006. Dynamics of photosynthesis in fluctuating light. Current Opinion in Plant Biology **9**, 671–678.

Saathoff AJ, Welles J. 2021. Gas exchange measurements in the unsteady state. Plant, Cell & Environment **44**, 3509–3523.

Downloaded from https://academic.oup.com/jxb/article/75/16/4904/7663878 by Bundesanstalt fuer Zuechtungsforschung an Kulturpflanzen, Hauptbibliothek user on 03 December 2025

Serbin SP, Dillaway DN, Kruger EL, Townsend PA. 2011. Leaf optical properties reflect variation in photosynthetic metabolism and its sensitivity to temperature. Journal of Experimental Botany **63**, 489–502.

Sharkey TD. 2016. What gas exchange data can tell us about photosynthesis. Plant, Cell & Environment **39**, 1161–1163.

Shrestha A, Cosenza F, van Inghelandt D, Wu PY, Li J, Casale FA, Weisweiler M, Stich B. 2022. The double round-robin population unravels the genetic architecture of grain size in barley. Journal of Experimental Botany **73**, 7344–7361.

Silva-Perez V, Molero G, Serbin SP, Condon AG, Reynolds MP, Furbank RT, Evans JR. 2017. Hyperspectral reflectance as a tool to measure biochemical and physiological traits in wheat. Journal of Experimental Botany **69**, 483–496.

Simkin AJ, López-Calcagno PE, Raines CA. 2019. Feeding the world: improving photosynthetic efficiency for sustainable crop production. Journal of Experimental Botany **70**, 1119–1140.

Theeuwen TP, Logie LL, Harbinson J, Aarts MG. 2022. Genetics as a key to improving crop photosynthesis. Journal of Experimental Botany **73**, 3122–3137.

Turnbull C, Lillemo M, Hvoslef-Eide TAK. 2021. Global regulation of genetically modified crops amid the gene edited crop boom – a review. Frontiers in Plant Science **12**, 630396.

van Bezouw RF, Keurentjes JJ, Harbinson J, Aarts MG. 2019. Converging phenomics and genomics to study natural variation in plant photosynthetic efficiency. The Plant Journal **97**, 112–133.

van Rooijen R, Aarts MGM, Harbinson J. 2015. Natural genetic variation for acclimation of photosynthetic light use efficiency to growth irradiance in Arabidopsis. Plant Physiology **167**, 1412–1429.

Verhulst P. 1838. Notice on the law that the population follows in its growth. Correspondance mathématique et physique **10**, 113–126.

Vicente R, Vergara-Díaz O, Medina S, Chairi F, Kefauver SC, Bort J, Serret MD, Aparicio N, Araus JL. 2018. Durum wheat ears perform better than the flag leaves under water stress: gene expression and physiological evidence. Environmental and Experimental Botany **153**, 271–285.

Visscher PM, Hill WG, Wray NR. 2008. Heritability in the genomics era—concepts and misconceptions. Nature Reviews Genetics **9**, 255–266.

Ward JH Jr. 1963. Hierarchical grouping to optimize an objective function. Journal of the American Statistical Association **58**, 236–244.

Weisweiler M, Montaigu AD, Ries D, Pfeifer M, Stich B. 2019. Transcriptomic and presence/absence variation in the barley genome assessed from multi-tissue mRNA sequencing and their power to predict phenotypic traits. BMC Genomics **20**, 787.

Wingler A, Marès M, Pourtau N. 2004. Spatial patterns and metabolic regulation of photosynthetic parameters during leaf senescence. New Phytologist **161**, 781–789.

Wu PY, Stich B, Weisweiler M, Shrestha A, Erban A, Westhoff P, Inghelandt DV. 2022. Improvement of prediction ability by integrating multi-omic datasets in barley. BMC Genomics **23**, 200.

Wullschleger SD. 1993. Biochemical limitations to carbon assimilation in C_3 plants—A retrospective analysis of the A/C_i curves from 109 species. Journal of Experimental Botany **44**, 907–920.

Yang F, Fan Y, Wu X, *et al*. 2018. Auxin-to-gibberellin ratio as a signal for light intensity and quality in regulating soybean growth and matter partitioning. Frontiers in Plant Science **9**, 56.

Yang W, Guo Z, Huang C, Wang K, Jiang N, Feng H, Chen G, Liu Q, Xiong L. 2015. Genome-wide association study of rice (*Oryza sativa* L.) leaf traits with a high-throughput leaf scorer. Journal of Experimental Botany **66**, 5605–5615.

Yendrek CR, Tomaz T, Montes CM, Cao Y, Morse AM, Brown PJ, McIntyre LM, Leakey ADB, Ainsworth EA. 2016. High-throughput phenotyping of maize leaf physiological and biochemical traits using hyperspectral reflectance. Plant Physiology **173**, 614–626.

Yin X, Struik PC. 2010. Modelling the crop: from system dynamics to systems biology. Journal of Experimental Botany **61**, 2171–2183.

Yin X, van der Linden CG, Struik PC. 2018. Bringing genetics and biochemistry to crop modelling, and vice versa. European Journal of Agronomy **100**, 132–140.

Zadoks JC, Chang TT, Konzak CF. 1974. A decimal code for the growth stages of cereals. Weed Research **14**, 415–421.

Zhu XG, Long SP, Ort DR. 2010. Improving photosynthetic efficiency for greater yield. Annual Review of Plant Biology **61**, 235–261.

Downloaded from https://academic.oup.com/jxb/article/75/16/4904/7663878 by Bundesanstalt fuer Zuechtungsforschung an Kulturpflanzen, Hauptbibliothek user on 03 December 2025

Supplementary Materials

Yanrong Gao[1,2], Merle Stein[1], Lilian Oshana[2], Wenxia Zhao[1,5], Shizue Matsubara[2,3], Benjamin Stich[1,3,4]

[1]Institute of Quantitative Genetics and Genomics of Plants, Heinrich Heine University, Düsseldorf, Germany

[2]IBG-2: Plant Sciences, Forschungszentrum Jülich, Jülich, Germany

[3]Cluster of Excellence on Plant Sciences (CEPLAS)

[4]Julius Kühn Institute (JKI) – Federal Research Centre for Cultivated Plants, Institute for Breeding Research on Agricultural Crops, Sanitz, Germany

[5]Xinjiang Seed Industry Development Center of China, Urumqi, China.

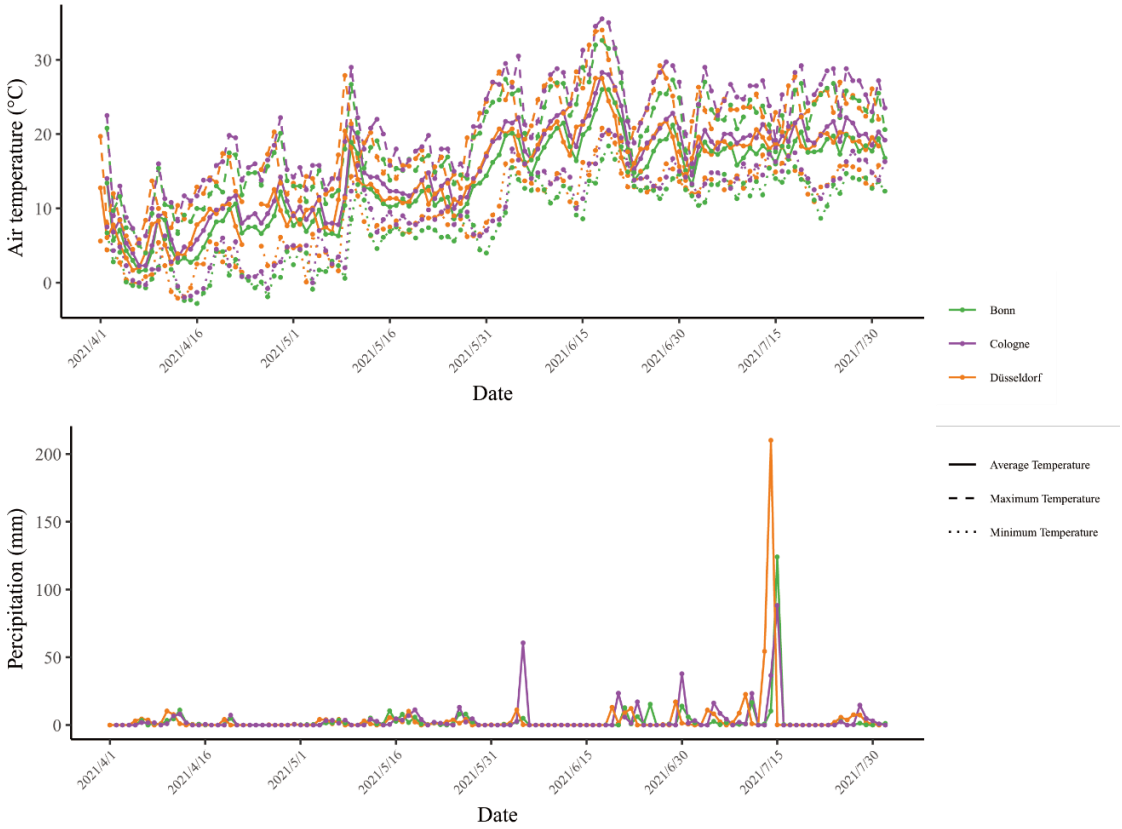

Supplementary Fig. S1: Air temperature and precipitation recorded during the field experiments in Bonn, Cologne, Düsseldorf. Dashed, solid, and dotted represent the maximum, average, and minimum temperature of one day, respectively. Green, purple and orange color represent three location Bonn, Cologne and Düsseldorf, respectively. The temperature data of Düsseldorf from 2021/04/24 to 2021/04/25 was missing.

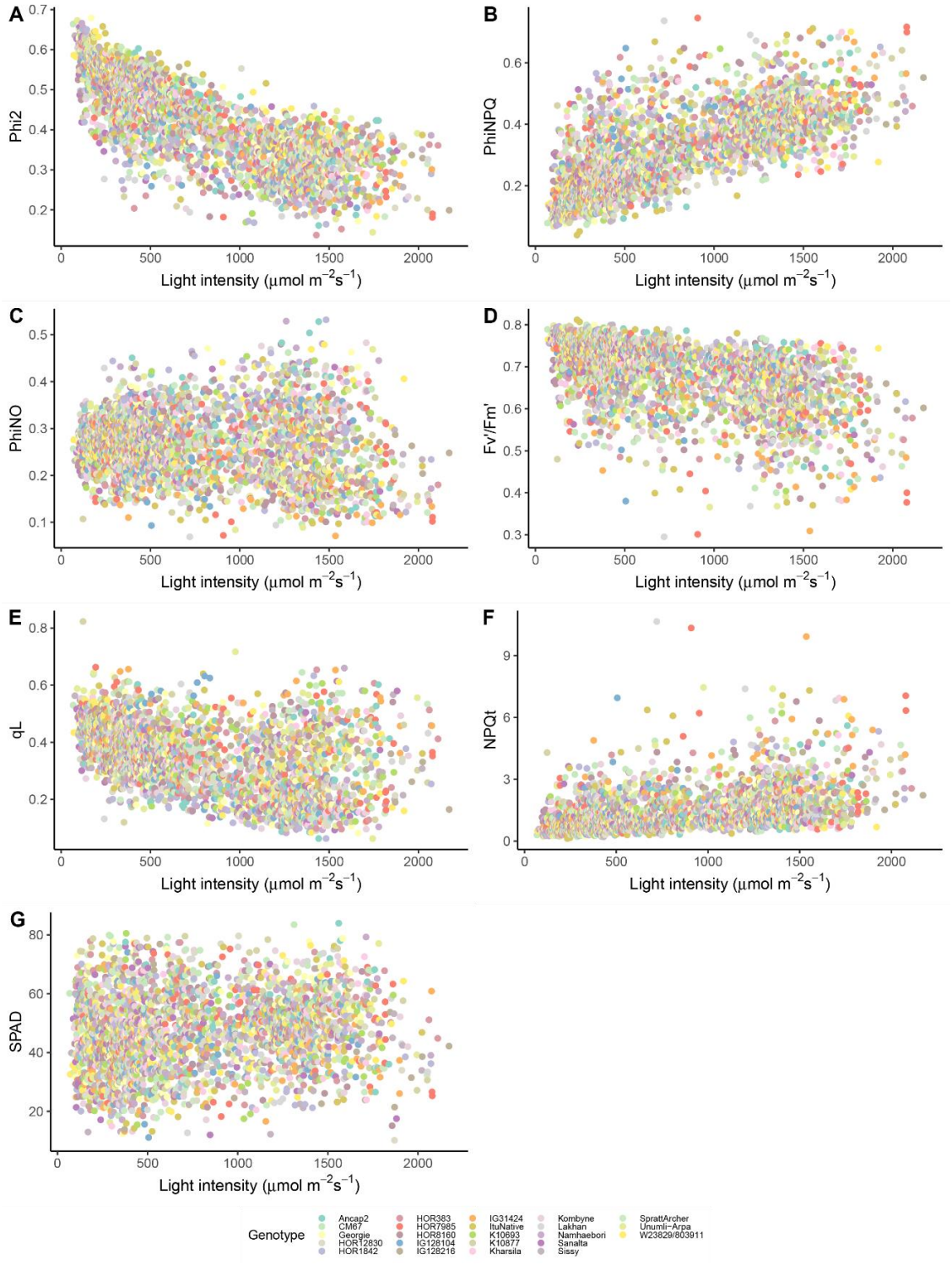

Supplementary Fig. S2: Light response curves of PSII parameters and SPAD for the 23 barley inbred lines. (A) Phi2, (B) PhiNPQ, (C) PhiNO, (D) Fv'/Fm', (E) qL, (F) NPQt and (G) SPAD.

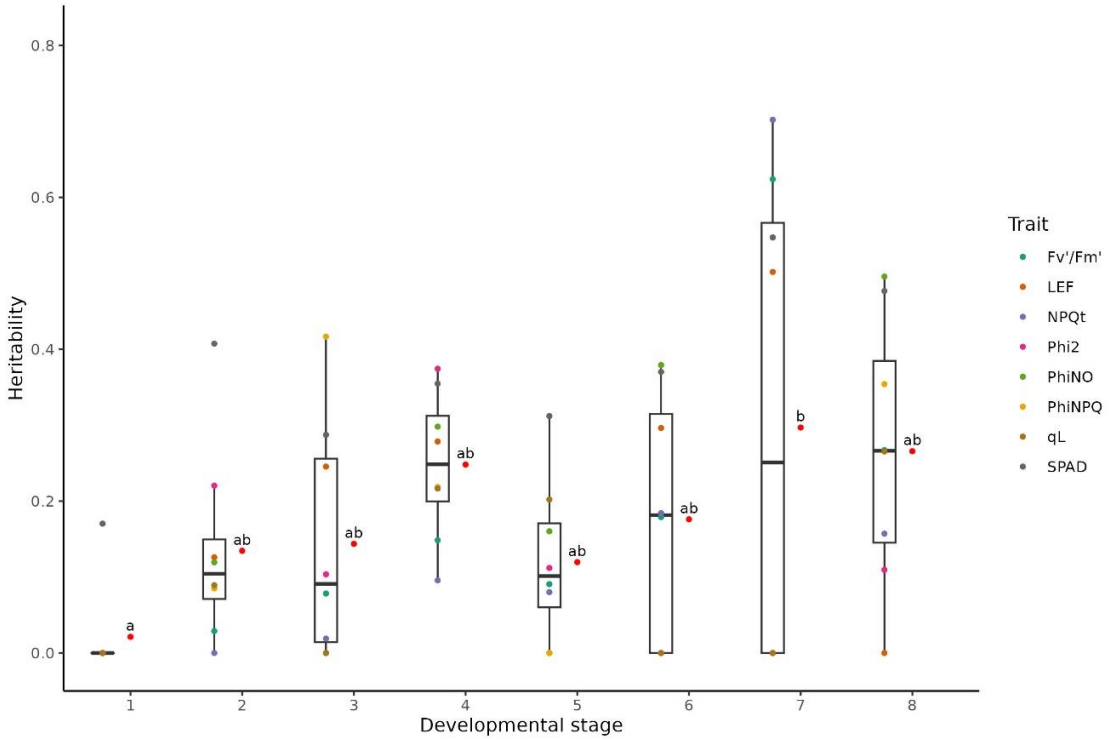

Supplementary Fig. S3: Developmental changes in heritability. Heritability of each PSII parameters and SPAD along the barley developmental stages defined by Zadok's growth scale. The red dot next to each box is the mean heritability of each stage. Different letters next to each box show significant differences by the Tukey-test ($P < 0.05$) between the mean heritability of different developmental stages.

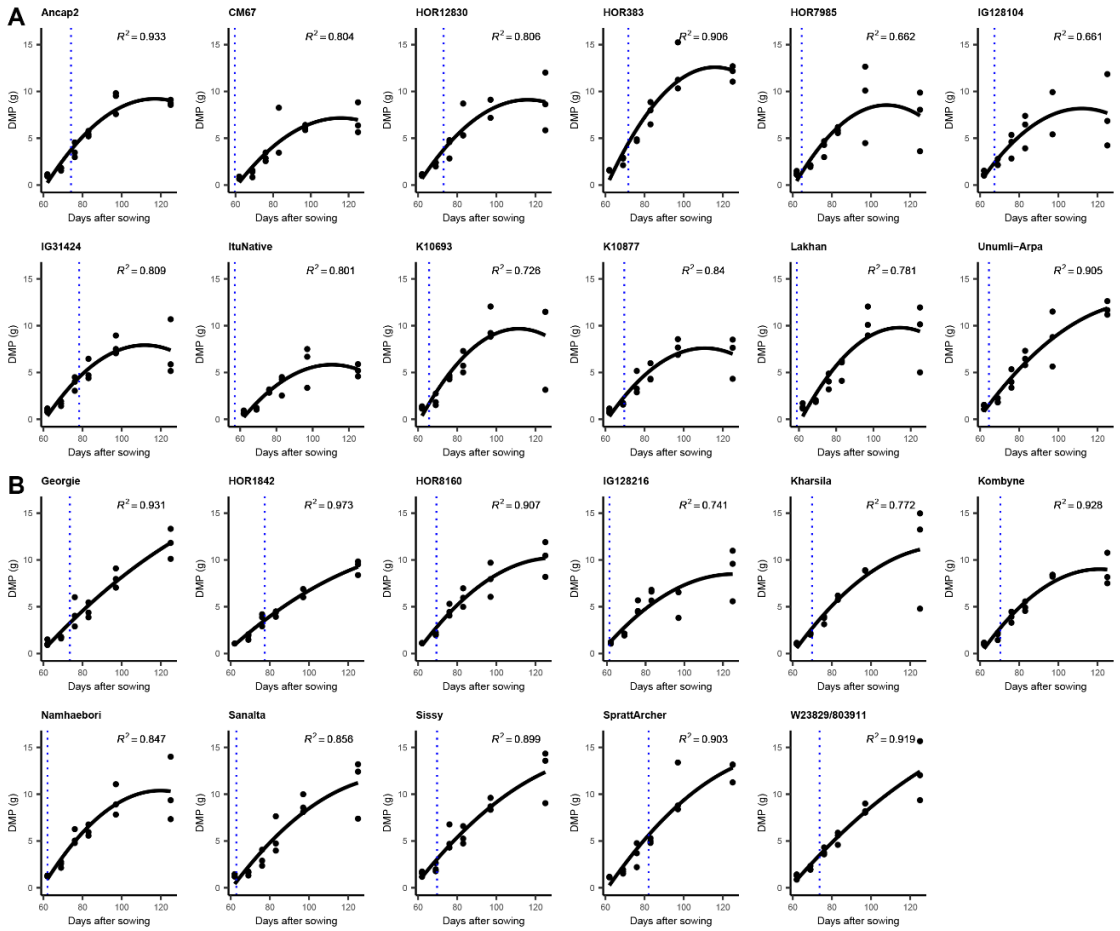

Supplementary Fig.S4: The growth trajectories for 23 barley inbred lines grown in the field. The black dots were the adjusted values of dry mass per plant (DMP) in each plot, the black lines were the DMP trajectory curves predicted by the quadratic model. The blue dashed line in each plot indicates flowering time (FT) for each inbred.

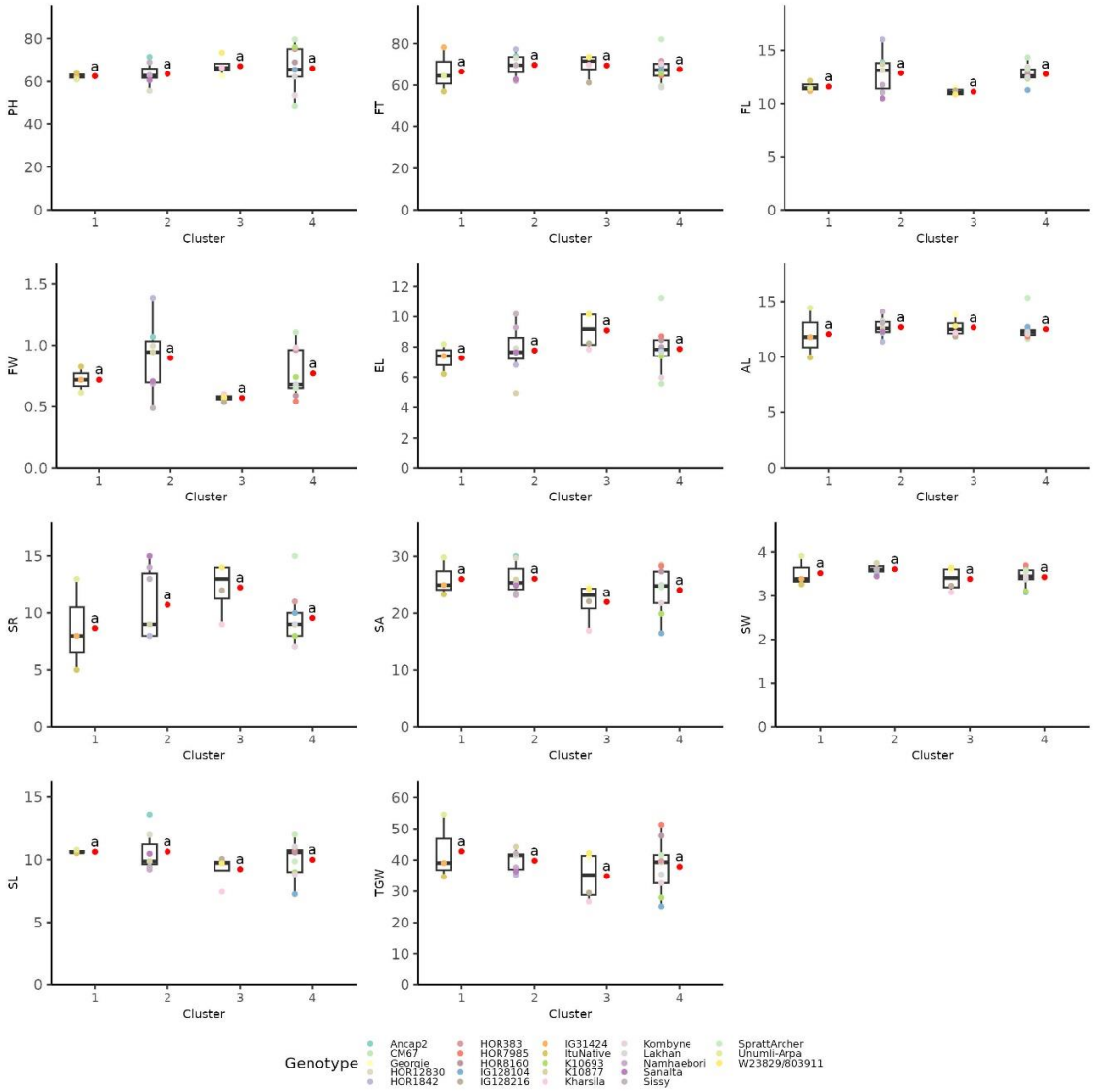

Supplementary Fig. S5: Boxplot of the adjusted entry means for 11 morphological traits of twenty-three barley inbred lines in multiple environments across multiple years experiments assigned to four clusters. The color dots represent the adjusted entry means of each morphological trait. The red dot next to each box are the mean of the trait for the genotypes in each cluster. The letters next to each box are the compact letters, which means the means for each parameter under different conditions which not sharing the same letters are significantly different based on the Tukey-test ($P < 0.05$).

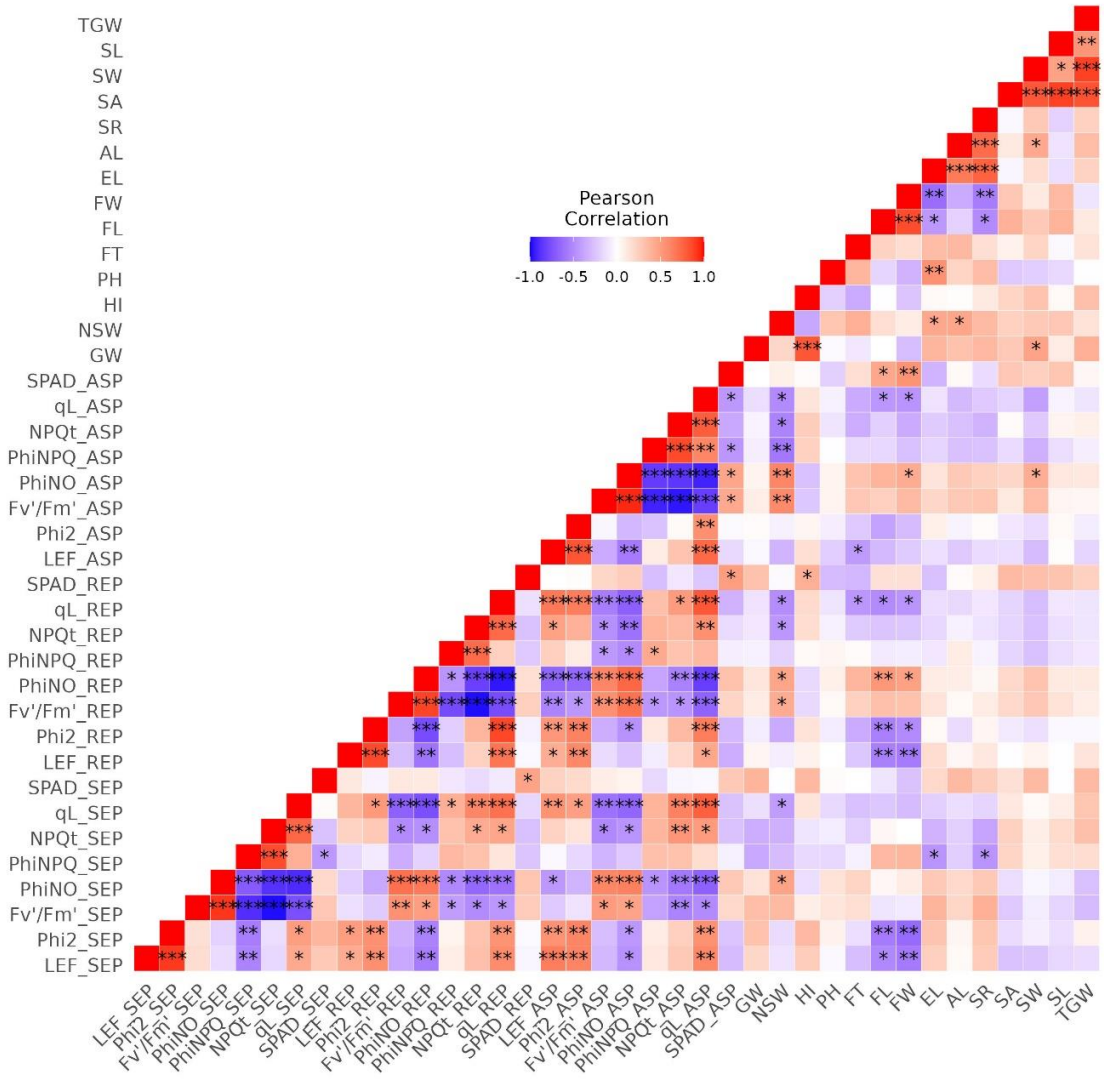

*Supplementary Fig. S6: Person correlation coefficients calculated between pairs of adjusted entry means based on each developmental phase of 23 barley inbreds for PSII parameters, SPAD and morphological traits collected from multiple environments and years in the field conditions. Asterisks indicate the significance level (***, **, * indicated P< .001, .01, .05 respectively)*

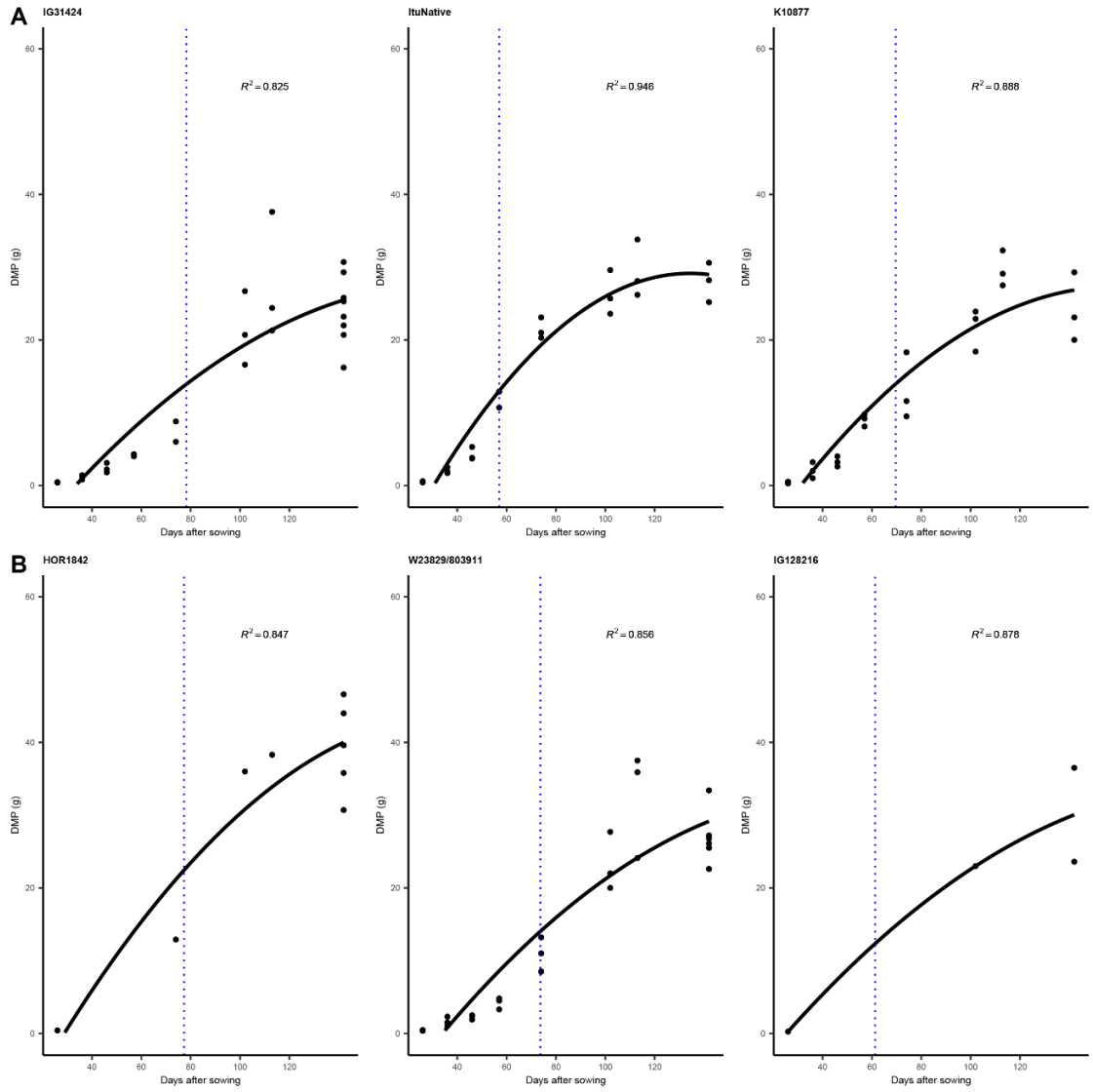

Supplementary Fig. S7: The growth trajectory curves for six barley inbred lines grown in the climate chamber condition. The black dots were the adjusted value of the total aboveground dry mass (DMP), the black lines were the DMP trajectories predicted by the logistic model. The blue dashed line in each plot indicated the flowering time (FT) for each barley inbred.

Chapter 3

The potential of considering photosynthesis parameters in crop yield breeding by genomic prediction

Yanrong Gao[1,2], Po-Ya Wu[1,3], Shizue Matsubara[4,5], Benjamin Stich[1,2,5,6,*]

Under review at Journal of Experimental Botany

Own contribution: I am the first author of this manuscript. I completed all experiments and analyzed the data. I contributed 90% of the data interpretation. My contribution to the final writing was 90%.

The potential of considering photosynthesis parameters in crop yield breeding by genomic prediction

Yanrong Gao[1,2], Po-Ya Wu[1,3], Shizue Matsubara[4,5], Benjamin Stich[1,2,5,6]

[1]Julius Kühn Institute (JKI) – Federal Research Centre for Cultivated Plants, Institute for Breeding Research on Agricultural Crops, Sanitz, Germany

[2]Institute of Quantitative Genetics and Genomics of Plants, Heinrich Heine University, Düsseldorf, Germany

[3]Leibniz Institute of Plant Genetics and Crop Plant Research (IPK) OT Gatersleben, Seeland, Germany

[4]IBG-2: Plant Sciences, Forschungszentrum Jülich, Jülich, Germany

[5]Cluster of Excellence on Plant Sciences (CEPLAS)

[6]Utilization of Plant Genetic Resources for Breeding Purposes, University of Rostock, Rostock

[*]Corresponding author: Benjamin Stich

Abstract

To meet the growing demand for agricultural products, optimizing photosynthesis is a promising strategy to improve the crop yields. Phenotypic variance in photosynthesis has been observed within or between species. To explore the potential of integrating photosynthetic parameters into crop breeding programs, we explored the genetic variation in photosynthesis by assessing photosynthesis-related parameters across plant development in 631 barley recombinant inbred lines (RILs) from eight HvDRR sub-populations under field conditions. The genetic complexity of these parameters was resolved by bi-parental and multi-parental quantitative trait loci (QTL) analyses. Finally, we examined the merit of integrating photosynthesis-related parameters in genomic prediction of yield and its components. Significant genotypic variations of the photosynthesis-related parameters were found among the RILs, with their heritability ranging from 0.38 to 0.54. The multiple QTL and dynamic QTL for photosynthesis observed across different developmental stages underlined the complexity of the genetics of photosynthesis in barley. The considerably higher percentage of phenotypic variance explained for genomic prediction than multi-parental QTL analysis illustrates that the photosynthesis-related parameters are inherited in a more complex way than classical agronomic traits. Notably, the prediction ability for yield was increased by integrating the photosynthesis-related parameters of some developmental stages into genomic prediction models. Therewith, our results suggest a novel perspective on increasing the efficiency of crop breeding programs by integrating photosynthesis-related parameters into prediction models.

Key words: Barley, photosynthesis, crop yield, plant development, genetics, QTL, genomic prediction.

1. Introduction

The crop yields need to be increased by the year 2050 by about 25-70% to meet the increasing demand for agricultural products (Hunter *et al.*, 2017). Yield can be defined in many ways from different perspectives. Centering around photosynthesis, yield is determined by variation in three main factors: light interception, harvest index, and photosynthetic efficiency (Bonington, 1977; Zhu *et al.*, 2010). Experimental but also theoretical studies suggest that the former two factors might be close to their theoretical maximum in various crop species (e.g., Long *et al.*, 2006a; Zhu *et al.*, 2010). In contrast, photosynthetic efficiency has not reached the theoretical maximum in C3 plants (Long *et al.*, 2006b; Zhu *et al.*, 2010; Prosekov and Ivanova, 2018), thus limiting the crop yield potential (Long *et al.*, 2006a; Prado *et al.*, 2013; Kromdijk and Long, 2016). Therefore, enhancing photosynthetic efficiency has become a priority to improve crop yields (Zhu *et al.*, 2010). Past conventional breeding activities, which were primarily targeting yield and its components, may have unintentionally and indirectly improved photosynthetic capacity (Ding *et al.*, 2025). However, due to the complexity of the relationship between photosynthesis and crop yields (e.g., Driever *et al.*, 2014), direct selection for crop yield is not sufficient to enhance photosynthesis or improve the utilization of genetic variance/variation for photosynthesis (Theeuwen *et al.*, 2022; Croce *et al.*, 2024). Instead, direct selection for photosynthesis-related parameters can contribute to optimizing photosynthesis and identifying its bottlenecks that limit crop yields (Theeuwen *et al.*, 2022).

Photosynthesis is a highly complex physiological process which not only depends on molecular, structural and physiological processes of the plant, but also highly dynamically responds to environmental conditions in both short and long term (Gifford, 1995; Kono and Terashima, 2014). For example, fluctuating light intensities, which are caused by e.g. moving clouds or leaves (Chazdon and Pearcy, 1991), can lead to both short-term and long-term adjustments (acclimation) of photosynthesis (Alter *et al.*, 2012; Vialet-Chabrand *et al.*, 2017). Photosynthesis is also influenced by internal factors such as growth and development of the plant (Gao *et al.*, 2024) or leaf (Wingler *et al.*, 2004; Bielczynski *et al.*, 2017). In addition, photosynthesis is potentially regulated by the sink, *i.e.* the plant's capacity to utilize or store the assimilates produced. For instance, when the sink size is small, accumulation of carbohydrates in source leaves can downregulate photosynthetic activity (Paul and Foyer, 2001).

From the point of view of crop breeding, the correlation of photosynthesis-related parameters to agronomic traits is still unclear, especially under dynamic environmental conditions. Their relationships are strongly influenced by genotype–environment interactions, can vary across growth stages and management conditions, and are often inconsistent between different studies (Driever *et al.*, 2014; Carmo-Silva *et al.*, 2017; Gao *et al.*, 2024). These aspects make it difficult to identify photosynthetic traits that are both heritable and reliably predictive of yield across diverse conditions (Chang *et al.*, 2019).

Several studies have shown that optimizing regulation of photosynthesis or its pathway components by genetic modification can improve crop yields, such as by targeting the Calvin–Benson cycle in wheat (Driever *et al.*, 2017), carbon transport in rice (Gong *et al.*, 2015), and soybean (Hay *et al.*, 2017), and photoprotection in tobacco (Kromdijk *et al.*, 2016) and soybean (De Souza *et al.*, 2022). Importantly, a growing number of studies have pointed out that the variation of photosynthesis can also be caused by genes outside ~100 core photosynthetic genes (Tyagi and Gaur, 2003; Berry *et al.*, 2013). For instance, several quantitative trait loci (QTL) for photosynthesis have been linked to indirect effects rather than direct effects by the core photosynthetic genes (Yin *et al.*, 2022). The potential of thousands of such genes, which indirectly affect photosynthesis, are yet to be explored.

To better understand and utilize genetic variations of photosynthesis for plant breeding, marker assisted breeding is an effective technique that has identified candidate loci for photosynthesis-related parameters in various crops (e.g., Ortiz *et al.*, 2017; Feldman *et al.*, 2018; Joynson *et al.*, 2021). Unlike other cereals, however, only a limited number of QTL studies have been performed in barley to identify the genetic factors contributing to variation of photosynthesis-related parameters. The few previous studies in barley were focused on a single developmental stage (Guo *et al.*, 2008; Liu *et al.*, 2015; Liu *et al.*, 2017; Salter *et al.*, 2020). Moreover, these studies used bi-parental populations (doubled haploid lines or recombinant inbred lines, RILs) to identify QTL for photosynthesis-related traits, which, due to the low number of involved parental genotypes and limited recombination events, led to a low mapping resolution (Huang *et al.*, 2012) and an incomplete capturing of the genetic architecture of a complex trait (Holland, 2007; reviewed by Scott *et al.*, 2020). Multi-parent population (MPP) QTL mapping is an alternative approach to overcome these issues (Scott *et al.*, 2020). The MPP QTL analyses were successfully deployed in

barley for agronomically important traits such as grain size (Shrestha *et al.*, 2022) and flowering time (Sannemann *et al.*, 2015; Cosenza *et al.*, 2024), but not yet for photosynthesis-related parameters.

Photosynthesis is a highly complex trait and variation is expected to be caused by many small-effect QTL (Theeuwen *et al.*, 2022). Due to the small effect sizes, genomic prediction (GP) is considered a very suitable approach to increase the genetic gain for complex traits in breeding programs (Meuwissen *et al.*, 2001; Desta and Ortiz, 2014). Instead of identifying QTL, GP obtains genomic estimated breeding values by estimating genome-wide marker effects of each individual (Meuwissen *et al.*, 2001). In contrast to yield-related traits (e.g., Beyene *et al.*, 2015; Millet *et al.*, 2019), GP has never been used in photosynthesis breeding programs. Estimating the prediction ability might give new insights into the potential to improve photosynthetic efficiency by predictive breeding approaches.

The overall objective of this study was to assess the potential to integrate photosynthesis-related parameters into crop and specifically barley breeding programs by 1) exploring the genetic variation of photosynthesis-related parameters in barley RILs across different developmental phases, 2) unraveling the genetic complexity of the photosynthesis-related parameters in barley by using bi-parental and MPP QTL analyses, and 3) examining the utility of integrating the photosynthesis-related parameters in GP of yield and its components.

2. Materials and methods

2.1 Plant materials and genotyping

The plant materials of this study comprised eight recombinant inbred line (RIL) populations which were selected from the *Hordeum vulgare* Double Round-Robin (HvDRR) population consisting of 45 RIL populations (Casale *et al.*, 2022; Shrestha *et al.*, 2022). The HvDRR population was derived from the crossings of 23 barley inbred lines that were selected from 224 barley landraces and cultivars (Weisweiler *et al.*, 2019), using the double round-robin design (Stich, 2009). Each HvDRR sub-population was established following a single seed decent strategy (Casale *et al.*, 2022). The eight RIL populations of our study were selected based on the contrasting phenotypes of their parental inbreds for photosynthesis-related parameters (Supplementary Table S1; Gao *et al.*, 2024).

The RILs of the HvDRR population were genotyped at the S4 generation using the 50K SNP genotyping array that includes 40,040 SNP markers (Bayer *et al.*, 2017).

2.2 Field experimental design

The above mentioned eight RIL populations were grown in Germany at Cologne in 2021 (Y21) and Düsseldorf in 2022 (Y22). In Cologne, two trials were performed with different plot sizes. These were named in the following as mini-big plot (2.25 m^2) with 200 plants, and big plot (10 m^2) with 1000 plants. In both trials, an augmented design was used. In Düsseldorf, one trial with 2.25 m^2 plots with 200 plants was performed, also by following an augmented design. The ten parental inbreds were used as checks in both years' trials. Air temperature and precipitation were recorded during the field experiments in both locations. The fields in Cologne and Düsseldorf have a para-brown soil. Fertilization and crop protection followed local practices.

2.3 Assessment of photosynthesis-related parameters and agronomic traits

In both years (Y21 and Y22), photosynthesis-related parameters were collected from the top fully expanded leaf of three replicates in each plot across multiple developmental stages of barley from seedling stage (ZS13, (Zadoks *et al.*, 1974)) to dough development (ZS87) using MultispeQ V2 device (Kuhlgert *et al.*, 2016). The measurements in Y21 were based on the protocol

"Photosynthesis RIDES" which sets the intensity of actinic light to the incident light intensity upon leaf. In Y22, we used the protocol "PSII measurements", by which the intensity of actinic light was always set to 1500 $\mu mol\, m^{-2} s^{-1}$. This light intensity was chosen to mimic the high light condition observed in the previous field experiments (Gao *et al.*, 2024). These two different but complementary measurement protocols were used to capture the genetic variation of photosynthesis under both variable (Y21) and high (Y22) light intensity conditions.

The following MultispeQ parameters were assessed in our study (see Kuhlgerd *et al.*, (2016) for instrument descriptions and the definitions of the parameters): linear electron flow (LEF), the fraction of PSII open centers (qL), quantum yield of PSII (Phi2), the maximum efficiency of PSII in light-adapted state (Fv'/Fm'), non-photochemical quenching (NPQt), quantum yield of non-photochemical quenching (PhiNPQ), quantum yield of non-regulated dissipation processes (PhiNO), and relative chlorophyll content (SPAD). In addition, MultispeQ also recorded environmental parameters, such as the ambient light intensity of photosynthetically active radiation (PAR), ambient temperature, and ambient humidity.

Agronomic traits were assessed in multi-year and multi-environment field experiments in the years 2017 to 2021 at Düsseldorf, Cologne, Eifel Mechernich, and Quedlinburg in Germany (Shrestha *et al.*, 2022; Cosenza *et al.*, 2024; Lapasiya *et al.*, 2025). Not every location was used every year to evaluate all parameters. Flag leaf length (FL, cm) and width (FW, cm) were measured by rulers when the flag leaf was fully expanded. Plant height (PH) was measured from the ground surface to the top of the spike when plants were fully developed. Flowering time (FT) was recorded as days after sowing when 50% of the plants within a row were flowering. Awn length (AWL, cm), spike length (SPL, cm), and spikelet number in one row of the spike (SPK) were assessed when the spike was fully developed. Seed length (SDL, mm), seed width (SDW, mm), seed area (SDA, mm^2), and thousand grain weight (TGW, g) were measured by MARViN seed analyser (MARViNTECH GmbH, Germany). Grain yield (GY, kg/10 m^2) and net straw yield (SY, kg/10 m^2) were measured at the harvest using a combine harvester.

2.4 Statistical analyses

Due to the dependence of photosynthesis on light intensity and temperature (Ogren, 1993; Yamasaki *et al.*, 2002; Coast *et al.*, 2022), these were considered during the analyses. Because of

the degradation of chlorophyll after senescence, all observations with SPAD values <10 were removed from the data set. We considered three main developmental phases (S) of barley in the statistical analysis: slow expansion phase (SEP) ($ZS < 30$), rapid expansion phase (REP) ($30 \leq ZS < 60$), as well as anthesis and senescence phase (ASP) ($ZS \geq 60$). In addition, we considered the time window (TW) of each measurement: every one hour was considered as one TW as block effect to model environmental differences that are not explained by the individual environmental factors.

The following mixed linear model was used to estimate adjusted entry means for photosynthesis-related parameters for the data set ALL (i.e., combining both Y21 and Y22):

$$y_{ijlknsopqr} = \mu + G_i + E_j + (G_{checks}{:}\,E)_{ij} + (S{:}\,E)_{lj} + (ZS{:}\,E)_{kj} + D_n + (TW{:}\,D)_{sn} + PAR_{ijlknsopqr} + T_{ijlknsopqr} + H_{ijlknsopqr} + (B{:}\,E)_{oj} + (R{:}\,B{:}\,E)_{poj} + (C{:}\,B{:}\,E)_{qoj} + \epsilon_{ijlknsopqr} \quad , [1]$$

where $y_{ijlknsopqr}$ was the observed MultispeQ parameter across all light conditions and all developmental stages, μ the general mean, G_i the effect of the i^{th} genotype, E_j the effect of the j^{th} location, $(G_{checks}{:}\,E)_{ij}$ the interaction between the i^{th} inbred (if it was a check) and the j^{th} location, $(S{:}\,E)_{lj}$ the effect of the l^{th} barley developmental phase nested within the j^{th} location, $(ZS{:}\,E)_{kj}$ the effect of the k^{th} Zadok's score of barley development nested within the j^{th} location, D_n the effect of measurement date n, $(TW{:}\,D)_{sn}$ the effect of the s^{th} time window nested in the n^{th} measurement date, $(B{:}\,E)_{oj}$ the effect of the o^{th} block nested within the j^{th} location, $(R{:}\,B{:}\,E)_{poj}$ the effect of the p^{th} range nested within the o^{th} block in the j^{th} location, $(C{:}\,B{:}\,E)_{qoj}$ the effect of the q^{th} row nested within the o^{th} block in the j^{th} location, $PAR_{jlknsopqr}$ the actinic light intensity of the MultispeQ during each measurement, $T_{jlknsopqr}$ the ambient temperature of each measurement, $H_{ijlknsopqr}$ the ambient humidity of each measurement, and $\epsilon_{ijlknsopqr}$ the random error. In this model, G_i, E_j, and $(S{:}\,E)_{kj}$ were treated as fixed effects and $(G_{checks}{:}\,E)_{ij}$, $(ZS{:}\,E)_{lj}$, D_n, $(TW{:}\,D)_{sn}$, $(B{:}\,E)_{oj}$, $(R{:}\,B{:}\,E)_{poj}$, and $(C{:}\,B{:}\,E)_{qoj}$ as random effects; $PAR_{ijlknsopqr}$, $T_{ijlknsopqr}$, and $H_{ijlknsopqr}$ were covariates.

One of our aims was to estimate the dynamic genetic influence on photosynthesis across different developmental phases in different years. Thus, we performed the above-described statistical

analysis based on six different data sets (i.e., combined analysis across the developmental phases and both years (ALL), three developmental phases separately (SEP, REP, and ASP) while combining the data from two years, and two years separately (Y21 and Y22) while combining the data from three developmental phases for each year) with three models (Supplementary Table S2). We also obtained adjusted entry means for each year across all developmental phases (Supplementary Table S2) as well as for each developmental phase in the two-year experiments.

The linear mixed models were fitted using ASReml 4.2 (Gilmour *et al.*, 2021), and if not mentioned differently, all the other statistical analyses were conducted in R program.

Broad-sense heritability (H^2) was estimated for each data set based on the following equation:

$$H^2 = \sigma_G^2/(\sigma_G^2 + \overline{v}_\delta^{BLUE}/2), \qquad [2]$$

where σ_G^2 was the genotypic variance of the RIL from model [1] with a random effect for G_i and $\overline{v}_\delta^{BLUE}$ was the mean variance of the difference between two adjusted entry means (Holland *et al.*, 2003; Piepho and Möhring, 2007).

The relationship between the photosynthesis-related parameters and the morphological or yield-related parameters of the RILs was evaluated by Pearson's correlation coefficient among adjusted entry means for each data set.

2.5 QTL analysis for photosynthesis-related parameters

The genetic maps for each HvDRR sub-population and the consensus map across all 45 linkage maps of HvDRR populations are available from Casale *et al.* (2022). The genetic map of each HvDRR sub-population was used for bi-parental population (BPP) QTL analyses. A consensus map (Casale *et al.*, 2022) was used for MPP QTL analysis.

BPP and MPP QTL analyses were conducted based on the adjusted entry means of the photosynthesis-related parameters for each RIL calculated from the corresponding data set (Supplementary Table S2).

For BPP QTL analysis, genetic probabilities were computed every centiMorgan (cM). The genome-wide scan was then performed by using the Haley-Knott regression algorithm (Haley and Knott, 1992). Then a forward and backward selection was performed for multiple QTL mapping (Shrestha *et al.*, 2022). The logarithm of the odds (LOD) score at a 0.05 significance level was set

as QTL threshold determined by 10000 permutations (Dupuis and Siegmund, 1999). The BPP QTL analysis was conducted with R/qtl (Broman *et al.*, 2003). The MPP QTL analysis was performed across the selected eight HvDRR sub-populations using the R/mppR package (Garin *et al.*, 2015). QTL were only mapped for a trait*HvDRR sub-population combination, for which phenotypic data were available for at least half of the individuals.

2.6 Genomic prediction of photosynthesis-related parameters

Genome-wide prediction was performed by genomic best linear unbiased prediction (GBLUP):

$\boldsymbol{y} = \mathbf{1}\mu + \mathbf{Z}\boldsymbol{u} + \boldsymbol{\varepsilon}$, [3]

where $\boldsymbol{y}$ was the vector of the adjusted entry means of the photosynthesis-related parameters, $\mathbf{1}$ the unit vector, μ the general mean, $\mathbf{Z}$ the incidence matrix of genotypic effects, $\boldsymbol{u}$ the vector of genotypic effects that were assumed to be normally distributed with $\boldsymbol{u} \sim N(0, \mathbf{G}\sigma_u^2)$, where $\mathbf{G}$ denotes the relationship matrix calculated on the basis of the SNP marker data (VanRaden, 2008), σ_u^2 the genetic variance, and $\boldsymbol{\varepsilon}$ the vector of residuals following a normal distribution $\boldsymbol{\varepsilon} \sim N(0, \mathbf{I}\sigma_\epsilon^2)$, where $\mathbf{I}$ was the identity matrix and σ_ϵ^2 the residual variance. In this study, only additive effects were considered. In addition, the G*E effect is confounded with the error variance. GBLUP model was fitted using the R package sommer (Giovanny, 2016)

2.7 Cross validation

To assess the performance of the GBLUP model, five-fold cross validation (CV) was conducted. Prediction abilities (*PA*) were calculated using Pearson's correlation coefficient (r) between observed and genomic estimated breeding values for each photosynthesis-related parameter. The median of the prediction ability across the five folds (each with 100 replicates) was considered as prediction ability. In order to allow a comparison to the results of the MPP QTL analyses, the proportion of phenotypic variance explained (PEV) for the genomic prediction models was calculated as the squared prediction ability: $PEV = PA^2 = r^2$.

We conducted the above-described five-fold cross validation for the aforementioned six different data sets (Supplementary Table S2). The adjusted entry means of these six data sets were estimated based on the models described above. To compare the prediction ability in the three developmental phases, we used 199 genotypes that were measured in all three developmental phases, thereby

eliminating the bias associated with sample size differences. Similarly, we selected the genotypes that were assessed in both years to conduct the five-fold cross validation using the data sets Y21 and Y22.

2.8 Assess the effect of different factors on genomic prediction ability for photosynthesis-related parameters.

Multiple analyses were conducted to assess the effects of 1) population size and 2) number of markers.

1) Population size

We systematically varied the number of RILs from 50 to 600 in increments of 50 RILs by using the adjusted entry means from the data set ALL. For each population size, five-fold cross validation was performed 20 times for each photosynthesis-related parameter. For LEF, Phi2, PhiNO, qL and SPAD, the prediction was relatively high, and the prediction ability changed marginally with the increasing population size. In comparison, PhiNPQ, NPQt and Fv'/Fm' had lower prediction ability and their prediction ability increased as the population size increased from 50 to approximately 150, and then remained largely stable at larger population sizes (Supplementary Fig. S1A).

2) Number of SNP markers

Different numbers of SNP were used for five-fold cross validation by using the data set ALL. The number of markers varied as follows: 3607, 7214, 10821, 14428, 18035, 21642, 25249, 28856, 32463, and 36070. The markers were randomly chosen in each replicate, but always including those of the lower number gene set in the next bigger gene set. This procedure was repeated 50 times. The prediction ability was independent of the number of SNP markers (Supplementary Fig. S1B)

3) Genomic prediction of agronomic traits based on photosynthesis-related parameters

One of the objectives of this study was to evaluate the potential of integrating photosynthesis-related parameters into breeding programs targeting crop yields. Hence, the photosynthesis-related parameters were used as the predictors of agronomic traits.

First, the prediction ability of the agronomic traits was investigated with the same GBLUP model [3] that was used to predict the photosynthesis-related parameters based on SNP information. This model served as a benchmark to evaluate the performance of integrating photosynthesis into genomic prediction.

Next, the prediction ability for agronomic traits was assessed with bivariate prediction models (Sun *et al.*, 2019) to evaluate whether agronomic traits share genetic covariance with photosynthesis-related parameters, and therefore whether the latter can act as informative secondary traits. Specifically, we estimated the prediction ability for the agronomic traits after integrating one photosynthesis-related parameter as a secondary trait separately:

$$\begin{bmatrix}\boldsymbol{y_1}\\ \boldsymbol{y_2}\end{bmatrix} = \mathbf{1}\begin{bmatrix}\mu_1\\ \mu_2\end{bmatrix} + \begin{bmatrix}\mathbf{Z_1} & 0\\ 0 & \mathbf{Z_2}\end{bmatrix}\begin{bmatrix}\boldsymbol{u_1}\\ \boldsymbol{u_2}\end{bmatrix} + \begin{bmatrix}\boldsymbol{\varepsilon_1}\\ \boldsymbol{\varepsilon_2}\end{bmatrix}, \quad [4]$$

where $\boldsymbol{y_i}$ was the vector of the adjusted entry means of genotypes for trait i, where $i \in$ [1: agronomic trait, and 2: photosynthesis-related parameter]. μ_i was the general mean for trait i, $\mathbf{Z_i}$ the incidence matrix of genotypic effects of trait i. In addition, $\boldsymbol{u_i}$ and $\boldsymbol{\varepsilon_i}$ were the vectors of random genetic effects and residuals for trait i, where $\begin{bmatrix}\boldsymbol{u_1}\\ \boldsymbol{u_2}\end{bmatrix}$ and $\begin{bmatrix}\boldsymbol{\varepsilon_1}\\ \boldsymbol{\varepsilon_2}\end{bmatrix}$ were assumed to be normally distributed $N(0, \mathbf{H} \otimes \mathbf{G})$ and $N(0, \mathbf{I} \otimes \mathbf{R})$, respectively, in which $\mathbf{G}$ was the relationship matrix calculated on the basis of the SNP marker data, $\mathbf{I}$ an identity matrix, $\mathbf{H}$ ($\mathbf{R}$) the genetic (residual) variance-covariance matrix for the two traits, and $\otimes$ the Kronecker product.

Third, we evaluated the contribution of all eight photosynthesis-related parameters together to the genomic prediction of agronomic traits using two alternative specifications of the same GBLUP model (Eq. [5]), namely by adding photosynthesis-related parameters as fixed or random effects. By adding the photosynthesis-related parameters as fixed effects, we estimated their common effects on agronomic traits for all genotypes. The addition of photosynthesis-related parameters as random effects allowed us to estimate the heterogenous effects of photosynthesis-related parameters on agronomic traits. In both cases, we fitted

$$\boldsymbol{y} = \mathbf{1}\mu + \mathbf{Z}\boldsymbol{u} + \mathbf{X}\boldsymbol{v} + \boldsymbol{\varepsilon}, \quad [5]$$

where $\boldsymbol{y}$ is the vector of agronomic trait observations, $\mathbf{X}$ was the matrix of the principal component analysis (PCA) on the photosynthesis-related parameters to avoid multicollinearity among these parameters, and $\mathbf{v}$ the vector of the regression coefficients. The remaining terms ($\mathbf{1}$, μ, $\mathbf{Z}$, $\boldsymbol{u}$, and $\boldsymbol{\varepsilon}$)

are defined as in the model [3]. For the first analysis, *i.e.*, adding the photosynthesis-related parameters as fixed effects, $\boldsymbol{\nu}$ was treated as fixed-effect vector so that the PCs of the photosynthesis-related parameters entered the GBLUP model as fixed covariates. In the second analysis, *i.e.*, adding the photosynthesis-related parameters as random effects, $\boldsymbol{\nu}$ was treated as a random-effect vector ($\boldsymbol{\nu} \sim N(0, I\sigma^2_{\boldsymbol{\nu}})$) so that the PCs defined an additional random term in the model. To quantify the effect of integrating photosynthesis-related parameters on the prediction of agronomic traits, we calculated the change in prediction ability (ΔPA) as the difference between the prediction ability obtained with the bivariate model and that obtained with the baseline univariate GBLUP model using genome-wide SNP markers only:

$$\Delta PA = PA_{bivariate} - PA_{univariate} \quad [6]$$

where both *PA* values refer to the same agronomic trait and were estimated using the same cross-validation scheme.

As a fourth approach, we assessed the performance of a joined weighted relationship matrix calculated from SNP markers and photosynthesis-related parameters to predict GY and SY. The joined weighted relationship matrix allows us to evaluate whether photosynthesis-related parameters capture the variation of agronomic traits that is not fully explained by SNP markers. In order to do so, the matrices $\mathbf{G}$ in model [3] of the two predictors (the photosynthesis-related parameters and SNP data) were weighted and summed up to a single joined weighted relationship matrix. The weight of each predictor was varied from 0 to 1 in increments of 0.1, resulting in eleven distinct combinations of joined weighted relationship matrices, where the sum of the two weights in each combination equaled 1. Five-fold cross validation (each with 50 times) was performed to assess the prediction ability of each model with different joined weighted relationship matrices.

3. Results

3.1 Phenotypic and genotypic variation

To characterize the photosynthesis-related parameters under field conditions, we first summarized the phenotypic variation and light-response patterns across a total of 631 RILs from eight HvDRR sub-populations and the corresponding ten parental inbreds. These were evaluated for seven photosystem II (PSII) related parameters and SPAD under a wide range of PAR in the field. In Y21, actinic PAR was equal to ambient PAR and LEF increased with increasing PAR (Fig. 1A), with larger deviation in the high PAR range. A decreasing trend of Phi2 with increasing PAR was observed (Supplementary Fig. S2A). In Y22, actinic PAR was 1500 $\mu mol\, m^{-2} s^{-1}$ and both LEF and Phi2 showed no dependence on ambient PAR (Fig. 1B; Supplementary Fig. S2B). The light response of NPQt was similar to that of PhiNPQ, and the light response of Phi2 was opposite to that of PhiNPQ in Y21, while no clear trend was observed in Y22. Unlike the PSII parameters, SPAD was not affected by PAR (Supplementary Fig. S2) and varied between 10 and 85 across the developmental stages studied.

3.2 Genetic variation across HvDRR sub-populations

In order to explore the genetic variation in photosynthesis-related parameters, we assessed the variance components and estimated the broad-sense heritability for each parameter.

For this two-year experiment (data set ALL), we observed significant ($P < 0.05$) effects of the Zadok's score nested in environment ($\sigma^2_{ZS:E}$), *i.e.* the development of barley, the date of the measurement (σ^2_D), the time window nested in day ($\sigma^2_{TW:D}$), and the genotype (σ^2_G) on all PSII parameters and SPAD (Table 1). The check*environment effect ($G_{checks}: E$) was significant ($P < 0.05$) for all photosynthesis-related parameters except for PhiNO (Table 1). On the basis of the data set ALL, the heritability on an entry mean basis (H^2) of all PSII parameters and SPAD ranged from 0.383 (NPQt) to 0.540 (SPAD). In Y21, when measurements were taken at various actinic PAR intensities, H^2 for PSII parameters were considerably lower, spanning between 0.075 (PhiNPQ) and 0.196 (qL). In Y22, PSII parameters were measured under the fixed high light condition, and the H^2 ranged from 0.415 (PhiNO) to 0.521 (PhiNPQ). Compared to PSII parameters which were sensitive to the instantaneous light intensity, SPAD was relatively stable.

The H^2 of SPAD in Y21 was lower (0.328) than in Y22 (0.496), which suggests that the difference in H^2 between the two years is not only due to the measurement protocol, but also due to additional environmental or experimental variability in the first vs. the second year. Nevertheless, the measurement protocol appears to be a major contributor to the difference in H^2 observed in PSII parameters between both years (Fig. 2). In addition, the H^2 also changed across the different developmental phases for each photosynthesis-related parameter. In general, the H^2 for the photosynthesis-related parameters in SEP was the lowest of the three developmental phases (Fig. 2).

A principal coordinate analysis based on 36077 SNP markers was performed to assess the population structure of the genetic materials of this study. The inbreds of the HvDRR sub-populations clustered together (Supplementary Fig. S3). The HvDRR sub-populations, which shared one of the inbred parents, were close to each other.

3.3 The phenotypic variation within HvDRR sub-populations

We assessed the phenotypic variation within each HvDRR sub-populations to determine whether individual HvDRR sub-populations provide useful segregating variation for photosynthesis-related parameters.

For each HvDRR sub-population, the adjusted entry means of the photosynthesis-related parameters of the parental inbreds were within the variation range of the values observed for the sub-population (Fig. 3), thus illustrating transgressive segregation. The coefficient of variation (Cov) for all RILs was ranging from 3.70% (Fv'/Fm') to 26.48% (NPQt). For each HvDRR sub-population, the highest Cov value was observed for NPQt, while the lowest value was observed for Fv'/Fm' (Table 2). HvDRR25 was the sub-population with the lowest Cov value for Fv'/Fm', LEF, NPQt, PhiNPQ and qL, while it showed the highest Cov for SPAD. In contrast, HvDRR35 had the highest CoV for Fv'/Fm', NPQt, and qL.

In order to assess the importance of epistatic variance, we compared for each HvDRR sub-population the differences between the means of the parameters for the parental inbreds and the corresponding RILs. For homozygous genotypes as in our RILs, the expected progeny mean equals the parental mean in the absence of epistasis. Significant deviations from parental means suggested that epistatic effects contribute to the phenotype under consideration. Using this comparison, we

observed significant ($P < 0.05$) differences for Phi2 in HvDRR25 and HvDRR27 and for Fv'/Fm', NPQt, and PhiNPQ in HvDRR32 (Fig. 3).

3.4 Correlations among and within photosynthesis-related parameters and agronomic traits.

In order to identify phenotypic traits that are most relevant for yield and its components, we examined the correlations within photosynthesis-related parameters and between these and agronomic traits across the developmental phases.

We observed a wide range of correlations among each pair of photosynthesis-related parameters (Fig. 4) when considering the adjusted entry means calculated for the data set ALL. For instance, SPAD was significantly positively correlated with Fv'/Fm' and PhiNO, while it was significantly negatively correlated with LEF, NPQt, Phi2, PhiNPQ and qL (Fig. 4). As expected, Phi2 and LEF were significantly positively correlated with each other. In contrast, Fv'/Fm' was significantly negatively correlated with all PSII parameters except PhiNO. While NPQt was positively correlated with Phi2, the correlation coefficient was low.

We also analyzed the correlation between the adjusted entry means of photosynthesis-related parameters in the data set ALL and the adjusted entry means of agronomic traits collected from multi-year and -environment experiments (Fig. 4). Since comparison between characters that have been assessed in different environments reduces the covariance due to error, this approach allows to directly obtain genotypic correlations (Holland, 2006; Piepho *et al.*, 2012). Notably, LEF, Phi2, and qL were significantly ($P < 0.05$) positively correlated with GY and also yield component traits, such as spike- and seed-related traits (AWL, SPL, SPK, SDW, SDA, and TGW). In contrast, PhiNO and SPAD were significantly ($P < 0.05$) negatively correlated with GY as well as its component traits.

In the next step, we studied the correlation between the same traits across the different developmental phases. We observed significantly ($P < 0.05$) positive correlations between the two developmental phases SEP and REP for LEF, Phi2, PhiNPQ and SPAD, while the correlations were only moderately positive for Fv'/Fm', NPQt, PhiNO and qL (Fig. 5). PhiNO and SPAD were the only parameters that showed significantly ($P < 0.05$) positive correlation between REP and ASP. No significant correlation was observed between SEP and ASP for PSII-related parameters

and SPAD. We then examined the correlation between the photosynthetic parameters assessed in the individual developmental phases and grain/straw yield (GY/SY), flag leaf dimensions (FL/FW), spike-related traits (SPL, AWL, SPK), and seed-related traits (SDW, SDL, SDA, TGW). We found SPAD in SEP and NPQt and PhiNPQ in REP were significantly ($P < 0.05$) negatively correlated with GY, while Fv'/Fm', Phi2 and LEF in REP were moderately positively correlated with GY. However, the significant positive correlation between Phi2 and GY observed across all developmental phases disappeared when considering each individual development phase. Specifically, we observed a change in the correlation coefficient across phases, from negative in SEP to positive in REP and then to negative again in ASP. The correlations between Phi2 and several spike- and seed-related traits remained significant in SEP and REP. In addition, we observed several parameters to be significantly ($P < 0.05$) positively correlated with SY, such as Fv'/Fm' and LEF in SEP or LEF and Phi2 in REP, while PhiNPQ and SPAD in SEP and SPAD in REP were negatively correlated with SY (Fig. 5). These correlation patterns observed across all HvDRR populations differed considerably from those found for individual HvDRR populations in individual developmental phases. For individual HvDRR sub-populations, we only observed significantly positive correlations between Fv'/Fm' and PhiNO and GY in REP for HVDRR34 and qL and GY in SEP for HvDRR31 (Supplementary Figs. S4 and S5). Although the correlation between Phi2 and GY showed a negative-positive-negative pattern across SEP, REP and ASP at the whole population level, this patten was not observed in all HvDRR sub-populations. For instance, in HvDRR31, Phi2 was positively correlated with GY in SEP, and negatively correlated with GY in REP and ASP (Supplementary Fig. S5).

3.5 QTL associated with photosynthesis-related parameters

In order to dissect the genetic architecture underlying variation in photosynthesis-related traits and to identify genomic regions contributing to these parameters (Objective 2), we performed BPP and MPP QTL analyses across datasets and developmental phases.

In total, 24 QTL were detected for the photosynthesis-related parameters using the BPP QTL analysis when considering all six data sets. The QTL were detected on all chromosomes except 6H. The PEV by individual QTL ranged from 15.36% to 45.28% (Supplementary Table S3).

The detected QTL were not consistent across the different data sets. For the data set ALL, nine QTL were identified for three HvDRR sub-populations: one QTL was detected for HvDRR02 for

SPAD, four QTL for HvDRR25 for LEF, Phi2 and SPAD, and four QTL for HvDRR27 for Fv'/Fm', NPQt, PhiNPQ and SPAD. The PEV of the simultaneous fit of all additive QTL was ranging from 15.43% (NPQt) to 42% (SPAD) (Supplementary Table S3).

For the data set Y21, two QTL associated with SPAD were detected in HvDRR27 and HvDRR35, while in the data set Y22 three QTL associated with LEF, Phi2 and NPQt were detected in HvDRR25 and HvDRR34. The two QTL for LEF and Phi2 were located in the same region of chromosome 5 in HvDRR25.

Notably, QTL changed across the different developmental phases. In SEP, two QTL were detected for Phi2 (HvDRR35). In REP, four QTL were associated with LEF (HvDRR27), Phi2 (HvDRR27), and SPAD (HvDRR02 and HvDRR25). In ASP, four QTL were associated with PhiNO (HvDRR25), qL (HvDRR32), and SPAD (HvDRR25, HvDRR27).

A total of 37 QTL were detected in the MPP QTL analysis across the different data sets (Supplementary Table S3). The PEV by individual QTL ranged from 2.3% (SPAD ALL and Phi2 for REP) to 15.21% (LEF, REP).

We summarized both BPP and MPP QTL into 18 consensus QTL based on the consensus map (Casale *et al*., 2022), in which 7 consensus QTL were detected by BPP as well as MPP mapping, 8 consensus QTL were detected only by MPP mapping, and 3 were detected by BPP QTL mapping (Supplementary Table S4).

3.6 Genomic prediction for photosynthesis-related parameters

We evaluated genomic prediction ability (PA) using the GBLUP method across years and developmental phases in order to assess whether photosynthesis-related parameters can be predicted from genome-wide markers and, thus, are of use in breeding programs.

In the first step, the PA of each photosynthesis-related parameter based on SNP markers was estimated using the GBLUP model (Eq. [3]). Using all RILs in data set ALL, the PA ranged from 0.25 for PhiNPQ to 0.57 for SPAD (Supplementary Fig. S6).

To compare PA between years, only genotypes evaluated in both years (Y21 and Y22) were considered. In Y21, the PA for photosynthesis-related parameters ranged from 0.25 (qL) to 0.56 (PhiNPQ), whereas in Y22, the PA ranged from 0.08 (NPQt) to 0.42 (SPAD) (Fig. 6A).

In the next step, we compared the PA for the photosynthesis-related parameters in different developmental phases. The PAs of the photosynthesis-related parameters were often higher in SEP and REP than in ASP (Fig. 6B). The PAs of Fv'/Fm', LEF, Phi2, and SPAD decreased in ASP compared to SEP and REP, while the heritability of these parameters showed the opposite trend (Fig. 2). Fv'/Fm' and NPQt had consistently low PAs across the developmental phases (Fig. 6B).

3.7 Prediction of agronomic traits by integrating photosynthesis-related parameters

Four different approaches were examined in order to evaluate whether the PA for GY and SY based on SNP markers can be improved by incorporating photosynthesis-related parameters as predictors.

By using a bivariate model to integrate the photosynthesis-related parameters as secondary trait in the model (Eq. [4]), the PAs for the agronomic traits were increased but not by all photosynthesis-related parameters. The difference between the PA of the bivariate model and the corresponding univariate model (GBLUP model) ranged from -0.13 to 0.01 (Supplementary Fig. S7, Supplementary Table S5). Overall, by using this bivariate model, the highest percentage of improved PA was 2% by adding PhiNPQ (SEP) as the secondary trait to predict HI. The PAs of FT, FL, PH, SDL, SDA, SPK, SPL, AWL, TGW, and GY were increased by adding the PSII-related parameters as secondary traits in the bivariate model in the data set ALL (Supplementary Fig. S7). For instance, the PA for GY was improved by adding NPQt (0.14%), Fv'/Fm' (0.14%) and LEF (0.08%) as secondary trait. Comparing the three different developmental stages, some of the photosynthesis-related parameters from both REP (PhiNPQ 0.98%, LEF 0.42%, Phi2 0.23%, and qL 0.16%) and ASP (LEF 0.11%, PhiNO 0.07%, and SPAD 0.03%) data set were able to improve the PA for GY, while no photosynthesis-related parameters from SEP could improve GY. The strongest improvement of about 1% was observed when considering PhiNPQ from REP. For SY, we observed a very small increase in PA when integrating qL (ASP, delta=0.0006) as secondary traits (Supplementary Fig.S7).

Next, the photosynthesis-related parameters were added to the GBLUP model as either fixed or random effect (Eq. [5], Fig. 7, Supplementary Fig. S8, Supplementary Table S5). The PA for the agronomic traits (SDA (9.1%), SDL (0.98%) and AWL (0.88%)) was improved by adding the photosynthesis-related parameters as fixed effect. Adding the photosynthesis-related parameters as random effects also slightly increased the PAs of three and two agronomic traits when

considering photosynthesis-related parameters from SEP and ASP, respectively. Interestingly, the improved PAs in SEP were observed for seed-related traits (SDL (3.8%), SDA (10.7%), and GY (0.45%)).

Lastly, joined weighted relationship matrices of the photosynthesis-related parameters and SNP markers were established (Eq. [3]; Fig. 8). First, for data set ALL, using the whole set of SNP markers, the PA of GY based purely on photosynthesis-related parameters (PA=0.348) was considerably lower than when calculated purely based on SNP markers (PA=0.605). Furthermore, none of the joined weighted matrices could improve PA for GY compared to that of the SNP markers. In contrast, the PAs of FL, FW, PH, SPK, SPL and HI were improved by the joined weighted matrices, and the improvements of PA ranged from 0.04% (FL, weight of SNP=0.8) to 1.86% (FW, weight of SNP=0.9) (Fig. 8). Using only those markers, which were detected in the QTL analysis of the photosynthesis-related parameters (Supplementary Table S3), to calculate the relationship matrix, we observed increases of the PA compare to the relationship matrix calculated for all SNP markers. Among all agronomic traits, the highest increase of the PA was observed for FW with an increase of 3.33%.

Notably, the PA improvement of GY varied between the two years (data set Y21 and Y22, Supplementary Fig. S10) and among the different developmental phases (data set SEP, REP, ASP, Supplementary Fig. S11). For Y21, consideration of the photosynthesis-related parameters, regardless of their weight, improved the PA of GY, ranging from 5.51% (weight of SNP=0.9) to 6.08% (weight of SNP=0.5), while for Y22, it did not improve the PA of GY under any weight level. (Supplementary Fig. S10). Integrating photosynthesis-related parameters assessed in the REP and SEP improved the PA for GY, ranging from 0.24% (SEP, weight of SNP=0.9) to 1.12% (REP, weight of SNP=0.7) (Supplementary Fig. S11). Doing the same analyses for all other agronomic traits, the percentage of improved PA by using a joined weighted relationship matrix compared to a purely SNP based matrix ranged from 0.00037% (TGW, REP, weight of SNP=0.9) to 11.1% (SDA, SEP, weight of SNP=0.4).

4 Discussion

Our study revealed high variability in the photosynthesis-related parameters in the eight HvDRR sub-populations grown under field conditions (Fig. 3). Consistent with our previous findings (Gao *et al.*, 2024), this high variability of the photosynthesis-related parameters was explained by environmental conditions, plant developmental phases, genetic effects, and the interaction between genotype and environment (Table 1). In order to evaluate the potential of classical plant breeding to optimize photosynthesis via phenotypic selection, it is crucial to consider the heritability of the photosynthesis-related parameters. In our two-year experiments, the broad sense heritability ranged from 0.393 (qL) to 0.540 (SPAD) for the different parameters (Table 1). The heritability observed for SPAD is in good agreement with what was reported earlier in barley under field conditions (Liu *et al.*, 2015; 0.50-0.58; Obsa *et al.*, 2016; 0.48-0.85). Consistent with our observation, these previous studies also suggested that the ranking of the genotypes is not stable across years, i.e., genotype by environment interaction has a major impact on photosynthetic phenotypes. In this study, the difference in the ranking of the genotypes between Y21 and Y22 might be partially explained by the different measurement protocols used. In Y21 we used the "Photosynthesis RIDES" protocol which measures the PSII-related parameters under the ambient light intensity, whereas in Y22 all measurements were conducted under the same light intensity of 1500 $\mu mol\, m^{-2} s^{-1}$. Although measuring photosynthesis under highly variable ambient light intensity reflects the reality in the field, using the same light intensity for all measurements could reduce PAR-dependent variations in the photosynthetic parameters (Fig. 1) and thereby increase the contribution of the genetic variation. The comparison of the genetic variance for each year in the data set ALL (Supplementary Fig. S12) revealed that the genetic variation for Y22 is higher than that for Y21 for all photosynthesis-related parameters measured in this study. A plausible explanation for this observation might be that reduced PAR-dependent variations by using a fixed actinic light intensity reduce the environmental noise. This in turn improves the ability of comparing the PSII-related parameters across genotypes and therewith increases the heritability. Therefore, measurement protocols with predefined actinic light intensity are recommendable when the primary objective is to quantify genetic variations in photosynthesis. In field conditions, such protocols can be applied using a hand-held device with a clamp-on chamber. On the other hand, photosynthesis measurements performed under ambient light intensities, such as for Y21, may

capture additional environment-dependent or G×E components that are relevant for yield formation and, thus, may improve prediction ability of yield. This is in accordance with our observation that for Y21, all considerations of the photosynthesis-related parameters, regardless of their weight in the joined weighted relatedness matrix, improved the prediction ability of GY while this was not the case for Y22 (Supplementary Fig. S10). Thus, fixed light intensities are recommendable for genetic dissection and robust genotype comparisons, whereas ambient light measurements may be advantageous when the main goal is prediction of yield under realistic field conditions.

4.1 Genetic complexity of photosynthesis-related parameters

We conducted both BPP and MPP QTL analyses in the eight barley HvDRR sub-populations to gain better insights into the genetic complexity of photosynthesis-related parameters. The BPP and MPP QTL analyses identified 28 and 35 QTL of the photosynthesis-related parameters, respectively (Supplementary Table S3). The higher number of QTL detected for the multi-population analysis is in accordance with the previous studies which showed a higher power of this analysis to detect QTL compared to the bi-parental analysis (cf. Shrestha *et al.*, 2022; Cosenza *et al.*, 2024).

Based on the consensus genetic map of BPP and MPP QTL, we identified 18 consensus QTL (Supplementary Table S4), of which eleven were associated with more than one photosynthesis-related parameter. A similar observation was also made in previous studies, e.g. for QTL associated with net photosynthesis rate, stomatal conductance, chlorophyll fluorescence parameters, or chlorophyll content (Guo *et al.*, 2008; Liu *et al.*, 2015; Liu *et al.*, 2017; Salter *et al.*, 2020). Since the photosynthesis-related parameters were strongly correlated with each other across all developmental phases (Fig. 4) or within each developmental phase (Fig. 5), their variations might share a common genetic basis.

We also observed that multiple QTL were associated with each trait (Supplementary Table S3), suggesting that the photosynthesis-related parameters were controlled by multiple QTL. This is in line with the findings of other studies in cereals, such as rice (Adachi *et al.*, 2017; Gu *et al.*, 2017; Adachi *et al.*, 2019; Wang *et al.*, 2020). Yet, the proportion of phenotypic variance explained by the detected QTL for the photosynthesis-related parameters was considerably lower than those explained by QTL for agronomic traits in the same populations (Supplementary Table S3)

(Shrestha *et al.*, 2022; Cosenza *et al.*, 2024; Lapasiya *et al.*, 2025). This might be explained by the highly variable nature of photosynthesis, which quickly and dynamically responds to environmental changes (Fig. 1; Supplementary Fig. S2) (Long *et al.*, 2022), as highlighted by the lower heritability for the photosynthesis-related traits than for the agronomic traits (Fig. 2) (Shrestha *et al.*, 2022; Cosenza *et al.*, 2024; Lapasiya *et al.*, 2025). An additional explanation for the considerably lower proportion of phenotypic variance explained by the photosynthesis-related QTL compared with the QTL for agronomic traits might be the higher genetic complexity of the former compared to the latter. Importantly, even when using MPP QTL analysis, the PEV of detected QTL was low, indicating that photosynthesis-related parameters might be controlled by many small-effect alleles that are difficult to detect. In contrast, the PEV of genomic prediction analysis, were three to seven times higher than the PEV of MPP QTL (Supplementary Table S6), suggesting that genomic prediction performs better for such complex photosynthesis process. In this case, GP might be a promising approach to improve photosynthesis-related parameters by classical breeding.

4.2 The potential to improve photosynthesis-related parameters by genomic prediction

By using all genome-wide available SNPs as predictor, the PA for the photosynthesis-related parameters of the data set ALL was ranging from 0.25 (PhiNPQ) to 0.58 (SPAD) (Fig. 6). These values are in the order of what was previously reported for *Arabidopsis thaliana* under controlled conditions (Farooq *et al.*, 2021) and suggest that data from field experiments can also be used to train genomic prediction models for photosynthesis-related parameters. From a biological and breeding perspective, predicting photosynthesis-related traits *per se* is relevant for several reasons. First, although genomic prediction is not a tool to investigate the underlying physiology processes, it can still contribute to our understanding of photosynthesis by quantifying how much of the phenotypic variation is consistently captured by genome-wide additive effects across environments and developmental phases (Fig. 6B). Secondly, photosynthesis-related parameters are promising targets for yield improvements (Croce *et al.*, 2024), and moderate optimizations of photosynthesis can already have cumulative effects to improve grain yields (reviewed by Simkin *et al.*, 2019). Therefore, genomic prediction for photosynthesis can provide breeders with a practical tool to directly select candidate genotypes for genetically determined variation in

photosynthesis. Finally, establishing predictive models for photosynthesis-related parameters provides a basis for subsequent analysis in which photosynthesis could be incorporated as additional information to improve genomic prediction of agronomic traits.

Despite the promising PAs observed for the photosynthesis-related traits in our study (Supplementary Fig. S6), the values were lower compared to those reported for agronomic traits in the HvDRR population. For instance, Shrestha *et al.* (2022) reported that the PAs for grain size and grain weight-related traits ranged from 0.83 to 0.86. Cosenza *et al.* (2024) also reported cross-validated PAs of 0.77 for both flowering time and plant height. However, given that a relatively low PA for photosynthesis-related parameters was reported in Arabidopsis under controlled conditions (Farooq *et al.*, 2021), the dynamic response of photosynthesis to environmental fluctuations in the field cannot fully explain the low PA.

One of the challenges in genomic prediction of photosynthetic traits is the complex effects of physiological and developmental processes on photosynthesis, including source-sink interaction (Paul and Foyer, 2001), leaf development and senescence (Wingler *et al.*, 2004), and circadian clock (Dodd *et al.*, 2014). As a result, photosynthesis measurements performed at a single time point (or a few time points) in a single developmental phase are not enough to capture the overall long-term performance of the plant that is evaluated by the end-point measurements of agronomic traits. Moreover, the high non-genetic variability of photosynthesis makes it more difficult to accurately predict photosynthesis based on genomic information alone. When environmental fluctuations during the measurements are unavoidable, one possibility to improve the PA for photosynthesis-related parameters might be to increase the frequency of assessment to capture, for example, diurnal and seasonal trends across different plant developmental phases. High-throughput photosynthetic phenotyping systems (reviewed by van Bezouw *et al.*, 2019) would facilitate such assessment under field conditions (Keller *et al.*, 2024).

4.3 The potential and challenge to improve crop yields by optimizing photosynthesis

Several approaches have been proposed to improve crop yield by optimizing photosynthesis (reviewed by Croce *et al.*, 2024). One of the challenges is the complex relationship between photosynthesis and yield (Croce *et al.*, 2024; Keller *et al.*, 2024). In our study on barley, the correlation between GY and the photosynthesis-related parameters varied across the

developmental phases (Fig. 4), as was shown previously (Gao *et al.*, 2024). We observed that LEF, Phi2, and qL were significantly ($P<0.05$) positively correlated with most of the agronomic traits, such as spike- and seed-related traits and also GY and SY (Fig. 4), while SPAD was significantly ($P<0.05$) negatively correlated with most of the agronomic traits (Fig. 4). Lower leaf chlorophyll content can lead to deeper light penetration into a dense canopy and may thereby improve whole-plant photosynthesis (Gu *et al.*, 2017; Rotasperti *et al.*, 2022; Cutolo *et al.*, 2023; Croce *et al.*, 2024).

To better understand how photosynthesis contributes to the formation of barley grain and straw yield and thereby improve strategies to integrate photosynthesis-related parameters into crop breeding programs aiming at yield improvements, we estimated the correlation between the photosynthesis-related parameters and yield components in each developmental phase separately. In line with our previous study (Gao *et al.*, 2024), the correlation between yield- and the photosynthesis-related parameters changed during plant growth and development (Fig. 5). For instance, a dynamic correlation was observed between Phi2 and GY, switching from negative in SEP to positive in REP and then to negative again in ASP (Fig. 5). In the case of Phi2, it was significantly positively correlated with spike- and seed-related parameters in SEP and REP, while the correlation was moderately negative in ASP.

The SEP comprises the spikelet initiation phase (Waddington 1 to 4.5), i.e. from apex development until the appearance of awn primordia. At the end of this phase, the number of primordia already reaches the maximum (Thirulogachandar and Schnurbusch, 2021; Celestina *et al.*, 2023), which determines the maximum yield potential of barley. Moreover, Křen *et al.* (2014) reported that tillering and beginning of stem elongation stage (also SEP in this study) is the crucial period for the formation of spring barley yield and grain quality. During REP, SPK reaches a plateau and then starts to decrease (Thirulogachandar and Schnurbusch, 2021). The increase in positive correlation coefficient found between SPK and Phi2 from SEP to REP might indicate that higher Phi2 can help maintain the number of fertile florets and, thus, suppress the decrease of SPK in REP (Arisnabarreta and Miralles, 2008). Furthermore, not only SPK but also grain weight is determined during the spike development stage, long before the grain filling stage (Distelfeld *et al.*, 2014). The positive correlation found between Phi2 and the spike- and seed-related traits (AWL, SPK, SPL, SDL, SDE, SDA and TGW) in SEP and REP may therefore illustrate the importance of

photosynthesis during these stages in determining the yield potential of barley, possibly through positive influence on SPK and grain weight.

In contrast, the correlations between the photosynthesis-related parameters and the spike/seed-related traits were considerably lower in ASP (Fig. 5). One reason could be that the main contributors to grain filling are not leaves but photosynthesis of the spike itself (reviewed by Sanchez-Bragado *et al.*, 2020). This is supported by the observations that the photosynthetic capacity of spikes is close to or even higher than that of leaves in the late grain filling stage (Abbad *et al.*, 2004; Maydup *et al.*, 2010; Sanchez-Bragado *et al.*, 2014). Another possible explanation for the low correlation coefficient between GY and the photosynthesis-related parameters in ASP is progression of leaf senescence. With increasing leaf senescence in the late stage of grain filling, soluble carbohydrates from stems may gain more importance in providing sugars for grain filling (Bingham *et al.*, 2007) besides the spike photosynthesis.

4.4 The potential to exploit photosynthesis-related parameters in crop breeding programs to improve yield

Having seen the above-described correlation patterns among the photosynthesis-related parameters and yield as well as its components, we evaluated the predictive power of the photosynthesis-related parameters towards yield by four different approaches.

First, in line with the correlation between the photosynthesis-related parameters, the PA of the photosynthesis-related parameters varied depending on the developmental phases in which these had been measured. This finding illustrates that, in order to exploit photosynthetic parameters for yield prediction, the most appropriate stage for their assessment needs to be determined. Furthermore, we observed that the PA for GY was lower when prediction was based on photosynthesis-related parameters alone compared to genomic prediction (Fig. 8, Supplementary Fig. S9-S11). In contrast, Keller *et al.* (2024) reported the potential of photosynthesis-related parameters to predict genotype*environment interaction of bean yield, which was higher than that of genomic prediction. Since our study used photosynthesis-related parameters obtained from a two-year experiment to predict the average crop yield assessed from multi-year and -environment experiments, it is possible that our analyses reflected genetic correlation more strongly than phenotypic correlation between crop yields and the photosynthesis-related parameters.

When combining the photosynthesis-related parameters with the genomic information to predict crop yield and its components, we observed only slight increases of the PA, with a maximum of 11.1% increase compared to using genomic information alone when considering a few selected developmental stages. In contrast, for most traits and developmental stages, no improvement was observed. The minor and inconsistent improvements might be due to the limitation of considering only PSII-related parameters and SPAD in this study, as these parameters are only related to the light reaction of photosynthesis at leaf level. In addition, more frequent assessment of photosynthesis-related parameters should allow better separation of signal from noise and, thus, increase the predictive performance.

Together, these findings suggest that the photosynthesis-related parameters carry some information on yield and its components that is different from the SNP-based relationship matrix. Therefore, photosynthesis-related parameters could provide valuable additional information that can be considered in future research to increase the PA of yield and its components, and therewith to improve the efficiency of crop breeding programs.

5 Conclusions

The results of this study highlight the considerable extent of genetic variation for photosynthesis-related parameters in barley segregating populations under field conditions compared to other sources of variation. Nevertheless, significant effects of environmental factors and significant interactions between genotype and environments on the photosynthesis-related parameters illustrate the potential of high-throughput and time-series measurements for understanding their genetics. Development of such devices is essential for exploiting the full potential of photosynthesis-related parameters in predicting yield and also for realizing yield improvements by genetic optimization of photosynthesis. The dynamic correlations between photosynthesis-related parameters and agronomic traits indicate that plant developmental effects should be taken into account when developing strategies for optimizing photosynthesis to improve crop yields. The considerably higher PEV of genomic prediction than QTL-based analyses illustrates that the photosynthesis-related parameters are inherited in a more complex way than classical agronomic traits. However, our results suggest that the PA for yield and yield components can be slightly increased by integrating photosynthesis-related parameters, which are assessed in selected developmental phases, into genomic prediction. This might open up a novel perspective on increasing the efficiency of crop breeding programs by integrating photosynthesis into prediction models, especially when high-throughput field phenotyping methods become available.

Acknowledgement

The authors would like to thank Florian Esser and George Alskief (Institute of Quantitative Genetics and Genomics of Plants, Biology Department, Heinrich Heine University, Düsseldorf, Germany) for the field management in Cologne and Düsseldorf in Germany. The authors thank Sarah Patrick (Heinrich Heine University, Düsseldorf, Germany) for the phenotyping in 2022. The work in BS and SM labs was supported by the Deutsche Forschungsgemeinschaft (DFG, German Research Foundation) through the Cluster of Excellence on Plant Sciences (CEPLAS, EXC2048). The authors thank two anonymous reviewers for helpful comments on an earlier version of the manuscript.

Declaration of Competing Interest

The authors declare no conflict of interest.

Author Contribution

BS, SM conceptualized the study, acquired funding and supervised the work; YG, SM, and BS designed the research. YG performed experiments and analyzed the data. PYW contributed to data analysis. YG, SM, and BS interpreted the results. YG drafted the manuscript, which was improved by SM and BS. All authors read and approved the final version of the manuscript.

Funding

The work in BS and SM labs was supported by the Deutsche Forschungsgemeinschaft (DFG, German Research Foundation) through the Cluster of Excellence on Plant Sciences (Heinrich Heine University, Düsseldorf, Germany) (CEPLAS, EXC2048).

Data Availability

The adjusted entry means of the barley parental inbreds and recombinant inbred lines for photosynthesis-related parameters of each data set have been deposited at Zenodo (https://doi.org/10.5281/zenodo.18695492)

Reference

Abbad H, El Jaafari S, Bort Pie J, Araus Ortega JL. 2004. Comparison of flag leaf and ear photosynthesis with biomass and grain yield of durum wheat under various water conditions and genotypes. Agronomie, 2004, vol. 24, num. 1, p. 19-28.

Adachi S, Yamamoto T, Nakae T, Yamashita M, Uchida M, Karimata R, Ichihara N, Soda K, Ochiai T, Ao R, others. 2019. Genetic architecture of leaf photosynthesis in rice revealed by different types of reciprocal mapping populations. Journal of Experimental Botany 70, 5131-44.

Adachi S, Yoshikawa K, Yamanouchi U, Tanabata T, Sun J, Ookawa T, Yamamoto T, Sage RF, Hirasawa T, Yonemaru J. 2017. Fine mapping of carbon assimilation rate 8, a quantitative trait locus for flag leaf nitrogen content, stomatal conductance and photosynthesis in rice. Frontiers in Plant Science 8, 60.

Alter P, Dreissen A, Luo FL, Matsubara S. 2012. Acclimatory responses of Arabidopsis to fluctuating light environment: Comparison of different sunfleck regimes and accessions. Vol. 113, 221-37.

Arisnabarreta S, Miralles DJ. 2008. Critical period for grain number establishment of near isogenic lines of two-and six-rowed barley. Field Crops Research 107, 196-202.

Bayer MM, Rapazote-Flores P, Ganal M, Hedley PE, Macaulay M, Plieske J, Ramsay L, Russell J, Shaw PD, Thomas W, Waugh R. 2017. Development and evaluation of a barley 50k iSelect SNP array. Frontiers in Plant Science 8.

Berry JO, Yerramsetty P, Zielinski AM, Mure CM. 2013. Photosynthetic gene expression in higher plants. Photosynthesis Research 117, 91-120.

Beyene Y, Semagn K, Mugo S, Tarekegne A, Babu R, Meisel B, Sehabiague P, Makumbi D, Magorokosho C, Oikeh S, Gakunga J, Vargas M, Olsen M, Prasanna BM, Banziger M, Crossa J. 2015. Genetic gains in grain yield through genomic selection in eight bi-parental maize populations under drought stress. Crop Science 55, 154-63.

Bielczynski LW, Łaçki MK, Hoefnagels I, Gambin A, Croce R. 2017. Leaf and plant age affects photosynthetic performance and photoprotective capacity. Plant Physiology 175, 1634-48.

Bingham IJ, Blake J, Foulkes MJ, Spink J. 2007. Is barley yield in the UK sink limited?: I. Post-anthesis radiation interception, radiation-use efficiency and source–sink balance. Field Crops Research 101, 198-211.

Bonington S. 1977. Climate and the efficiency of crop production in Britain. Philosophical Transactions of the Royal Society of London. B, Biological Sciences 281, 277-94.

Broman KW, Wu H, Sen Ś, Churchill GA. 2003. R/qtl: QTL mapping in experimental crosses. bioinformatics 19, 889-90.

Carmo-Silva E, Andralojc PJ, Scales JC, Driever SM, Mead A, Lawson T, Raines CA, Parry MAJ. 2017. Phenotyping of field-grown wheat in the UK highlights contribution of light response of photosynthesis and flag leaf longevity to grain yield. Journal of experimental botany 68, 3473-86.

Casale F, Inghelandt DV, Weisweiler M, Li J, Stich B. 2022. Genomic prediction of the recombination rate variation in barley – A route to highly recombinogenic genotypes. Plant Biotechnology Journal 20, 676-90.

Celestina C, Hunt J, Brown H, Huth N, Andreucci M, Hochman Z, Bloomfield M, Porker K, McCallum M, Harris F, others. 2023. Scales of development for wheat and barley specific to either single culms or a population of culms. European Journal of Agronomy 147, 126824.

Chang TG, Chang S, Song QF, Perveen S, Zhu XG. 2019. Systems models, phenomics and genomics: Three pillars for developing high-yielding photosynthetically efficient crops. In Silico Plants 1, 1-13.

Chazdon RL, Pearcy RW. 1991. The Importance of Sunflecks for Forest Understory Plants Photosynthetic machinery appears adapted to brief, unpredictable periods of radiation.

Coast O, Posch BC, Rognoni BG, Bramley H, Gaju O, Mackenzie J, Pickles C, Kelly AM, Lu M, Ruan Y-L, others. 2022. Wheat photosystem II heat tolerance: evidence for genotype-by-environment interactions. The Plant Journal 111, 1368-82.

Cosenza F, Shrestha A, Inghelandt DV, Casale FA, Wu PY, Weisweiler M, Li J, Wespel F, Stich B. 2024. Genetic mapping reveals new loci and alleles for flowering time and plant height using the double round-robin population of barley. Journal of Experimental Botany 75, 2385-402.

Croce R, Carmo-Silva E, Cho YB, Ermakova M, Harbinson J, Lawson T, McCormick AJ, Niyogi KK, Ort DR, Patel-Tupper D, Pesaresi P, Raines C, Weber APM, Zhu X-G. 2024. Perspectives on improving photosynthesis to increase crop yield. The Plant Cell 36, 3944-73.

Cutolo EA, Guardini Z, Dall'Osto L, Bassi R. 2023. A paler shade of green: engineering cellular chlorophyll content to enhance photosynthesis in crowded environments. New Phytologist 239, 1567-83.

De Souza AP, Burgess SJ, Doran L, Hansen J, Manukyan L, Maryn N, Gotarkar D, Leonelli L, Niyogi KK, Long SP. 2022. Soybean photosynthesis and crop yield are improved by accelerating recovery from photoprotection. Science 377, 851-54.

Desta ZA, Ortiz R. 2014. Genomic selection: Genome-wide prediction in plant improvement. Trends in plant science 19, 592-601.

Ding Q, Zhen X, Sadok W. 2025. Photosynthesis-driven yield gains in global wheat breeding trials. Crop Science 65, e70005.

Distelfeld A, Avni R, Fischer AM. 2014. Senescence, nutrient remobilization, and yield in wheat and barley. Journal of experimental botany 65, 3783-98.

Dodd AN, Kusakina J, Hall A, Gould PD, Hanaoka M. 2014. The circadian regulation of photosynthesis. Photosynthesis research 119, 181-90.

Driever SM, Lawson T, Andralojc PJ, Raines CA, Parry MAJ. 2014. Natural variation in photosynthetic capacity, growth, and yield in 64 field-grown wheat genotypes. Journal of Experimental Botany 65, 4959-73.

Driever SM, Simkin AJ, Alotaibi S, Fisk SJ, Madgwick PJ, Sparks CA, Jones HD, Lawson T, Parry MAJ, Raines CA. 2017. Increased sbpase activity improves photosynthesis and grain yield in wheat grown in greenhouse conditions. Philosophical Transactions of the Royal Society B: Biological Sciences 372.

Dupuis J, Siegmund D. 1999. Statistical methods for mapping quantitative trait loci from a dense set of markers. Genetics 151, 373-86.

Farooq M, Van Dijk ADJ, Nijveen H, Aarts MGM, Kruijer W, Nguyen T-P, Mansoor S, de Ridder D. 2021. Prior biological knowledge improves genomic prediction of growth-related traits in Arabidopsis thaliana. Frontiers in genetics 11, 609117.

Feldman MJ, Ellsworth PZ, Fahlgren N, Gehan MA, Cousins AB, Baxter I. 2018. Components of water use efficiency have unique genetic signatures in the model C4 grass Setaria. Plant physiology 178, 699-715.

Gao Y, Stein M, Oshana L, Zhao W, Matsubara S, Stich B. 2024. Exploring natural genetic variation in photosynthesis-related traits of barley in the field. Journal of Experimental Botany 75, 4904-25.

Garin V, Wimmer V, Malosetti M. 2015. mppR: an R package for QTL analysis in multi-parent populations using linear mixed models. R Vignette. https://cran. r-project. org/package= mppR/vignettes/mppR_vignette. pdf.

Gifford RM. 1995. Whole plant respiration and photosynthesis of wheat under increased CO2 concentration and temperature: long-term vs. short-term distinctions for modelling. Global Change Biology 1, 385-96.

Gilmour AR, Gogel BJ, Welham SJ. 2021. User Guide Release 4.2 Functional Specification.

Giovanny C-P. 2016. Genome assisted prediction of quantitative traits using the R package sommer. PLoS ONE 11, 1-15.

Gong HY, Li Y, Fang G, Hu DH, Jin WB, Wang ZH, Li YS. 2015. Transgenic rice expressing Ictb and FBP/Sbpase derived from cyanobacteria exhibits enhanced photosynthesis and mesophyll conductance to CO2. PLoS ONE 10, 1-23.

Gu J, Zhou Z, Li Z, Chen Y, Wang Z, Zhang H. 2017. Rice (Oryza sativa L.) with reduced chlorophyll content exhibit higher photosynthetic rate and efficiency, improved canopy light distribution, and greater yields than normally pigmented plants. Field Crops Research 200, 58-70.

Guo P, Baum M, Varshney RK, Graner A, Grando S, Ceccarelli S. 2008. QTLs for chlorophyll and chlorophyll fluorescence parameters in barley under post-flowering drought. Euphytica 163, 203-14.

Haley CS, Knott SA. 1992. A simple regression method for mapping quantitative trait loci in line crosses using flanking markers. 315-24.

Hay WT, Bihmidine S, Mutlu N, Hoang KL, Awada T, Weeks DP, Clemente TE, Long SP. 2017. Enhancing soybean photosynthetic CO2 assimilation using a cyanobacterial membrane protein, ictB. Journal of Plant Physiology 212, 58-68.

Holland JB. 2006. Estimating genotypic correlations and their standard errors using multivariate

restricted maximum likelihood estimation with SAS Proc MIXED. Crop science 46, 642-54.

Holland JB. 2007. Genetic architecture of complex traits in plants. Current opinion in plant biology 10, 156-61.

Holland JB, Nyquist WE, Cervantes-Martínez CT, Janick J. 2003. Estimating and interpreting heritability for plant breeding: an update. Plant breeding reviews 22.

Huang BE, George AW, Forrest KL, Kilian A, Hayden MJ, Morell MK, Cavanagh CR. 2012. A multiparent advanced generation inter-cross population for genetic analysis in wheat. Plant Biotechnology Journal 10, 826-39.

Hunter MC, Smith RG, Schipanski ME, Atwood LW, Mortensen DA. 2017. Agriculture in 2050: Recalibrating targets for sustainable intensification. BioScience 67, 386-91.

Joynson R, Molero G, Coombes B, Gardiner L-J, Rivera-Amado C, Piñera-Chávez FJ, Evans JR, Furbank RT, Reynolds MP, Hall A. 2021. Uncovering candidate genes involved in photosynthetic capacity using unexplored genetic variation in Spring Wheat. Plant Biotechnology Journal 19, 1537-52.

Keller B, Soto J, Steier A, Portilla-Benavides AE, Raatz B, Studer B, Walter A, Muller O, Urban MO. 2024. Linking photosynthesis and yield reveals a strategy to improve light use efficiency in a climbing bean breeding population. Journal of Experimental Botany 75, 901-16.

Kono M, Terashima I. 2014. Long-term and short-term responses of the photosynthetic electron transport to fluctuating light. Journal of Photochemistry and Photobiology B: Biology 137, 89-99.

Křen J, Klem K, Svobodová I, Míša P, Neudert L. 2014. Yield and grain quality of spring barley as affected by biomass formation at early growth stages.

Kromdijk J, Głowacka K, Leonelli L, Gabilly ST, Iwai M, Niyogi KK, Long SP. 2016. Improving photosynthesis and crop productivity by accelerating recovery from photoprotection. Science 354, 857-61.

Kromdijk J, Long SP. 2016. One crop breeding cycle from starvation? How engineering crop photosynthesis for rising CO2 and temperature could be one important route to alleviation. Proceedings of the Royal Society B: Biological Sciences 283.

Kuhlgert S, Austic G, Zegarac R, Osei-Bonsu I, Hoh D, Chilvers MI, Roth MG, Bi K, TerAvest D, Weebadde P, Kramer DM. 2016. MultispeQ Beta: A tool for large-scale plant phenotyping connected to the open photosynQ network. Royal Society Open Science 3.

Lapasiya T, Gao Y, Wu P-Y, Haweit A, van Inghelandt D, Stich B, Shrestha A. 2025. Genetic architecture and cellular basis of flag leaf size in barley. Journal of Experimental Botany, eraf487.

Liu L, Sun G, Ren X, Li C, Sun D. 2015. Identification of QTL underlying physiological and morphological traits of flag leaf in barley. BMC Genetics 16, 1-10.

Liu X, Fan Y, Mak M, Babla M, Holford P, Wang F, Chen G, Scott G, Wang G, Shabala S,

Zhou M, Chen ZH. 2017. QTLs for stomatal and photosynthetic traits related to salinity tolerance in barley. BMC Genomics 18, 1-13.

Long SP, Ainsworth EA, Leakey ADB, Nösbsrger J, Ort DR. 2006a. Food for thought: Lower-than-expected crop yield stimulation with rising CO2 concentrations. Science 312, 1918-21.

Long SP, Taylor SH, Burgess SJ, Carmo-Silva E, Lawson T, De Souza AP, Leonelli L, Wang Y. 2022. Into the shadows and back into sunlight: photosynthesis in fluctuating light. Annual review of plant biology 73, 617-48.

Long SP, Zhu XG, Naidu SL, Ort DR. 2006b. Can improvement in photosynthesis increase crop yields? Plant, Cell and Environment 29, 315-30.

Maydup ML, Antonietta M, Guiamet JJ, Graciano C, López JR, Tambussi EA. 2010. The contribution of ear photosynthesis to grain filling in bread wheat (Triticum aestivum L.). Field crops research 119, 48-58.

Meuwissen TH, Hayes BJ, Goddard M. 2001. Prediction of total genetic value using genome-wide dense marker maps. genetics 157, 1819-29.

Millet EJ, Kruijer W, Coupel-Ledru A, Prado SA, Cabrera-Bosquet L, Lacube S, Charcosset A, Welcker C, Eeuwijk Fv, Tardieu F. 2019. Genomic prediction of maize yield across European environmental conditions. Nature genetics 51, 952-56.

Obsa BT, Eglinton J, Coventry S, March T, Langridge P, Fleury D. 2016. Genetic analysis of developmental and adaptive traits in three doubled haploid populations of barley (Hordeum vulgare L.). Theoretical and Applied Genetics 129, 1139-51.

Ogren E. 1993. Convexity of the Photosynthetic Light-Response Curve in Relation to lntensity and Direction of Light during Growth '. Plant Physiology, 1013-19.

Ortiz D, Hu J, Salas Fernandez MG. 2017. Genetic architecture of photosynthesis in Sorghum bicolor under non-stress and cold stress conditions. Journal of experimental botany 68, 4545-57.

Paul MJ, Foyer CH. 2001. Sink regulation of photosynthesis. Journal of experimental botany 52, 1383-400.

Piepho HP, Möhring J. 2007. Computing heritability and selection response from unbalanced plant breeding trials. Genetics 177, 1881-88.

Piepho HP, Möhring J, Schulz-Streeck T, Ogutu JO. 2012. A stage-wise approach for the analysis of multi-environment trials. Biometrical Journal 54, 844-60.

Prado SA, Gallardo JM, Serrago RA, Kruk BC, Miralles DJ. 2013. Comparative behavior of wheat and barley associated with field release and grain weight determination. Field Crops Research 144, 28-33.

Prosekov AY, Ivanova SA. 2018. Food security: The challenge of the present. Geoforum 91, 73-77.

Rotasperti L, Tadini L, Chiara M, Crosatti C, Guerra D, Tagliani A, Forlani S, Ezquer I, Horner DS, Jahns P, others. 2022. The barley mutant happy under the sun 1 (hus1): an additional contribution to pale green crops. Environmental and Experimental Botany 196,

104795.

Salter WT, Li S, Dracatos PM, Barbour MM. 2020. Identification of quantitative trait loci for dynamic and steady-state photosynthetic traits in a barley mapping population. AoB PLANTS 12, 1-10.

Sanchez-Bragado R, Elazab A, Zhou B, Serret MD, Bort J, Nieto-Taladriz MT, Araus JL. 2014. Contribution of the ear and the flag leaf to grain filling in durum wheat inferred from the carbon isotope signature: genotypic and growing conditions effects. Journal of integrative plant biology 56, 444-54.

Sanchez-Bragado R, Vicente R, Molero G, Serret MD, Maydup ML, Araus JL. 2020. New avenues for increasing yield and stability in C3 cereals: exploring ear photosynthesis. Current Opinion in Plant Biology 56, 223-34.

Sannemann W, Huang BE, Mathew B, Léon J. 2015. Multi-parent advanced generation inter-cross in barley: high-resolution quantitative trait locus mapping for flowering time as a proof of concept. Molecular Breeding 35.

Scott MF, Ladejobi O, Amer S, Bentley AR, Biernaskie J, Boden SA, Clark M, Dell'Acqua M, Dixon LE, Filippi CV, Fradgley N, Gardner KA, Mackay IJ, O'Sullivan D, Percival-Alwyn L, Roorkiwal M, Singh RK, Thudi M, Varshney RK, Venturini L, Whan A, Cockram J, Mott R. 2020. Multi-parent populations in crops: a toolbox integrating genomics and genetic mapping with breeding. Heredity 125, 396-416.

Shrestha A, Cosenza F, Inghelandt Dv, Wu PY, Li J, Casale FA, Weisweiler M, Stich B. 2022. The double round-robin population unravels the genetic architecture of grain size in barley. Journal of Experimental Botany 73, 7344-61.

Simkin AJ, López-Calcagno PE, Raines CA. 2019. Feeding the world: improving photosynthetic efficiency for sustainable crop production. Journal of Experimental Botany 70, 1119-40.

Stich B. 2009. Comparison of mating designs for establishing nested association mapping populations in maize and Arabidopsis thaliana. Genetics 183, 1525-34.

Sun J, Poland JA, Mondal S, Crossa J, Juliana P, Singh RP, Rutkoski JE, Jannink J-L, Crespo-Herrera L, Velu G. 2019. High-throughput phenotyping platforms enhance genomic selection for wheat grain yield across populations and cycles in early stage. Theoretical and Applied Genetics 132, 1705-20.

Theeuwen TPJM, Logie LL, Harbinson J, Aarts MGM. 2022. Genetics as a key to improving crop photosynthesis. Journal of Experimental Botany 73, 3122-37.

Thirulogachandar V, Schnurbusch T. 2021. 'Spikelet stop'determines the maximum yield potential stage in barley. Journal of Experimental Botany 72, 7743-53.

Tyagi AK, Gaur T. 2003. Light Regulation of Nuclear Photosynthetic Genes in Higher Plants. Critical Reviews in Plant Sciences 22, 417-52.

van Bezouw RFHM, Keurentjes JJB, Harbinson J, Aarts MGM. 2019. Converging phenomics and genomics to study natural variation in plant photosynthetic efficiency. The Plant Journal 97, 112-33.

VanRaden PM. 2008. Efficient methods to compute genomic predictions. Journal of dairy science

91, 4414-23.

Vialet-Chabrand S, Matthews JSA, Simkin AJ, Raines CA, Lawson T. 2017. Importance of fluctuations in light on plant photosynthetic acclimation. Plant Physiology 173, 2163-79.

Wang Z, Wang S, Yu C, Han X, Zou D. 2020. QTL analysis of rice photosynthesis-related traits under the cold stress across multi-environments. Euphytica 216, 116.

Weisweiler M, Montaigu AD, Ries D, Pfeifer M, Stich B. 2019. Transcriptomic and presence/absence variation in the barley genome assessed from multi-tissue mRNA sequencing and their power to predict phenotypic traits. BMC Genomics 20, 1-15.

Wingler A, Marès M, Pourtau N. 2004. Spatial patterns and metabolic regulation of photosynthetic parameters during leaf senescence. New Phytologist 161, 781-89.

Yamasaki T, Yamakawa T, Yamane Y, Koike H, Satoh K, Katoh S. 2002. Temperature acclimation of photosynthesis and related changes in photosystem II electron transport in winter wheat. Plant Physiology 128, 1087-97.

Yin X, Gu J, Dingkuhn M, Struik PC. 2022. A model-guided holistic review of exploiting natural variation of photosynthesis traits in crop improvement. Journal of Experimental Botany 73, 3173-88.

Zadoks JC, Chang TT, Konzak CF. 1974. A decimal code for the growth stages of cereals. Weed Research 14, 415-21.

Zhu XG, Long SP, Ort DR. 2010. Improving photosynthetic efficiency for greater yield. Annual Review of Plant Biology 61, 235-61.

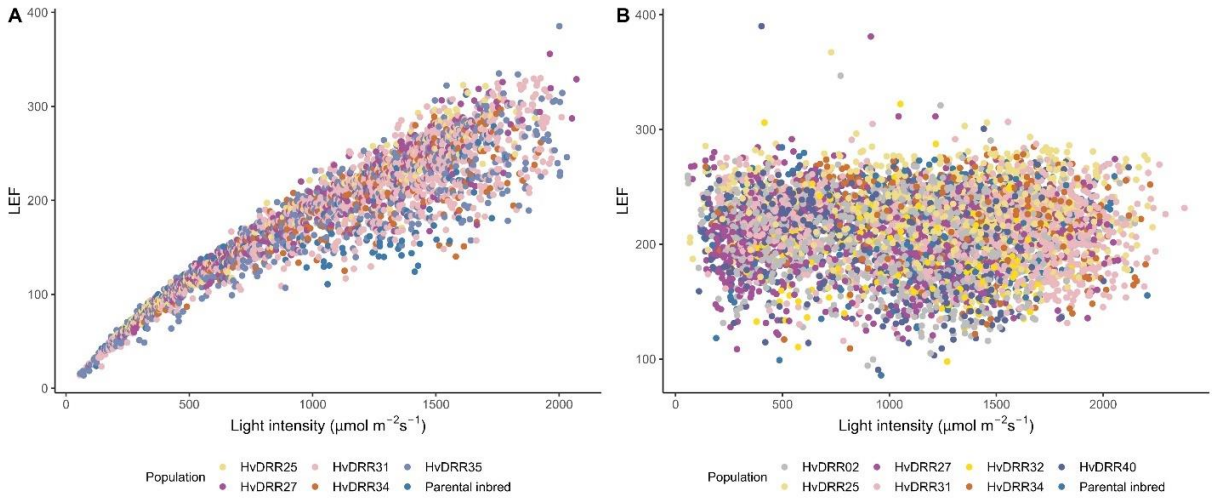

Fig. 1 Linear electron flow (LEF) for the ten barley parental inbred lines (gray dots) and the derived recombinant inbred lines in relation to changing ambient light intensity in field experiments in Year 2021 (dataset Y21, A) and Year 2022 (dataset Y22, B). The different colors represent the different genetic material groups.

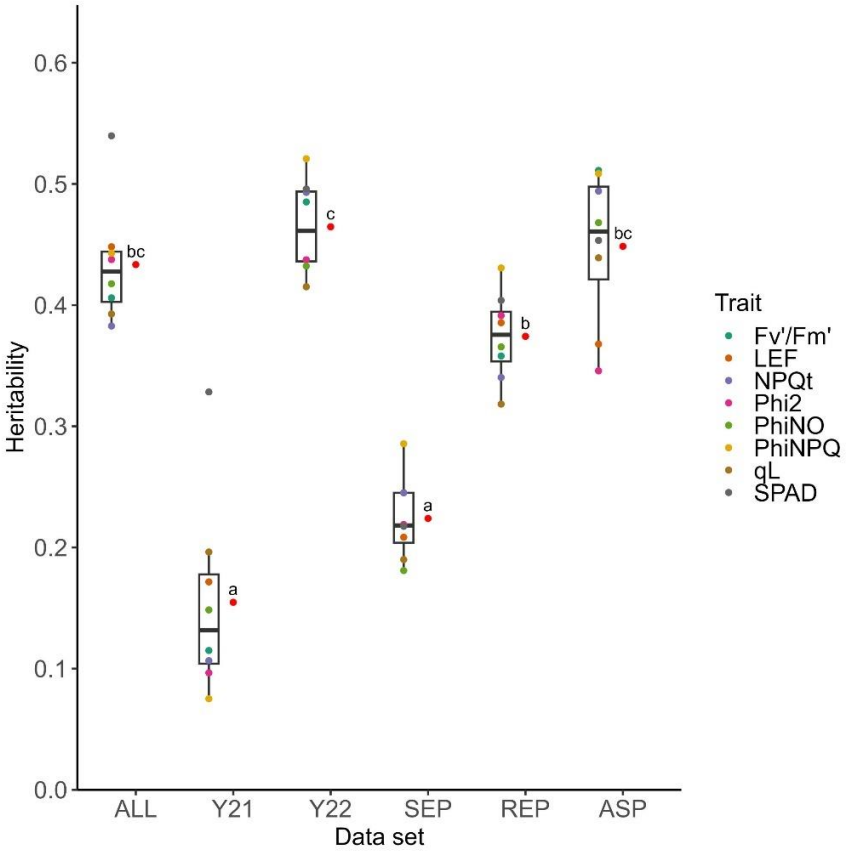

Fig. 2 Heritability of photosystem II parameters and SPAD in different data sets. Y21: experiment in year 2021; Y22: experiment in year 2022; SEP: slow expansion phase (Zadoks score (ZS) from 10 to 29); REP: rapid expansion phase (ZS from 30 to 59); ASP: anthesis and senescence phase (ZS from 60 to 87). The red point next to each box plot indicates the mean heritability across all traits for each data set. Different letters next to each box plot indicate significant differences based on Tukey-test ($P < 0.05$) among the mean heritabilities.

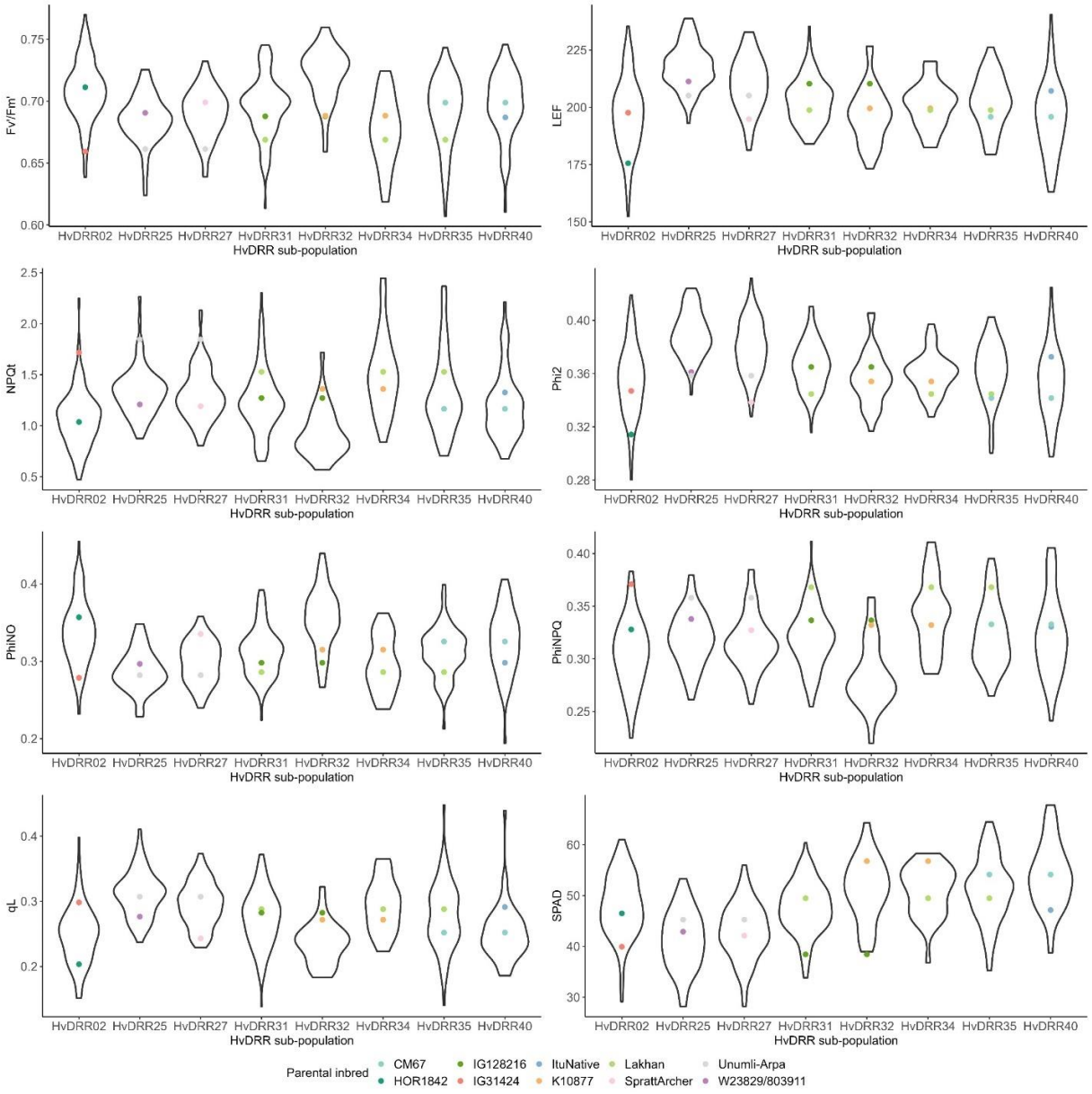

Fig. 3 Violin plots of adjusted entry means of the photosynthesis-related parameters of each HvDRR sub-population of the data set ALL. The colored points represent the adjusted entry means of the parental inbreds of the corresponding sub-population.

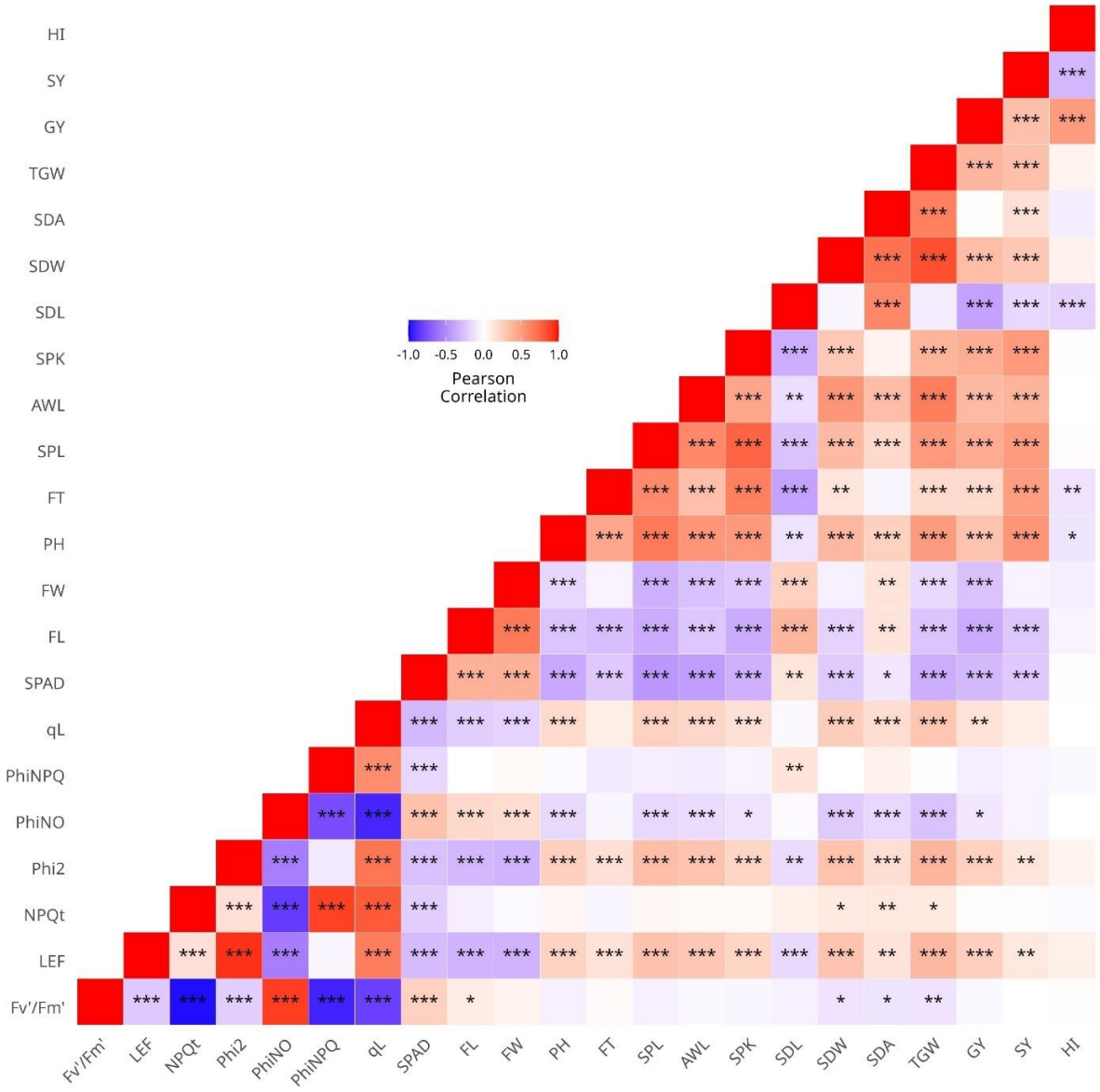

Fig. 4 Pearson correlation coefficients calculated between pairs of adjusted entry means across all barley recombinant inbred lines for the photosynthesis-related parameters from the ALL data set, and the agronomic traits collected in multi-year and –environment field experiments. Flag leaf length (FL), flag leaf width (FW), plant height (PH), flowering time (FT), spike length (SPL), awn length (AWL), spikelet number per row (SPK), seed length (SD), seed width (SDW), seed area (SDA), thousand grain weight (TGW), grain yield (GY), straw yield (SY), and harvest index (HI). Asterisks indicate the significance level (***, **, * indicated P < 0.001, 0.01, 0.05 respectively).

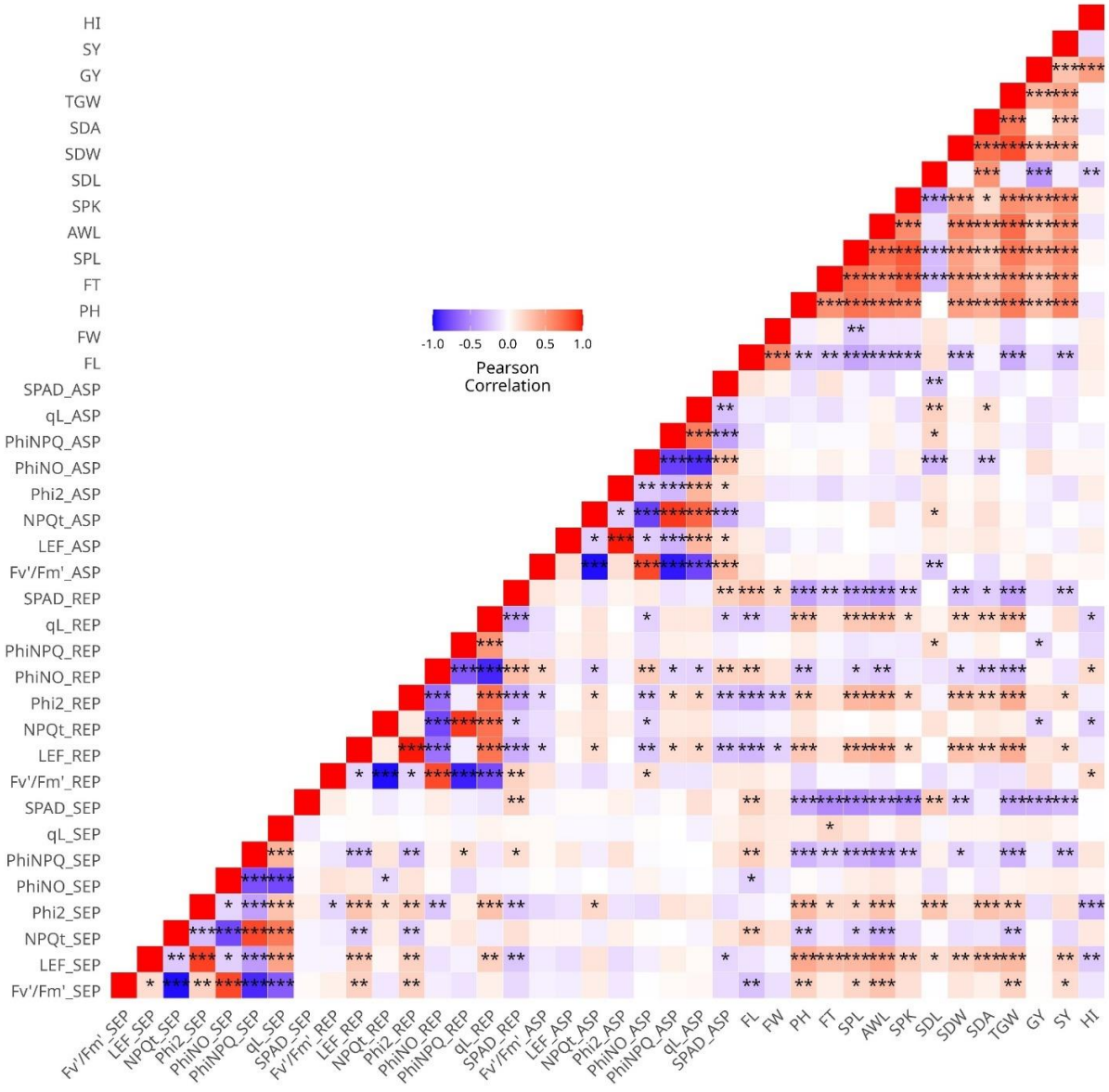

Fig. 5 Pearson correlation coefficients calculated between pairs of adjusted entry means across all barley recombinant inbred lines for the photosynthesis-related parameters of three developmental phases in the two-year experiments, and the agronomic traits collected in multi-year and –environment field experiments. For abbreviations of the agronomic traits, see Fig. 4 legend. Asterisks indicate the significance level (***, **, * indicated P < 0.001, 0.01, 0.05 respectively).

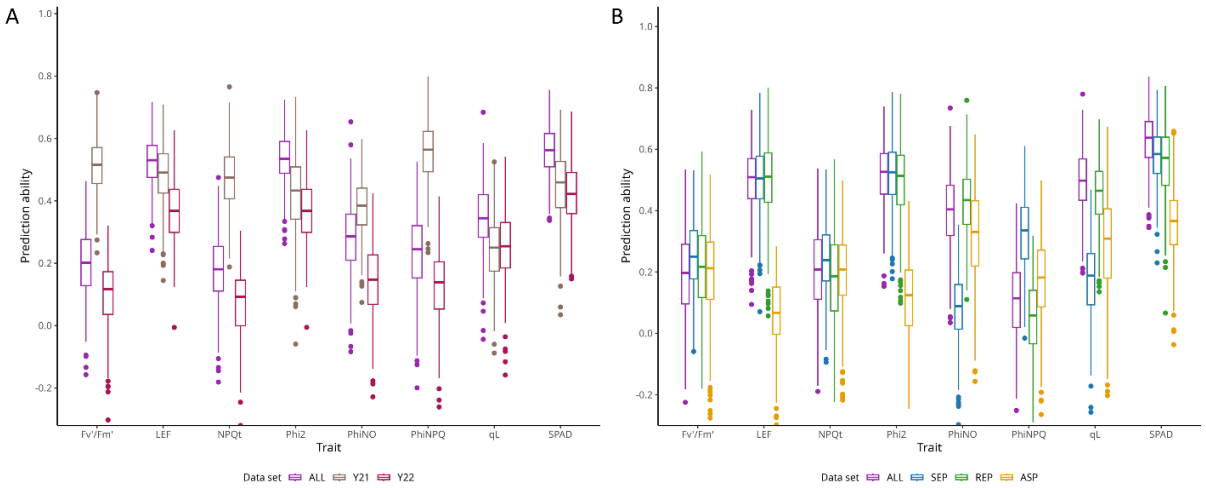

Fig. 6 Prediction abilities of the photosynthesis-related parameters. A. Prediction abilities across different years. Y21 and Y22 represent the adjusted entry means calculated from the experiment from year 2021 and 2022, respectively. ALL represents the adjusted entry means calculated from the combined datasets Y21 and Y22. The prediction ability was calculated by using five-fold cross-validation with 100 replications. B. Prediction abilities across different developmental phases. SEP, REP, and ASP represent the adjusted entry means calculated from the measurements taken in slow expansion phase, rapid expansion phase, and anthesis and senescence phase, respectively. The common 199 genotypes across the three data sets were used for five-fold cross-validation with 100 replications. ALL represents the adjusted entry means calculated from the combined datasets of the three developmental phases.

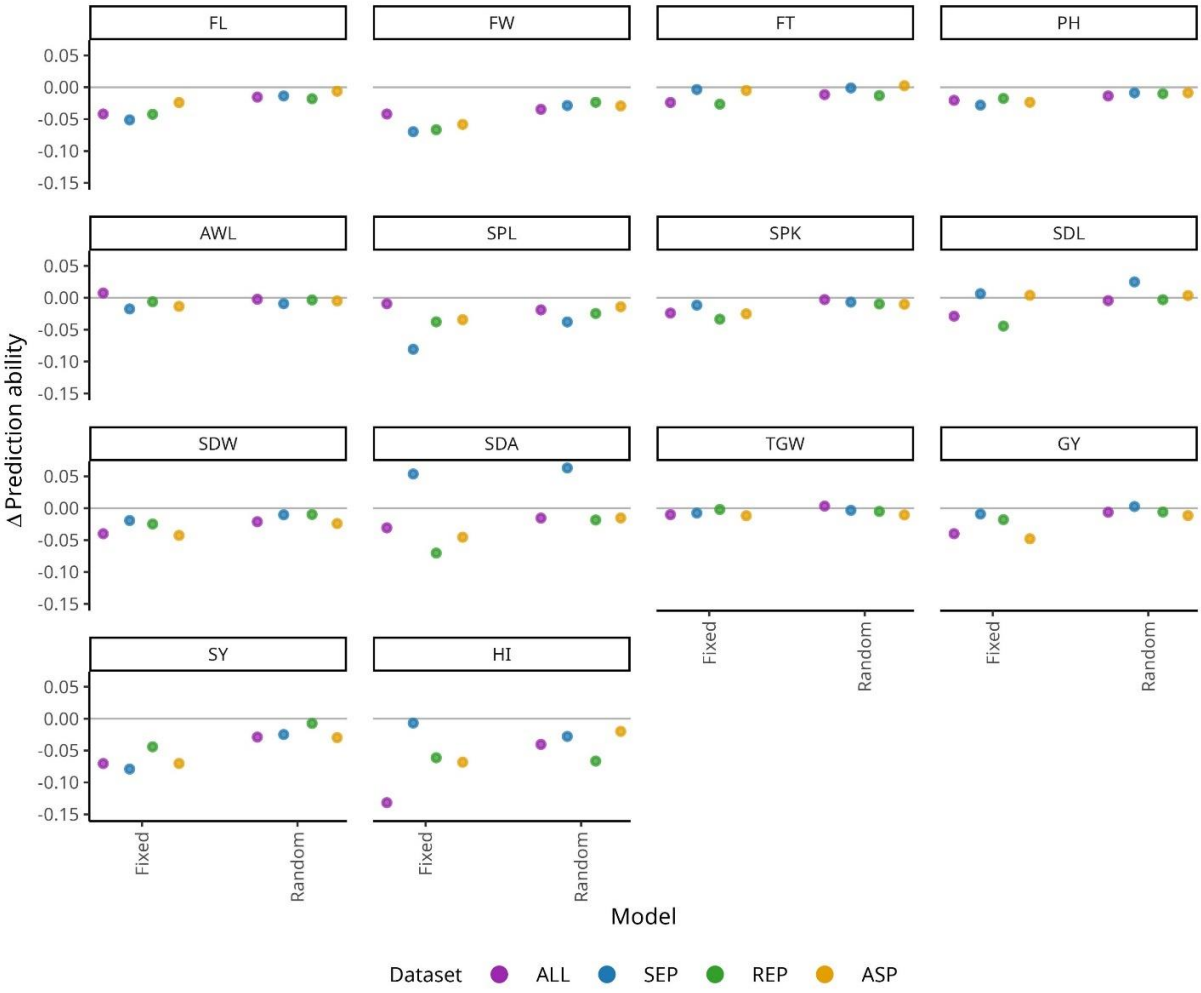

Fig. 7 Difference in the prediction ability between a GBLUP model in which photosynthesis-related parameters were considered as fixed or random effects together with a SNP based relationship matrix compared to a model which only relied on SNP data. SEP, REP, and ASP represent the adjusted entry means calculated from the measurements taken in slow expansion phase, rapid expansion phase, and anthesis and senescence phase, respectively.

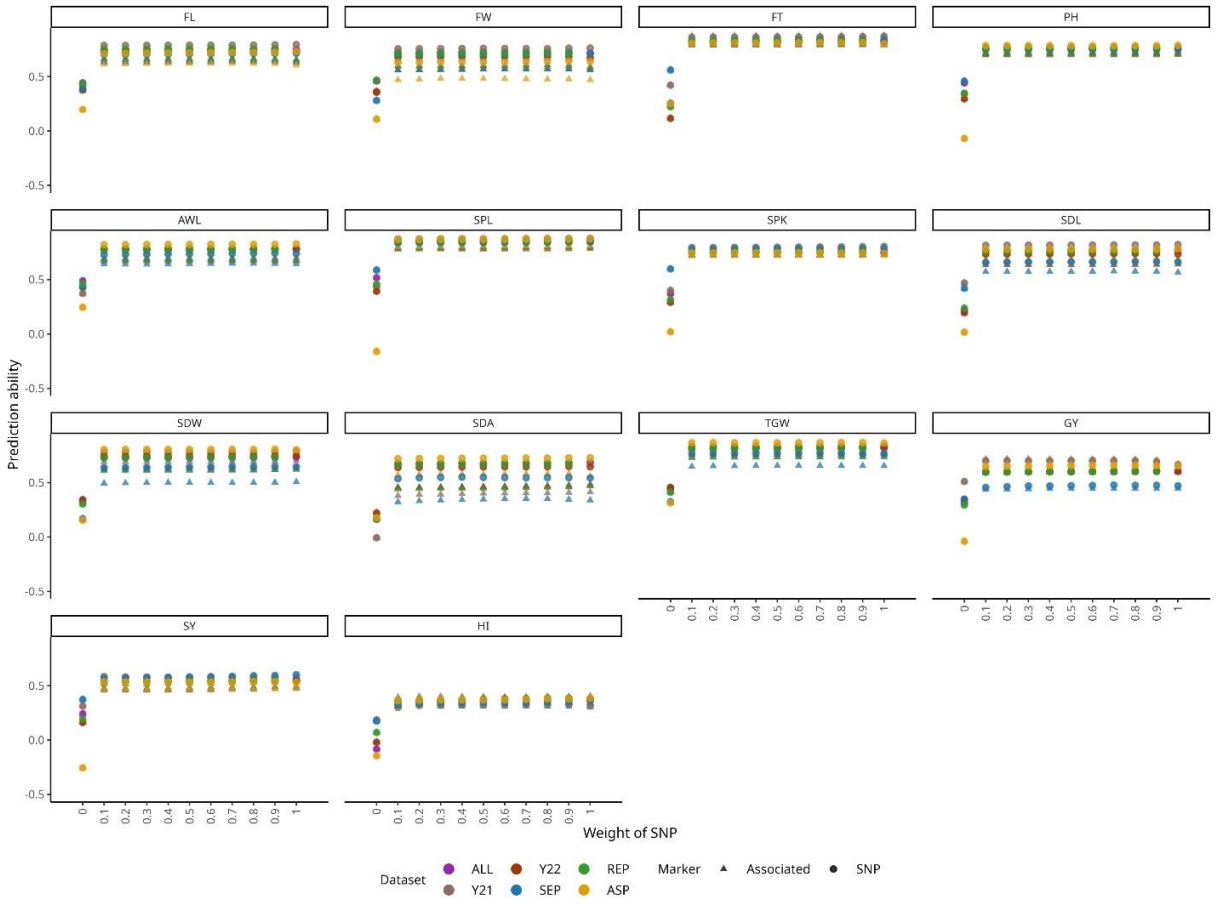

Fig. 8 Prediction abilities of the agronomic traits using SNPs, the photosynthesis-related parameters, or joined relationship matrices. Flag leaf length (FL), flag leaf width (FW), plant height (PH), flowering time (FT), spike length (SPL), awn length (AWL), spikelet number per row (SPK), seed length (SD), seed width (SDW), seed area (SDA), thousand grain weight (TGW), grain yield (GY), straw yield (SY), and harvest index (HI). The different colors represent the adjusted entry mean of the photosynthesis-related parameters from different data sets. The triangles show the prediction abilities using the 62 associated SNP markers to calculate the joint weighted relationship matrix. The circles show the prediction abilities using all genome-wide SNP markers to calculate the joint weighted relationship matrix.

Table 1: Variance components and broad-sense heritability (H^2) for photosystem II related parameters and SPAD measured in the field experiments by using the entire data set (ALL), where σ^2_G is genotypic variance; $\sigma^2_{G_{checks}:E}$ the variance component of the interaction between parental inbreds (as checks) and location; $\sigma^2_{ZS:E}$ the variance component of the Zadok's score nested in location; σ^2_D the variance component of date of measurement, $\sigma^2_{E:B}$ the variance component of block effects nested within location, $\sigma^2_{E:B:R}$ variance component of range nested within the block in location, $\sigma^2_{E:B:C}$ the variance component of row nested within the block in location, σ^2_ϵ the variance component of residual, and H^2 the heritability.

Note that the values of variance components of six photosynthesis-related parameters (Phi2, Fv'/Fm', PhiNO, PhiNPQ, NPQt, and qL) were multiplied with 1000.

Data set	Trait	σ^2_G	$\sigma^2_{G_{checks}:E}$	$\sigma^2_{ZS:E}$	σ^2_D	$\sigma^2_{TW:D}$	$\sigma^2_{B:E}$	$\sigma^2_{R:B:E}$	$\sigma^2_{C:B:E}$	σ^2_ϵ	H^2
ALL	Fv'/Fm'	0.232***	0.567***	0.157***	1.076***	0.116***	0.247	0.017*	0.021**	2.880	0.395
ALL	LEF	54.915***	205.646***	23.119***	82.108***	43.075***	110.083*	1.716	8.769***	697.578	0.394
ALL	NPQt	36.602***	122.781***	29.018***	155.362***	21.627***	27.136	2.635*	2.852*	496.880	0.372
ALL	Phi2	0.198***	1.525***	0.067***	0.511***	0.187***	0.756***	0.001	0.025**	2.149	0.433
ALL	PhiNO	0.475***	0.278	0.213***	1.424***	0.369***	0.009	0.034*	0.037**	5.638	0.414
ALL	PhiNPQ	0.398***	2.392***	0.155***	2.512***	0.184***	1.615***	0.041***	0.029*	4.263	0.429
ALL	qL	0.666***	0.859**	0.634***	1.103***	0.446***	0.328	0.018	0.089***	8.499	0.393
ALL	SPAD	18.810***	17.962***	5.283***	49.279***	3.747***	0.000	1.441***	2.441***	117.129	0.540

Table 2: Coefficients of variation (Cov) across all eight HvDRR sub-populations and the ten parental inbreds for the photosynthesis-related parameters.

Population	Fv'/Fm'	LEF	NPQt	Phi2	PhiNO	PhiNPQ	qL	SPAD
HvDRR02	3.214	8.142	24.587	7.229	12.033	10.020	16.515	12.477
HvDRR25	2.690	5.349	17.631	4.189	9.024	7.607	10.834	13.576
HvDRR27	2.768	5.122	19.269	5.230	8.768	8.403	11.086	12.508
HvDRR31	3.401	6.056	25.517	4.769	9.837	8.682	15.218	10.520
HvDRR32	3.019	6.418	26.622	5.391	11.410	11.351	13.348	11.649
HvDRR34	3.905	5.773	25.199	4.095	11.482	9.721	13.140	9.449
HvDRR35	3.922	6.802	29.871	5.816	9.835	9.601	17.740	12.288
HvDRR40	3.767	7.988	27.200	7.098	12.777	11.909	16.364	11.575
Parental inbreds	2.479	5.237	19.366	4.640	8.138	5.053	11.105	12.672

Supplementary materials

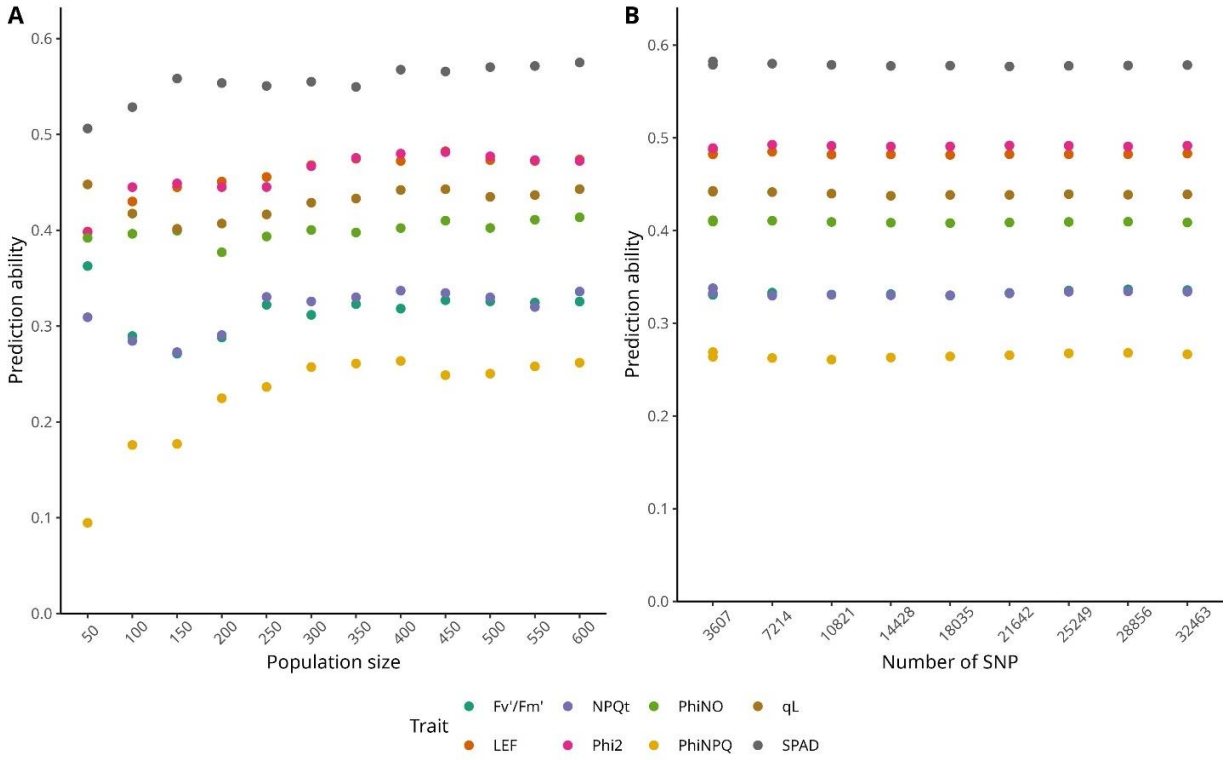

Supplementary Fig. S1 A. The prediction ability of each photosynthesis-related parameter from five-fold cross validation by using different population sizes. The size of the population was varied between 50 and 600 RILs, in increments of 50 RILs. B. The prediction ability of each photosynthesis-related parameters from five-fold cross validation by using different number of SNPs.

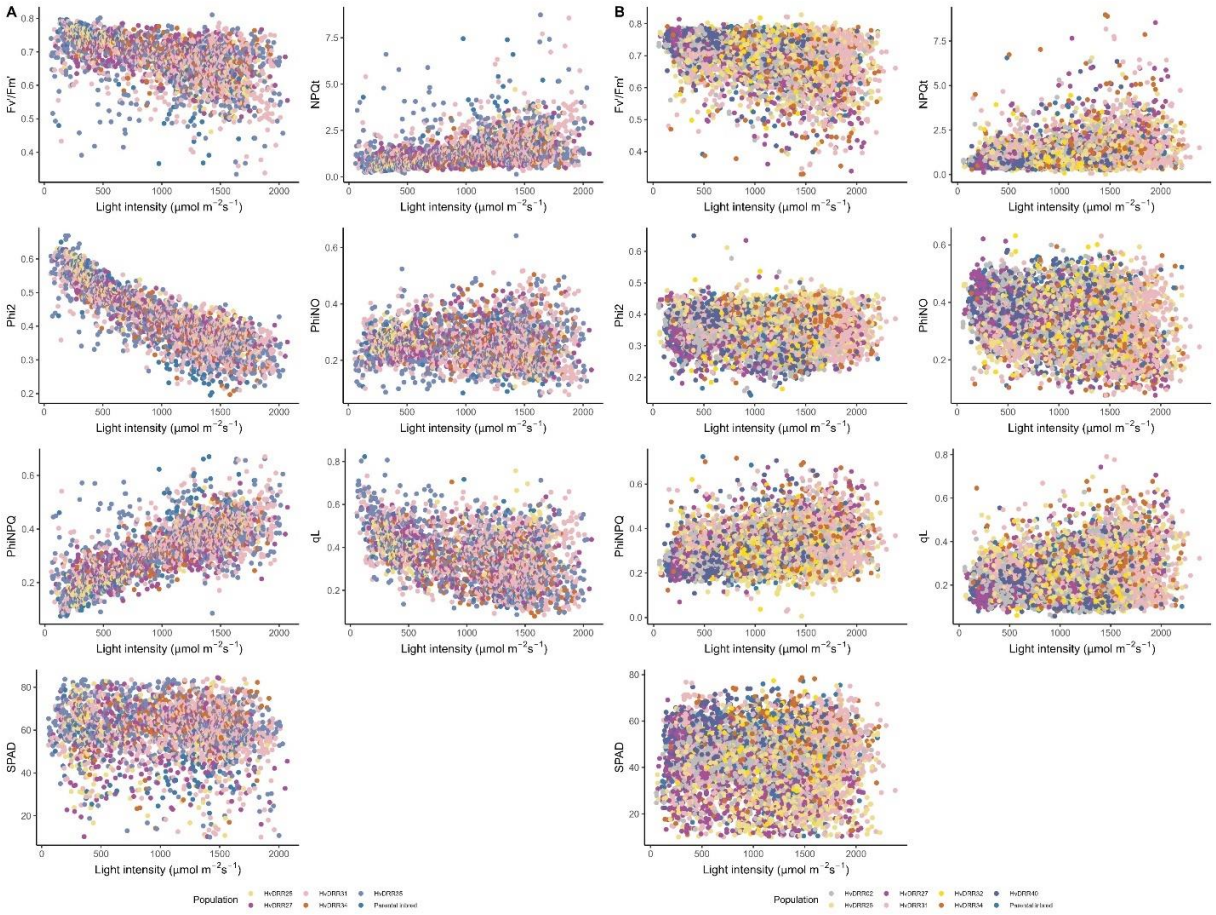

Supplementary Fig. S2 Photosynthesis-related parameters for ten barley parental inbred lines (gray dots) and the derived recombinant inbred lines in relation to ambient light intensity in field experiments. A. Year 2021. B. Year 2022. The different colors of the dots represent the different HvDRR sub-populations and the parental inbreds.

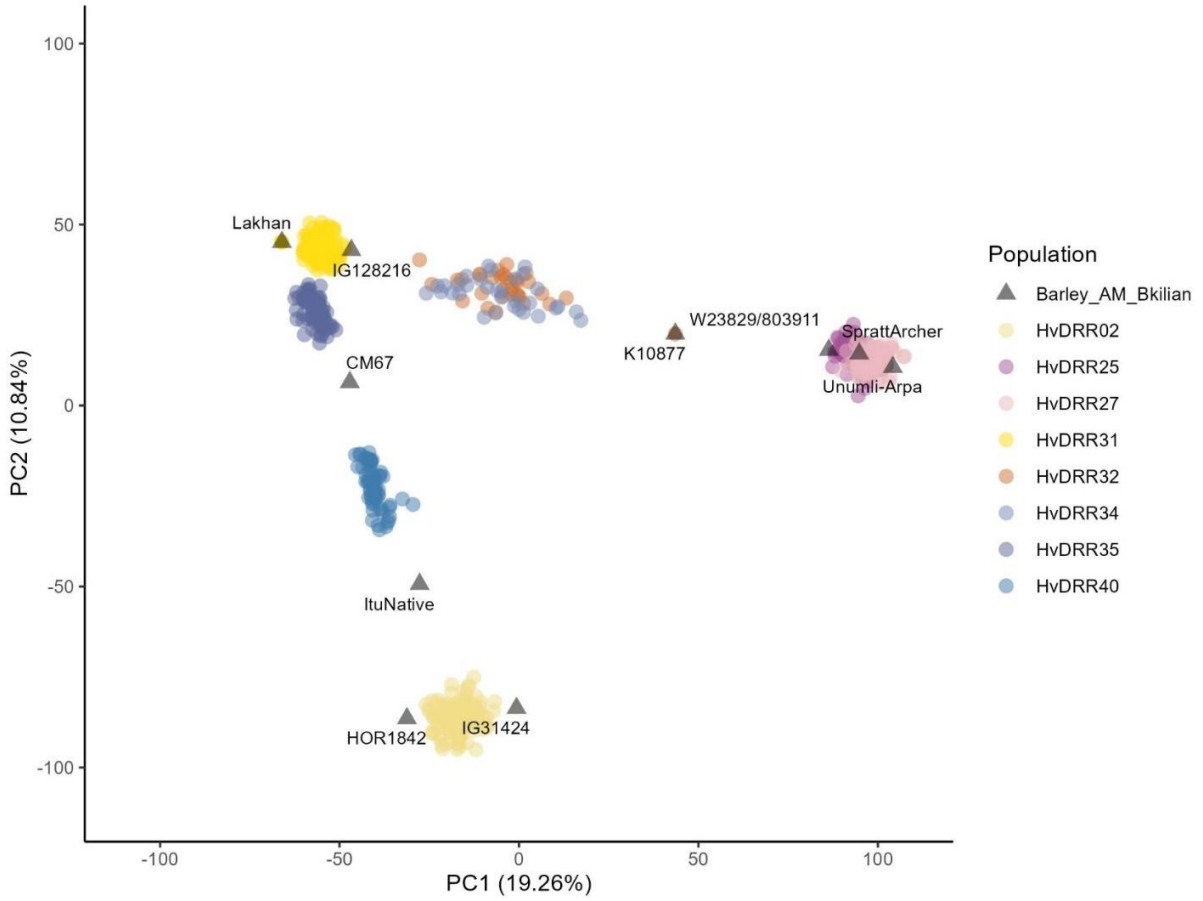

Supplementary Fig. S3 Principal coordinate analysis of the HvDRR populations of barley and their parental inbreds based on 36 077 SNP markers. PC1 and PC2 are the first and second principal coordinate, respectively. Numbers in parentheses refer to the proportion of variance explained by the principal coordinate.

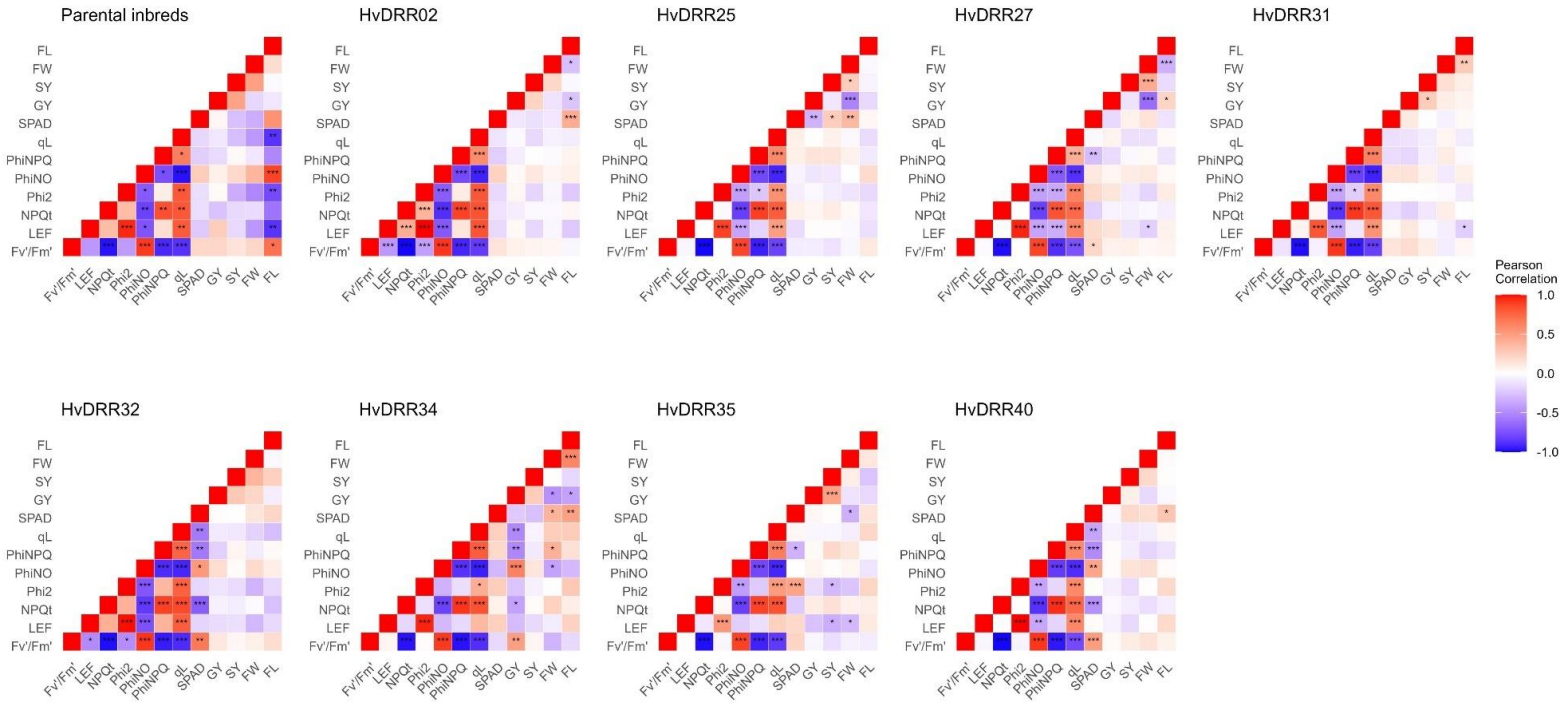

Supplementary Fig. S4 Pearson correlation coefficients calculated between pairs of adjusted entry means of the photosynthesis-related parameters and some agronomic traits for each HvDRR sub-population and the ten parental inbreds. The photosynthesis-related parameters are from the ALL data set. Grain yield (GY), straw yield (SY), flag leaf length (FL), and flag leaf width (FW) were collected from the multi-year and -environment field experiments. Asterisks indicate the significance level (***, **, * indicated $P < 0.001$, 0.01, 0.05 respectively).

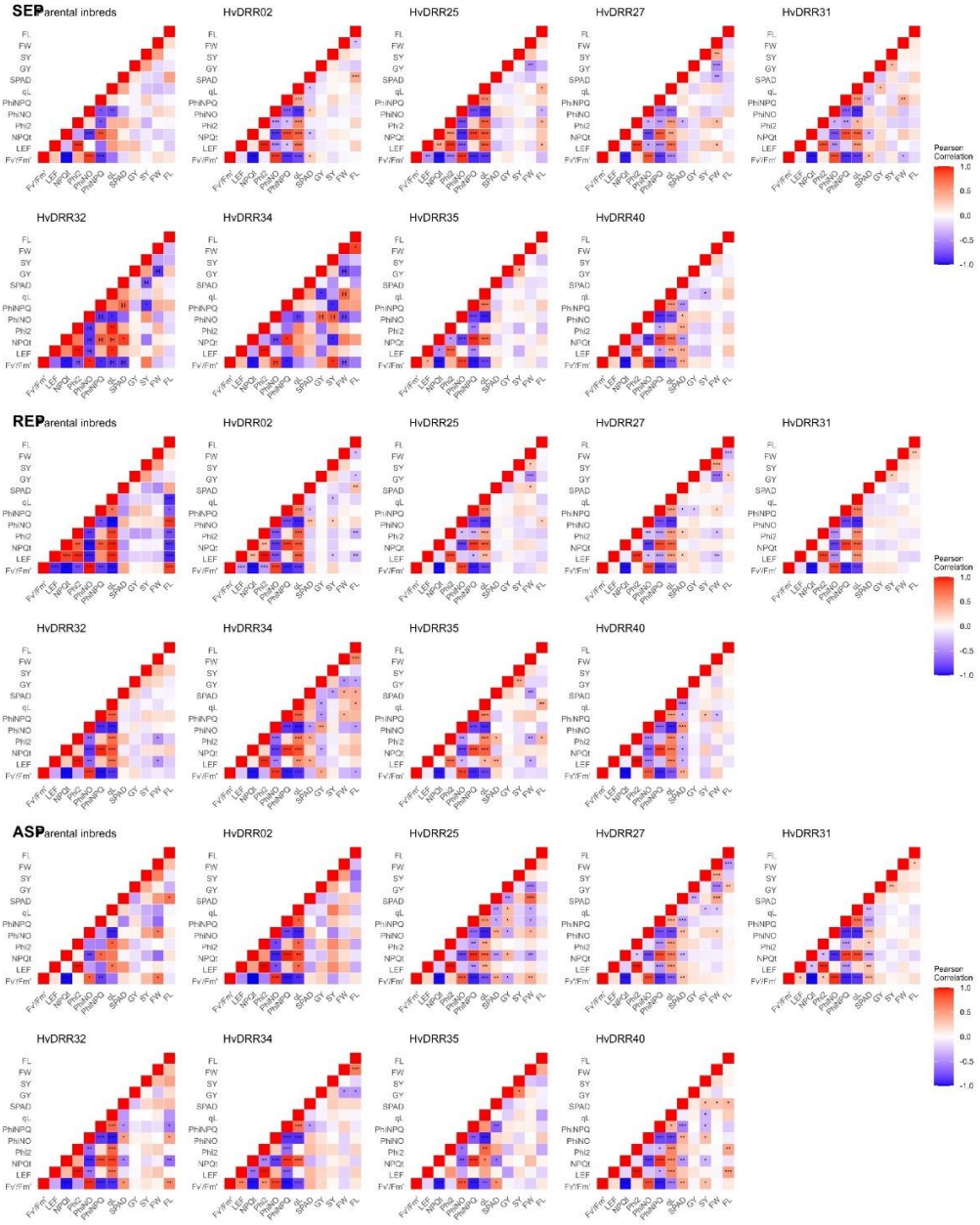

Supplementary Fig. S5 Pearson correlation coefficients calculated between pairs of adjusted entry means of the photosynthesis-related parameters and some agronomic traits for each HvDRR sub-population and the ten parental inbreds. The photosynthesis-related parameters are from slow expansion phase (SEP), rapid expansion phase (REP), and anthesis and senescence (ASP). Grain yield (GY), straw yield (SY), flag leaf length (FL), and flag leaf width (FW) were collected from the multi-year and -environment field experiments. Asterisks indicate the significance level (***, **, * indicated $P < 0.001$, 0.01, 0.05 respectively).

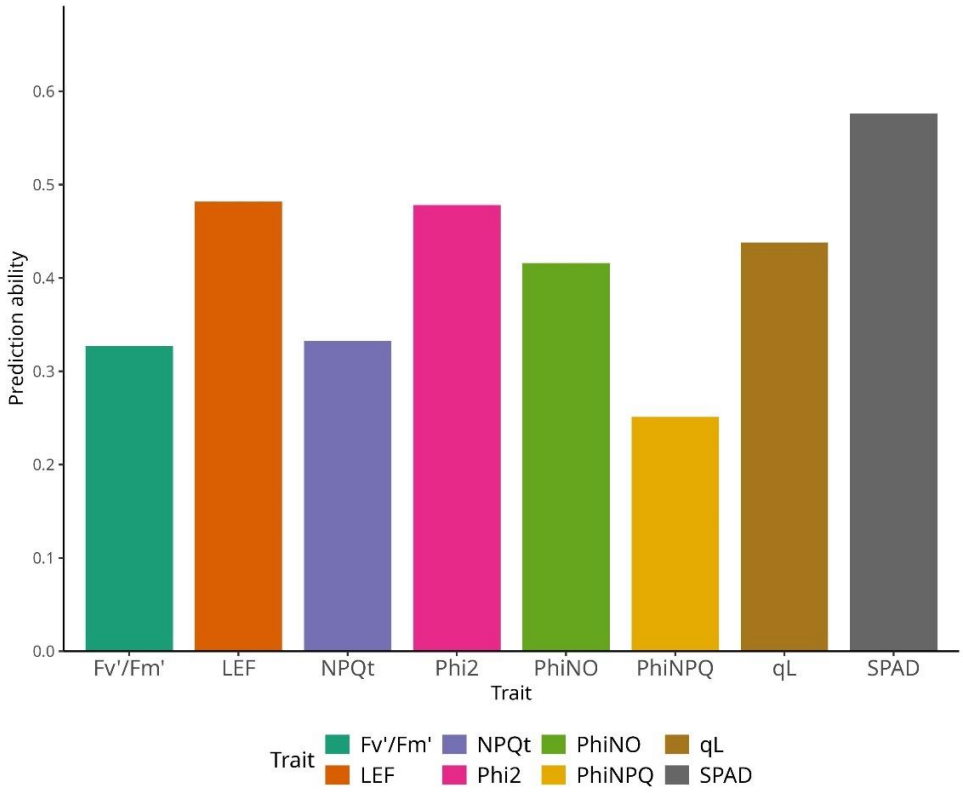

Supplementary Fig. S6 Prediction abilities of the photosynthesis-related parameters across two years for data set ALL. The prediction ability was calculated as median across five-fold cross-validation with 100 replications.

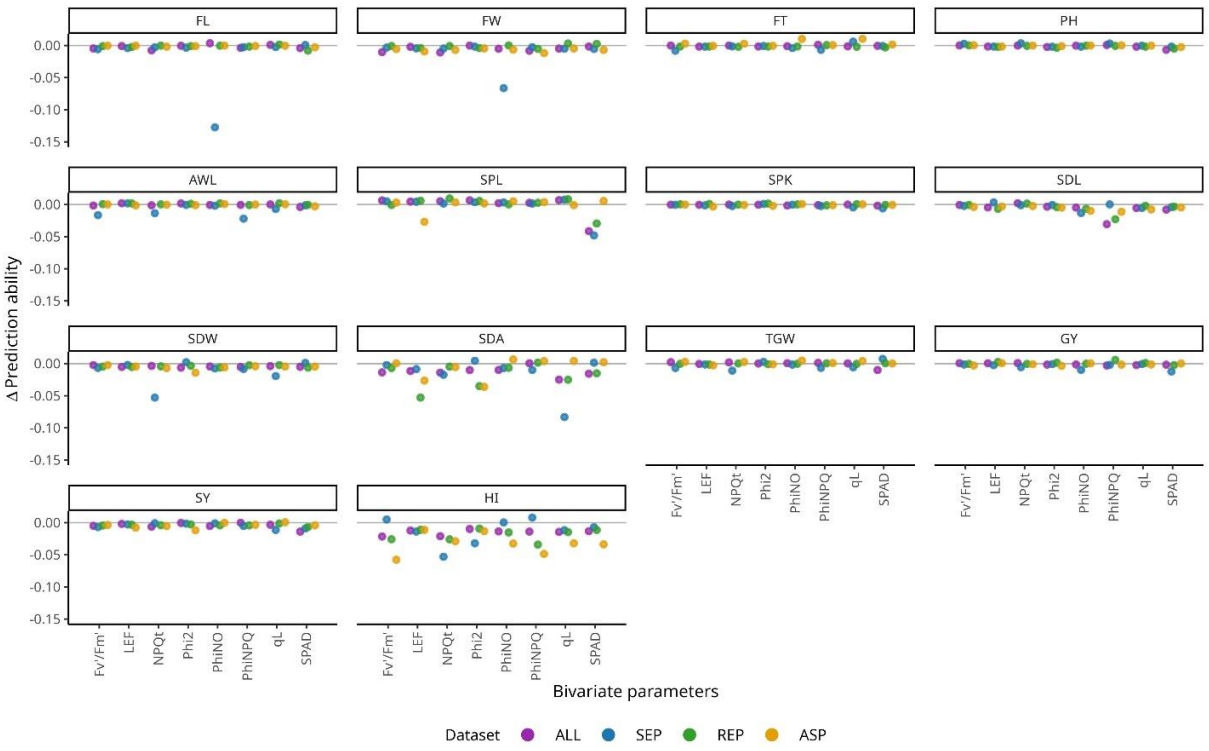

Supplementary Fig. S7 Difference in the prediction ability for the agronomic traits of the bivariate model compared to the univariate model. SEP, REP, and ASP represent the adjusted entry mean calculated from the measurements taken in slow expansion phase, rapid expansion phase, and anthesis and senescence phase, respectively. The considered agronomic traits are: flag leaf length (FL), flag leaf width (FW), flowering time (FT), plant height (PH), awn length (AWL), spike length (SPL), spikelet number per row (SPK), seed length (SDL), seed width (SDW), seed area (SDA), thousand grain weight (TGW), grain yield (GY), straw yield (SY), and harvest index (HI).

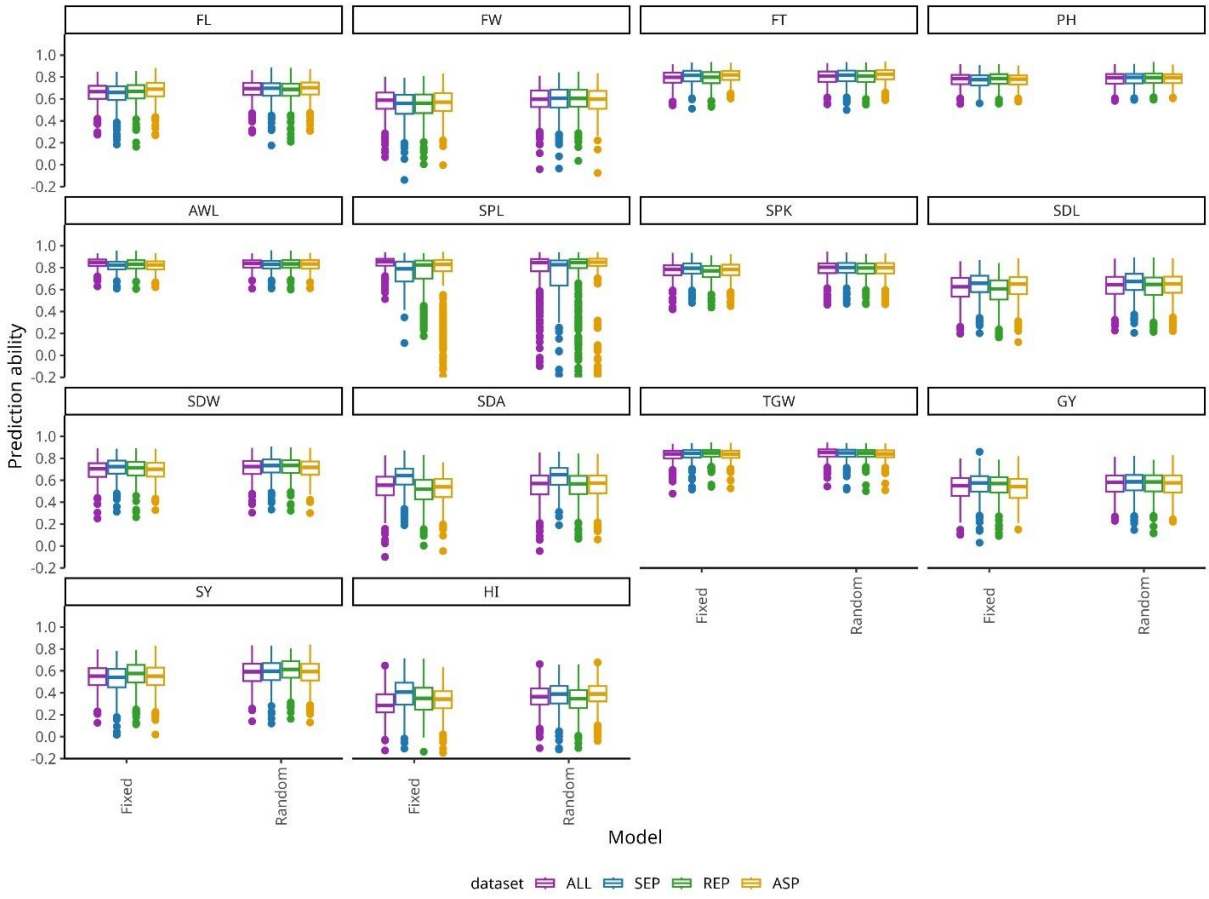

Supplementary Fig. S8 The prediction ability of GBLUP model by adding photosynthesis-related parameters as fixed or random effects. SEP, REP, and ASP represent the adjusted entry means calculated from the measurements taken in slow expansion phase, rapid expansion phase, and anthesis and senescence phase, respectively.

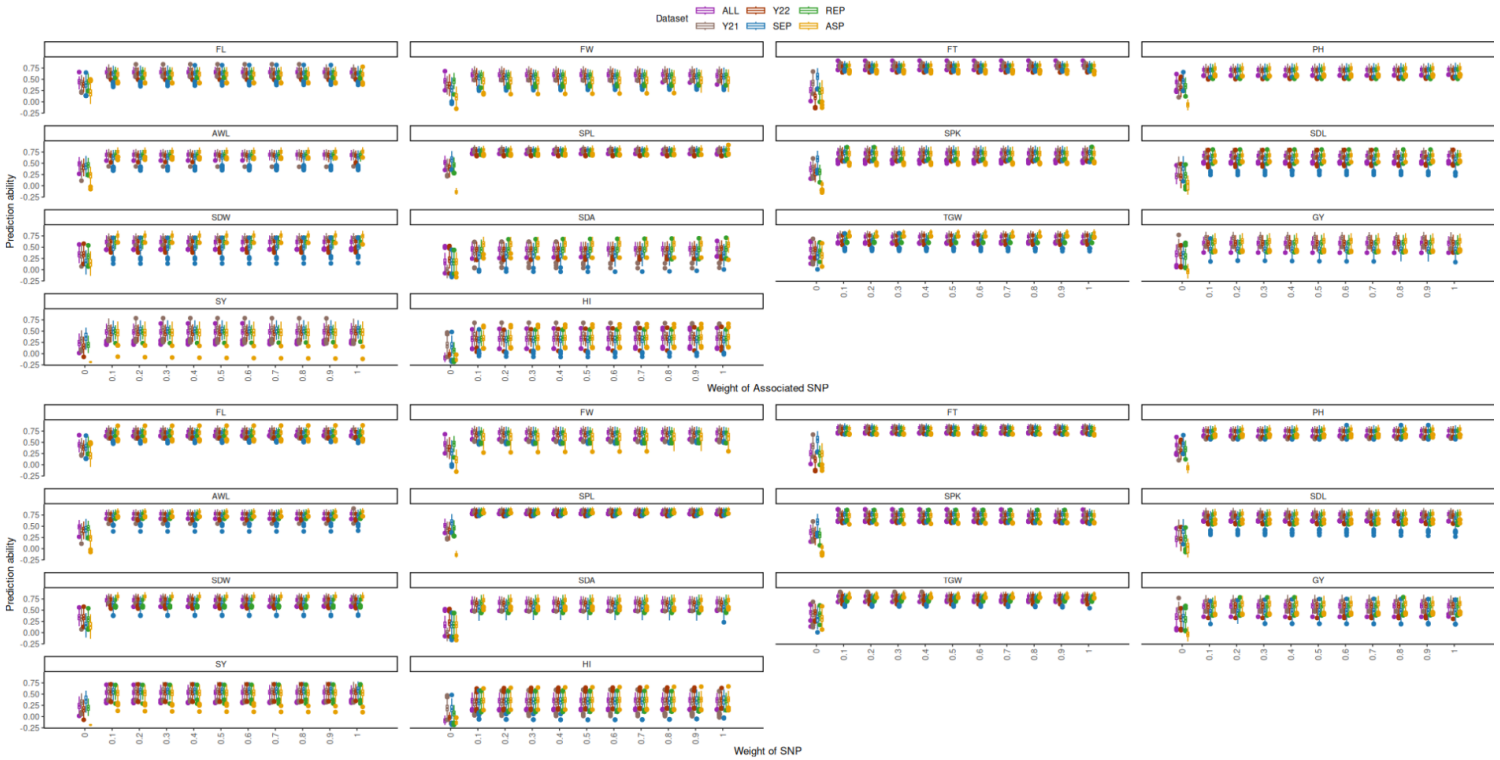

Supplementary Fig. S9 Prediction abilities of the agronomic traits using SNPs, the photosynthesis-related parameters, or joined relationship matrices. Flag leaf length (FL), flag leaf width (FW), plant height (PH), flowering time (FT), spike length (SPL), awn length (AWL), spikelet number per row (SPK), seed length (SD), seed width (SDW), seed area (SDA), thousand grain weight (TGW), grain yield (GY), straw yield (SY), and harvest index (HI). The different colors represent the adjusted entry mean of the photosynthesis-related parameters from different data sets. A. Prediction abilities using the 62 associated SNP markers to calculate the joint weighted relationship matrix. B. Prediction abilities using all genome-wide SNP markers to calculate the joint weighted relationship matrix.

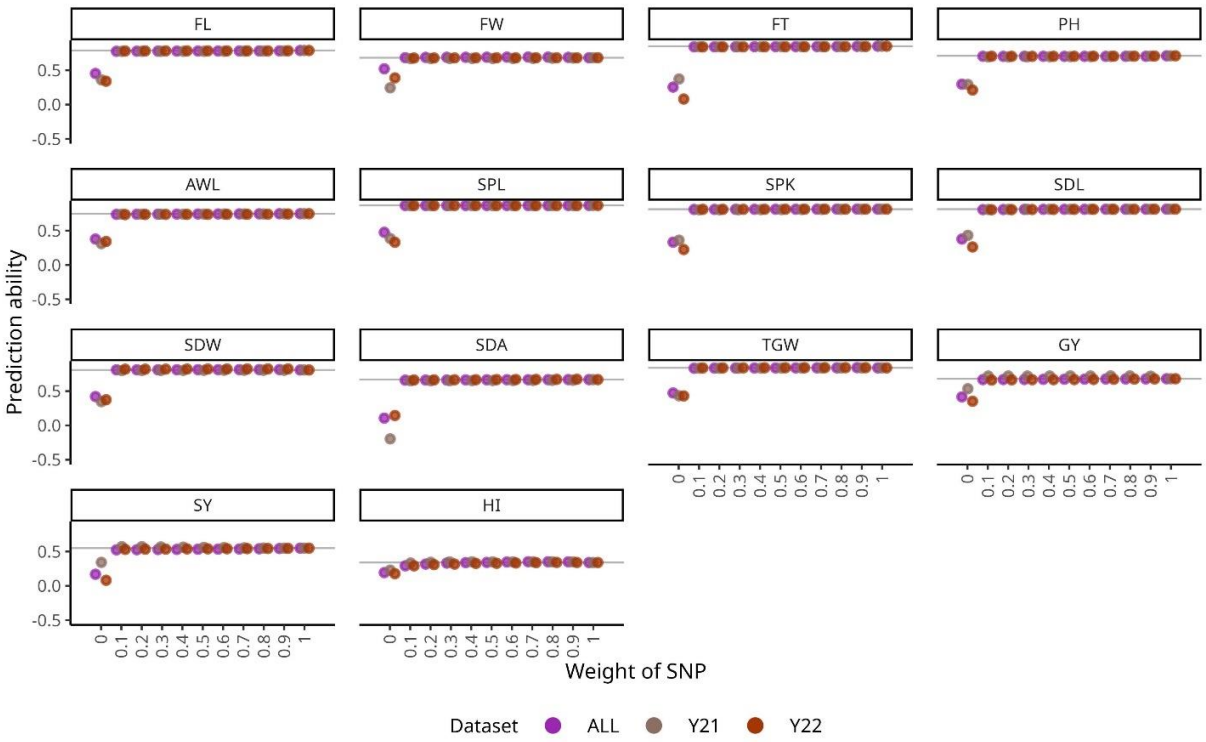

Supplementary Fig. S10 Prediction abilities of the agronomic traits using SNPs, the photosynthesis-related parameters, or joined relationship matrices. Flag leaf length (FL), flag leaf width (FW), plant height (PH), flowering time (FT), spike length (SPL), awn length (AWL), spikelet number per row (SPK), seed length (SD), seed width (SDW), seed area (SDA), thousand grain weight (TGW), grain yield (GY), straw yield (SY), and harvest index (HI). The different colors represent the adjusted entry means of the photosynthesis-related parameters from different data sets. The grey line is the prediction ability for each agronomic trait when only SNP markers are used as predictor (Weight of SNP = 1). The common 270 genotypes across the three data sets were used for five-fold cross-validation.

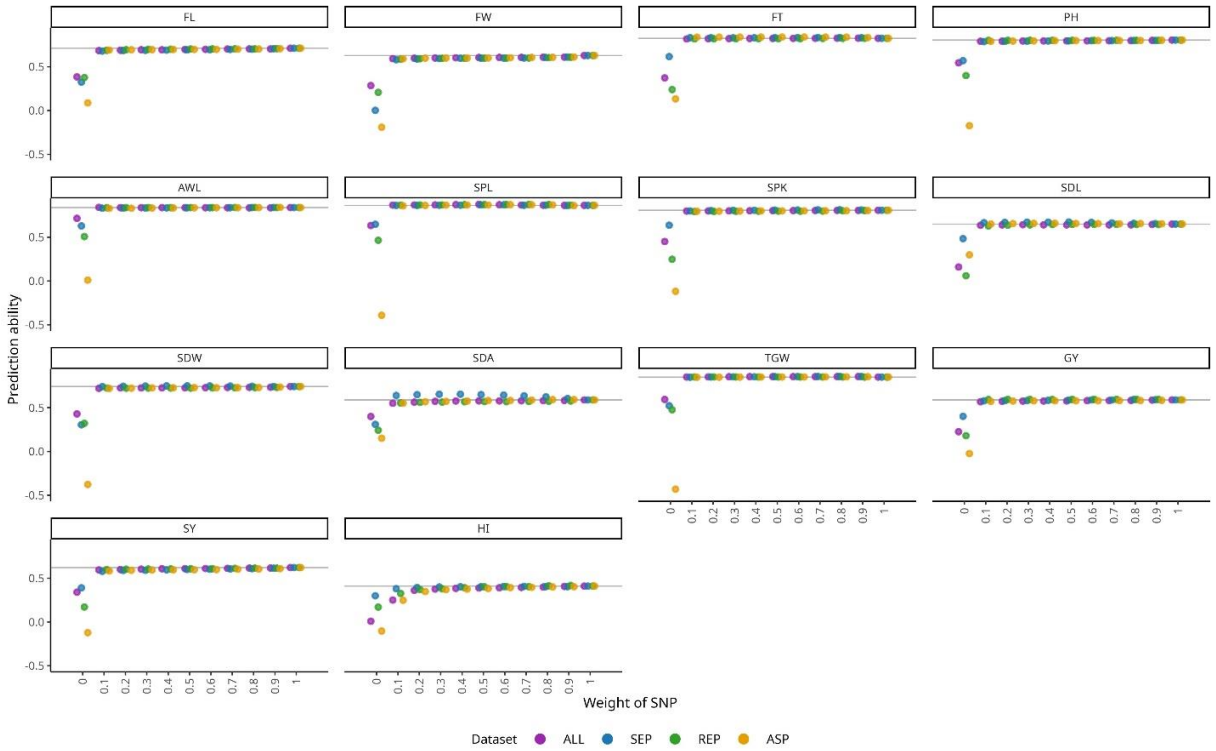

Supplementary Fig. S11 Prediction abilities of the agronomic traits using SNPs, the photosynthesis-related parameters, or joined relationship matrices. Flag leaf length (FL), flag leaf width (FW), plant height (PH), flowering time (FT), spike length (SPL), awn length (AWL), spikelet number per row (SPK), seed length (SD), seed width (SDW), seed area (SDA), thousand grain weight (TGW), grain yield (GY), straw yield (SY), and harvest index (HI). The different colors represent the adjusted entry means of the photosynthesis-related parameters from different data sets. The grey line is the prediction ability for each agronomic trait when only SNP markers are used as predictor (Weight of SNP = 1). The common 142 genotypes across the three data sets were used for five-fold cross-validation.

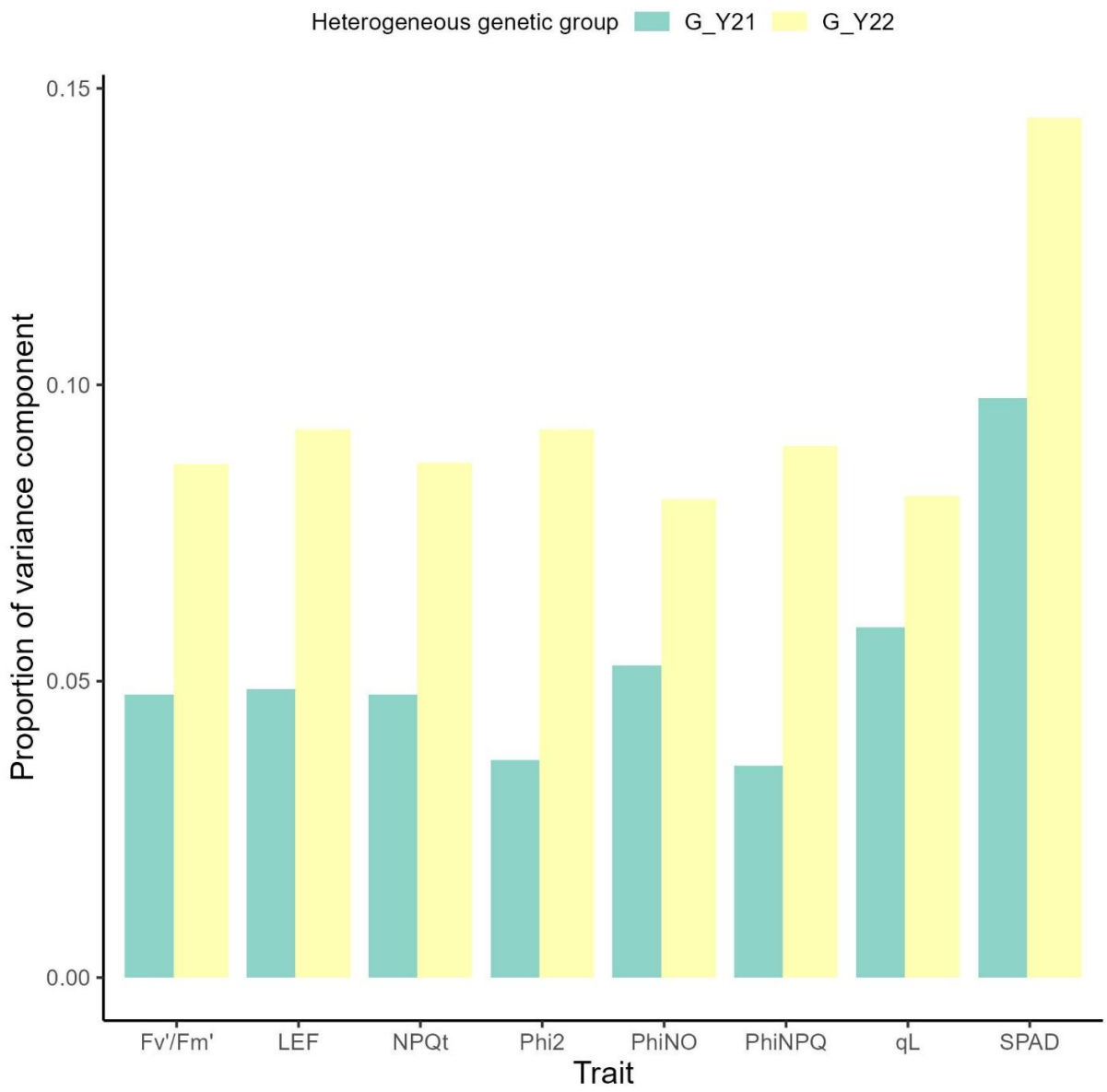

Supplementary Fig. S12 The proportion of genetic variance assessed separately for the two years (G_Y21 and G_Y22).

Supplementary Table S1 Summary of HvDRR sub-populations included in field experiments.

Populations	Parental inbred A	Parental inbred B	Year 2021	2022
HvDRR02	HOR1842	IG31424		X
HvDRR25	W23829/803911	Unumli-Arpa	X	X
HvDRR27	Unumli-Arpa	SprattArcher	X	X
HvDRR31	Lakhan	IG128216	X	X
HvDRR32	IG128216	K10877		X
HvDRR34	K10877	Lakhan	X	X
HvDRR35	Lakhan	CM67	X	
HvDRR40	ItuNative	CM67		X

Supplementary Table S2 Summary of data analyses and the mixed liner model used for each data set. *y*, the observed MultispeQ parameter across all light conditions and all developmental stages; μ, the general mean; G_i, the effect of the i^{th} genotypes; E_j, the effect of the j^{th} Location; $(G_{checks}\colon E)_{ij}$, the interaction between the i^{th} inbred (if it was a check) and the j^{th} location; $(S\colon E)_{lj}$, the effect of the l^{th} barley developmental phase nested within the j^{th} location; $(ZS\colon E)_{kj}$, the effect of the k^{th} Zadok's score of barley development nested within the j^{th} location; D_n, the effect of measurement date n; $(TW\colon D)_{sn}$, the effect of the s^{th} time window in the n^{th} measurement date; $(B\colon E)_{oj}$, the effect of the o^{th} block nested within the j^{th} location; $(R\colon B\colon E)_{poj}$, the effect of the p^{th} range nested within the o^{th} block in the j^{th} location; $(C\colon B\colon E)_{qoj}$, the effect of the q^{th} row nested within the o^{th} block in the j^{th} location; PAR, the actinic light intensity of each measurement; T, the ambient temperature of each measurement; H, the ambient humidity of each measurement; and ϵ, the random error.

Data set	Year of experiment	Developmental phase	Statistical model
ALL	2021 and 2022	All 3 developmental phases	$y_{ijlknsopqr} = \mu + G_i + E_j + (G_{checks}\colon E)_{ij} + (S\colon E)_{lj} + (ZS\colon E)_{kj} + D_n + (TW\colon D)_{sn} + PAR_{ijlknsopqr} + T_{ijlknsopqr} + H_{ijlknsopqr} + (B\colon E)_{oj} + (R\colon B\colon E)_{poj} + (C\colon B\colon E)_{qoj} + \epsilon_{ijlknsopqr}$
Y21	2021	All 3 developmental phases	$y_{ilknsopqr} = \mu + G_i + S_l + ZS_k + D_n + (TW\colon D)_{sn} + PAR_{ilknsopqr} + T_{ilknsopqr} + H_{ilknsopqr} + B_o + (R\colon B)_{po} + (C\colon B)_{qo} + \epsilon_{ilknsopqr}$
Y22	2022	All 3 developmental phases	
SEP	2021 and 2022	SEP	$y_{ijknsopqr} = \mu + G_i + E_j + (G_{checks}\colon E)_{ij} + (ZS\colon E)_{kj} + D_n + (TW\colon D)_{sn} + PAR_{ijknsopqr} + T_{ijknsopqr} + H_{ijknsopqr} + (B\colon E)_{oj} + (R\colon B\colon E)_{poj} + (C\colon B\colon E)_{qoj} + \epsilon_{ijknsopqr}$
REP	2021 and 2022	REP	
ASP	2021 and 2022	ASP	

Supplementary Table S2 Summary of data analyses and the mixed liner model used for each data set. *y*, the observed MultispeQ parameter across all light conditions and all developmental stages; μ, the general mean; G_i, the effect of the i^{th} genotypes; E_j, the effect of the j^{th} Location; $(G_{checks}\colon E)_{ij}$, the interaction between the i^{th} inbred (if it was a check) and the j^{th} location; $(S\colon E)_{lj}$, the effect of the l^{th} barley developmental phase nested within the j^{th} location; $(ZS\colon E)_{kj}$, the effect of the k^{th} Zadok's score of barley development nested within the j^{th} location; D_n, the effect of measurement date n; $(TW\colon D)_{sn}$, the effect of the s^{th} time window in the n^{th} measurement date; $(B\colon E)_{oj}$, the effect of the o^{th} block nested within the j^{th} location; $(R\colon B\colon E)_{poj}$, the effect of the p^{th} range nested within the o^{th} block in the j^{th} location; $(C\colon B\colon E)_{qoj}$, the effect of the q^{th} row nested within the o^{th} block in the j^{th} location; PAR, the actinic light intensity of each measurement; T, the ambient temperature of each measurement; H, the ambient humidity of each measurement; and ϵ, the random error.

Data set	Year of experiment	Developmental phase	Statistical model
ALL	2021 and 2022	All 3 developmental phases	$y_{ijlknsopqr} = \mu + G_i + E_j + (G_{checks}\colon E)_{ij} + (S\colon E)_{lj} + (ZS\colon E)_{kj} + D_n + (TW\colon D)_{sn} + PAR_{ijlknsopqr} + T_{ijlknsopqr} + H_{ijlknsopqr} + (B\colon E)_{oj} + (R\colon B\colon E)_{poj} + (C\colon B\colon E)_{qoj} + \epsilon_{ijlknsopqr}$
Y21	2021	All 3 developmental phases	$y_{ilknsopqr} = \mu + G_i + S_l + ZS_k + D_n + (TW\colon D)_{sn} + PAR_{ilknsopqr} + T_{ilknsopqr} + H_{ilknsopqr} + B_o + (R\colon B)_{po} + (C\colon B)_{qo} + \epsilon_{ilknsopqr}$
Y22	2022	All 3 developmental phases	
SEP	2021 and 2022	SEP	$y_{ijknsopqr} = \mu + G_i + E_j + (G_{checks}\colon E)_{ij} + (ZS\colon E)_{kj} + D_n + (TW\colon D)_{sn} + PAR_{ijknsopqr} + T_{ijknsopqr} + H_{ijknsopqr} + (B\colon E)_{oj} + (R\colon B\colon E)_{poj} + (C\colon B\colon E)_{qoj} + \epsilon_{ijknsopqr}$
REP	2021 and 2022	REP	
ASP	2021 and 2022	ASP	

Supplementary Table S3. Summary of quantitative trait loci (QTLs) detected in HvDRR sub-populations for photosynthesis-related parameters by two methods, bi-parental population QTL analysis (BPP) and multi-parental population QTL analysis (MPP). The genetic and physical position of peak markers, the markers flanking the confidence interval of the QTL and the percentage of explained phenotypic variance are reported. In addition, the percentage of explained phenotypic variance for all QTL of of one trait are given.

									Marker position						LOD of start				LOD of stop	Additive	Percentage of explained	Simultane
Data	Method	Population	Allele A	Allele B	Individuals	Traits	QTL	Chr	Peak [cM]	[bp]	Associated marker	LOD	Start [cM]	Start position [bp]	Start marker	marker	Stop [cM]	Stop position [bp]	Stop marker	marker	effect	phenotypic variance	ous fit
ALL	BPP	HvDRR02	HOR1842	IG31424	121	SPAD	1	5	202.888	528905621	JHI-Hv50k-2016-336335	5.670	196.919	523791649	JHI-Hv50k-2016-333385	4.118	213.979	530327920	JHI-Hv50k-2016-337089	3.598	-2.791	19.411	
ALL	BPP	HvDRR25	W23829/8039	Unumli-Arpa	73	LEF	1	5	206.376	529178521	JHI-Hv50k-2016-336527	3.654	194.120	522211296	JHI-Hv50k-2016-332467	0.886	221.446	538629843	JHI-Hv50k-2016-341114	1.820	4.541	20.589	
ALL	BPP	HvDRR25	W23829/8039	Unumli-Arpa	73	Phi2	1	5	206.376	529178521	JHI-Hv50k-2016-336527	3.391	194.120	522211296	JHI-Hv50k-2016-332467	1.089	221.446	538629843	JHI-Hv50k-2016-341114	1.824	0.008	19.260	
ALL	BPP	HvDRR25	W23829/8039	Unumli-Arpa	73	SPAD	1	2	33(37.020)	24596729	JHI-Hv50k-2016-72947	3.769	10.206	7966422	SCRI_RS_232722	2.265	50.048	30044023	BOPA1_8787-1459	2.066	-2.367	15.570	
ALL	BPP	HvDRR25	W23829/8039	Unumli-Arpa	73	SPAD	2	3	104.937	521727040	JHI-Hv50k-2016-195277	6.314	95.504	509740908	JHI-Hv50k-2016-193704	3.733	109.794	529852053	JHI-Hv50k-2016-197208	3.437	3.155	28.380	42.001
ALL	BPP	HvDRR27	Unumli-Arpa	SprattArcher	93	FvFm	1	2	286.449	659298954	JHI-Hv50k-2016-145127	3.861	273.566	646453774	JHI-Hv50k-2016-137311	1.968	290.228	665302017	SCRI_RS_206020	3.027	0.008	17.403	
ALL	BPP	HvDRR27	Unumli-Arpa	SprattArcher	93	NPQt	1	2	286.449	659298954	JHI-Hv50k-2016-145127	3.386	273.566	646453774	JHI-Hv50k-2016-137311	1.719	290.228	665302017	SCRI_RS_206020	2.662	-0.097	15.438	
ALL	BPP	HvDRR27	Unumli-Arpa	SprattArcher	93	PhiNPQ	1	2	284.539	653915743	JHI-Hv50k-2016-141266	4.760	273.108	644730189	JHI-Hv50k-2016-136125	3.083	290.228	665297458	JHI-Hv50k-2016-148274	3.218	-0.012	21.000	
ALL	BPP	HvDRR27	Unumli-Arpa	SprattArcher	93	SPAD	1	2	97.794	63790068	JHI-Hv50k-2016-81372	3.759	75.214	43259727	JHI-Hv50k-2016-77905	1.314	185.734	589291459	JHI-Hv50k-2016-109569	1.331	-2.217	16.986	
Y21	BPP	HvDRR27	Unumli-Arpa	SprattArcher	88	SPAD	1	2	55.310	29981630	JHI-Hv50k-2016-74940	3.186	36.555	22283006	JHI-Hv50k-2016-71918	1.042	62.760	33158437	SCRI_RS_192657	1.326	-3.999	15.359	
Y21	BPP	HvDRR35	Lakhan	CM67	79	SPAD	1	4	16.743	7780789	JHI-Hv50k-2016-228627	3.435	5.331	3416507	JHI-Hv50k-2016-227243	1.697	35.312	13331321	JHI-Hv50k-2016-230694	1.468	2.556	18.148	
Y22	BPP	HvDRR25	W23829/8039	Unumli-Arpa	72	LEF	1	5	206.376	529178521	JHI-Hv50k-2016-336527	3.690	194.120	522211296	JHI-Hv50k-2016-332467	0.887	226.700	541006821	JHI-Hv50k-2016-342543	1.416	6.621	21.022	
Y22	BPP	HvDRR25	W23829/8039	Unumli-Arpa	72	Phi2	1	5	206.376	529178521	JHI-Hv50k-2016-336527	3.692	194.120	522211296	JHI-Hv50k-2016-332467	0.889	226.700	541006821	JHI-Hv50k-2016-342543	1.417	0.011	21.034	
Y22	BPP	HvDRR34	K10877	Lakhan		NPQt	1	1	203.9782	490443608	JHI-Hv50k-2016-48141	3.280	191.396	488,045,874	BOPA1_1923-265	1.072	210.2905	491121252	JHI-Hv50k-2016-48473	1.549	0.359	38.566	
SPE	BPP	HvDRR35	Lakhan	CM67	38	Phi2	1	5	2(288.270)	548785518	JHI-Hv50k-2016-346290	5.232	279.884	540622415	JHI-Hv50k-2016-342331	3.064	301.722	556120346	JHI-Hv50k-2016-349097	1.753	0.035	40.090	
SPE	BPP	HvDRR35	Lakhan	CM67	38	Phi2	2	7	11.095	10054685	JHI-Hv50k-2016-445022	3.243	0.000	219512	BOPA2_12_10036	2.090	239.651	573389555	JHI-Hv50k-2016-494113	1.125	-0.024	21.800	54.713
REP	BPP	HvDRR02	HOR1842	IG31424	119	SPAD	1	5	199.037	526701121	SCRI_RS_201248	5.733	197.517	525051210	JHI-Hv50k-2016-333872	3.808	213.979	530327920	JHI-Hv50k-2016-337089	3.350	-3.260	19.896	
REP	BPP	HvDRR25	W23829/8039	Unumli-Arpa	73	SPAD	1	3	49.931	29205608	JHI-Hv50k-2016-162598	6.031	43.785	22680293	JHI-Hv50k-2016-160987	4.163	53.145	33364832	JHI-Hv50k-2016-163568	3.970	3.375	31.647	
REP	BPP	HvDRR27	Unumli-Arpa	SprattArcher	93	LEF	1	2	114.873	216431557	JHI-Hv50k-2016-91855	4.115	83.869	56835897	JHI-Hv50k-2016-80633	2.596	128.334	539925262	JHI-Hv50k-2016-101321	2.058	-5.466	18.435	
REP	BPP	HvDRR27	Unumli-Arpa	SprattArcher	93	Phi2	1	2	114.440	173277622	JHI-Hv50k-2016-90999	3.422	76.991	43974996	JHI-Hv50k-2016-78081	1.805	128.334	539925262	JHI-Hv50k-2016-101321	1.837	-0.009	15.588	
ASP	BPP	HvDRR25	W23829/8039	Unumli-Arpa	40	PhiNO	1	2	49.448	28308142	JHI-Hv50k-2016-74431	3.385	28.786	20871415	SCRI_RS_66401	0.957	71.411	44129811	JHI-Hv50k-2016-78167	1.479	-0.034	32.275	
ASP	BPP	HvDRR25	W23829/8039	Unumli-Arpa	40	SPAD	1	2	37.020	24596729	JHI-Hv50k-2016-72947	4.107	28.786	20871415	SCRI_RS_66401	1.993	50.048	30044023	BOPA1_8787-1459	2.355	-9.902	37.677	
ASP	BPP	HvDRR27	Unumli-Arpa	SprattArcher	77	SPAD	1	2	33.506	20825164	SCRI_RS_185319	4.351	6.269	10631847	JHI-Hv50k-2016-64423	1.946	48.042	26363248	JHI-Hv50k-2016-73697	2.273	6.682	22.913	
ASP	BPP	HvDRR32	IG128216	K10877	30	qL	1	4	84.448	484423020	JHI-Hv50k-2016-249584	3.928	79.133	449611912	SCRI_RS_181886	1.856	91.415	515793342	JHI-Hv50k-2016-252905	1.622	0.042	45.280	
ALL	MPP					LEF	1	1	66.418	38603975	JHI-Hv50k-2016-18239	3.606	57.046	32486241	JHI-Hv50k-2016-17394		87.975	305664801	BOPA2_12_10300			3.640	
ALL	MPP					LEF	2	4	15.720	10281223	JHI-Hv50k-2016-229859	3.033	13.374	9459865	JHI-Hv50k-2016-229205		23.974	12950458	JHI-Hv50k-2016-230594			2.750	6.07
ALL	MPP					NPQt	1	4	0.000	4906733	JHI-Hv50k-2016-227950	3.120	0.000	4906733	JHI-Hv50k-2016-227950		13.374	9459660	JHI-Hv50k-2016-229207			2.890	
ALL	MPP					Phi2	1	1	66.418	38603975	JHI-Hv50k-2016-18239	3.299	55.325	31502766	JHI-Hv50k-2016-17085		88.062	306458264	BOPA1_ABC11913-1-1-104			3.050	
ALL	MPP					PhiNO	1	1	60.548	35004618	SCRI_RS_170869	3.575	55.325	31502766	JHI-Hv50k-2016-17085		84.927	102621085	JHI-Hv50k-2016-20766			3.290	
ALL	MPP					SPAD	1	2	115.793	127569542	JHI-Hv50k-2016-89203	4.930	107.066	90,566,215	BOPA1_5113-624		121.595	200870898	JHI-Hv50k-2016-91451			4.000	
ALL	MPP					SPAD	2	3	157.272	527642156	JHI-Hv50k-2016-196749	3.175	141.516	508264337	JHI-Hv50k-2016-193149		181.648	547806515	JHI-Hv50k-2016-201055			2.300	
ALL	MPP					SPAD	3	5	224.651	526967552	JHI-Hv50k-2016-335087	5.285	218.937	523882465	JHI-Hv50k-2016-333135		230.077	529895058	JHI-Hv50k-2016-336985			4.380	10.880
Y21	MPP					LEF	1	7	67.659	41060990	JHI-Hv50k-2016-457630	3.559	43.533	26522983	JHI-Hv50k-2016-453933		72.424	44059048	SCRI_RS_155061			4.630	
Y21	MPP					Phi2	1	4	90.497	435922595	JHI-Hv50k-2016-243980	3.345	85.814	79993625	JHI-Hv50k-2016-238832		100.113	499941334	BOPA1_8034-315			4.360	
Y21	MPP					PhiNO	1	7	80.541	49222284	JHI-Hv50k-2016-461558	3.324	74.822	45582370	JHI-Hv50k-2016-460846		83.088	50945241	SCRI_RS_202061			4.330	
Y21	MPP					PhiNPQ	1	2	205.812	608449388	JHI-Hv50k-2016-116511	3.279	205.395	608212869	JHI-Hv50k-2016-116402		219.493	616031394	JHI-Hv50k-2016-119531			4.270	
Y21	MPP					SPAD	1	2	42.701	28819655	JHI-Hv50k-2016-74683	3.279	37.524	26372182	JHI-Hv50k-2016-73723		48.755	31811486	BOPA1_7144-973			5.040	
Y22	MPP					LEF	1	5	224.651	526967552	JHI-Hv50k-2016-335087	3.023	217.453	523055067	JHI-Hv50k-2016-332921		231.182	530485399	SCRI_RS_237494			3.110	
Y22	MPP					Phi2	1	5	224.651	526967552	JHI-Hv50k-2016-335087	3.026	217.453	523055067	JHI-Hv50k-2016-332921		231.182	530485399	SCRI_RS_237494			3.120	
Y22	MPP					SPAD	1	2	21.982	18266158	JHI-Hv50k-2016-70046	3.594	0.000	5314030	JHI-Hv50k-2016-62362		44.606	29916306	JHI-Hv50k-2016-74880			3.610	
Y22	MPP					SPAD	2	2	294.702	656801113	JHI-Hv50k-2016-142842	3.184	285.079	651302139	JHI-Hv50k-2016-139420		303.232	662073104	JHI-Hv50k-2016-147075			3.020	6.770
SEP	MPP					NPQt	1	7	149.490	429001069	JHI-Hv50k-2016-486426	3.595	137.620	147306628	JHI-Hv50k-2016-475622		154.827	480644340	JHI-Hv50k-2016-488121			3.230	
SEP	MPP					PhiNPQ	1	4	3.924	6251543	BOPA2_12_11485	3.201	0.000	4906733	JHI-Hv50k-2016-227950		13.454	9486748	JHI-Hv50k-2016-229244			4.830	
SEP	MPP					SPAD	1	5	220.674	524805000	JHI-Hv50k-2016-333747	3.508	207.363	517488826	SCRI_RS_239128		231.182	530485399	SCRI_RS_237494			5.620	
REP	MPP					LEF	1	2	37.503	26362729	JHI-Hv50k-2016-73712	4.145	27.612	21396801	JHI-Hv50k-2016-71784		47.666	31307172	JHI-Hv50k-2016-75278			3.460	
REP	MPP					LEF	2	2	177.660	585633374	JHI-Hv50k-2016-109411	3.373	172.919	580590717	JHI-Hv50k-2016-109128		179.899	587949701	JHI-Hv50k-2016-109442			2.090	
REP	MPP					LEF	3	4	120.426	551568896	JHI-Hv50k-2016-258388	4.204	119.504	550293012	JHI-Hv50k-2016-258057		137.279	565947460	JHI-Hv50k-2016-260417			3.990	
REP	MPP					LEF	4	6	203.810	559969823	JHI-Hv50k-2016-433097	3.031	194.565	555268907	JHI-Hv50k-2016-429588		207.306	561748098	BOPA2_12_30956			1.510	
REP	MPP					LEF	5	7	96.722	60492758	JHI-Hv50k-2016-465556	3.357	91.508	56563165	SCRI_RS_157816		108.416	70855127	JHI-Hv50k-2016-468564			4.360	15.21
REP	MPP					Phi2	1	2	17.382	15967496	JHI-Hv50k-2016-68511	3.135	10.966	12199300	SCRI_RS_150792		50.015	32486733	JHI-Hv50k-2016-75493			2.640	
REP	MPP					Phi2	2	2	178.951	587010446	JHI-Hv50k-2016-109414	3.788	174.999	582813388	BOPA1_6752-1013		182.716	599,395,161	SCRI_RS_222876			2.300	
REP	MPP					Phi2	3	4	136.338	565295698	JHI-Hv50k-2016-260357	4.065	128.654	559218292	SCRI_RS_200957		138.955	567110223	JHI-Hv50k-2016-261147			3.810	
REP	MPP					Phi2	4	7	96.158	60038184	JHI-Hv50k-2016-465287	3.046	91.508	56563165	SCRI_RS_157816		108.416	70855127	JHI-Hv50k-2016-468564			3.620	13.610
REP	MPP					PhiNO	1	1	60.548	35004618	SCRI_RS_170869	5.117	55.960	31866857	JHI-Hv50k-2016-17165		81.399	72455950	JHI-Hv50k-2016-19938			5.590	
REP	MPP					PhiNO	2	4	135.944	565019581	JHI-Hv50k-2016-260353	3.666	128.678	559240806	JHI-Hv50k-2016-259359		139.310	567359933	JHI-Hv50k-2016-261178			3.100	7.790
REP	MPP					qL	1	7	95.841	59783628	JHI-Hv50k-2016-465225	3.371	73.171	44535834	JHI-Hv50k-2016-460651		118.147	82293783	JHI-Hv50k-2016-469990			3.340	
REP	MPP					SPAD	1	2	238.002	625816080	SCRI_RS_708	3.703	227.961	620576003	JHI-Hv50k-2016-122320		241.914	627833511	JHI-Hv50k-2016-127015			2.510	
REP	MPP					SPAD	2	5	225.100	527215217	JHI-Hv50k-2016-335374	4.823	222.569	525813906	JHI-Hv50k-2016-334166		230.258	529993198	JHI-Hv50k-2016-336955			4.500	6.910
ASP	MPP					FvFm	1	1	134.952	450053813	JHI-Hv50k-2016-37618	3.477	134.485	449503017	SCRI_RS_21080		140.575	455497281	JHI-Hv50k-2016-37651			5.070	
ASP	MPP					qL	1	2	44.606	29916306	JHI-Hv50k-2016-74880	5.036	40.018	27583311	JHI-Hv50k-2016-74134		50.015	32486733	JHI-Hv50k-2016-75493			7.140	
ASP	MPP					SPAD	1	2	30.036	22496450	SCRI_RS_159228	9.035	27.612	21396801	JHI-Hv50k-2016-71784		36.947	26107957	JHI-Hv50k-2016-73663			11.980	

Supplementary table 4 Summary of consense quantitative trait loci (QTLs) detected in HvDRR sub-populations for photosynthesis-related parameters. The genetic and physical position of peak markers, the markers flanking the confidence interval of the QTL and the percentage of explained phenotypic variance are reported.

Data	Method	Population	Allele A	Allele B	Individuals	Traits	QTL	Chr	Peak [cM]	Marker position [bp]	Associated marker	LOD	Start [cM]	Start position [bp]	Start marker	start marker	Stop [cM]	Stop position [bp]	Stop marker	LOD of stop marker	Additive effect	Percentage of explained phenotypic variance	Consensus QTL for photosynthesis	Including method
ALL	MPP					PhiNO	1	1	60.548	35,004,618	SCRI_RS_170869	3.575	55.325	31,502,766	JHI-Hv50k-2016-17085		84.927	102,621,085	JHI-Hv50k-2016-20766			3.290		
REP	MPP					PhiNO	1	1	60.548	35,004,618	SCRI_RS_170869	5.117	55.960	31,866,857	JHI-Hv50k-2016-17165		81.399	72,455,950	JHI-Hv50k-2016-19938			5.590		
ALL	MPP					LEF	1	1	66.418	38,603,975	JHI-Hv50k-2016-18239	3.606	57.046	32,486,241	JHI-Hv50k-2016-17394		87.975	305,664,801	BOPA2_12_10300			3.640		
ALL	MPP					Phi2	1	1	66.418	38,603,975	JHI-Hv50k-2016-18239	3.299	55.325	31,502,766	JHI-Hv50k-2016-17085		88.062	306,458,264	BOPA1_ABC11913-1-1-104			3.050	qHvDRR-PS-1	MPP
ASP	MPP					FvFm	1	1	134.952	450,053,813	JHI-Hv50k-2016-37618	3.477	134.485	449,503,017	SCRI_RS_21080		140.575	455,497,281	JHI-Hv50k-2016-37651			5.070	qHvDRR-PS-2	MPP
Y22	BPP	HvDRR34	K10877	Lakhan		NPQt	1	1	203.978	490,443,608	JHI-Hv50k-2016-48141	3.280	191.396	488,045,874	BOPA1_1923-265	1.072	210.291	491,121,252	JHI-Hv50k-2016-48473	1.549	0.359	38.566	qHvDRR-PS-3	BPP
Y22	MPP					SPAD	1	2	21.982	18,266,158	JHI-Hv50k-2016-70046	3.594	0.000	5,314,030	JHI-Hv50k-2016-62362		44.606	29,916,306	JHI-Hv50k-2016-74880			3.610		
ALL	BPP	HvDRR25	23829/8039	Unumli-Arpa	73	SPAD	1	2	33(37.020	24,596,729	JHI-Hv50k-2016-72947	3.769	10.206	7,966,422	SCRI_RS_232722	2.265	50.048	30,044,023	BOPA1_8787-1459	2.066	-2.367	15.570		
ASP	BPP	HvDRR27	Unumli-Arpa	SprattArcher	77	SPAD	1	2	33.506	20,825,164	SCRI_RS_185319	4.351	6.269	10,631,847	JHI-Hv50k-2016-64423	1.946	48.042	26,363,248	JHI-Hv50k-2016-73697	2.273	6.682	22.913		
REP	MPP					Phi2	1	2	17.382	15,967,496	JHI-Hv50k-2016-68511	3.135	10.966	12,199,300	SCRI_RS_150792		50.015	32,486,733	JHI-Hv50k-2016-75493			2.640		
ASP	BPP	HvDRR25	23829/8039	Unumli-Arpa	40	PhiNO	1	2	49.448	28,308,142	JHI-Hv50k-2016-74431	3.385	28.786	20,871,415	SCRI_RS_66401	0.957	71.411	44,129,811	JHI-Hv50k-2016-78167	1.479	-0.034	32.275		
ASP	BPP	HvDRR25	23829/8039	Unumli-Arpa	40	SPAD	1	2	37.020	24,596,729	JHI-Hv50k-2016-72947	4.107	28.786	20,871,415	SCRI_RS_66401	1.993	50.048	30,044,023	BOPA1_8787-1459	2.355	-9.902	37.677		
REP	MPP					LEF	1	2	37.503	26,362,729	JHI-Hv50k-2016-73712	4.145	27.612	21,396,801	JHI-Hv50k-2016-71784		47.666	31,307,172	JHI-Hv50k-2016-75278			3.460		
ASP	MPP					SPAD	1	2	30.036	22,496,450	SCRI_RS_159228	9.035	27.612	21,396,801	JHI-Hv50k-2016-71784		36.947	26,107,957	JHI-Hv50k-2016-73663			11.980		
Y21	BPP	HvDRR27	Unumli-Arpa	SprattArcher	88	SPAD	1	2	55.310	29,981,630	JHI-Hv50k-2016-74940	3.186	36.555	22,283,006	JHI-Hv50k-2016-71918	1.042	62.760	33,158,437	SCRI_RS_192657	1.326	-3.999	15.359		
Y21	MPP					SPAD	1	2	42.701	28,819,655	JHI-Hv50k-2016-74683	3.279	37.524	26,372,182	JHI-Hv50k-2016-73723		48.755	31,811,486	BOPA1_7144-973			5.040		
ASP	MPP					qL	1	2	44.606	29,916,306	JHI-Hv50k-2016-74880	5.036	40.018	27,583,311	JHI-Hv50k-2016-74134		50.015	32,486,733	JHI-Hv50k-2016-75493			7.140	qHvDRR-PS-4	6MPP,5BPP
ALL	BPP	HvDRR27	Unumli-Arpa	SprattArcher	93	SPAD	1	2	97.794	63,790,068	JHI-Hv50k-2016-81372	3.759	75.214	43,259,727	JHI-Hv50k-2016-77905	1.314	185.734	589,291,459	JHI-Hv50k-2016-109569	1.331	-2.217	16.986		
REP	BPP	HvDRR27	Unumli-Arpa	SprattArcher	93	Phi2	1	2	114.440	173,277,622	JHI-Hv50k-2016-90999	3.422	76.991	43,974,996	JHI-Hv50k-2016-78081	1.805	128.334	539,925,262	JHI-Hv50k-2016-101321	1.837	-0.009	15.588		
REP	BPP	HvDRR27	Unumli-Arpa	SprattArcher	93	LEF	1	2	114.873	216,431,557	JHI-Hv50k-2016-91855	4.115	83.869	56,835,897	JHI-Hv50k-2016-80633	2.596	128.334	539,925,262	JHI-Hv50k-2016-101321	2.058	-5.466	18.435		
ALL	MPP					SPAD	1	2	115.793	127,569,542	JHI-Hv50k-2016-89203	4.930	107.066	90,566,215	BOPA1_5113-624		121.595	200,870,898	JHI-Hv50k-2016-91451			4.000	qHvDRR-PS-5	3BPP, 1MPP
REP	MPP					LEF	2	2	177.660	585,633,374	JHI-Hv50k-2016-109411	3.373	172.919	580,590,717	JHI-Hv50k-2016-109128		179.899	587,949,701	JHI-Hv50k-2016-109442			2.090		
REP	MPP					Phi2	2	2	178.951	587,010,446	JHI-Hv50k-2016-109414	3.788	174.999	582,813,388	BOPA1_6752-1013		182.716	599,395,161	SCRI_RS_222876			2.300	qHvDRR-PS-6	MPP
Y21	MPP					PhiNPQ	1	2	205.812	608,449,388	JHI-Hv50k-2016-116511	3.279	205.395	608,212,869	JHI-Hv50k-2016-116402		219.493	616,031,394	JHI-Hv50k-2016-119531			4.270		
REP	MPP					SPAD	1	2	238.002	625,816,080	SCRI_RS_708	3.703	227.961	620,576,003	JHI-Hv50k-2016-122320		241.914	627,833,511	JHI-Hv50k-2016-127015			2.510	qHvDRR-PS-7	MPP
ALL	BPP	HvDRR27	Unumli-Arpa	SprattArcher	93	PhiNPQ	1	2	284.539	653,915,743	JHI-Hv50k-2016-141266	4.760	273.108	644,730,189	JHI-Hv50k-2016-136125	3.083	290.228	665,297,458	JHI-Hv50k-2016-148274	3.218	-0.012	21.000		
ALL	BPP	HvDRR27	Unumli-Arpa	SprattArcher	93	FvFm	1	2	286.449	659,298,954	JHI-Hv50k-2016-145127	3.861	273.566	646,453,774	JHI-Hv50k-2016-137311	1.968	290.228	665,302,017	SCRI_RS_206020	3.027	0.008	17.403		
ALL	BPP	HvDRR27	Unumli-Arpa	SprattArcher	93	NPQt	1	2	286.449	659,298,954	JHI-Hv50k-2016-145127	3.386	273.566	646,453,774	JHI-Hv50k-2016-137311	1.719	290.228	665,302,017	SCRI_RS_206020	2.662	-0.097	15.438		
Y22	MPP					SPAD	2	2	294.702	656,801,113	JHI-Hv50k-2016-142842	3.184	285.079	651,302,139	JHI-Hv50k-2016-139420		303.232	662,073,104	JHI-Hv50k-2016-147075			3.020	qHvDRR-PS-8	3BPP, 1MPP
REP	BPP	HvDRR25	23829/8039	Unumli-Arpa	73	SPAD	1	3	49.931	29,205,608	JHI-Hv50k-2016-162598	6.031	43.785	22,680,293	JHI-Hv50k-2016-160987	4.163	53.145	33,364,832	JHI-Hv50k-2016-163568	3.970	3.375	31.647	qHvDRR-PS-9	BPP
ALL	BPP	HvDRR25	23829/8039	Unumli-Arpa	73	SPAD	2	3	104.937	521,727,040	JHI-Hv50k-2016-195277	6.314	95.504	509,740,908	JHI-Hv50k-2016-193704	3.733	109.794	529,852,053	JHI-Hv50k-2016-197208	3.437	3.155	28.380		
ALL	MPP					SPAD	2	3	157.272	527,642,156	JHI-Hv50k-2016-196749	3.175	141.516	508,264,337	JHI-Hv50k-2016-193149		181.648	547,806,515	JHI-Hv50k-2016-201055			2.300	qHvDRR-PS-10	1BPP, 1MPP
Y21	BPP	HvDRR35	Lakhan	CM67	79	SPAD	1	4	16.743	7,780,789	JHI-Hv50k-2016-228627	3.435	5.331	3,416,507	JHI-Hv50k-2016-227243	1.697	35.312	13,331,321	JHI-Hv50k-2016-230694	1.468	2.556	18.148		
ALL	MPP					NPQt	1	4	0.000	4,906,733	JHI-Hv50k-2016-227950	3.120	0.000	4,906,733	JHI-Hv50k-2016-227950		13.374	9,459,660	JHI-Hv50k-2016-229207			2.890		
SEP	MPP					PhiNPQ	1	4	3.924	6,251,543	BOPA2_12_11485	3.201	0.000	4,906,733	JHI-Hv50k-2016-227950		13.454	9,486,748	JHI-Hv50k-2016-229244			4.830		
ALL	MPP					LEF	2	4	15.720	10,281,223	JHI-Hv50k-2016-229859	3.033	13.374	9,459,865	JHI-Hv50k-2016-229205		23.974	12,950,458	JHI-Hv50k-2016-230594			2.750	qHvDRR-PS-11	1BPP, 3MPP
Y21	MPP					Phi2	1	4	90.497	435,922,595	JHI-Hv50k-2016-243980	3.345	85.814	79,993,625	JHI-Hv50k-2016-238832		100.113	499,941,334	BOPA1_8034-315			4.360		
ASP	BPP	HvDRR32	IG128216	K10877	30	qL	1	4	84.448	484,423,020	JHI-Hv50k-2016-249584	3.928	79.133	449,611,912	SCRI_RS_181886	1.856	91.415	515,793,342	JHI-Hv50k-2016-252905	1.622	0.042	45.280	qHvDRR-PS-12	1MPP, 1BPP
REP	MPP					LEF	3	4	120.426	551,568,896	JHI-Hv50k-2016-258388	4.204	119.504	550,293,012	JHI-Hv50k-2016-258057		137.279	565,947,460	JHI-Hv50k-2016-260417			3.990		
REP	MPP					Phi2	3	4	136.338	565,295,698	JHI-Hv50k-2016-260357	4.065	128.654	559,218,292	SCRI_RS_200957		138.955	567,110,223	JHI-Hv50k-2016-261147			3.810		
REP	MPP					PhiNO	2	4	135.944	565,019,581	JHI-Hv50k-2016-260353	3.666	128.678	559,240,806	JHI-Hv50k-2016-259359		139.310	567,359,933	JHI-Hv50k-2016-261178			3.100	qHvDRR-PS-13	MPP
ALL	BPP	HvDRR02	HOR1842	IG31424	121	SPAD	1	5	202.888	528,905,621	JHI-Hv50k-2016-336335	5.670	196.919	523,791,649	JHI-Hv50k-2016-333385	4.118	213.979	530,327,920	JHI-Hv50k-2016-337089	3.598	-2.791	19.411		
ALL	BPP	HvDRR25	23829/8039	Unumli-Arpa	73	LEF	1	5	206.376	529,178,521	JHI-Hv50k-2016-336527	3.654	194.120	522,211,296	JHI-Hv50k-2016-332467	0.886	221.446	538,629,843	JHI-Hv50k-2016-341114	1.820	4.541	20.589		
ALL	BPP	HvDRR25	23829/8039	Unumli-Arpa	73	Phi2	1	5	206.376	529,178,521	JHI-Hv50k-2016-336527	3.391	194.120	522,211,296	JHI-Hv50k-2016-332467	1.089	221.446	538,629,843	JHI-Hv50k-2016-341114	1.824	0.008	19.260		
Y22	BPP	HvDRR25	23829/8039	Unumli-Arpa	72	LEF	1	5	206.376	529,178,521	JHI-Hv50k-2016-336527	3.690	194.120	522,211,296	JHI-Hv50k-2016-332467	0.887	226.700	541,006,821	JHI-Hv50k-2016-342543	1.416	6.621	21.022		
Y22	BPP	HvDRR25	23829/8039	Unumli-Arpa	72	Phi2	1	5	206.376	529,178,521	JHI-Hv50k-2016-336527	3.692	194.120	522,211,296	JHI-Hv50k-2016-332467	0.889	226.700	541,006,821	JHI-Hv50k-2016-342543	1.417	0.011	21.034		
SPE	BPP	HvDRR35	Lakhan	CM67	38	Phi2	1	5	92(288.27(	548,785,518	JHI-Hv50k-2016-346290	5.232	279.884	540,622,415	JHI-Hv50k-2016-342331	3.064	301.722	556,120,346	JHI-Hv50k-2016-349097	1.753	0.035	40.090		
REP	BPP	HvDRR02	HOR1842	IG31424	119	SPAD	1	5	199.037	526,701,121	SCRI_RS_201248	5.733	197.517	525,051,210	JHI-Hv50k-2016-333872	3.808	213.979	530,327,920	JHI-Hv50k-2016-337089	3.350	-3.260	19.896		
ALL	MPP					SPAD	3	5	224.651	526,967,552	JHI-Hv50k-2016-335087	5.285	218.937	523,882,465	JHI-Hv50k-2016-333135		230.077	529,895,058	JHI-Hv50k-2016-336985			4.380		
Y22	MPP					LEF	1	5	224.651	526,967,552	JHI-Hv50k-2016-335087	3.023	217.453	523,055,067	JHI-Hv50k-2016-332921		231.182	530,485,399	SCRI_RS_237494			3.110		
Y22	MPP					Phi2	1	5	224.651	526,967,552	JHI-Hv50k-2016-335087	3.026	217.453	523,055,067	JHI-Hv50k-2016-332921		231.182	530,485,399	SCRI_RS_237494			3.120		
SEP	MPP					SPAD	1	5	220.674	524,805,000	JHI-Hv50k-2016-333747	3.508	207.363	517,488,826	SCRI_RS_239128		231.182	530,485,399	SCRI_RS_237494			5.620		
REP	MPP					SPAD	2	5	225.100	527,215,217	JHI-Hv50k-2016-335374	4.823	222.569	525,813,906	JHI-Hv50k-2016-334166		230.258	529,993,198	JHI-Hv50k-2016-336955			4.500	qHvDRR-PS-14	7BPP, 5MPP
REP	MPP					LEF	4	6	203.810	559,969,823	JHI-Hv50k-2016-433097	3.031	194.565	555,268,907	JHI-Hv50k-2016-429588		207.306	561,748,098	BOPA2_12_30956			1.510	qHvDRR-PS-15	MPP
SPE	BPP	HvDRR35	Lakhan	CM67	38	Phi2	2	7	11.095	10,054,685	JHI-Hv50k-2016-445022	3.243	0.000	219,512	BOPA2_12_10036	2.090	239.651	573,389,555	JHI-Hv50k-2016-494113	1.125	-0.024	21.800	qHvDRR-PS-16	BPP
Y21	MPP					LEF	1	7	67.659	41,060,990	JHI-Hv50k-2016-457630	3.559	43.533	26,522,983	JHI-Hv50k-2016-453933		72.424	44,059,048	SCRI_RS_155061			4.630		
REP	MPP					qL	1	7	95.841	59,783,628	JHI-Hv50k-2016-465225	3.371	73.171	44,535,834	JHI-Hv50k-2016-460651		118.147	82,293,783	JHI-Hv50k-2016-469990			3.340		
Y21	MPP					PhiNO	1	7	80.541	49,222,284	JHI-Hv50k-2016-461558	3.324	74.822	45,582,370	JHI-Hv50k-2016-460846		83.088	50,945,241	SCRI_RS_202061			4.330		
REP	MPP					LEF	5	7	96.722	60,492,758	JHI-Hv50k-2016-465556	3.357	91.508	56,563,165	SCRI_RS_157816		108.416	70,855,127	JHI-Hv50k-2016-468564			4.360		
REP	MPP					Phi2	4	7	96.158	60,038,184	JHI-Hv50k-2016-465287	3.046	91.508	56,563,165	SCRI_RS_157816		108.416	70,855,127	JHI-Hv50k-2016-468564			3.620	qHvDRR-PS-17	MPP
SEP	MPP					NPQt	1	7	149.490	429,001,069	JHI-Hv50k-2016-486426	3.595	137.620	147,306,628	JHI-Hv50k-2016-475622		154.827	480,644,340	JHI-Hv50k-2016-488121			3.230	qHvDRR-PS-18	MPP

Supplementary Table S5 Prediction ability of five-fold cross-validation for the agronomic traits when considering a SNP-based relationship matrix. Only genotypes with phenotypic records available for the photosynthesis-related parameters in all three data sets (SEP, REP, and ASP) were included.

Agronomic trait	Prediction ability
SDL	0.650551
SDW	0.742726
SDA	0.589196
TGW	0.850571
PH	0.80504
FT	0.824579
FL	0.710947
FW	0.628368
GY	0.589425
SY	0.622076
HI	0.410124
AWL	0.839056
SPL	0.864324
SPK	0.808071

Supplementary Table S6 The percentage of phenotypic variance explained (PVE) of multi-parental QTL and genomic prediction analysis of data set ALL for each photosynthesis-related parameter.

Data set	Trait	MPP_PVE (%)	GP_PVE (%)
ALL	Fv'/Fm'	-	10.69
ALL	LEF	6.07	23.23
ALL	NPQt	2.89	11.09
ALL	Phi2	3.05	22.85
ALL	PhiNO	3.29	17.31
ALL	PhiNPQ	-	6.30
ALL	qL	-	19.18
ALL	SPAD	10.88	33.18

Chapter 4

Genetic architecture and cellular basis of flag leaf size variation in barley

Twinkal Lapasiya[1,3,4+], Yanrong Gao[1,3+], Po-Ya Wu[1,3], Amirah Haweit[1], Delphine van Inghelandt[1,3,5], Benjamin Stich[1,2,3,4*], Asis Shrestha[1,3*]

Accepted pending revision at Journal of Experimental Botany

Own contribution: I am the first author of this paper, I completed 50% of the experiments, I conducted 50% of data analysis and interpretation. Together with my coauthor Twinkal, I drafted the manuscript.

Genetic architecture and cellular basis of flag leaf size variation in barley

Twinkal Lapasiya[1,2,3,†], Yanrong Gao[1,2,†], Po-Ya Wu[1,2], Amirah Haweit[1], Delphine van Inghelandt[1,2,4], Benjamin Stich[1,2,3,5,*], and Asis Shrestha[1,2,*]

[1] Quantitative Genetics and Genomics of Plants, Heinrich-Heine-University Düsseldorf, Universitätsstraße 1, D-40225 Düsseldorf, Germany

[2] Institute for Breeding Research on Agricultural Crops, Julius Kühn-Institute, Federal Research Center for Cultivated Plants, Rudolf-Schick-Platz 3a, D-18190 Sanitz, Germany

[3] Utilization of Plant Genetic Resources for Breeding Purposes, University of Rostock, D-18051 Rostock, Germany

[4] Leibniz Institute of Plant Genetics and Crop Plant Research (IPK) OT Gatersleben, Corrensstrasse 3, D-06466 Seeland, Germany

[5] The Cluster of Excellence on Plant Sciences, Heinrich-Heine-University Düsseldorf, D-40225 Düsseldorf, Germany

[†] These authors contributed equally to this work

[*]Corresponding author: Benjamin Stich; Asis Shrestha

Abstract

The flag leaf is a major contributor of photosynthetic assimilates to developing grains. We investigated the genetic architecture and cellular basis of flag leaf length (FLL) and width (FLW) in a multiparent population of 45 recombinant inbred line (RIL) populations (HvDRR) in barley. Fine-mapping of a major quantitative trait locus (QTL) was performed to prepare the isolation of the causal gene. Natural variation of FLL and FLW across environments was highly heritable, and genotypes from warm climates produced longer and wider flag leaves than those from cooler regions. Variation in flag leaf size was quantitatively inherited and influenced by 24 consensus QTLs, of which 17 have not previously been reported. Validation of QTLs qHvDRR-FLS-8 and qHvDRR-FLS-17 in nearly isogenic RILs showed that these QTLs also controlled length and width of leaves older than the flag leaf. The number of epidermal cells primarily determined FLL, whereas the number and size of epidermal cells collectively determined FLW differences. In addition, we identified the previously unknown effect of genic allele and epiallele at Vrn-H1 on flag leaf size variation in spring barley. Furthermore, we fine-mapped qHvDRR-FLS-8, narrowing the interval from 8.7 Mb to 3.5 Mb. In conclusion, our study identified the genomic regions associated with morphological and anatomical variation for leaf size and set the stage to uncover causal genes.

Keywords: Barley, fine mapping, flag leaf, genetics, QTL, QTL mapping.

1. Introduction

Photosynthesis is central to plant production and productivity (Long et al., 2006) as it plays a vital role in production and accumulation of organic material in plants (Gautam et al., 2022), and the leaf represents the most important photosynthetic organ (Blum, 1985; Wang et al., 2016). Because of this important role of leaves for photosynthesis, in the 1960s Donald (1968) and Jennings (1964) proposed a model for enhancing grain yield potential by modifying phenotypic characters such as leaf area in cereals using 'ideotype' breeding. This theory was then supported by the observations that longer flag leaves contributed to higher yields in rice (Rahman et al., 2014), and larger and heavier leaf blades also led to high grain output in six-rowed barley (Alqudah and Schnurbusch, 2015).

The position of individual leaves affects their contribution to grain yield. During the grain-filling stage of wheat, it was reported that the photosynthetic carbon assimilation of flag leaves (the final leaf to emerge before the spike) supplies >80% of the carbohydrate substrates for starch synthesis (Wu et al., 2012; Fan et al., 2017; Yang et al., 2022). In rice, the flag leaf, produces >50% of the carbohydrates that accumulate in grains (Gladun, 1993). A similar observation in barley (Zheng, 1999) suggests that the size of the flag leaf is central to single plant yield. This observation supports the relevance of understanding the genetic architecture of this phenotypic character.

Grass leaves have three distinct areas, namely the proximal sheath, distal blade, and blade sheath boundary (auricle and ligule) (Richardson et al., 2024). The aforementioned leaf morphology is initiated as the leaf primordium at the fringes of the shoot apical meristem. The primordium growth and patterning occur in three axes: the adaxial–abaxial, proximal–distal, and medial–lateral plane (Richardson et al., 2021). The basic genetic framework of leaf development from meristematic cells has been extensively studied using leaf shape and size mutants in maize (Juarez et al., 2004; Nardmann et al., 2004; Nogueira et al., 2009; Conklin et al., 2020; Zhang et al., 2020; Richardson et al., 2021). Analysis of rolled leaf 1 showed that the spatiotemporal expression of the Homeodomain-Leucine Zipper III gene via the miRNA166 pathway is the central regulator of abaxial–adaxial polarity of the developing leaf in maize (Juarez et al., 2004). Likewise, the cell proliferation along the medial–lateral plane in the leaf primordium is regulated by genetically redundant loci NARROWSHEATH1 (Ns1) and Ns2 which encode WUSCHEL-RELATED HOMEOBOX 3 (Wox3) (Richardson et al., 2021). Wox3 genes are expressed in the marginal rims. The double mutants ns1/ns2 failed to maintain

leaf margin identity and produced a narrow leaf blade and sheath, but comparable leaf length with that of the wild type. Recently, it was shown that Wox3 genes are involved in auxin biosynthesis and the development of blade sheath boundary tissues, illustrating their multiple roles in proximal–distal and medial–lateral patterning (Zhang et al., 2020; Satterlee et al., 2023). Furthermore, cell division arrests at the tip of the leaf and proceeds in a basipetal direction, and gradually transits for cell proliferation to cell expansion during leaf development (Vanhaeren et al., 2017; Lu et al., 2021).

Likewise, Narrow leaf 2 (Nal2) and Nal3 are the rice orthologs of Ns1 and Ns2, where the nal2/nal3 double mutant in rice showed a similar narrow leaf phenotype to the ns1/ns2 mutant in maize (Ishiwata et al., 2013). Several genes controlling flag leaf traits have been identified in rice, such as NARROW LEAF 7 (Nal7) (Fujino et al., 2008), NARROW LEAF 1 (Nal1) (Qi et al., 2008), SHALLOT-LIKE 1 (Sll1) (G.-H. Zhang et al., 2009), NARROW AND ROLLED LEAF 1 (Nrl1) (Hu et al., 2010), and SEMI-ROLLED LEAF 1 (Srl1) (Xiang et al., 2012; Li et al., 2017). By mutant analysis of these genes, it has been found that changes in leaf shape and size resulted from changes in cell division and/or expansion. For instance, Jiang et al. (2015) have found that leaf length and width are reduced by 50% in nal1-2 and nal1-3 rice mutants, which was caused by suppression of cell division. In addition, natural variation for flag leaf area and related traits was studied using quantitative trait locus (QTL) mapping in rice. Such studies identified additional genomic regions compared with those from mutant-based analyses, suggesting that the genetic network underlying leaf size variation in rice is not yet fully uncovered (Zhang et al., 2015; Wu et al., 2017; Tang et al., 2018; Wen et al., 2020; Wang et al., 2022; Wang et al., 2023).

In comparison with the large number of leaf mutants available in rice and maize (Neuffer et al., 1997), only a few leaf mutants are available for barley, and even fewer have been characterized. The available barley leaf mutants have been categorized as having narrow (e.g. angustifolium, fol), wide (e.g. Broad leaf1, Blf1; Broad leaf13, Blf13), long (e.g. Curly3, Cur3), or short leaves (e.g. Curly dwarf1, Cud1; Elongation1-5, Elo1-5). For some of these mutants, chromosomal positions have been determined (Druka et al., 2011).

Yet, the underlying genes for only three barley leaf mutations have been identified and functionally characterized. Narrow leafed dwarf1 (nld1) is the barley ortholog of Ns1/Ns2. The recessive nld1 allele in barely produced short plants with a narrow leaf blade, while the leaf blade length corresponded to that of wild-type plants. In contrast to Nld1, the barley mutants

Blf1 and Blf13 are characterized by wide leaf blades compared with the wild type, which is caused by an increased number of cells along the medial–lateral axis (Jöst et al., 2016, 2024). Blf1 has no significant effect on the width of the leaf sheath. In contrast, the width of the palea and lemma of blf1 mutants increases, which suggests the existence of shared genetic mechanisms to control the medial–lateral growth between these organs and the leaf blade. The effect of blf1 on blade width appears from plastochron 6 (P6) onward, indicating that Blf1 functions to limit cell proliferation in the medial–lateral axis during blade outgrowth, but does not affect the recruitment of leaf founder cells as Ns1/2 does (Jöst et al., 2016, 2024). The Blf1 locus encodes an INDETERMINATE-domain protein that is expressed in the nuclei of the shoot apical meristem, and epidermal and subepidermal cells at the base of P2 and P3 leaf primordia, and later throughout the epidermis (P5/P6), especially corresponding to presumptive veins (Jöst et al., 2016). The T189P substitution in the conserved motif of the HvHNT1 protein caused the Blf13 mutants to produce wider leaf primordia (after passing the P2 stage) and, hence, wider leaf blades than the wild type (Jöst et al., 2024). To our knowledge, no earlier studies have explored the presence of natural allelic variation at Nld1, Blf1, and Blf13.

In addition to these three mutant-based approaches mentioned above, several studies have employed the existing natural variation for leaf size in cultivated barley to unravel its genetics using genome-wide association mapping. Digel et al. (2016) have assessed the leaf blade width and length variation in a diverse panel of European winter barley cultivars and observed that the Ppd-H1 locus is associated with the studied traits. The recessive late flowering allele at ppd-H1 showed a pleiotropic effect on leaf size, producing greater blade width and length due to an extended vegetative phase. A similar observation has been reported by Alqudah et al. (2018) in a spring barley association panel. Similarly, the semi-dwarf mutations also had pleiotropic effects on leaf size where the dwarfing allele was associated with a short, narrow, and erect flag leaf in barley (Kuczyńska et al., 2013).

In addition, some studies on QTLs for flag leaf length and width have been conducted in bi-parental populations (Gyenis et al., 2007; Xue et al., 2008; Liu et al., 2015; Vafadar Shamasbi et al., 2017; Niu et al., 2022). The above-mentioned studies detected various QTLs for flag leaf size across all the chromosomes of barley. Some studies (Liu et al., 2015; Niu et al., 2022) detected QTLs which co-localized with those of the other studies (Gyenis et al., 2007; Xue et al., 2008; Du et al., 2019). Furthermore, many QTLs have been detected around the Vrs1 locus (Liu et al., 2015). One of the reasons for the relatively few detected novel QTLs in the above-

mentioned studies might be because of the limited genetic variation captured by a single bi-parental population.

The objectives of this study were to: (i) assess the genetic complexity of flag leaf size variation using a multiparent population (MPP) resource, the double round-robin population of barley (HvDRR); (ii) identify the allelic series at each QTL and a subset of the QTLs of candidate genes by local association mapping exploiting genome-wide variant information of parental inbreds as well as classical fine-mapping; and (iii) assess the potential cellular cause of flag leaf size variation for a subset of the QTLs.

2. Materials and methods

2.1 Plant materials

Our study was based on the spring barley diversity panel described by Haseneyer et al. (2010). In addition, we have selected from this panel the 23 inbreds that maximize a genotypic and trait diversity index (Weisweiler et al., 2019) and crossed them in the double round-robin design (Stich, 2009). From each of the 45 crosses, a recombinant inbred line (RIL) population was developed following the single seed descent principle. The 50 K barley single nucleotide polymorphism (SNP) array (Bayer et al., 2017) was used to genotype 35–146 RILs from each of the 45 HvDRR subpopulations in the F4 generation. As described by Casale et al. (2022), the genetic map for individual HvDRR subpopulations and a consensus map across the HvDRR population were established, and used for linkage mapping described below.

2.2 Field experiment and data collection

From 2019 to 2021, each RIL was grown in field experiments at two different locations in Germany: Köln and Mechernich in 2019 and 2020; and Düsseldorf and Mechernich in 2021. We followed an augmented incomplete block design with one replicate for each RIL in each of the six environments as well as 16–20 replicates for each of the 23 parental inbreds. The RILs from a single HvDRR subpopulation were sown in a randomized way in adjacent rows or columns with 30 seeds per entry in a 160 cm long row. The spring barley diversity panel with 224 inbreds was included in each environment.

The flag leaf length (FLL) of the main culm in centimeters was collected from 3–5 random plants of each entry in each of the six environments. In the years 2020 and 2021, from the same leaf, the flag leaf width (FLW) was also assessed in centimeters.

2.3 Statistical analyses

Data were processed and statistical analyses were performed using R software (R Core Team, 2023). Upon the removal of outliers with residuals >2.5 times the SD of the residuals from a fitted linear model (Equation 1), the measurements made for FLL and FLW in the above-described experiment were analyzed using the following mixed model:

$$y_{ijk} = \mu + G_i + E_j + (G \times E)_{ij} + e_{ijk}, \qquad (1)$$

where, yijk was the observed phenotypic value for the ith genotype in the jth environment for the kth replication, μ the general mean, Gi the effect of the ith genotype, Ej the effect of the jth

environment, (G×E)ij the interaction of the ith genotype with the jth environment, and eijk the residual. For the calculation of adjusted entry means, the genotype effect G was considered as fixed and the other effects were considered as random. For the calculation of the broad sense heritability on an entry mean basis (H2), the genotypic variance σ2g was calculated based on the above model, but with a random genotype effect. H2 was then calculated according to Piepho and Möhring (2007).

Further, we performed a single population QTL analysis for FLL and FLW in the 45 HvDRR subpopulations using the R/qtl package (Broman et al., 2003) as described in detail by Shrestha et al. (2022). First, genotype probabilities of every 1 cM were estimated, followed by a genome-wide scan for QTLs using Haley–Knott regression. A forward search algorithm was then applied to perform multiple QTL mapping. A permutation test with 4000 runs was performed, and the logarithm of the odds (LOD) score at a 0.05 significance level was set as a threshold for QTL detection. QTLs were added to the model as long as these were significant at the above-mentioned threshold.

A 1.5 LOD drop sets the confidence interval on either side of the detected QTLs (Dupuis and Siegmund, 1999). The co-localized QTLs for FLL and FLW with an overlapping confidence interval detected across the HvDRR subpopulations were summarized as consensus QTLs. The confidence interval of consensus QTLs was defined across subpopulations and phenotypes by using the shortest possible confidence interval of co-located QTLs and referred as flag leaf size- (FLS) associated loci detected in the HvDRR population (qHvDRR-FLS). The percentage of explained phenotypic variance (PEV) for these consensus QTLs was summarized as the range of the lowest and highest PEV explained by the individual populations belonging to the respective consensus QTLs.

We also performed MPP QTL analysis (Garin et al., 2017) using a consensus map across the RILs of the 45 HvDRR subpopulations. The parental model was applied to estimate the multi-QTL effect, with the assumption that (i) each parent contributes a unique allele at a QTL, and (ii) the effect of the parental inbred is constant across the subpopulations involving the parent in question. QTL scanning for FLL and FLW was performed according to the procedure described in Shrestha et al. (2022).

2.4 Genomic prediction

Genome-wide prediction for FLL and FLW was performed by genomic best linear unbiased prediction (GBLUP) using the following model (VanRaden, 2008):

$$\boldsymbol{y} = \mathbf{1}\mu + \boldsymbol{Zu} + \boldsymbol{\varepsilon}, \quad (2)$$

where y was the vector of the adjusted entry means of the HvDRR population for FLL and FLW, 1 the unit vector, μ the general mean, Z the incidence matrix of genotypic effects, u the vector of genotypic effects that were assumed to be normally distributed, with $\boldsymbol{u} \sim N(0, \mathbf{G}\sigma_u^2)$, where G denotes the relationship matrix calculated on the basis of the SNP marker data and σ_u^2 the genetic variance, and ε isthe vector of residuals following the normal distribution $\boldsymbol{\varepsilon} \sim N(0, \mathbf{I}\sigma_\varepsilon^2)$, where I was the identity matrix and σ_ε^2 the residual variance. In this study, only additive effects were considered. The GBLUP model was performed using the R package sommer (Covarrubias-Pazaran, 2016). Five-fold cross-validation was applied to evaluate the performance of the GBLUP model. Prediction ability was estimated as the Pearson's correlation coefficient between the observed and genomic estimated breeding value (GEBV). The median prediction ability across the 5-fold cross-validation was calculated for each of the 50 replicates. The PEV by the GBLUP model was the square of the median prediction ability.

2.5 Candidate gene analysis

We carried out candidate gene analysis for the consensus QTLs that were smaller than 10 Mb. For these QTLs, the list of high confidence genes was obtained from the plant genomics and phenomics research data repository from IPK Gatersleben, Germany (https://doi.ipk-gatersleben.de/DOI/d5f552ae-e6d3-4030-8c0e-4b1effc5b615/1b08648e-99af-4bb1-b32a-24576f0ee57f/2). The annotation and coordinates were based on the Morex v3 gene models (Mascher et al., 2021). The genes that displayed polymorphisms among the concerned parental inbreds were then selected using the variant calling data gathered from the whole-genome sequencing project of the 23 parental inbreds (Weisweiler et al., 2022) and were then designated candidate genes. Further, we looked for non-synonymous (amino acid substitutions) sequence variants categorized as tolerated or deleterious mutations; indels in the coding region; and indels and structural variants (SVs) in the 5'-end regulatory region (5 kb upstream of the start codon).

2.6 Detailed characterization of the effect of quantitative trait loci qHvDRR-FLS-8 and qHvDRR-FLS-17 on leaf and cell properties

We validated two QTLs, namely qHvDRR-FLS-8 and qHvDRR-FLS-17, and dissected the epidermal cell size and number on the leaf blade. Four RILs, two carrying the Georgie allele (Hv.2018S.7.02932 and Hv.2018S.7.02664) and two carrying the HOR8160 allele

(Hv.2018S.8.02731 and Hv.2018S.7.02921), at qHvDRR-FLS-8 were evaluated. Georgie and HOR8160 are the parental inbreds of the HvDRR14 subpopulation. At qHvDRR-LS-17, three RILs, namely Hv.2018S.7.03209, Hv.2018S.7.03211 (Georgie allele), and Hv.2018S.7.03369 (Lakhan allele) from the HvDRR33 subpopulation were used for QTL validation. The pair of RILs for a QTL was selected such that they were polymorphic at the QTL of interest but monomorphic at all other QTLs detected in that subpopulation, and furthermore were monomorphic for the highest number of molecular markers for the rest of the genome. Six plants of each of the seven RILs and three parental inbreds were grown in a lattice design under controlled conditions. Each plant was grown in a 1.5 liter pot filled with a mixture of sand and soil (30:70 w/w peat-based soil 'Einheitserde Deklarationstyp 3'). The day length was set to 16 h followed by 8 h darkness. The light intensity was set to 300 µmol m−2 s−1, 50 cm away from the light source, and the relative humidity to 55%. The temperature under daylight was 20 °C and the night temperature was 18 °C.

We measured the length and width of the flag leaf (FL) and the second (L2), third (L3), and fourth (L4) fully expanded leaf from the top of the main culm. The collected data of leaf size were then analyzed using the following fixed model:

$$z_{ijmnk} = \mu + \alpha_i + \beta_j + (\alpha \times \beta)_{ij} + \delta_m + \gamma_n + e_{ijmnk}, \quad (3)$$

where, zijmnk was the observed phenotypic value for the ith genotype for the jth leaf type at the mth row and the nth tray for the kth replication, µ the general mean, αi the effect of the ith genotype, βj the effect of the jth leaf type, (α×β)ij the interaction of the ith genotype with the jth leaf type, δm the effect of the mth row, γn the effect of the nth tray, and eijmnk the residual. For the calculation of adjusted entry means, all the effects were considered as fixed.

From the same plants, leaf imprints were taken from the top three leaves for QTL qHvDRR-FLS-8 and the top two leaves for QTL qHvDRR-FLS-17 for the significantly different RILs to assess cell size and cell number. We prepared epidermal imprints from the middle of the adaxial side of the leaf in the direction of the leaf length. This was realized by applying a film of transparent nail polish which was then transferred with transparent adhesive tape to microscope slides. Images of the epidermal cells from the imprints were recorded from two field of views using a Nikon SMZ18 stereo microscope equipped with a Nikon DS-Fi2 camera at ×10 magnification. The software ImageJ (Schneider et al., 2012) was used to assess the length of lateral cells and count the number of cell files. The length was measured for all the lateral cells

per row per imprint bordering the stomata cell files (Supplementary Fig. S1). The collected cell dimensions were then analyzed using Equation 3.

2.7 Fine-mapping of quantitative trait locus qHvDRR-FLS-8 on chromosome 2H

We developed a high-resolution mapping population by crossing two RILs from the HvDRR14 subpopulation that were also included in the above-described experiment, namely Hv.2018S.7.02932 and Hv.2018S.7.02921 that harbored Georgie and the HOR8160 allele at QTL qHvDRR-FLS-8 on chr2H. Then, we genotyped the left border (LB) and the right border (RB) of the QTL interval in 1890 F2 progenies using Kompetitive allele-specific PCR (KASP PCR) markers (Supplementary Table S1). DNA was extracted from 7- to 10-day-old seedlings for genotyping, and the KASP™ assay was performed using a Quantstudio5 real-time PCR machine (Thermo Fischer Scientific). The recombinants between LB and RB were transplanted to 1.5 liter pots. The recombinants were further genotyped inside the QTL interval (Supplementary Table S1) and were grown in the greenhouse until maturity.

Further, the F3 progenies derived from the above-mentioned recombinants were grown in the field between March and July 2024 at Groß Lüsewitz in Germany, following an augmented block design with two replicates. The experiment contained two blocks (the replicates) with 30 seeds per recombinant in a 160 cm long row in each block; each recombinant appeared only once in one block. At the heading stage, when the flag leaf was fully developed, leaf length was evaluated from three different randomly selected plants per row.

Then, phenotypic data of F3 progenies were analyzed using the following model:

$$y_{ijm} = \mu + \alpha_i + \beta_j + \lambda_m + e_{ijm} \qquad (4)$$

where, where, yijm was the observed phenotypic value for the ith genotype in the jth block at the mth range, μ the general mean, αi the effect of the ith genotype, βj the effect of the jth block, λm the effect of the mth range, and eijm the residual. For the calculation of adjusted entry means, all the effects were considered as fixed. We performed marker trait correlation with the adjusted entry means of FLL and the genotypic data of the F2 progenies using an additive and dominance effects model.

3. Results

3.1 Phenotypic variation for flag leaf length and width

FLL and FLW phenotypes were collected across six and four environments, respectively, for ~3866 RILs from the 45 HvDRR subpopulations as well as the diversity panel. The parental inbreds were replicated 16–20 times in each environment as repeated checks to account for field heterogeneity. We observed a significant variation in the phenotype FLL and FLW among the inbreds of the diversity panel originating from different continents, with genotypes from South Asia and East Asia producing comparatively longer and wider flag leaves (Fig. 1). Smaller flag leaves were common among the genotypes from Europe, except southern Europe. Notably, we also observed a considerable diversity for FLL and FLW across the RILs of the HvDRR population. The adjusted entry means of RILs across six environments for FLL varied between 5.6 cm and 19.1 cm (Fig. 2, File 1 at Zenodo). For FLW, the range on a proportional scale was even larger at 0.25–2 cm (Fig. 2, File 1 at Zenodo). The range of FLL and FLW of RILs from 45 subpopulations was the same as those observed for the diversity panel. The subpopulation with the highest diversity for FLL was HvDRR43, with a coefficient of variation (CV) of 18.8%, whereas HvDRR08 had the lowest CV (7.4%). CV of FLL for the diversity panel (14%) fell between the above-mentioned two extreme cases. This trend was different for FLW, where the highest CV was observed for the diversity panel with 41.6%. The CVs for the HvDRR subpopulations were lower, ranging from 12.8% (HvDRR07) to 28% (HvDRR47) (Supplementary Table S2). The majority of these differences were due to genetics as the H2 on an entry mean basis was 0.77 for FLL and 0.58 for FLW (Table 1). We observed a correlation coefficient of 0.62 (Supplementary Fig. S2A) for the correlation between FLL and FLW across all the evaluated entries. However, the level of association differed considerably between the different characterized material groups. The correlation coefficient was 0.62 for the diversity panels and ranged from −0.24 to 0.87 for the individual HvDRR subpopulations (Supplementary Figs S2A, B, S3). In 40 HvDRR subpopulations and the diversity panel, the correlation between FLL and FLW was significantly ($P<0.05$) different from 0 (Supplementary Fig. S3).

3.2 Quantitative trait loci associated with flag leaf size

First, we performed MPP analyses that detected 15 and 12 QTLs associated with FLL and FLW, respectively. Seven of these QTLs were associated with both FLL and FLW (Fig. 3). In the next step, we performed subpopulation-specific QTL analysis and detected a total of 79

QTLs for FLL and FLW. The QTLs were detected in 29 and 15 of the HvDRR subpopulations for FLL and FLW, respectively (Fig. 4). Among the detected QTLs, 36, 11, and 12 were located on chromosomes 2H, 3H, and 5H, respectively. The number of QTLs on the remaining chromosomes varied between four and six (Fig. 4; Supplementary Tables S3, S4). Except for a locus on chr2H (qFL2-2, qFW2-2), all the MPP QTLs were detected at the same position in the subpopulation-specific analyses, which illustrated the accuracy of the QTLs identified in the study. The PEV for individual QTLs varied from 3% to 46% (Supplementary Tables S3, S4). About 77% of the QTLs detected in our study explained ≥10% of the phenotypic variance for the associated characteristics (Supplementary Tables S3, S4). We further summarized these 79 QTLs into 24 consensus QTLs based on their overlapping confidence intervals. Of these 24 consensus QTLs, 12 QTLs were shared between FLL and FLW. Moreover, 10 QTLs were only associated with FLL, of which nine were unique to individual subpopulations. The remaining two consensus QTLs were detected only for FLW, of which one QTL was unique to subpopulation HvDRR31 (Supplementary Table S5). The PEV explained by a GBLUP model across all genome-wide SNPs across the entire HvDRR population was 61.2% (FLL) and 51.9% (FLW).

When mapping the epistatic QTL for each HvDRR subpopulation, one pair of epistatic QTLs was detected in HvDRR38 for FLW, which were located on chr6H and chr7H at 162 cM and 221 cM, respectively. In addition, we detected significant interactions among the main effect QTLs in HvDRR31 for FLL and in HvDRR30 and HvDRR32 for FLW. The main effect QTL associated with FLL from HvDRR31, qFL_Hv31_2H_1, showed a significant interaction with three QTLs, namely qFL_Hv31_2H_2, qFL_Hv31_2H_3, and qFL_Hv31_7H_1. In addition, we also detected significant interactions between the two main effect QTLs qFL_Hv31_2H_2 and qFL_Hv31_7H_1 in the same subpopulation. In addition, we observed a significant interaction between three pairs of major effect QTLs linked to FLW in HvDRR30 and one pair of major effect QTLs in HvDRR32.

Next, we estimated the additive effect of each parental inbred across the MPP QTLs. The QTL allele effects ranged from −1.04 cm to 0.72 cm and from −0.09 cm to 0.08 cm for FLL and FLW, respectively (Supplementary Fig. S4). Furthermore, the frequency of QTLs with minor effect was higher compared with those with large effect (Supplementary Fig. S4). In addition, the crossing design of the HvDRR population allows estimation of the allelic series for QTL effect discussed above. At each MPP QTL, we observed an allelic series for both FLL and FLW (Fig. 5). These observations illustrated that the phenotypic variation for FLL and FLW

in the HvDRR population was controlled by the cumulative effect of minor effect alleles and a few large effect alleles (Fig. 5; Supplementary Fig. S4).

3.3 Candidate genes associated with flag leaf length and width

The variant calling data from the whole-genome sequencing of the 23 parental inbreds, including SNP annotations, indels, and predicted SVs (Weisweiler et al., 2022), were used to select the candidate genes in the consensus QTL interval that were smaller than 10 Mb, which was the case for nine QTLs (qHvDRR-FLS-2, qHvDRR-FLS-3, qHvDRR-FLS-7, qHvDRR-FLS-8, qHvDRR-FLS-15, qHvDRR-FLS-17, qHvDRR-FLS-19, qHvDRR-FLS-20, and qHvDRR-FLS-23). For these nine consensus QTLs, we found a total of 900 positional candidate genes. The number of positional candidate genes for each consensus QTL varied between 11 and 206 (Supplementary Table S6).

Out of the 24 consensus QTLs, 12 contained the closest barley orthologs of genes involved in developmental processes in barley or other crops (Supplementary Tables S5, S7). Allelic variations in the regulatory or coding region for some of these orthologs were found among the parental inbreds of QTL-bearing subpopulations (Supplementary Tables S5, S6). For example, we found indels in the promoter region of Tcp5 and Grf5 genes residing in qHvDRR-FLS-2 which are known to be involved in defining organ size in Arabidopsis (Horiguchi et al., 2005; van Es et al., 2018; Yu et al., 2021). At qHvDRR-FLS-2, we found 5–13 bp deletions in the promoter region of the Tcp5 gene in HOR1842, HOR12830, and K10693 (contributing to a longer/wider FL) compared with ItuNative (contributing to a shorter/narrower FL), indicating a possible cis-regulatory effect (Supplementary Fig. S5). Likewise, 6 bp deletions in the 5'-untranslated region (UTR) and 25 bp deletions in the first intron of CM67 (contributing to a longer FL) compared with ItuNative (contributing to a shorter FL) in Grf5 was the promising candidate gene for qHvDRR-FLS-15 (Supplementary Fig. S6). In addition, we also detected QTLs for FLL and FLW at major flowering time loci in barley (Supplementary Fig. S7; Table 2; Supplementary Tables S8, S9). The hypermethylated epiallele and intron variation allele Vrn-H1-3 associated with earlier flowering contributed to a longer FL (Table 2; Supplementary Fig. S7).

3.4 Validation and characterization of quantitative trait loci qHvDRR-FLS-8 and qHvDRR-FLS-17 under controlled conditions

qHvDRR-FLS-8 on chr2H was one of the major effect QTLs for FLS, with PEV ranging from 8% to 32% across the individual HvDRR subpopulations (Supplementary Table S5). We validated the effect of qHvDRR-FLS-8 on FLL in the HvDRR14 subpopulation by comparing RILs Hv.2018S.7.02932 and Hv.2018S.7.02664 carrying the Georgie allele with RILs Hv.2018S.8.02731 and Hv.2018S.7.02921 carrying HOR8160 allele at qHvDRR-FLS-8 while the rest of the genome was close to isogenic. We observed that the FL, L2, and L3 of one of the RIL with the Georgie allele (Hv.2018S.7.02932) were significantly longer ($P<0.05$, $n=6$) compared with the RILs carrying the HOR8160 allele at this QTL. However, for the other RIL with the Georgie allele (Hv.2018S.7.02664), the corresponding tests for L3 were not significant due to a lower number of observations ($n = 5$). This trend between the RILs with significantly different leaf length was consistent with the QTL effect detected in our analysis. However, it contradicted the leaf size phenotype of the parental inbreds, where Georgie had shorter leaves than HOR8160, particularly for L2 and L3 (Fig. 6A–B). This subpopulation also harbors an additional QTL, qHvDRR-FLS-22 on chr6H, where the HOR8160 allele contributes to longer flag leaves. The selected RIL pairs are only polymorphic at QTL qHvDRR-FLS-8, and all the four RILs carry the Georgie allele at QTL qHvDRR-FLS-22. In contrast, the parental inbreds are polymorphic for all the QTLs detected in this subpopulation, which is the reason behind the observation that HOR8160 has longer leaves (FL, L2 and L3) than Georgie despite the fact that HOR8160 carries the allele at qHvDRR-FLS-8, which causes a shorter flag leaf.

Next, we measured the length of lateral cells in the qHvDRR-FLS-8 RIL pairs and the parental inbreds and further used these data to estimate the number of lateral cells per file across the leaf length. This was done in order to determine if leaf length differences are due to longer lateral cells or more lateral cells. We observed a significant difference in the length of the lateral cells between the parental inbreds (Supplementary Fig. S8). However, the RIL pairs with a contrasting allele at qHvDRR-FLS-8 showed a significant difference in the number of lateral cells per file across the leaf length which indicates that at this QTL the difference in the leaf length might be due to a difference in cell proliferation (Fig. 6C–G).

qHvDRR-FLS-17 on chr4H was another major effect QTL for FLS, with PEV ranging from 13% to 28% across the HvDRR subpopulations (Supplementary Table S5). We validated qHvDRR-FLS-17 for FLW in the HvDRR33 subpopulation by comparing RILs

Hv.2018S.7.03209 and Hv.2018S.7.03211 carrying the Georgie allele, and Hv.2018S.7.03369 carrying the Lakhan allele at this QTL. A significantly narrower FL and L2 were observed for the RIL with the Georgie allele (Hv.2018S.7.03209) compared to those with the Lakhan allele (Hv.2018S.7.03369) at qHvDRR-FLS-17. However, the other RIL (Hv.2018S.7.03211) with the Georgie allele had an FL and L2 width intermediate between those of Hv.2018S.7.03209 and Hv.2018S.7.03369. This trend between the RILs with significantly different leaf width was in accordance with the QTL effect observed in the QTL analysis and also in line with the parental inbreds, where Georgie had narrower leaves than Lakhan (Fig. 7A).

Next, we estimated the total number of cells files across the leaf width and the average width of lateral cells (Fig. 7B–F; Supplementary Fig. S9). At the QTL qHvDRR-FLS-17, the total number of cell files along the leaf width and the average width of cell files might collectively influence the difference in FLW between the RIL pairs (Fig. 7F; Supplementary Fig. S9).

3.5 Fine-mapping of quantitative trait locus qHvDRR-FLS-8 on chr2H

For fine-mapping, we obtained the segregating population from the genetic cross between the above-mentioned RILs from the HvDRR14 subpopulation, Hv.2018S.7.02932 and Hv.2018S.7.02921 that are carrying the Georgie allele and the HOR8160 allele, respectively, at qHvDRR-FLS-8. To enhance the resolution, 222 F2 plants that were recombinant between the markers flanking the QTL were further genotyped inside the interval. Later, F3 seeds of those recombinants were grown in the field and FLL was evaluated at the heading stage, and was found to range from 4.8 cm to 18.2 cm. The H2 was 48% for FLL in this segregating population. Collectively, the genotypic data of the F2 population and phenotypic data from the F3 population were used for single marker regression analysis. The segregating non-recombinants carrying the Georgie allele at all the markers had significantly longer flag leaves than the individuals carrying the HOR8160 allele which additionally validated the QTL (Fig. 8). The heterozygous individuals in the QTL region mimicked the phenotype of the individuals carrying the HOR8160 allele. The recombination analysis allowed us to delimit the QTL interval between M7 and M47 (626.5–629.9 Mb) consisting of 77 high confidence genes inside the new interval (Supplementary Table S10).

4. Discussion

Leaf size is unquestionably a key agronomic phenotype as the leaf is the main source of photosynthetic assimilates. Leaf size differences, and the flag leaf in particular, are associated

with yield potential in different plant species (Williams and Hayes, 1979). With this study, we aimed to understand the genetic complexity of FLL and FLW variation in barley.

4.1 Flag leaf size variation and its association with the geographic origin

The length and width of the flag leaf of inbreds from warm regions of the world were greater than those from cold regions (Fig. 1). The observation contradicts the theory of a daytime energy budget (carbon assimilation versus water loss) where larger leaves are disadvantageous in warmer regions (Wright et al., 2017). One explanation for our finding might be that spring barley is cultivated from autumn (sown in October/November) to spring season (harvested in March/April) in warm and arid regions (Tabarzad et al., 2016), which reduces the high temperature constraint. On the other hand, spring barley in Europe and North America is grown from spring to summer (Wiersma and Ransom, 2005; Marcinkowski and Piniewski, 2018), which rules out that smaller leaves compensate for frost tolerance. However, the aforementioned trend that inbreds from warm regions had longer and wider flag leaves than those from colder regions was evident even within the European continent. FLL and FLW were greater in the inbreds from Southern Europe than those from Northern Europe. Likewise, the inbreds from Central Asia with a harsh winter showed FLL and FLW characteristics similar to those of Europe and North America, indicating a consistent spread of flag leaf characters along the temperature gradient.

It is also possible that the difference in leaf size can be compensated through the number of tillers and leaf number per culm in the inbreds from the temperate regions. Such studies at the population level are not available. However, on a physiological level, barley plants produce more tillers and final shoot biomass when grown at 15 °C compared with those grown at 25 °C (Hemming et al., 2012). Hence, the FLS alone might not be a good predictor of a vegetation model for the energy balance theory in barley and grasses in general. One approach to better understand this leaf size and temperature relationship on an ecological scale is to assess the effect of the individual genes contributing to leaf size variation.

4.2 Genetic factors play a major role in controlling flag leaf size characteristics in barley

In our study, we identified a high genetic contribution in defining FLS characteristics in HvDRR, with the H2 on an entry mean basis of ~77% for FLL and ~58% for FLW (Table 1). The H2 of FLL and FLW observed in our study corresponded to previous reports (Liu et al.,

2015; Digel et al., 2016; Alqudah et al., 2018; Jabbari et al., 2018; Du et al., 2019), indicating that a significant component of natural variation is under genetic control, enabling isolation of causative genes.

The range of FLL (5.6–19 cm) and FLW (0.25 to 2.03 cm) observed in RILs of the HvDRR population was greater than those reported by Jabbari et al. (2018) in an association mapping panel, indicating greater phenotypic diversity in the HvDRR population. This was further supported by the observation that phenotypic variation for FLL and FLW among the RILs of HvDRR was similar to those observed in the diversity panel evaluated in the current study. This finding illustrated the potential of the HvDRR population for genetic, physiological, and ecological analyses.

The ranges reported by bi-parental population studies for FLL can be divided into two groups, the first one that observed a wide range of phenotypic variation: Gyenis et al. (2007) recorded a range of 8–34 cm; Vafadar Shamasbi et al. (2017), 3.9–13.4 cm; and Niu et al. (2022), 5–31 cm. The high range of variation can be attributed to favorable controlled conditions (Liu et al., 2015; Digel et al., 2016; Alqudah et al., 2018) or single selected environmental conditions (Du et al., 2019) that were used in the respective studies. On the other hand, a limited range of variation for FLL was reported for some studies, 17–19 cm (Liu et al., 2015) and 12–14 cm (Du et al., 2019). In addition, the phenotypic range of FLW in previous studies in barley (Gyenis et al., 2007; Liu et al., 2015; Vafadar Shamasbi et al., 2017) was also narrower than those observed in our study. The above-described limited range of FLL and FLW can be explained by the fact that those studies were conducted in individual bi-parental populations and the genetic divergence among the two parental genotypes was low. In contrast, the parents of the HvDRR population were selected to maximize genotypic and phenotypic diversity (Weisweiler et al., 2019).

4.3 Genetic complexity of flag leaf size variation

Seventy-nine subpopulation-specific QTLs detected in our study coincided with those detected using MPP QTL analysis for flag leaf size variation (Figs 3, 4). The significance of QTLs detected in the MPP analysis was higher than those detected in subpopulation-specific QTL analysis (Fig. 3; Supplementary Tables S3, S4). We summarized these QTLs into 24 consensus QTLs. Furthermore, we compared the physical interval of these 24 consensus QTLs with those reported in previous studies, whenever possible. We found that seven of the 24 consensus QTLs have been reported previously, which highlights the accuracy of the QTLs detected in our study

(Supplementary Table S5). On the other hand, however, we detected 17 novel loci that explained between 3% and 44% phenotypic variance (Supplementary Tables S3, S4). This observation illustrated the potential and statistical power of a large and diverse MPP to detect novel and rare variants. Nevertheless, our findings suggest that even all consensus QTLs together explained just ~60% of the total phenotypic variance, illustrating the genetic complexity of the studied traits.

Regardless of the significant genetic complexity of the investigated characteristics across all HvDRR subpopulations, the proportion of the QTLs explaining ≥10% PEV was high. In addition, we observed an allelic series for the detected QTLs (Fig. 5). These findings suggest that fine-mapping and, eventually, reverse genetics approaches to isolate the underlying genes will be possible for a substantial number of the detected QTLs when the most relevant subpopulations are studied.

4.4 The function of some developmental genes might be conserved in crops

We detected QTLs for FLL and FLW harboring/residing close to known flowering time genes such as Ppd-H1, Vrn-H1, and Vrn-H2 (Supplementary Table S5). In addition, 83% of the QTLs detected in our study co-localized with QTLs previously detected for grain size, flowering time, and plant height in the HvDRR population (Shrestha et al., 2022; Cosenza et al., 2024). Flowering time genes are reported to have pleiotropic effects on root and shoot growth (Arifuzzaman et al., 2016; Voss-Fels et al., 2018; Cosenza et al., 2024). For example, the late flowering allele of Ppd-H1 (reduced photoperiod sensitivity) produced larger leaves in barley (Alqudah et al., 2018) than the early alleles (Ppd-H1, photoperiod sensitive). This report is in accordance to our observation that in the subpopulations HvDRR18 and HvDRR30, the parental inbred that contributed to the early flowering allele at the Ppd-H1 locus had a smaller flag leaf than those associated with the late flowering allele. However, the opposite trend was observed for HvDRR26 and HvDRR39 where the early flowering allele at Ppd-H1 was associated with a longer and wider leaf (Supplementary Table S8). This result contradicted those of Digel et al. (2016) where under long-day conditions Ppd-H1 (late allele) produced larger leaves than the genotypes carrying the early alleles. This finding might indicate that there is an additional gene located next to Ppd-H1 which contributes to leaf size variation in the subpopulations HvDRR26 and HvDRR39.

Vrn-H1 and Vrn-H2 separate winter and spring type in barley. Although our parental inbreds have been classified as spring type (Cosenza et al., 2024), we detected heading date (Cosenza

et al., 2024) and leaf size QTLs at Vrn-H1 and Vrn-H2. However, we have observed no association between the presence of the late flowering allele and larger leaf size at QTLs co-localizing with Vrn-H2 in HvDRR30, HvDRR33, and HvDRR43 (Supplementary Table S9). Therefore, there might be a gene independent of Vrn-H2 in the aforementioned QTL interval which is regulating the leaf size. On the other hand, we reported for the first time that allelic variation of Vrn-H1 influenced FLL in spring barley in long-day conditions. The 11 kb long intron 1 regulates the cold responsiveness, and the deletion mutation in intron 1 bypasses the vernalization requirement in spring barley (Hemming et al., 2009). We found an allelic series for the deletion mutation in intron 1 (Supplementary Fig. S7) affecting the flowering time in spring barley (Table 2). The early flowering allele Vrn-H1-3 was associated with a longer flag leaf (Table 2). In addition to the intron deletion, we found that hypermethylation of a 116 bp region in intron 1 (chr5H: 528 153 135–528 153 251) (Kühl et al., 2025) reduced flowering time and increased FLL. Hence, our study uncovered a previously unknown association of Vrn-H1 with flag leaf size in spring barley.

The pleiotropic effect of the flowering time loci on above-ground biomass can be attributed to the duration of vegetative growth before transition to the reproductive phase (Neumann et al., 2017). However, the widely accepted correlation between early flowering and smaller leaf did not align perfectly with the flowering time-associated loci in our study. This might be caused by the differences in the number of leaves or tillers between early and late flowering genotypes compensating for the differences in leaf size.

In addition to flowering time genes, we also detected QTLs that harbored orthologs of genes involved in leaf size variation in other plant species (Supplementary Table S5). For instance, in the consensus QTL qHvDRR-FLS-2, a barley gene (HORVU.MOREX.r3.1HG0077830) which is an ortholog of Tcp5 resides. Tcp5 belongs to the TCP family of transcription factor-containing protein genes and is the most promising candidate gene underlying qHvDRR-FLS-2. Yu et al. (2021) observed that the TCP5–KNAT3/SAW1 pathway plays an important role in defining the leaf margin in Arabidopsis.

The consensus QTL qHvDRR-FLS-15 on chr4H in our study overlapped with the previously detected QTL cluster C4 (Du et al., 2019), and this region harbors the barley ortholog (HORVU.MOREX.r3.4HG0339430) of Arabidopsis Growth-Regulating Factor (GRF5) (Supplementary Table S5). Grf5 belongs to the plant-specific family of transcription factor genes which are known to be involved in different plant development processes (Hewezi et al.,

2012; Kim et al., 2012; Bao et al., 2014; Debernardi et al., 2014; Liang et al., 2014; Liu et al., 2014; Pajoro et al., 2014). In Arabidopsis, GRF5 was seen to interact with AN3 and manipulate cell proliferation in leaf primordia (Horiguchi et al., 2005). The polymorphisms in Tcp5 and Grf5 genes between the small and large FL were located in the promoter region (Supplementary Figs S5, S6), indicating a possible cis-regulatory difference.

Also, we found HORVU.MOREX.r3.4HG0402190, which is the ortholog of NARROW LEAF7 (Nal7) residing in the consensus QTL qHvDRR-FLS-16 on chr4H. Nal7 belongs to the flavin-containing monoxygenase family and is known to control the width of the leaf blade in rice (Fujino et al., 2008). Hence, the function of the barley orthologs of Tcp5, Nal7, and Grf5 might be conserved and worth investigating in barley using transgenesis.

For other QTLs that explained a high proportion of genotypic variance for leaf size, we did not find plausible candidate genes inside the confidence interval. The number of annotated genes in the confidence intervals, however, was too high for a direct transgenic validation. Therefore, fine-mapping is one of the promising approaches to isolate underlying genes for such QTLs.

In the present study, we fine-mapped the QTL qHvDRR-FLS-8 which is significantly associated with FLL. Using only eight markers across the initial confidence interval of 8.7 Mb, we were able to reduce the region by two-fifths. Seventy-seven annotated high confidence genes are located in the reduced interval (Supplementary Table S10). Among them, 75 are polymorphic between the parental inbreds, which makes a prioritization difficult (Supplementary Table S10). However, the number of recombination events between M7 and M47 is four, which will allow us to further narrow down the interval by genotyping additional markers in the interval (Fig. 8). Furthermore, ~300 additional recombinants are selected in the F4 generation. Nevertheless, two genes are compelling candidates among the 75 polymorphic genes in the narrowed genomic interval. The first, HORVU.MOREX.r3.2HG0201480, is the ortholog of SMALL AUXIN-UP RNA 23 (OsSAUR23), which was recently reported to control organ size in rice (Huang et al., 2025). Another candidate gene is HORVU.MOREX.r3.2HG0202180, which is the ortholog of ILI1-binding bHLH protein 1 (IBH1) which regulates cell elongation in Arabidopsis (L.-Y. Zhang et al., 2009; Ikeda et al., 2012; Lu et al., 2021).

4.5 Quantitative trait loci qHvDRR-FLS-8 and qHvDRR-FLS-17 also determine the size of leaves older than the flag leaf

We characterized the effect of qHvDRR-FLS-8 and qHvDRR-FLS-17 in detail, as well as examining the anatomy of the leaf epidermis to understand the link between leaf size and pavement cell size. Although these QTLs were detected based on the dimensions of the FL, they also influenced the size of older leaves (Figs 6, 7). For example, we saw that the leaf length was significantly different for the top three leaves, whereas the fourth leaf showed no significant variation. For leaf width, the significant differences were limited to the top two leaves.

The above findings are in contrast to results for the genes Blf1 and Nld1 which are known to influence the width of all the leaves in barley (Jöst et al., 2016; Yoshikawa et al., 2016). The same observation was made in rice for Nal1 and Nal2 (Ishiwata et al., 2013). Our observation is in agreement with the results of Zanella et al. (2023) who studied an MPP of wheat. In this study, FLL5A was observed to control the size of the flag leaf, but the effect was gradually decreasing down towards the third leaf. One of the reasons that the behavior of QTLs detected in our study and that of Zanella et al. (2023) is different from that of the known genes influencing leaf size might be that the QTLs studied here represent natural variation and not knockout/overexpression lines. Therefore, the differences between alleles, for example with respect to their gene expression but also protein functionality, may be smaller.

It is known that leaf shape and size are the result of coordinated action of cell proliferation in the primordium and cell expansion during leaf blade elongation (Donnelly et al., 1999; Nath et al., 2003). For a better understanding of leaf size modulation, we characterized the QTLs qHvDRR-FLS-8 and qHvDRR-FLS-17 by analyzing the cells in the adaxial epidermis of the leaf blade. We measured the length of the lateral cells adjacent to the stomatal rows. The differences in FLS between parental inbreds might be associated with lateral cell expansion. A similar behavior was observed in the parental inbreds of wheat. Zanella et al. (2023) reported that cell size determined the leaf length at FLL5A. When we compared the RILs polymorphic only at qHvDRR-FLS-8, we found that the difference in FLL was caused by cell division but not longitudinal epidermal cell expansion.

Further, RILs carrying an allele associated with a wider leaf blade at qHvDRR-FLS-17 showed differences in both the number and size of cell files on the lateral plane in both FL. In contrast, L2 was characterized by a significant difference only in number of cell files related to

transverse/lateral cell proliferation Similarly, Jöst et al. (2016, 2024) and Yoshikawa et al. (2016) observed that in their mutant-based studies in barley, the change in the leaf width was due to change in the cell file number.

5. Conclusion

The study identified a previously unknown association of a longer and wider flag leaf in genotypes adapted to warm regions in a barley natural population. In addition, we provided a comprehensive genetic control of FLL and FLW variation in barley and detected 17 novel genetic loci associated with flag leaf size. Furthermore, we identified subpopulations for fine-mapping major effect QTLs detected in the study. We also illustrated this by fine-mapping of qHvDRR-FLS-8, and we are one step closer to isolating the causal gene. Thereby, our study opens the door to functional validation of isolated candidate genes using transgenesis to unravel the underlying basis of the leaf size gradient across the globe but also to optimize leaf size with respect to carbon assimilation.

Acknowledgements

The authors would like to thank Konstantin Shek and Stephanie Krey (Quantitative Genetics and Genomics of Plants, Heinrich-Heine-University) for field and greenhouse management in Dusseldorf and Cologne. We are grateful to Vasantha Nagam, Anna-Lena Hippel, Bjarne Michelsen, Uwe Gräf, Brigit Lemcke, Benjamin Brüdigam, Petra Müller, Grit Waldbauer, Jens Rokitte, Bernd Keding (Institute for Breeding Research on Agricultural Crops, Julius Kühn Institute) for their support in management of greenhouse and field experiments in Groß Lüsewitz. We also thank our student helpers Michael-Tobias Borghorst, Anabelle Odebrecht, and Maximilian Maßling (Heinrich-Heine-University) for their help in leaf sampling. Finally, we would like to thank Anjali Walpola, Aashu and Kefas Baiyi (Institute for Breeding Research on Agricultural Crops, Julius Kühn-Institute) for offering helping hands during field harvesting. We gratefully acknowledge Bernd Hackauf for his constant support and for the information and discussions regarding rice orthologs in barley, which greatly facilitated our project.We gratefully acknowledge the editor and reviewers for their valuable feedback and thoughtful suggestions, which significantly improved this work.

Author contributions

BS and AS: conceptualized the study and supervised the work; BS: acquired the funding; TL, YG, and AS: conducted the experiments; TL, YG, PW, BS, and AS: analyzed the data; DVI and AS: designed and executed the field trials; TL, BS, and AS: wrote the manuscript. All authors read, corrected, and approved the manuscript.

Conflict of interest

None declared.

Funding

We would like to thank the Deutsche Forschungsgemeinschaft (DFG, German Research Foundation) for financially supporting this work of the project ‘Fitness effect of molecular variants of leaf area and economics spectrum of Hordeum vulgare’ within the transregional collaborative research center TRR341 ‘Plant Ecological Genetics’. We also acknowledge the computational platform provided by the Centre of Information and Media Technology at Heinrich-Heine-University Düsseldorf and the department for Digitalisation and Artificial Intelligence of the Julius Kühn-Insitute. We would also like to acknowledge that this work was

supported by de.NBI Cloud within the German Network for Bioinformatics Infrastructure (de.NBI) and ELIXIR-DE (Forschungszentrum Jülich and W-de.NBI-001, W-de.NBI-004, W-de.NBI-008, W-de.NBI-010, W-de.NBI-013, W-de.NBI-014, W-de.NBI-016, W-de.NBI-022).

Data availability

The data across all environments, adjusted entry means of the parental inbreds, and recombinant inbred lines of 45 HvDRR subpopulations and QTL validation experiment data have been deposited at Zenodo (https://zenodo.org/records/16982834). Genetic maps and variant calling data can be obtained from Casale et al. (2022) and Weisweiler et al. (2022). The scripts used for data analysis and to prepare the graphs are deposited at GitHub (https://github.com/Twinkallapasiya/QTLmapping). Requests for seeds of RILs from the HvDRR population or subpopulations should be directed to the corresponding authors.

References

Alqudah AM, Schnurbusch T. 2015. Barley leaf area and leaf growth rates are maximized during the pre-anthesis phase. Agronomy 5, 107–129.

Alqudah AM, Youssef HM, Graner A, Schnurbusch T. 2018. Natural variation and genetic make-up of leaf blade area in spring barley. Theoretical and Applied Genetics 131, 873–886.

Arifuzzaman M, Günal S, Bungartz A, Muzammil S, Afsharyan NP, Léon J, Naz AA. 2016. Genetic mapping reveals broader role of Vrn-H3 gene in root and shoot development beyond heading in barley. PLoS One 11, e0158718.

Bao M, Bian H, Zha Y, Li F, Sun Y, Bai B, Chen Z, Wang J, Zhu M, Han N. 2014. miR396a-mediated basic helix–loop–helix transcription factor bHLH74 repression acts as a regulator for root growth in Arabidopsis seedlings. Plant and Cell Physiology 55, 1343–1353.

Bayer MM, Rapazote-Flores P, Ganal M, et al. 2017. Development and evaluation of a barley 50k iSelect SNP array. Frontiers in Plant Science 8, 1792.

Blum A. 1985. Photosynthesis and transpiration in leaves and ears of wheat and barley varieties. Journal of Experimental Botany 36, 432–440.

Casale F, Van Inghelandt D, Weisweiler M, Li J, Stich B. 2022. Genomic prediction of the recombination rate variation in barley—a route to highly recombinogenic genotypes. Plant Biotechnology Journal 20, 676–690.

Conklin PA, Johnston R, Conlon BR, Shimizu R, Scanlon MJ. 2020. Plant homeodomain proteins provide a mechanism for how leaves grow wide. Development 147, dev193623.

Cosenza F, Shrestha A, Van Inghelandt D, Casale FA, Wu PY, Weisweiler M, Li J, Wespel F, Stich B. 2024. Genetic mapping reveals new loci and alleles for flowering time and plant height using the double round-robin population of barley. Journal of Experimental Botany 75, 2385–2402.

Covarrubias-Pazaran G. 2016. Genome-assisted prediction of quantitative traits using the R package sommer. PLoS One 11, e0156744.

Debernardi JM, Mecchia MA, Vercruyssen L, Smaczniak C, Kaufmann K, Inze D, Rodriguez RE, Palatnik JF. 2014. Post-transcriptional control of GRF transcription factors by microRNA miR396 and GIF co-activator affects leaf size and longevity. The Plant Journal 79, 413–426.

Digel B, Tavakol E, Verderio G, Tondelli A, Xu X, Cattivelli L, Rossini L, von Korff M. 2016. Photoperiod-H1 (Ppd-H1) controls leaf size. Plant Physiology 172, 405–415.

Donald CM. 1968. The breeding of crop ideotypes. Euphytica 17, 385–403.

Donnelly PM, Bonetta D, Tsukaya H, Dengler RE, Dengler NG. 1999. Cell cycling and cell enlargement in developing leaves of Arabidopsis. Developmental Biology 215, 407–419.

Druka A, Franckowiak J, Lundqvist U, et al. 2011. Genetic dissection of barley morphology and development. Plant Physiology 155, 617–627.

Du B, Liu L, Wang Q, Sun G, Ren X, Li C, Sun D. 2019. Identification of QTL underlying the leaf length and area of different leaves in barley. Scientific Reports 9, 4431.

Dupuis J, Siegmund D. 1999. Statistical methods for mapping quantitative trait loci from a dense set of markers. Genetics 151, 373–386.

Fan Y, Tian Z, Yan Y, Hu C, Abid M, Jiang D, Ma C, Huang Z, Dai T. 2017. Winter night-warming improves post-anthesis physiological activities and sink strength in relation to grain filling in winter wheat (Triticum aestivum L). Frontiers in Plant Science 8, 992.

Fujino K, Matsuda Y, Ozawa K, Nishimura T, Koshiba T, Fraaije MW, Sekiguchi H. 2008. NARROW LEAF 7 controls leaf shape mediated by auxin in rice. Molecular Genetics and Genomics 279, 499–507.

Garin V, Wimmer V, Mezmouk S, Malosetti M, van Eeuwijk F. 2017. How do the type of QTL effect and the form of the residual term influence QTL detection in multi-parent populations? A case study in the maize EU-NAM population. Theoretical and Applied Genetics 130, 1753–1764.

Gautam H, Fatma M, Sehar Z, Iqbal N, Albaqami M, Khan NA. 2022. Exogenously-sourced ethylene positively modulates photosynthesis, carbohydrate metabolism, and antioxidant defense to enhance heat tolerance in rice. International Journal of Molecular Sciences 23, 1031.

Gladun I. 1993. Distribution of assimilates from the flag leaf of rice during the reproductive period of development. Russian Journal of Plant Physiology 40, 215–219.

Gyenis L, Yun S, Smith K, Steffenson B, Bossolini E, Sanguineti MC, Muehlbauer G. 2007. Genetic architecture of quantitative trait loci associated with morphological and agronomic trait differences in a wild by cultivated barley cross. Genome 50, 714–723.

Haseneyer G, Stracke S, Paul C, Einfeldt C, Broda A, Piepho HP, Graner A, Geiger HH. 2010. Population structure and phenotypic variation of a spring barley world collection set up for association studies. Plant Breeding 129, 271–279.

Hemming MN, Fieg S, James Peacock W, Dennis ES, Trevaskis B. 2009. Regions associated with repression of the barley (Hordeum vulgare) VERNALIZATION1 gene are not required for cold induction. Molecular Genetics and Genomics 282, 107–117.

Hemming MN, Walford SA, Fieg S, Dennis ES, Trevaskis B. 2012. Identification of high-temperature-responsive genes in cereals. Plant Physiology 158, 1439–1450.

Hewezi T, Maier TR, Nettleton D, Baum TJ. 2012. The Arabidopsis microRNA396–GRF1/GRF3 regulatory module acts as a developmental regulator in the reprogramming of root cells during cyst nematode infection. Plant Physiology 159, 321–335.

Horiguchi G, Kim GT, Tsukaya H. 2005. The transcription factor AtGRF5 and the transcription coactivator AN3 regulate cell proliferation in leaf primordia of Arabidopsis thaliana. The Plant Journal 43, 68–78.

Hu J, Zhu L, Zeng D, et al. 2010. Identification and characterization of NARROW AND ROLLED LEAF 1, a novel gene regulating leaf morphology and plant architecture in rice. Plant Molecular Biology 73, 283–292.

Huang S, Zhou B, Gao Z, Li H, Ding Z. 2025. Increased expression of OsSAUR23 and OsRR9 regulates rice plant and organ size. The Crop Journal 13, 350–359.

Ikeda M, Fujiwara S, Mitsuda N, Ohme-Takagi M. 2012. A triantagonistic basic helix–loop–helix system regulates cell elongation in Arabidopsis. The Plant Cell 24, 4483–4497.

Ishiwata A, Ozawa M, Nagasaki H, et al. 2013. Two WUSCHEL-related homeobox genes, narrow leaf2 and narrow leaf3, control leaf width in rice. Plant and Cell Physiology 54, 779–792.

Jabbari M, Fakheri BA, Aghnoum R, Mahdi Nezhad N, Ataei R. 2018. GWAS analysis in spring barley (Hordeum vulgare L.) for morphological traits exposed to drought. PLoS One 13, e0204952.

Jennings PR. 1964. Plant type as a rice breeding objective. Crop Science 4, 13–15.

Jiang D, Fang J, Lou L, Zhao J, Yuan S, Yin L, Sun W, Peng L, Guo B, Li X. 2015. Characterization of a null allelic mutant of the rice NAL1 gene reveals its role in regulating cell division. PLoS One 10, e0118169.

Jöst M, Hensel G, Kappel C, et al. 2016. The INDETERMINATE DOMAIN protein BROAD LEAF1 limits barley leaf width by restricting lateral proliferation. Current Biology 26, 903–909.

Jöst M, Soltani O, Kappel C, Janiak A, Chmielewska B, Szurman-Zubrzycka M, McKim SM, Lenhard M. 2024. The gain-of-function mutation blf13 in the barley orthologue of the rice growth regulator NARROW LEAF1 is associated with increased leaf width. Journal of Experimental Botany 75, 850–867.

Juarez MT, Twigg RW, Timmermans MCP. 2004. Specification of adaxial cell fate during maize leaf development. Development 131, 4533–4544.

Kim J-S, Mizoi J, Kidokoro S, et al. 2012. Arabidopsis GROWTH-REGULATING FACTOR7 functions as a transcriptional repressor of abscisic acid- and osmotic stress-responsive genes, including DREB2A. The Plant Cell 24, 3393–3405.

Kuczyńska A, Surma M, Adamski T, Mikołajczak K, Krystkowiak K, Ogrodowicz P. 2013. Effects of the semi-dwarfing sdw1/denso gene in barley. Journal of Applied Genetics 54, 381–390.

Kühl, M, P.-Y. Wu, A. Shrestha, J. Engelhorn, S. Mukherjee, T. Hartwig, and B. Stich. 2025. Methylome differences among barley inbreds and their association with genomic, transcriptomic, and phenotypic variation. Journal of Experimental Botany:eraf422.

Li WQ, Zhang MJ, Gan PF, Qiao L, Yang SQ, Miao H, Wang GF, Zhang MM, Liu WT, Li HF. 2017. CLD 1/SRL 1 modulates leaf rolling by affecting cell wall formation, epidermis integrity and water homeostasis in rice. The Plant Journal 92, 904–923.

Liang G, He H, Li Y, Wang F, Yu D. 2014. Molecular mechanism of microRNA396 mediating pistil development in Arabidopsis. Plant Physiology 164, 249–258.

Liu H, Guo S, Xu Y, Li C, Zhang Z, Zhang D, Xu S, Zhang C, Chong K. 2014. OsmiR396d-regulated OsGRFs function in floral organogenesis in rice through binding to their targets OsJMJ706 and OsCR4. Plant Physiology 165, 160–174.

Liu L, Sun G, Ren X, Li C, Sun D. 2015. Identification of QTL underlying physiological and morphological traits of flag leaf in barley. BMC Genetics 16, 29.

Long SP, Zhu X-G, Naidu SL, Ort DR. 2006. Can improvement in photosynthesis increase crop yields? Plant, Cell & Environment 29, 315–330.

Lu R, Zhang J, Wu Y-W, Wang Y, Zhang J, Zheng Y, Li Y, Li X-B. 2021. bHLH transcription factors LP1 and LP2 regulate longitudinal cell elongation. Plant Physiology 187, 2577–2591.

Marcinkowski P, Piniewski M. 2018. Effect of climate change on sowing and harvest dates of spring barley and maize in Poland. International Agrophysics 32, 265–271.

Mascher M, Wicker T, Jenkins J, et al. 2021. Long-read sequence assembly: a technical evaluation in barley. The Plant Cell 33, 1888–1906.

Nardmann J, Ji J, Werr W, Scanlon MJ. 2004. The maize duplicate genes narrow sheath1 and narrow sheath2 encode a conserved homeobox gene function in a lateral domain of shoot apical meristems. Development 131, 2827–2839.

Nath U, Crawford BC, Carpenter R, Coen E. 2003. Genetic control of surface curvature. Science 299, 1404–1407.

Neuffer MG, Coe EH, Wessler SR. 1997. Mutants of maize. Cold Spring Harbor, NY: Cold Spring Harbor Laboratory Press.

Neumann K, Zhao Y, Chu J, Keilwagen J, Reif JC, Kilian B, Graner A. 2017. Genetic architecture and temporal patterns of biomass accumulation in spring barley revealed by image analysis. BMC Plant Biology 17, 137.

Niu Y, Chen T, Zheng Z, Zhao C, Liu C, Jia J, Zhou M. 2022. A new major QTL for flag leaf thickness in barley (Hordeum vulgare L). BMC Plant Biology 22, 305.

Nogueira FTS, Chitwood DH, Madi S, Ohtsu K, Schnable PS, Scanlon MJ, Timmermans MCP. 2009. Regulation of small RNA accumulation in the maize shoot apex. PLoS Genetics 5, e1000320.

Pajoro A, Madrigal P, Muiño JM, et al. 2014. Dynamics of chromatin accessibility and gene regulation by MADS-domain transcription factors in flower development. Genome Biology 15, R41.

Piepho H-P, Möhring J. 2007. Computing heritability and selection response from unbalanced plant breeding trials. Genetics 177, 1881–1888.

Qi J, Qian Q, Bu Q, et al. 2008. Mutation of the rice narrow leaf1 gene, which encodes a novel protein, affects vein patterning and polar auxin transport. Plant Physiology 147, 1947–1959.

R Core Team. 2023. A language and environment for statistical computing. Vienna, Austria: R Foundation for Statistical Computing.

Rahman MA, Haque M, Sikdar B, Islam MA, Matin MN. 2014. Correlation analysis of flag leaf with yield in several rice cultivars. Journal of Life and Earth Science 8, 49–54.

Richardson A, Jones H, Bartlett M. 2024. Grass awns: morphological diversity arising from developmental constraint. Current Opinion in Plant Biology 82, 102663.

Richardson AE, Cheng J, Johnston R, Kennaway R, Conlon BR, Rebocho AB, Kong H, Scanlon MJ, Hake S, Coen E. 2021. Evolution of the grass leaf by primordium extension and petiole–lamina remodeling. Science 374, 1377–1381.

Satterlee JW, Evans LJ, Conlon BR, et al. 2023. A Wox3-patterning module organizes planar growth in grass leaves and ligules. Nature Plants 9, 720–732.

Schneider CA, Rasband WS, Eliceiri KW. 2012. NIH Image to ImageJ: 25 years of image analysis. Nature Methods 9, 671–675.

Shrestha A, Cosenza F, van Inghelandt D, Wu PY, Li J, Casale FA, Weisweiler M, Stich B. 2022. The double round-robin population unravels the genetic architecture of grain size in barley. Journal of Experimental Botany 73, 7344–7361.

Stich B. 2009. Comparison of mating designs for establishing nested association mapping populations in maize and Arabidopsis thaliana. Genetics 183, 1525–1534.

Tabarzad A, Ghaemi AA, Zand-Parsa S. 2016. Barley grain yield and protein content response to deficit irrigation and sowing dates in semi-arid region. Modern Applied Science 10, 193–207.

Tang X, Gong R, Sun W, Zhang C, Yu S. 2018. Genetic dissection and validation of candidate genes for flag leaf size in rice (Oryza sativa L). Theoretical and Applied Genetics 131, 801–815.

Vafadar Shamasbi U, Jamali SH, Sadeghzadeh B, Abdollahi Mandoulakani B. 2017. Genetic mapping of quantitative trait loci for yield-affecting traits in a barley doubled haploid population derived from clipper×sahara 3771. Frontiers in Plant Science 8, 688.

van Es SW, Silveira SR, Rocha DI, Bimbo A, Martinelli AP, Dornelas MC, Angenent GC, Immink RG. 2018. Novel functions of the Arabidopsis transcription factor TCP 5 in petal development and ethylene biosynthesis. The Plant Journal 94, 867–879.

Vanhaeren H, Nam Y-J, De Milde L, Chae E, Storme V, Weigel D, Gonzalez N, Inzé D. 2017. Forever young: the role of ubiquitin receptor DA1 and E3 ligase BIG BROTHER in controlling leaf growth and development. Plant Physiology 173, 1269–1282.

VanRaden PM. 2008. Efficient methods to compute genomic predictions. Journal of Dairy Science 91, 4414–4423.

Voss-Fels KP, Robinson H, Mudge SR, Richard C, Newman S, Wittkop B, Stahl A, Friedt W, Frisch M, Gabur I. 2018. VERNALIZATION1 modulates root system architecture in wheat and barley. Molecular Plant 11, 226–229.

Wang H, Hou L, Wang M, Mao P. 2016. Contribution of the pod wall to seed grain filling in alfalfa. Scientific Reports 6, 26586.

Wang J, Wang T, Wang Q, et al. 2022. QTL mapping and candidate gene mining of flag leaf size traits in Japonica rice based on linkage mapping and genome-wide association study. Molecular Biology Reports 49, 63–71.

Wang N, Wang X, Qian Y, Bai D, Bao Y, Zhao X, Xu P, Li K, Li J, Li K. 2023. Genome-wide association analysis of rice leaf traits. Agronomy 13, 2687.

Weisweiler M, Montaigu A, Ries D, Pfeifer M, Stich B. 2019. Transcriptomic and presence/absence variation in the barley genome assessed from multi-tissue mRNA sequencing and their power to predict phenotypic traits. BMC Genomics 20, 787.

Weisweiler M, Arlt C, Wu PY, Van Inghelandt D, Hartwig T, Stich B. 2022. Structural variants in the barley gene pool: precision and sensitivity to detect them using short-read sequencing and their association with gene expression and phenotypic variation. Theoretical and Applied Genetics 135, 3511–3529.

Wen Y, Fang Y, Hu P, Tan Y, Wang Y, Hou L, Deng X, Wu H, Zhu L, Zhu L. 2020. Construction of a high-density genetic map based on SLAF markers and QTL analysis of leaf size in rice. Frontiers in Plant Science 11, 1143.

Wiersma JJ, Ransom JK. 2005. The small grains field guide. St. Paul, MN: University of Minnesota Extension Service.

Williams R, Hayes J. 1979. Relationships between photosynthetic area and other growth attributes with grain yield in 6- and 2-row barley genotypes. Annals of Applied Biology 91, 391–395.

Wright IJ, Dong N, Maire V, et al. 2017. Global climatic drivers of leaf size. Science 357, 917–921.

Wu J, Qi Y, Hu G, Li J, Li Z, Zhang H. 2017. Genetic architecture of flag leaf length and width in rice (Oryza sativa L.) revealed by association mapping. Genes & Genomics 39, 341–352.

Wu XY, Kuai BK, Jia JZ, Jing HC. 2012. Regulation of leaf senescence and crop genetic improvement. Journal of Integrative Plant Biology 54, 936–952.

Xiang J-J, Zhang G-H, Qian Q, Xue H-W. 2012. Semi-rolled leaf1 encodes a putative glycosylphosphatidylinositol-anchored protein and modulates rice leaf rolling by regulating the formation of bulliform cells. Plant Physiology 159, 1488–1500.

Xue D, Chen M, Zhou M, Chen S, Mao Y, Zhang G. 2008. QTL analysis of flag leaf in barley (Hordeum vulgare L.) for morphological traits and chlorophyll content. Journal of Zhejiang University: Science: B 9, 938–943.

Yang H, Fang C, Li Y, Wu Y, Fransson P, Rillig MC, Zhai S, Xie J, Tong Z, Zhang Q. 2022. Temporal complementarity between roots and mycorrhizal fungi drives wheat nitrogen use efficiency. New Phytologist 236, 1168–1181.

Yoshikawa T, Tanaka S-Y, Masumoto Y, Nobori N, Ishii H, Hibara K-I, Itoh J-I, Tanisaka T, Taketa S. 2016. Barley NARROW LEAFED DWARF1 encoding a WUSCHEL-RELATED HOMEOBOX 3 (WOX3) regulates the marginal development of lateral organs. Breeding Science 66, 416–424.

Yu H, Zhang L, Wang W, et al. 2021. TCP5 controls leaf margin development by regulating KNOX and BEL-like transcription factors in Arabidopsis. Journal of Experimental Botany 72, 1809–1821.

Zanella CM, Rotondo M, McCormick-Barnes C, et al. 2023. Longer epidermal cells underlie a quantitative source of variation in wheat flag leaf size. New Phytologist 237, 1558–1573.

Zhang B, Ye W, Ren D, et al. 2015. Genetic analysis of flag leaf size and candidate genes determination of a major QTL for flag leaf width in rice. Rice 8, 39.

Zhang G-H, Xu Q, Zhu X-D, Qian Q, Xue H-W. 2009. SHALLOT-LIKE1 is a KANADI transcription factor that modulates rice leaf rolling by regulating leaf abaxial cell development. The Plant Cell 21, 719–735.

Zhang L-Y, Bai M-Y, Wu J, et al. 2009. Antagonistic HLH/bHLH transcription factors mediate brassinosteroid regulation of cell elongation and plant development in rice and arabidopsis. The Plant Cell 21, 3767–3780.

Zhang Z, Runions A, Mentink RA, et al. 2020. A WOX/Auxin biosynthesis module controls growth to shape leaf form. Current Biology 30, 4857–4868.

Zheng T. 1999. Effects of some photosynthetic organs on milking and grain yield of barley. Barley Science 1, 21–22.

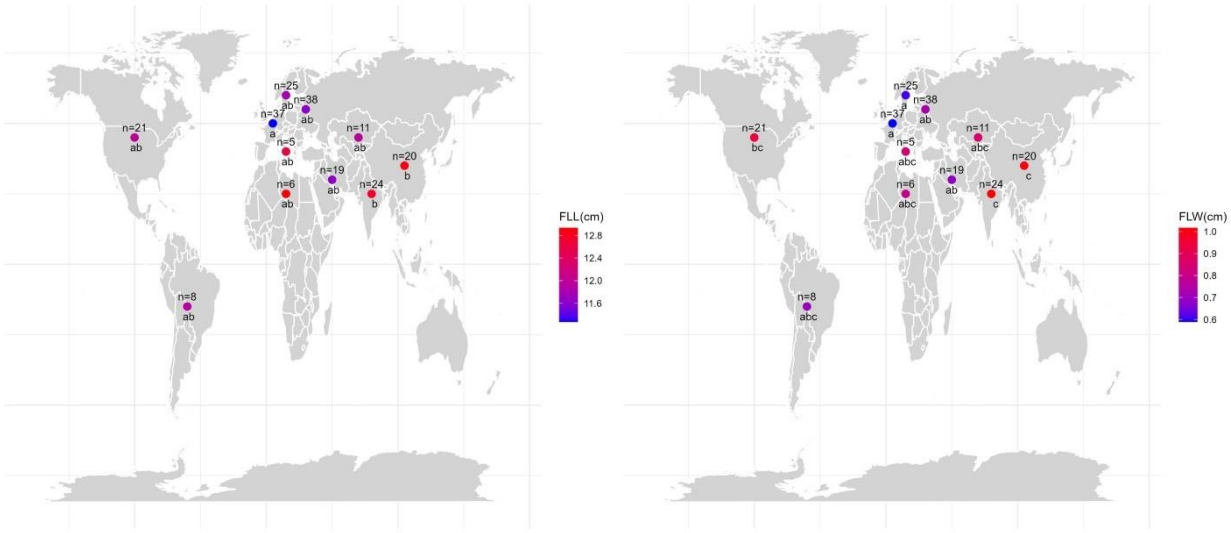

Fig. 1. Variation of flag leaf size based on the geographical origin. Heat map of adjusted entry means for (A) flag leaf length (FLL) and (B) flag leaf width (FLW) in centimeters in the barley diversity panel according to their geographical origin. Letters below the dots indicate significant differences in the trait value among the accessions from the respective geographical region ($P<0.05$) not sharing the same letter. The values above the dots denote the number of accessions from the diversity panel belonging to the respective geographical region.

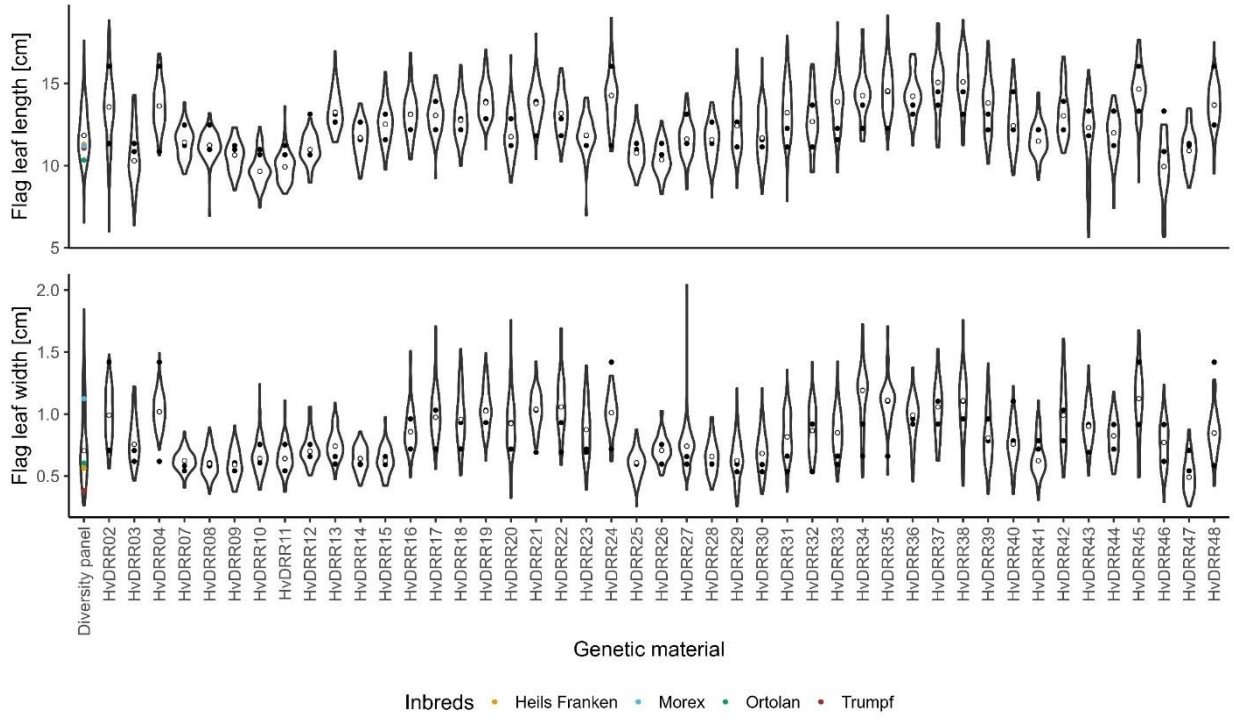

Fig. 2. Violin plot for flag leaf size across 45 HvDRR subpopulations. The distribution of adjusted entry means of (A) flag leaf length (FLL) and (B) flag leaf width (FLW) of recombinant inbred lines with each subpopulation estimated across six environments (n=3866). The white dot within each violin denotes the median values across all RILs, and the two black dots in each violin highlight the adjusted entry means of FLL and FLW of the parental inbreds of each subpopulation. The colored points represent the FLL and FLW of Morex and three German cultivars. n, number of RILs.

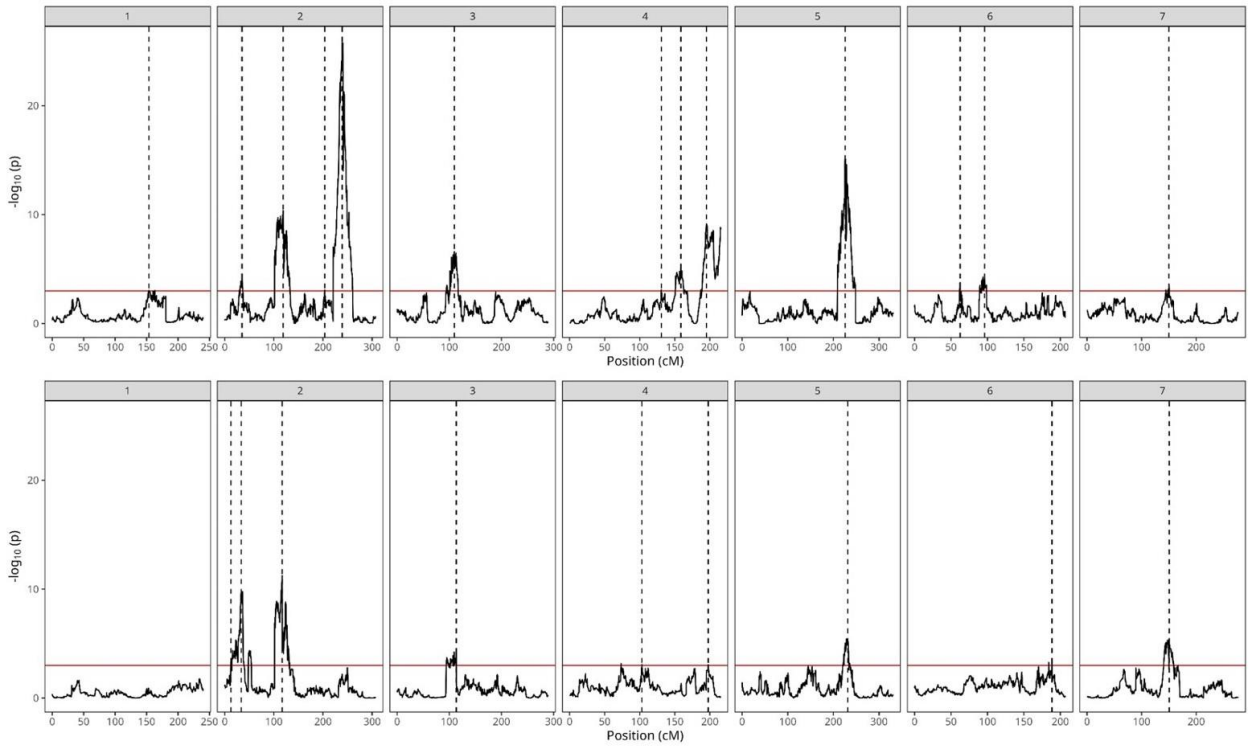

Fig. 3. Profiles of quantitative trait loci (QTLs) associated with flag leaf size from multiparent population analysis across the 45 HvDRR subpopulations using the parental model. QTL profile for (A) flag leaf length and (B) flag leaf width. The QTLs were detected across all seven chromosomes using composite interval mapping [significant threshold of −log10(P)=3]. The horizontal red line indicates the significance threshold, and the vertical dashed lines indicate the positions of the detected QTLs.

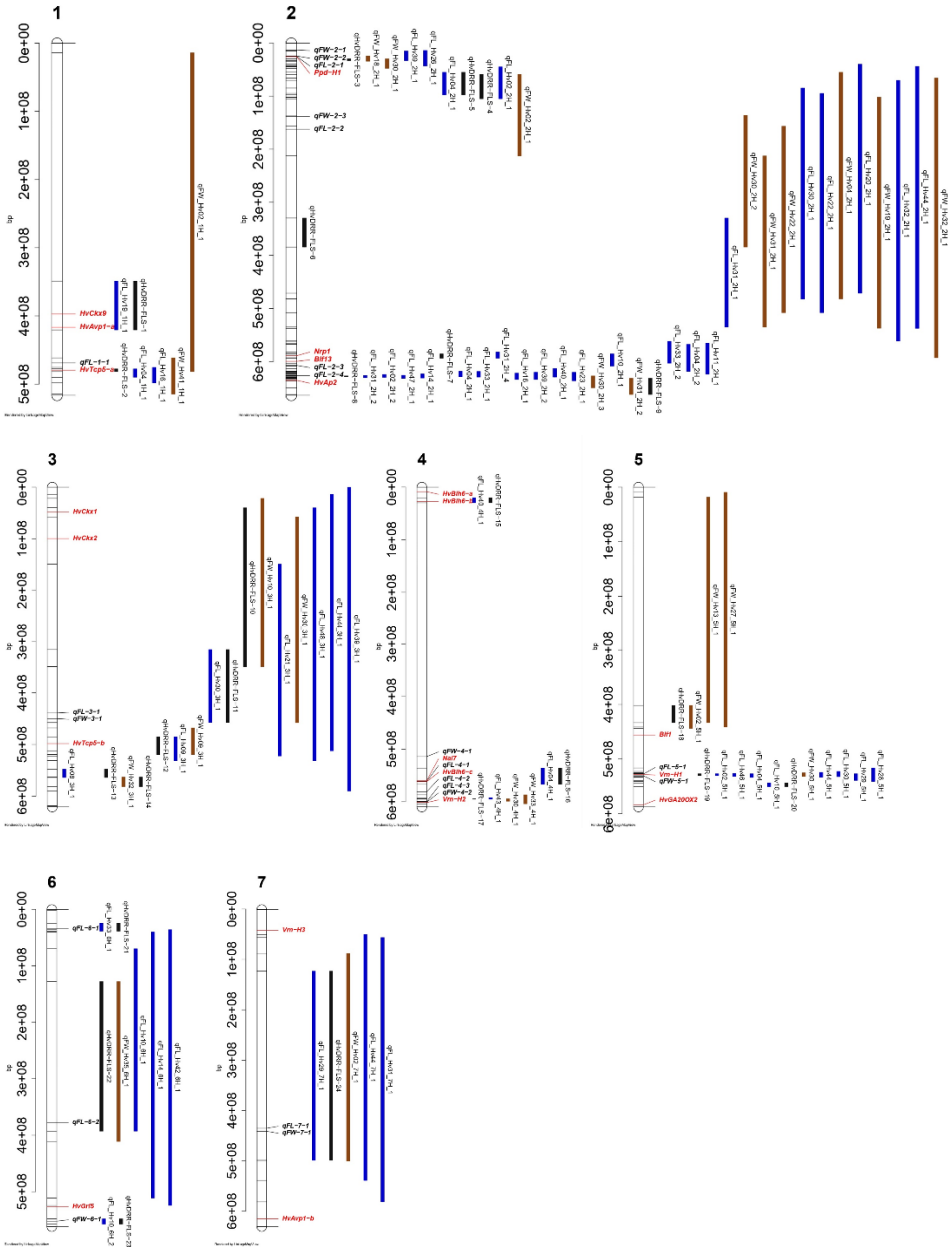

Fig. 4. Confidence interval of QTLs detected in individual HvDRR subpopulations. Flag leaf length (FLL) was assessed in six environments and flag leaf width (FLW) in four environments. The blue, brown, and black color bars indicate the physical interval of QTLs associated with FLL, FLW, and consensus QTLs, respectively. The positions of known genes controlling developmental phenotypes such as leaf size, flowering time, plant height, and spikelet branching are indicated in italics and red font. The positions of QTLs detected from multiparent population analysis using a parental model are indicated in italics and black font. The physical positions of the top and bottom five markers of the genetic map, and the markers flanking the QTL interval are indicated in the plot as a black line in the sketched chromosomes.

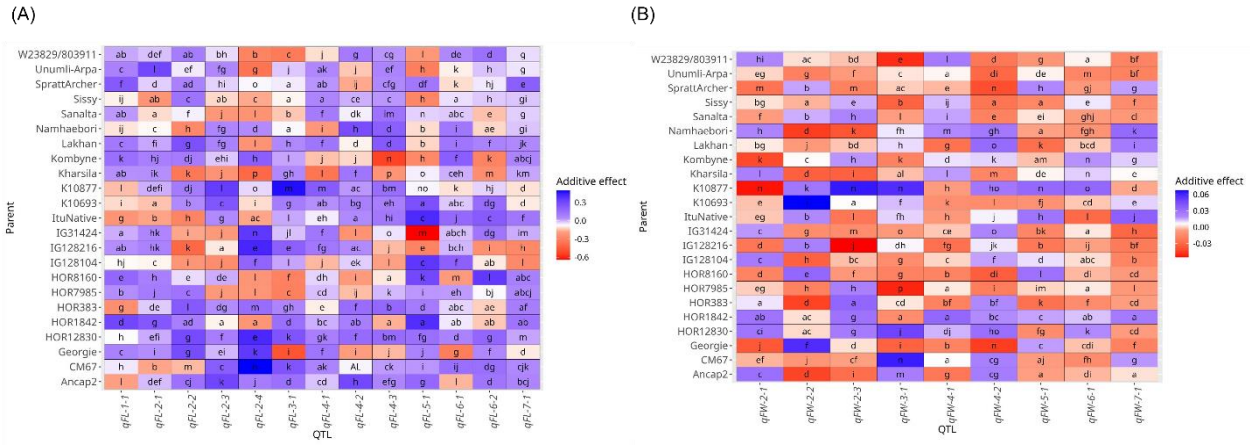

Fig. 5. Heat map of the effects of the parental inbreds at the quantitative trait loci (QTLs) detected through multiparent population analysis using a parental model. Multiple comparisons of the standardized allele effect for (A) flag leaf length (FLL) and (B) width (FLW) at corresponding QTLs. The standardized allele effect for an inbred is the difference between the mean of the estimated allele effect for 23 inbreds and the estimated additive effect of the corresponding inbred. The color code indicates the magnitude of the standardized allele effect. Letters indicate the significant difference ($P \leq 0.05$) between the genotypes not sharing the same letter by Tukey's HSD test (index AL in the figure represents the letter abcdefghijkl).

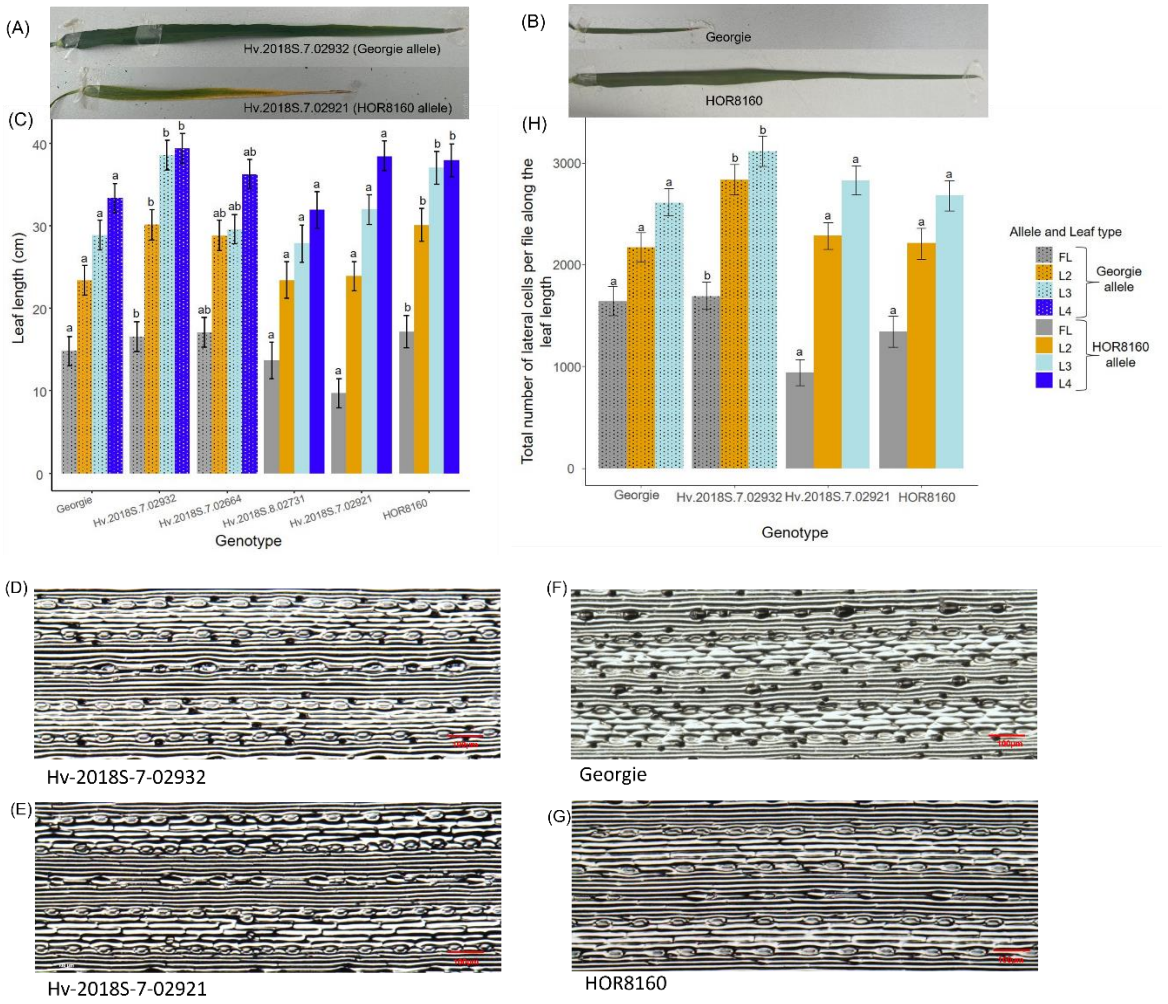

Fig. 6. Validation of a major QTL qHvDRR-FLS-8 associated with flag leaf length. qHvDRR-FLS-8 was detected on chr2H and the validation was done in the HvDRR14 subpopulation. Images of flag leaf of (A) recombinant inbred lines (RILs). (B) The length of flag leaf and older leaves in RILs and parental inbreds of subpopulation HvDRR14. RILs were polymorphic for qHvDRR-FLS-8 but isogenic for the other QTLs detected in the HvDRR14 subpopulation. Images of flag leaf imprints of RILs (C) Hv.2018S.7.02932, (D) Hv.2018S.7.02921, and parental inbreds (E) Georgie and (F) HOR8160 at ×10 magnification under the stereo microscope. (G) The number of lateral cells per file along the leaf length. The bar indicates leaf length/total number of lateral cells per file along the leaf length (AEM ±SE, n=4–6). Gray, yellow, light blue, and dark blue bars represent the flag leaf (FL), and the second (L2), third (L3), and fourth leaf from the top (L4), respectively. Patterned bars in the graph represent Georgie or RILs with the Georgie allele, and non-patterned bars represent HOR8160 or RILs with the HOR8160 allele at qHvDRR-FLS-8. Bars of the same color not sharing the same letter above the bar are significantly different from each other ($P<0.05$). AEM, adjusted entry mean; n, number of replicates.

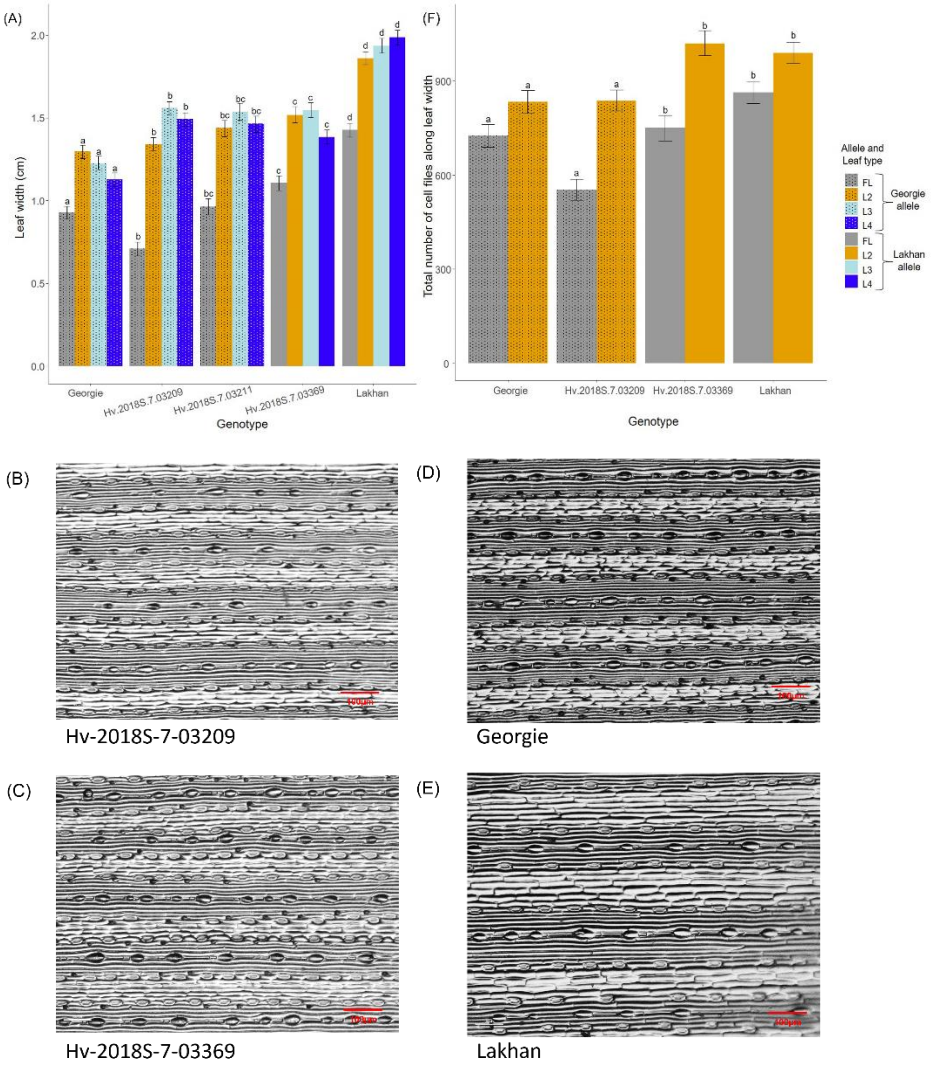

Fig. 7. Validation of a major QTL qHvDRR-FLS-17 associated with flag leaf width. qHvDRR-FLS-17 was detected on chr4H and the validation was done in the HvDRR33 subpopulation. (A) The width of the flag leaf and older leaves in RILs and parental inbreds of subpopulation HvDRR33. RILs were polymorphic for qHvDRR-FLS-17 but isogenic for the other QTLs in the HvDRR33 subpopulation. Images of flag leaf imprints of RILs (B) Hv.2018S.7.03209, (C) Hv.2018S.7.03369, and parental inbreds (D) Georgie and (E) Lakhan at ×10 magnification under the stereo microscope. (F) The number of cell files along the leaf width. The bar indicates leaf width/total number of cell files along the leaf width (AEM ±SE, n=5–6). Gray, yellow, light blue, and dark blue bars represent the flag leaf (FL), and the second (L2), third (L3), and fourth leaf from the top (L4), respectively. Patterned bars in the graph represent Georgie or RILs with the Georgie allele, and non-patterned bars represent Lakhan or RILs with the Lakhan allele at qHvDRR-FLS-17. Bars of the same color not sharing the same letter above the bar are significantly different from each other ($P<0.05$). AEM, adjusted entry mean; n, number of replicates.

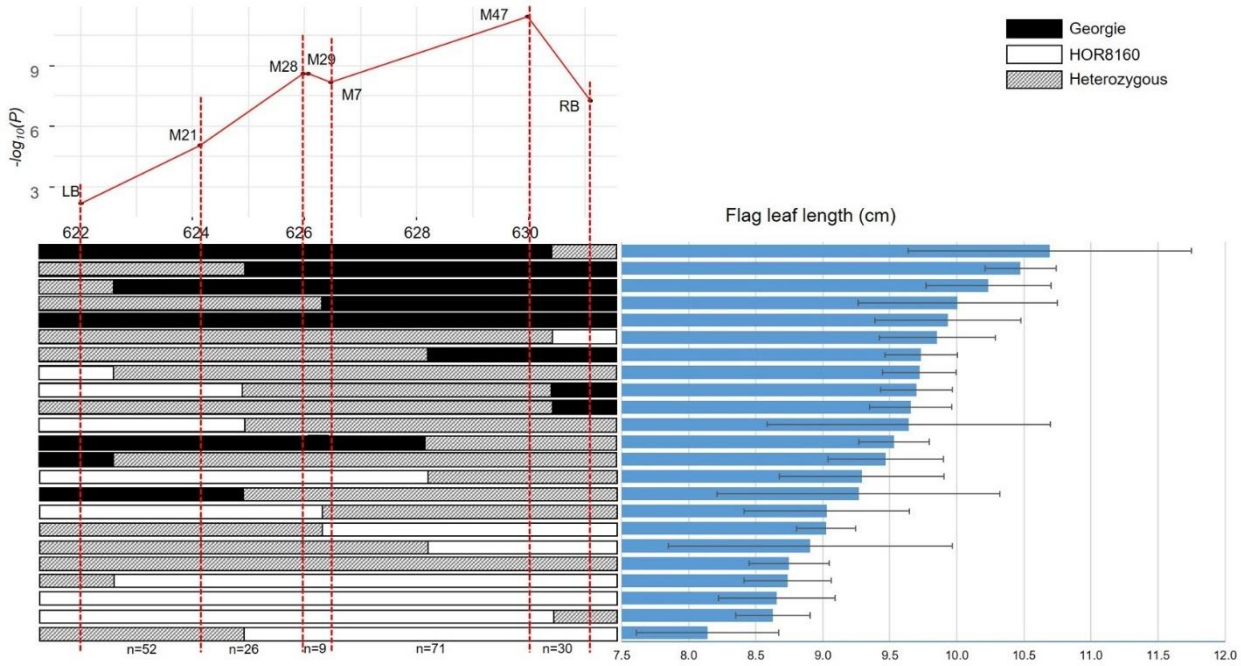

Fig. 8. Fine-mapping of qHvDRR-FLS-8 on chromosome 2H. The panel on the left is the visual representation of the genotype of the individuals at the corresponding markers in the QTL interval. The black, white, and gray bars represent Georgie, HOR8160, and the heterozygous allele, respectively. The number below the left panel represents the number of recombinants between the respective adjacent markers. The positions of corresponding markers are indicated in million base pairs. The graph on the right is the flag leaf length (AEM ±SE, n ~1374) of the corresponding individual. The top graph is the −log10(P) of single marker regression analysis performed using the genotypic data of F2 individuals and phenotypic data of F3 individuals. AEM, adjusted entry mean; n, number of flag leaves measured.

Table 1: Variance components and broad-sense heritability (H^2) of flag leaf length and flag leaf width

Phenotype	**Genotype**	**Environment**	**G*E**	**Error**	***H²***
Flag leaf length	2.82	1.18	0.76	3.62	0.77
Flag leaf width	0.034	0.01	0.01	0.04	0.58

Table 2: The allele of the Vrn-H1 gene among the parental inbreds. The table summarizes the deletion and differential methylation (epiallele) for the parental inbreds of those sub-populations where a QTL was detected for flag leaf length (FLL) and width (FLW) at the Vrn-H1 locus. The nomenclature for the intron deletion detected was adapted from Hemming et al. (2008) and the epiallele was adapted from Kühl et al. (2024). The flowering time QTLs detected by Cosenza et al. (2024) were used to compare the association of the effect of late or early Vrn-H1 flowering time (FT) allele with FLL.

Population	Parent 1 (P1)	Parent 2 (P2)	Intron allele P1	Intron allele P2	Epiallele P1	Epiallele P2	Variation	QTL at *Vrn-H1* for FT	Late FT allele	Larger FLL allele	Additive effect (cm)
HvDRR02	HOR1842	IG31424	*Vrn-H1-3*	*Vrn-H1-1*	Not defined	Hypo	Intron	Very close to it	IG31421	HOR1842	1.3
HvDRR04	HOR1842	Kharsila	*Vrn-H1-3*	*Vrn-H1-1*	Not defined	Hyper	Intron	Yes	Kharsila	HOR1842	0.5
HvDRR28	UnumliArpa	HOR8160	*Vrn-H1-1*	*Vrn-H1-1*	Hyper	Hyper	No variation	Yes	UnumliArpa	HOR8160	0.5
HvDRR29	HOR8160	IG128216	*Vrn-H1-1*	*Vrn-H1-1*	Hyper	Hyper	No variation	No		HOR8160	0.6
HvDRR30	IG128216	Georgie	*Vrn-H1-1*	*Vrn-H1-1*	Hyper	Hyper	No variation	No		Georgie	0.4
HvDRR44	IG128104	Kombyne	*Vrn-H1-3*	*Vrn-H1-1*	Not defined	Hypo	Intron	Yes	Kombyne	IG128104	0.7
HvDRR46	Kharsila	Kombyne	*Vrn-H1-1*	*Vrn-H1-1*	Hyper	Hypo	Epiallele	Yes	Kombyne	Kharsila	1.3

Supplementary materials

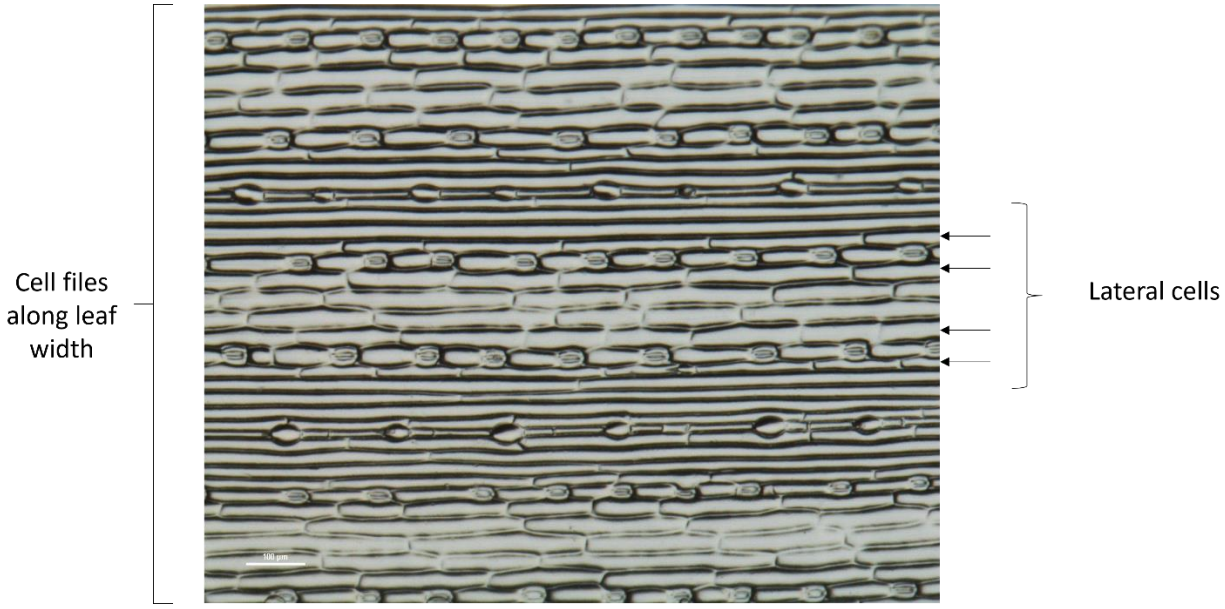

Supplementary Fig. S1 Leaf imprint of the epidermal cells at 10x magnification under stereo microscope.

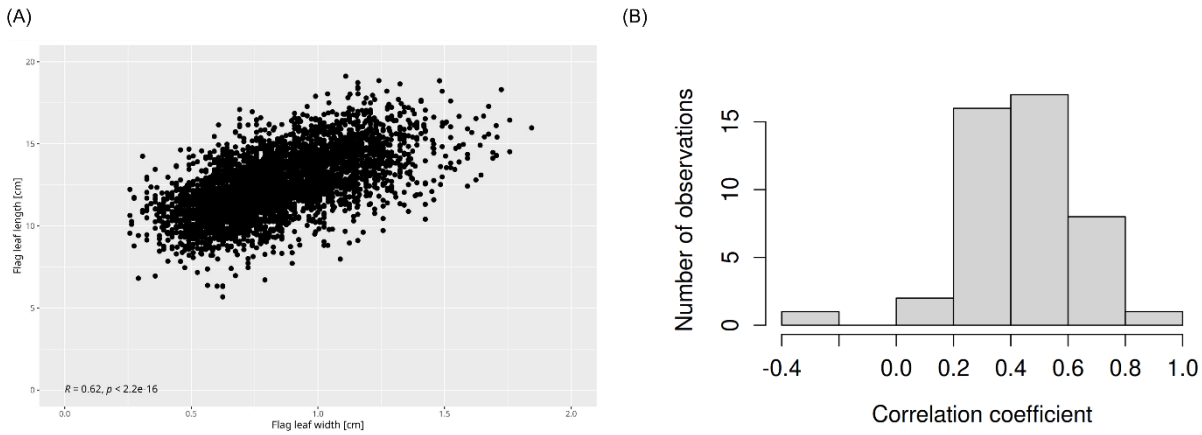

Supplementary Fig. S2. Correlation coefficient of flag leaf length, FLL and flag leaf width, FLW (A) across all the evaluated entries and (B) across 45 HvDRR population.

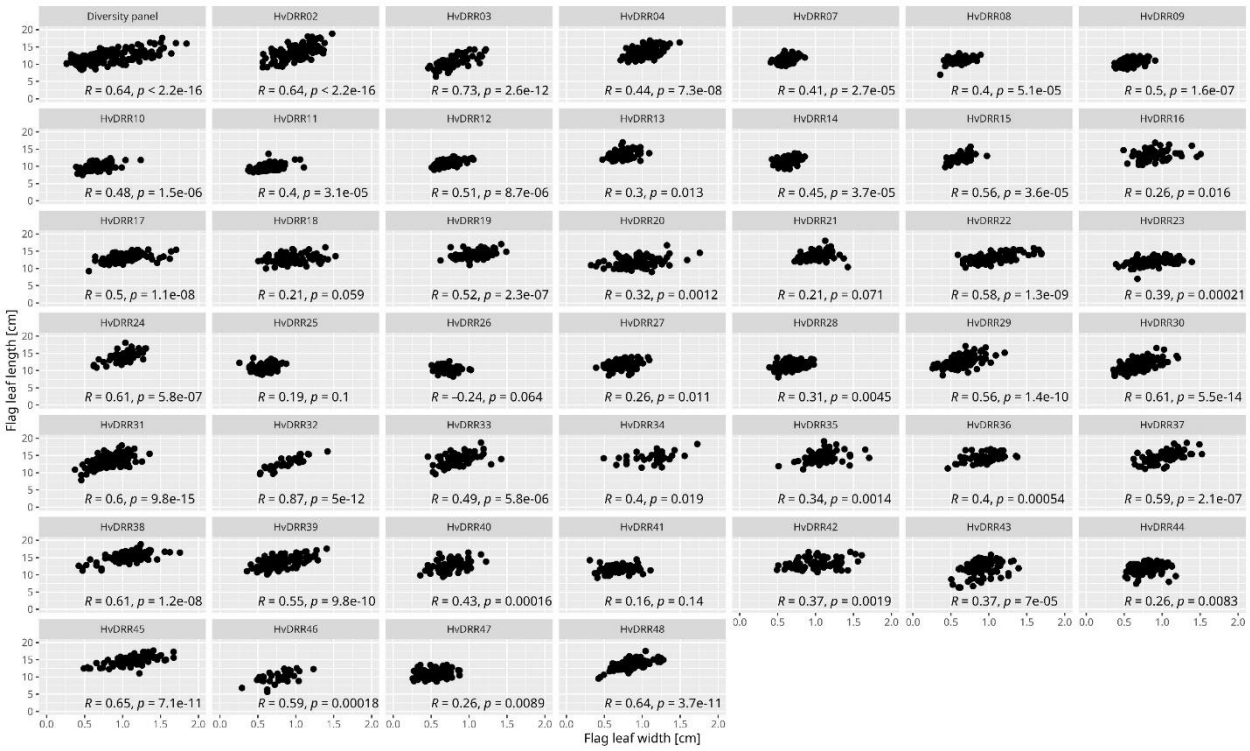

Supplementary Fig. S3. Correlation analysis between the two traits i.e. FLL in cm and FLW in cm across 45 HvDRR sub-populations.

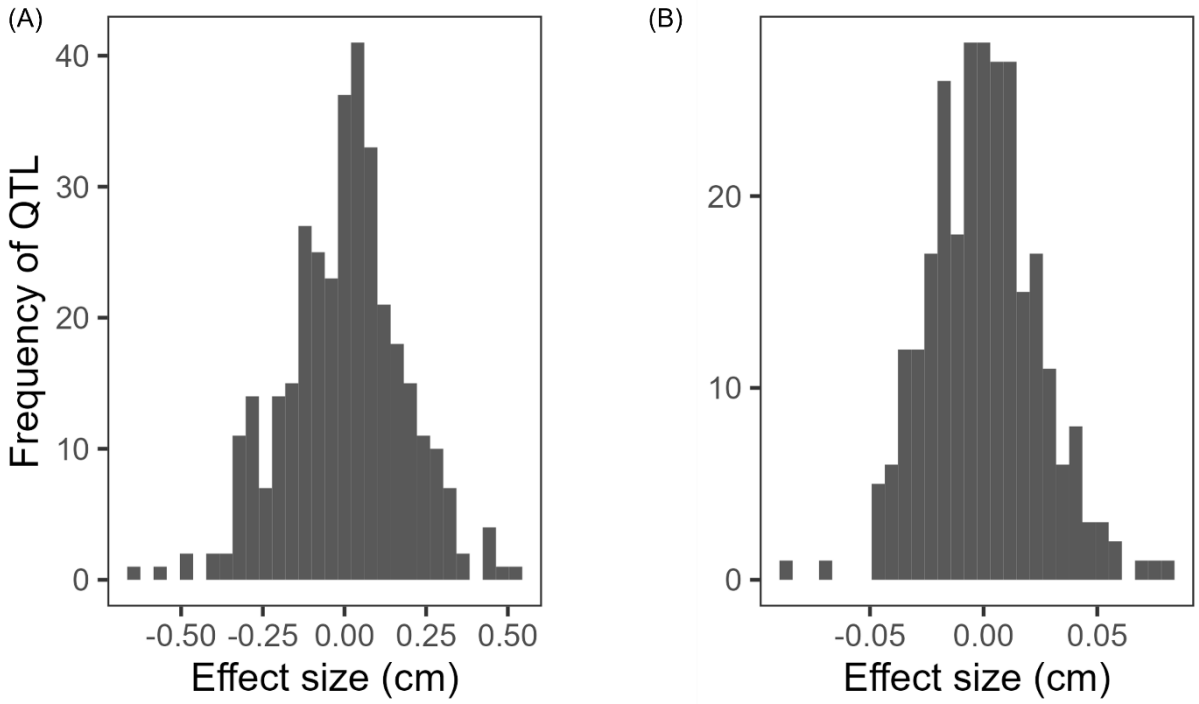

Supplementary Fig. S4. Standardized allele effect estimates for quantitative trait loci (QTLs) detected in multi-parent population analysis of 45 HvDRR sub-populations using a parental model for (A) flag leaf length, and (B) flag leaf width. The standardized allele effect for an inbred was the difference between the mean of the estimated allele effects for the 23 parental inbreds and the estimated allele effect of the considered inbred.

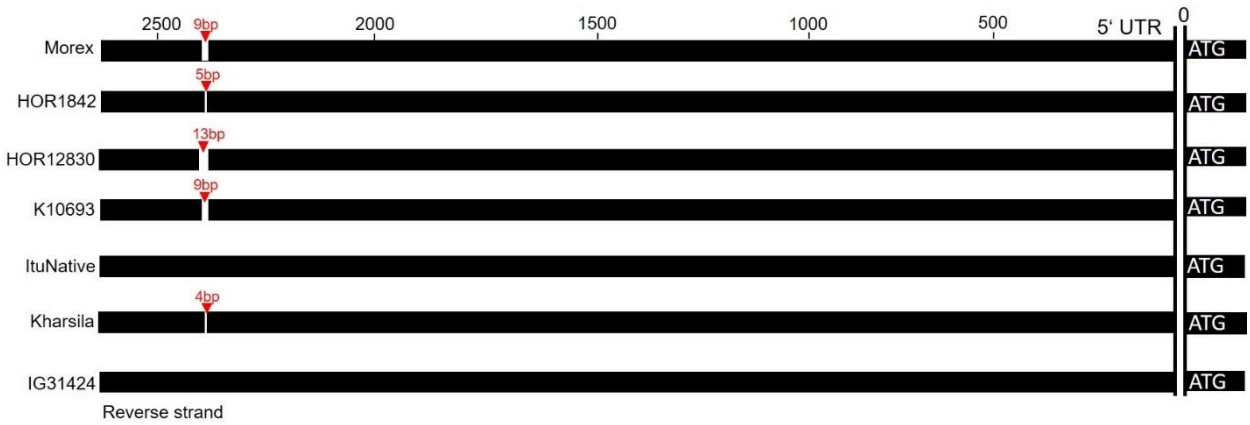

Supplementary Fig. S5. Allelic variation at *Tcp5*. *Tcp5* (*HORVU.MOREX.r3.1HG0077830)* is a candidate gene underlying *qHvDRR-FLS-2* on chromosome 1H encodes Growth regulating factor and was associated flag leaf length. Indels were detected in the promoter region of *Tcp5* between the parental inbreds. HOR1842, HOR12830 and K10693 alleles at the QTL contributed to longer/wider flag leaf.

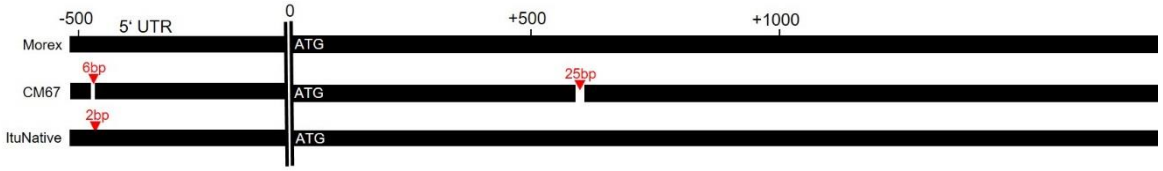

Supplementary Fig. S6. Allelic variation at *Grf5*. *Grf5* (*HORVU.MOREX.r3.4HG0339430)* is a candidate gene underlying *qHvDRR-FLS-15* on chromosome 4H encodes Growth regulating factor and was associated flag leaf length. Indels were detected in 5 UTR and first intron of *Grf5* between the parental inbreds and CM67 allele at the QTL contributed to longer flag leaf.

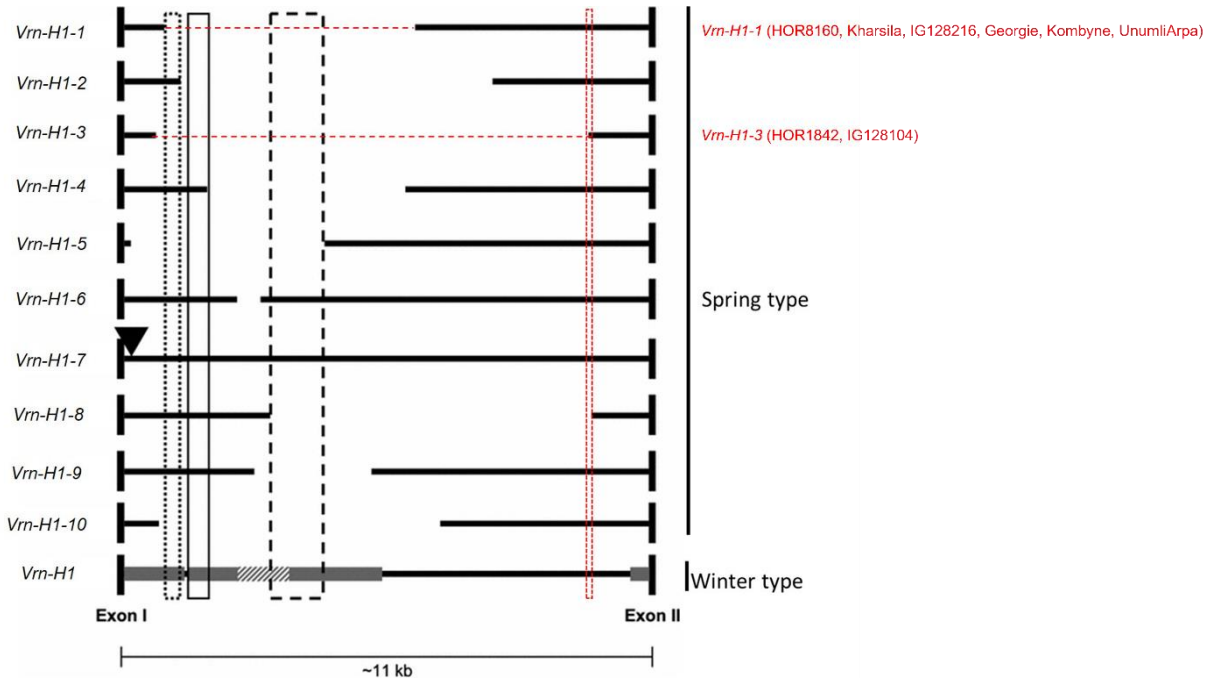

Supplementary Fig. S7. Allelic variation at *Vrn-H1*. *Vrn-H1* (*HORVU.MOREX.r3.5HG0511210*) was the candidate gene underlying *qHvDRR-FLS-19* on chromosome 5H and encodes MADS box transcription factor. The allelic series in the intron 1 of *Vrn-H1* was adopted from Hemming et al. (2009). *Vrn-H1* allele of the respective parental inbreds at *qHvDRR-FLS-19* is indicated in red font. The region covered by the red dotted rectangle indicate the differentially methylated region (DMR) in the intron 1 described in Kühl et al. (2025). HOR1842, HOR8160, Georgie, IG1282104 and Kharsila allele at the QTL contributed to longer flag leaf.

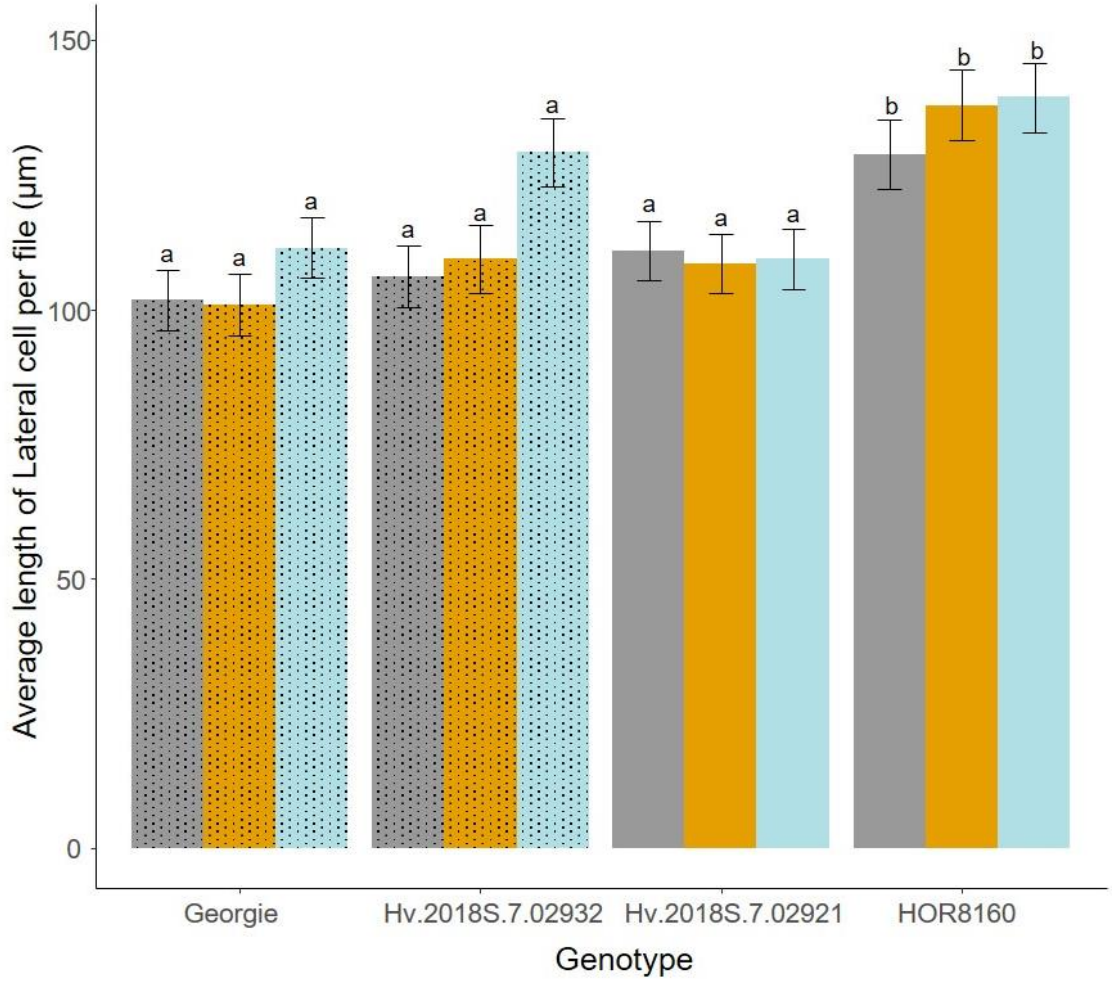

Supplementary Fig. S8. Validation of a major QTL *qHvDRR-FLS-8* associated with flag leaf length. *qHvDRR-FLS-8* was detected on chr2H and the validation was done in the HvDRR14 sub-population. The above graph indicates average length of lateral cell per file (AEM ±SE, n = 4-6). Grey, yellow and light blue bars represents flag leaf (FL), second (L2) and third leaf from the top (L3), respectively. Patterned bar in the graph represents Georgie or RILs with Georgie allele and non-patterned bars represents HOR8160 or RILs with HOR8160 allele at *qHvDRR-FLS-8*. Bars of the same color not sharing the same letter above the bar are significantly different from each other ($p < 0.05$). AEM, adjusted entry mean; SE, standard error; n, number of replicates.

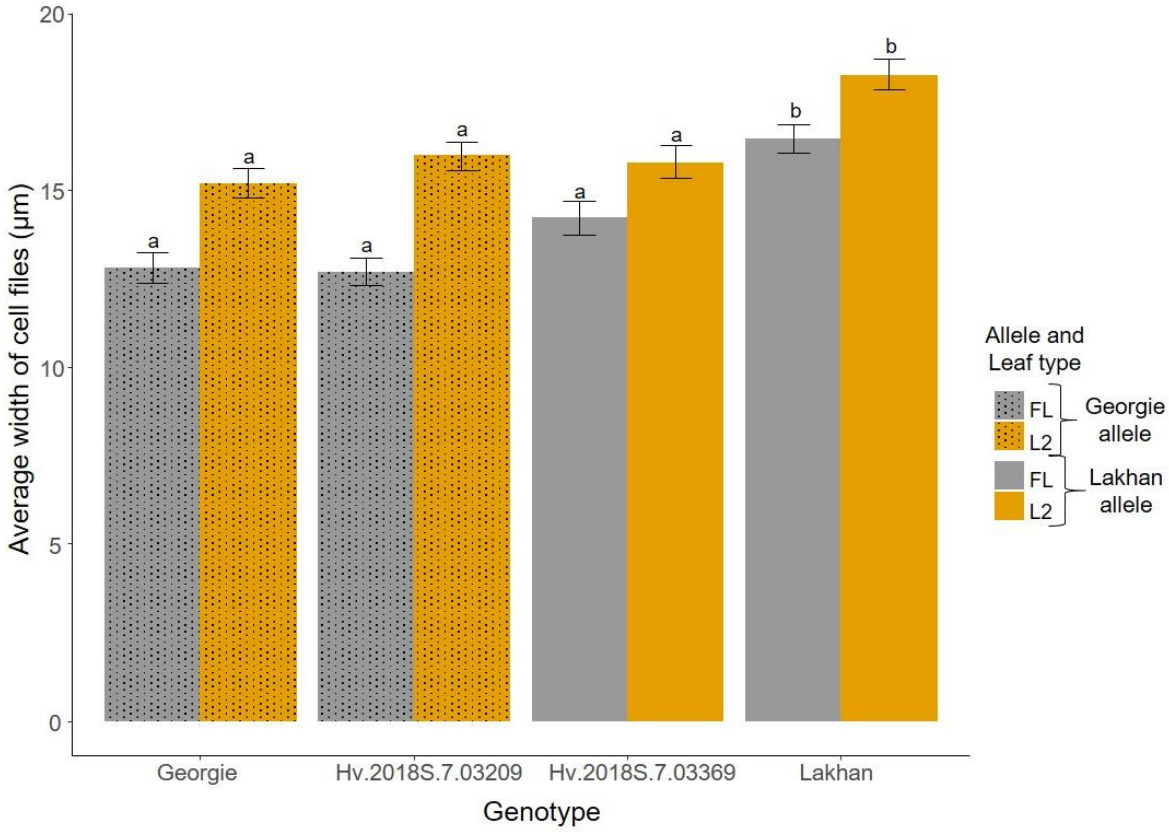

Supplementary Fig. S9. Validation of a major QTL *qHvDRR-FLS-17* associated with flag leaf width. *qHvDRR-FLS-17* was detected on chr4H and the validation was done in the HvDRR33 sub-population. The above bars represent average width of cell file (AEM ±SE, n = 5-6). Grey and yellow bars represents flag leaf (FL) and second leaf from the top (L2), respectively. Patterned bar in the graph represents Georgie or RILs with Georgie allele and non-patterned bars represents Lakhan or RILs with Lakhan allele at *qHvDRR-FLS-17*. Bars of the same color not sharing the same letter above the bar are significantly different from each other ($p < 0.05$). AEM, adjusted entry means; SE, standard error; n, number of replicates.

Supplementary Table S1. Single nucleotide polymorphic locus (SNP) used to desing Kompetitive allele specific PCR for fine-mapping of *qHvDRR-FLS-8*. SNPs are indicated in square brackets.

KASP marker name	Sequence	Purpose
SCRI_RS_154954	AGAGGTTCCAAGCCCAAGTACAGAGGCAAGTACGTGTAGTGATGAAAACACTCTGGGGTC[A/G]ATGACAATTTTGTTGATCTTCTGTTGTTTGTATCTCTCAGTGATGGTTCTTGTATGGCTT	Fine-mapping of *qHvDRR-FLS-8.* Genotyping at left border
M21	ATCTCTATCAGTATCTGTATCAGTCCCTGACTCGGCATCTGTATCAGTCCCTGACTCGTCATCTGTATCAGACCCTGACTCGTCATCTTGATCGATATATGTTTCGTCATCCATATTGGCATCCGTTCCGCCATCTGGATAGGTACCTGATTCGCCATCTAAATAGGTGTCCGACAGACCAGTCTCTGATTCAGCATCAGGCAAATCGTTTGCCATCTTGTCATTTGGACCCAGAAGCAACAGCGACAGC[A/G]CTTGCAGGTTCTTGGCGTTGAGAAGCAAGGCGACGACCGACCGGACGGCATGATCAGTGAGCAATCTGCCCTGGAGGCTCAGCTCCGTGAGGTTGTCCAGTCCGCGCAAGACGCTCGTGAGCAGGCTGCTGTAGTAGGCCATTGATGGGTGCAAGGAAAGGTGCAGATATCTCAAGCGTTCGCACCGGCTGATGAGCGTCGTGACCGGAGCAACCTCCGACGGACCTTTGCTGGAGAGGTCTTCGCAGAT	Fine-mapping of *qHvDRR-FLS-8.* Genotyping at marker M21
M28	TTAGCTCTACAGGAGGGATGCTTAACTAAGTATCTGCCTTCTACAAACATTGGTGTTTACCAAGAAACTGGTTTATTTTTCTAAACGTATTGCATTGTGTAGGGTCTAATAGTACGTAGCAAATAATGATGCGCGCCTAGTGCAGAGGCAAGGGAACTGAAATTCGTCGCCCATAAAGGAGATTTGATCTTGGAACTTTACGCTTATTAGCCATGAATAGGTTGAGATGGCCGGATAAGGCTAAACGCA[C/T]GCGATGCAGTCCCGCGGCCGGTGGCTTACTCTAGCGTTCAGGTCTAGCCGCCATCGCTCGTGGGGGATCTGGCGGCTCTAGGTTCTCCTGCCTAGGACCTGGCTACAGTTCGTTCGATGAGGATGCTCCTCCGGCCGTCGGCGTCTCCATGCCTCTAGACGTCTTGGGCATCGAAGACGAGGGCTCGGGATGGACGCTGGTTGTCGGTAGGAGGAGGAAGACTGAGGCGGAGTTGGTGAGGGAATTTTG	Fine-mapping of *qHvDRR-FLS-8.* Genotyping at marker M28
M29	GTAATTAGCTACAAATTAGGCAGCGAACCAGGGCTATCCGCTTTACGACCATTTCCAGGAAGGAAGTTACGACCTTTCTGATGAAAAAGGTCATTGGTATTTGGGTTAGGACCCCTCCGAACAGCTTACGACCAATTGGTCTCAAATAGTCATAGATTTGCGACCATTTCTGCGAGCGTCACTGCCAAAAGGTCGTTAGTTGACATATTTCTTGTAGTGCGCGTGTGACAAGTTTCATGTCAACGGATCT[C/G]GAGAGTAGGACTCAGATCCGCTACCCACCATGCTGGAGACCGTGGGAGATCACCGAACGAAAGCTTGTGGGCGGAGGGGAGTGAACTGGGTTGAAATGCGGCTAGAATTTCATCTGGAGTACGTATATGGTCCTATTTATGTGGGGTTGGGTGGGTGAGAGTGGGCATAATCCAACGTGATTGACGCGTCCCGTTGTTCCATATTCGGCCCAGATTTGGATGGTCAATCCGAGCGTTTGAGCCGAATATG	Fine-mapping of *qHvDRR-FLS-8.* Genotyping at marker M29
M7	ATCGGCACGGTCCAGTCGCTCGCCTGGCTCCGCCGCGCCGTGCGGCGGTGGCGCTCCAGGTCGGCGGCCTCGGTGCGGCGGCTTGCCAAGGACATGCTGGACGCCGCGGTGCCGGCGGGGCACGTGGCGGTGCGCGCGGAGGGCAGCGGCGCCGGTGAGTCGTCGTCGAGGCGGTTCGCGGTGCCGCTGGCGCAGCTGAGCCACCCGGCGTTCTGGGAGCTGCTGCGTCAGGCGGAGGAGGAGTACGGCT[T/C]CCCGTCGGCCCCCGGCCCCCTCGTGCTCCCATGCGACGAGGGCCACCTCCGCGACGTCCTCCGCCGCGTCTCCTCGTCGAACGCCGAAGGGTGCCGCTCATTCCGGCGCCGCAGCGTCATGGCGGCGCCCCTGCTGCAGGGCGCACGATGACTCTGGCGCCATGGTGGCGCCGCCTCGTCTCGTGATCGACCGGCCGTTCGTTCGTGCGCCCAGCCACCGTACATCGCAGAAGCGGGATAGCCGTGTCAA	Fine-mapping of *qHvDRR-FLS-8.* Genotyping at marker M7
M47	ACAGTTACATTGACTATTTGGATGCACTTGGTTATGGCCAAAGGCATGCTCCCATTCTCTCTAAAGGTTGGCCGTACGGAAAATGTCCAAGACCATGTATAATGCCATGTCACAAAGTCGTCGATGCCCTCAGACATTTACAGGGATTTTAGTAATTCATGTGTCGTCGACCAGAGAAAATACATCAAAATAAAAACTTTTCAATTTACGAACCAACCTGTGTTTAGATGGTTAGGAGGATAATGGTATT[C/T]TAAGTTCACTAGAGTTTAAGTTGGGGTGCTCGCATTTATTCTGAATTTATTTTTAGGATTTCCGACAATGCGCGTTCACTTTGAGGAGACTTTCCGTCGACTACGAGGCGCCTACGATGACTTCGTAAAATTTTAAGATGATATGCCGCTTCGGTTTCTCGAAGATATTCATACAGATAAGGTGTGTGTGCTCGTTCATAGGAGTAAGTTTCTGCACGTATGTATTAGCGCTTGTCTCTATCTAGTGTTAA	Fine-mapping of *qHvDRR-FLS-8.* Genotyping at marker M47
JHI-Hv50k-2016-128391	ACGCAAGGCCCAACCCGTCGTCGTCGTTTTCGGCGGTGGAGGCTGCTAAGGACGCGCATC[C/G]TGGGCACGCAAGTCCTCCTCGCACTTGTTGTCGATAGCATGTGCACTCCTGTATTGTACA	Fine-mapping of *qHvDRR-FLS-8.* Genotyping at right border

Supplementary Table S2. Coefficient of variation of flag leaf size characteristics across diversity panel and all 45 HvDRR population.

Population	Flag leaf length	Flag leaf width
Diversity panel	14.00	41.64
HvDRR02	15.61	20.84
HvDRR03	16.71	22.90
HvDRR04	10.00	13.82
HvDRR07	8.06	12.78
HvDRR08	7.41	17.62
HvDRR09	8.48	19.54
HvDRR10	9.88	21.00
HvDRR11	8.92	19.58
HvDRR12	7.66	16.73
HvDRR13	8.74	16.19
HvDRR14	9.16	15.47
HvDRR15	9.65	17.29
HvDRR16	10.14	21.03
HvDRR17	8.40	21.06
HvDRR18	9.83	22.84
HvDRR19	7.95	16.32
HvDRR20	11.50	25.87
HvDRR21	8.89	13.93
HvDRR22	9.45	22.03
HvDRR23	9.36	24.63
HvDRR24	11.69	16.24
HvDRR25	9.30	18.64
HvDRR26	9.00	14.88
HvDRR27	9.81	25.10
HvDRR28	9.96	20.25
HvDRR29	12.90	26.88
HvDRR30	13.40	24.47
HvDRR31	12.87	22.31
HvDRR32	12.90	23.03
HvDRR33	11.57	21.41
HvDRR34	10.28	22.76
HvDRR35	10.38	16.19
HvDRR36	8.44	18.80
HvDRR37	11.69	20.29
HvDRR38	10.37	24.97
HvDRR39	11.74	26.31
HvDRR40	12.72	22.21
HvDRR41	8.57	23.54
HvDRR42	11.25	26.56
HvDRR43	18.79	18.48
HvDRR44	11.61	18.84
HvDRR45	10.54	23.42
HvDRR46	18.16	25.50
HvDRR47	10.51	28.05
HvDRR48	10.07	20.89

Supplementary Table S3. Summary of quantitative trait loci (QTLs) detected in HvDRR sub-populations for flag leaf length. Composite interval mapping was performed using the Rqtl package. The genetic and physical position of peak markers, the markers flanking the confidence interval of the QTL and the percentage of explained phenotypic variation are reported. Parent and parental alleles contributing to positive additive effect to flagleaf length are indicated in the table. Cross denotes the row type of parents used to develop the corresponding recombinant inbred line populations. LOD, logarithm of odds

Individual QTL nam	Population	Allele.A	Allele.B	Chr	Peak (cM)	ated marker positi	Associated marker	LOD	Start.cM.	Start position (bp)	Start marker	of.start.m	Stop.cM.	Stop position (bp)	Stop marker	Lod.of.stop.marker	Additive effect	Parent allele	Variance	Cross
qFL_Hv04_1H_1	HvDRR04	HOR1842	Kharsila	1	168.64	479463108	JHI-Hv50k-2016-43233	5.726	166.3836	477753148	JHI-Hv50k-2016-42547	3.99478	187.149	489934013	JHI-Hv50k-2016-47631	1.863628	-0.44016	HOR1842	9.89	6*6
qFL_Hv16_1H_1	HvDRR16	K10693	HOR12830	1	205.8388	486469504	JHI-Hv50k-2016-46410	3.285	194.3421	475528198	SCRI_RS_213675	1.45436	249.453	498234809	JHI-Hv50k-2016-51097	1.767968	0.4645	HOR12830	12.03	6*6
qFL_Hv19_1H_1	HvDRR19	HOR383	Ancap2	1	101.95	370993763	BOPA2_12_30348	3.47291	95.3402	348962948	JHI-Hv50k-2016-26883	1.96559	128.334	420546148	JHI-Hv50k-2016-33883	1.636644	0.481	Ancap2	17.52629	6*6
qFL_Hv02_2H_1	HvDRR02	HOR1842	IG31424	2	90	43264415	BOPA1_3709-716	4.234	78.5427	45010188	BOPA1_7623-818	2.36832	123.966	105155499	JHI-Hv50k-2016-87726	2.35136	-0.6369	HOR1842	7.425	2*6
qFL_Hv02_2H_2	HvDRR02	HOR1842	IG31424	2	229.7	627833511	JHI-Hv50k-2016-127015	5.433	223.5262	624258629	JHI-Hv50k-2016-124850	3.92449	233.679	629738879	JHI-Hv50k-2016-127673	3.312741	0.6664	IG31424	9.729	2*6
qFL_Hv04_2H_1	HvDRR03	Kharsila	IG31424	2	210.16	625015892	JHI-Hv50k-2016-125310	3.924	200.2362	618255091	BOPA2_12_20649	2.37655	214.74	628668569	JHI-Hv50k-2016-127384	1.981402	0.8899	IG31424	24.27189	2*6
qFL_Hv04_2H_1	HvDRR04	HOR1842	Kharsila	2	101.57228	68535202	JHI-Hv50k-2016-82337	7.944	96.76403	55248853	JHI-Hv50k-2016-80337	5.38443	108.77	97734016	JHI-Hv50k-2016-86810	6.244112	-0.54275	HOR1842	14.285	6*6
qFL_Hv04_2H_2	HvDRR04	HOR1842	Kharsila	2	222.8759	615914301	JHI-Hv50k-2016-119520	3.464	171.6086	567600323	JHI-Hv50k-2016-106493	1.37898	229.437	618549746	JHI-Hv50k-2016-120912	1.928674	-0.34664	HOR1842	5.746	6*6
qFL_Hv10_2H_1	HvDRR10	Sanalta	/23829/8039′	2	142	602063649	JHI-Hv50k-2016-113922	2.715	121.0001	585633374	JHI-Hv50k-2016-109411	1.02212	150.989	608449388	JHI-Hv50k-2016-116511	0.9288282	0.26955	W23829/803911	6.277	2*2
qFL_Hv11_2H_1	HvDRR11	Sanalta	Sissy	2	99.6	590210213	JHI-Hv50k-2016-109902	3.11574	79.96328	565277907	JHI-Hv50k-2016-105797	1.41992	145.101	623724437	JHI-Hv50k-2016-124462	1.558875	0.32793	Sissy	13.75023	2*2
qFL_Hv14_2H_1	HvDRR14	Georgie	HOR8160	2	185.5	627460411	JHI-Hv50k-2016-126728	7.49357	182.0054	623310808	SCRI_RS_152659	5.16426	188.555	631087116	JHI-Hv50k-2016-128391	4.246666	-0.65143	Georgie	32.84	2*2
qFL_Hv16_2H_1	HvDRR16	K10693	HOR12830	2	259.61	628647280	JHI-Hv50k-2016-127369	5.953	246.9457	621785852	JHI-Hv50k-2016-123148	2.98201	266.078	633709959	JHI-Hv50k-2016-130169	3.26646	0.6787	HOR12830	23.48	6*6
qFL_Hv20_2H_1	HvDRR20	IG128104	HOR383	2	113.18	389936575	JHI-Hv50k-2016-93371	4.09769	52.29381	40139656	JHI-Hv50k-2016-77326	2.49428	116.125	471271325	JHI-Hv50k-2016-96857	2.255852	0.6044	HOR383	17.35465	6*6
qFL_Hv22_2H_1	HvDRR22	HOR383	Namhaebori	2	78.96	156851351	JHI-Hv50k-2016-90462	6.70355	72.24183	95111881	JHI-Hv50k-2016-86345	2.70195	90.5151	508011086	JHI-Hv50k-2016-99117	4.659865	-0.6827	HOR383	29.03694	6*6
qFL_Hv23_2H_1	HvDRR23	IG128104	Namhaebori	2	269.5659	629738879	JHI-Hv50k-2016-127673	3.1712	241.1168	620212020	JHI-Hv50k-2016-121840	1.26057	281.004	636169880	JHI-Hv50k-2016-131231	1.543617	-0.4705	IG128104	16.49765	6*6
qFL_Hv26_2H_1	HvDRR26	Unumli-Arpa	Sanalta	2	24	19297474	SCRI_RS_153226	6.36955	18.66076	14,076,281	JHI-Hv50k-2016-67667	4.6805	54.0611	43,264,415	BOPA1_3709-716	2.688459	-0.6328	Unumli-Arpa	41.91144	2*2
qFL_Hv30_2H_1	HvDRR30	IG128216	Georgie	2	117.35606	462113813	JHI-Hv50k-2016-95965	9.37546	92.13718	84978683	JHI-Hv50k-2016-85000	6.58521	123.814	482310420	JHI-Hv50k-2016-98244	7.778172	0.7292	Georgie	20.272	2*6
qFL_Hv31_2H_1	HvDRR31	Lakhan	IG128216	2	169.276	476073145	SCRI_RS_140618	7.89491	155.9958	329832133	SCRI_RS_147644	5.60503	175.789	535050261	JHI-Hv50k-2016-100559	4.533057	-0.7105	Lakhan	13.479	6*6
qFL_Hv31_2H_2	HvDRR31	Lakhan	IG128216	2	315.9892	627268913	JHI-Hv50k-2016-126411	9.71803	314.5159	626362954	JHI-Hv50k-2016-126024	6.41462	318.515	630366144	JHI-Hv50k-2016-127867	7.390829	0.7372	IG128216	17.175	6*6
qFL_Hv31_2H_4	HvDRR31	Lakhan	IG128216	2	251.1939	588639100	JHI-Hv50k-2016-109506	5.92313	247.2072	582019742	JHI-Hv50k-2016-109198	3.77136	254.233	593687880	JHI-Hv50k-2016-110773	4.238003	-0.6056	Lakhan	9.746	6*6
qFL_Hv32_2H_1	HvDRR32	IG128216	K10877	2	87.511	102240001	JHI-Hv50k-2016-87488	4.15649	79.29014	70465309	JHI-Hv50k-2016-82602	2.23694	121.513	561314845	JHI-Hv50k-2016-105024	2.442915	1.0453	K10877	40.38919	6*6
qFL_Hv33_2H_1	HvDRR33	Georgie	Lakhan	2	269	623238282	SCRI_RS_151129	6.46804	258.2583	618549453	JHI-Hv50k-2016-120916	4.28026	273.244	629176434	JHI-Hv50k-2016-127582	4.832706	-0.8332	Georgie	25.02	2*6
qFL_Hv33_2H_2	HvDRR33	Georgie	Lakhan	2	226.6	598817584	JHI-Hv50k-2016-112588	3.24791	194.2232	561797694	JHI-Hv50k-2016-105103	1.72095	237.693	603090194	JHI-Hv50k-2016-114276	1.594649	0.5494	Lakhan	11.39	2*6
qFL_Hv39_2H_1	HvDRR39	HOR12830	ItuNative	2	52	26541621	JHI-Hv50k-2016-73812	3.16623	21.14156	15,252,254	JHI-Hv50k-2016-68007	1.05039	65.735	33267074	JHI-Hv50k-2016-75728	1.313059	-0.5285	HOR12830	9.34	6*6
qFL_Hv39_2H_2	HvDRR39	HOR12830	ItuNative	2	228.818	623237567	JHI-Hv50k-2016-124322	3.52732	221.6221	620196496	BOPA1_5541-418	1.87917	238.821	633708485	JHI-Hv50k-2016-130184	1.966279	-0.519	HOR12830	10.49	6*6
qFL_Hv40_2H_1	HvDRR40	ItuNative	CM67	2	403.5113	623724097	JHI-Hv50k-2016-124463	5.40165	379.5814	613238587	JHI-Hv50k-2016-118422	3.53025	418.431	629176434	JHI-Hv50k-2016-127582	3.520657	0.8006	CM67	21.43	6*6
qFL_Hv44_2H_1	HvDRR44	IG128104	Kombyne	2	103	499539670	SCRI_RS_171203	5.41818	81.22101	44083536	JHI-Hv50k-2016-78108	2.0061	113.351	537485237	JHI-Hv50k-2016-101074	2.404752	0.5912	Kombyne	15.4	6*6
qFL_Hv47_2H_1	HvDRR47	IG31424	Sissy	2	293	628305145	JHI-Hv50k-2016-127068	4.48285	288.423	625812989	JHI-Hv50k-2016-125778	2.59757	299.985	631591390	JHI-Hv50k-2016-128653	2.949886	-0.5296	IG31424	18.65272	2*2
qFL_Hv08_3H_1	HvDRR08	HOR7985	/23829/8039′	3	218(220.3)	560042382	SCRI_RS_150944	4.139	201.1679	547809052	JHI-Hv50k-2016-201048	2.03443	224.549	563918935	SCRI_RS_103215	2.025	-0.37741	HOR7985	18.00675	2*2
qFL_Hv09_3H_1	HvDRR09	Sissy	/23829/8039′	3	129	508112937	JHI-Hv50k-2016-193119	4.12376	116.2172	485184975	JHI-Hv50k-2016-189281	2.4081	142.511	531393278	SCRI_RS_198609	2.11557	-0.38521	Sissy	17.29633	2*2
qFL_Hv21_3H_1	HvDRR21	Ancap2	Namhaebori	3	102.7575	493379778	SCRI_RS_155609	3.15383	71.37604	149021252	JHI-Hv50k-2016-167285	1.56871	119.987	522262890	JHI-Hv50k-2016-195438	1.648014	-0.5485	Ancap2	18.73743	6*6
qFL_Hv30_3H_1	HvDRR30	IG128216	Georgie	3	104.62897	448939623	JHI-Hv50k-2016-184166	9.7	83.23102	316292294	SCRI_RS_151545	8.16184	106.322	457448846	SCRI_RS_162838	8.175991	-0.754	IG128216	21.108	2*6
qFL_Hv39_3H_1	HvDRR39	HOR12830	ItuNative	3	10.069	1799813	JHI-Hv50k-2016-149285	2.68641	0	189466	JHI-Hv50k-2016-148570	2.38782	277.91	590116967	SCRI_RS_144559	1.005952	-0.4909	HOR12830	7.84	6*6
qFL_Hv44_3H_1	HvDRR44	IG128104	Kombyne	3	74.74	21147821	JHI-Hv50k-2016-160219	2.30269	56.65957	13963213	JHI-Hv50k-2016-156630	0.63656	214.095	512328642	JHI-Hv50k-2016-194685	0.5548681	0.3509	Kombyne	6.049	6*6
qFL_Hv48_3H_1	HvDRR48	HOR1842	HOR7985	3	89.34988	435394636	JHI-Hv50k-2016-182785	3.365	77.77252	39932180	JHI-Hv50k-2016-164435	1.23433	131.53	531392349	JHI-Hv50k-2016-197535	1.667503	-0.5737	HOR1842	16.84641	2*6
qFL_Hv04_4H_1	HvDRR04	HOR1842	Kharsila	4	100.12	549542165	JHI-Hv50k-2016-257876	3.082	89.40577	535994280	JHI-Hv50k-2016-255256	1.24288	117.187	567085052	JHI-Hv50k-2016-261131	0.9385072	-0.31783	HOR1842	5.078	6*6
qFL_Hv40_4H_1	HvDRR40	ItuNative	CM67	4	76.87972	21474863	JHI-Hv50k-2016-232198	3.00488	72.15089	20250693	JHI-Hv50k-2016-232016	1.02328	95.3704	29792174	JHI-Hv50k-2016-233646	0.9665596	0.567	CM67	11.02	6*6
qFL_Hv43_4H_1	HvDRR43	Kombyne	Namhaebori	4	131.07	595132794	JHI-Hv50k-2016-268870	4.5666	127.4267	592351923	JHI-Hv50k-2016-268238	2.94682	131.066	595132794	JHI-Hv50k-2016-268870	4.566603	0.9378	Namhaebori	16.84581	6*6
qFL_Hv02_5H_1	HvDRR02	HOR1842	IG31424	5	202.6	529178521	JHI-Hv50k-2016-336527	16.858	201.0852	527026791	JHI-Hv50k-2016-335111	14.9715	213.979	530327920	JHI-Hv50k-2016-337089	13.75349	-1.3126	HOR1842	37.077	2*6
qFL_Hv04_5H_1	HvDRR04	HOR1842	Kharsila	5	216.96	529123801	JHI-Hv50k-2016-336517	7.944	213.3985	527040691	JHI-Hv50k-2016-335186	6.46548	224.854	533637328	JHI-Hv50k-2016-338274	3.485346	-0.53419	HOR1842	14.526	6*6
qFL_Hv10_5H_1	HvDRR10	Sanalta	/23829/8039′	5	183	547530586	JHI-Hv50k-2016-345254	8.399	178.4558	543847341	SCRI_RS_198008	5.25703	186.404	550650607	JHI-Hv50k-2016-346813	6.602106	-0.49096	Sanalta	22.65	2*2
qFL_Hv28_5H_1	HvDRR28	Unumli-Arpa	HOR8160	5	185.4522	527565899	JHI-Hv50k-2016-335708	4.35112	174.6496	516375191	JHI-Hv50k-2016-328519	2.84733	199.988	541120940	JHI-Hv50k-2016-342734	1.294803	0.5421	HOR8160	21.91546	2*2
qFL_Hv29_5H_1	HvDRR29	HOR8160	IG128216	5	244.26	530674618	JHI-Hv50k-2016-337251	3.612	225.6032	527055864	JHI-Hv50k-2016-335244	2.07049	253.495	539249747	JHI-Hv50k-2016-341797	1.24906	-0.576	HOR8160	11.52	2*6
qFL_Hv30_5H_1	HvDRR30	IG128216	Georgie	5	198.5285	528152948	BOPA2_12_30930	3.9109	184.1453	522599333	JHI-Hv50k-2016-332745	1.93693	213.716	532352878	JHI-Hv50k-2016-337901	2.398587	0.446	Georgie	7.602	2*6
qFL_Hv44_5H_1	HvDRR44	IG128104	Kombyne	5	258.83	525535984	JHI-Hv50k-2016-334016	5.68257	257.3967	524452711	JHI-Hv50k-2016-333647	3.37645	264.769	533307510	JHI-Hv50k-2016-338130	2.948324	-0.662	IG128104	16.261	6*6
qFL_Hv46_5H_1	HvDRR46	Kharsila	Kombyne	5	357.6118	529817938	JHI-Hv50k-2016-336914	4.6734	352.3798	526495342	JHI-Hv50k-2016-334451	2.94263	360.024	531927248	JHI-Hv50k-2016-337782	2.821254	-1.3311	Kharsila	45.93098	6*6
qFL_Hv10_6H_1	HvDRR10	Sanalta	/23829/8039′	6	75	235389805	JHI-Hv50k-2016-394928	6.146	56.92453	69752125	JHI-Hv50k-2016-388660	4.2553	77.1013	392824650	JHI-Hv50k-2016-402874	4.512595	0.41346	W23829/803911	15.576	2*2
qFL_Hv10_6H_2	HvDRR10	Sanalta	/23829/8039′	6	157	555457083	SCRI_RS_10655	5.7	147.7477	548283757	JHI-Hv50k-2016-426825	3.51666	159.931	557402082	JHI-Hv50k-2016-431100	4.162361	0.37762	W23829/803911	14.272	2*2
qFL_Hv14_6H_1	HvDRR14	Georgie	HOR8160	6	65	367032871	SCRI_RS_195914	5.302	46.70355	40183383	JHI-Hv50k-2016-384569	3.4041	101.076	511222059	JHI-Hv50k-2016-414666	3.155441	0.53506	HOR8160	21.65	2*2
qFL_Hv33_6H_1	HvDRR33	Georgie	Lakhan	6	63.57793	29222745	JHI-Hv50k-2016-380678	3.96657	55.36104	24625256	JHI-Hv50k-2016-379580	1.2383	79.3823	38663939	JHI-Hv50k-2016-384305	2.056443	0.6022	Lakhan	14.21	2*6
qFL_Hv42_6H_1	HvDRR42	Ancap2	ItuNative	6	120.9406	45151546	JHI-Hv50k-2016-385708	3.87132	107.8953	35994893	JHI-Hv50k-2016-383480	2.24984	245.828	524387861	JHI-Hv50k-2016-417315	1.777368	0.6958	ItuNative	21.93375	6*6
qFL_Hv29_7H_1	HvDRR29	HOR8160	IG128216	7	164	323336489	JHI-Hv50k-2016-481738	4.30976	150.5146	123258022	JHI-Hv50k-2016-481098	2.00352	177.361	498857616	JHI-Hv50k-2016-489537	2.517499	-0.6173	HOR8160	13.95	2*6
qFL_Hv31_7H_1	HvDRR31	Lakhan	IG128216	7	111.4	61640902	BOPA2_12_10696	3.023	75.6667	56385693	JHI-Hv50k-2016-464490	1.34071	211.521	581389148	JHI-Hv50k-2016-497323	1.090956	-0.3797	Lakhan	4.715	6*6
qFL_Hv44_7H_1	HvDRR44	IG128104	Kombyne	7	177.92	517521225	JHI-Hv50k-2016-491200	4.39271	91.26959	50380828	JHI-Hv50k-2016-461900	2.16967	182.811	539028571	JHI-Hv50k-2016-491516	2.667218	0.4909	Kombyne	12.163	6*6

Supplementary Table S4. Summary of quantitative trait loci (QTLs) detected in 45 HvDRR sub-populations for flag leaf width. Composite interval mapping was performed using the Rqtl package. The genetic and physical position of peak markers, the markers flanking the confidence interval of the QTL and the percentage of explained phenotypic variation are reported. Parent and parental alleles contributing to positive additive effect to flag leaf width are indicated in the table. Cross denotes the row type of parents used to develop the corresponding recombinant inbred line populations. LOD, logarithm of odds; FLW. flag leaf width

Individual.QTL.name	Population	Allele.A	Allele.B	Chr	Peak.cM.	Associated marker pos	Associated.marker	LOD	Start.cM.	Start position (bp)	Start.marker	Lod.of.sta	Stop.cM.	Stop position (bp)	Stop.marker	Lod.of.sto	Additive.effect	Parent.allele	Variance	Cross
qFW_Hv02_1H_1	HvDRR02	HOR1842	IG31424	1	52.23212	24193269	JHI-Hv50k-2016-16067	1.7423634	22.00408	14149277	JHI-Hv50k-2016-12117	0.11254	177.979	481729844	JHI-Hv50k-2016-44236	0.21283	0.0408	IG31424	3.679	2*6
qFW_Hv41_1H_1	HvDRR41	ItuNative	K10693	1	137.4359	468600756	JHI-Hv50k-2016-39498	3.2016091	133.1986	461485901	JHI-Hv50k-2016-38105	1.33395	218.598	514697022	JHI-Hv50k-2016-57299	0.74228	0.06117	K10693	15.4261	6*6
qFW_Hv02_2H_1	HvDRR02	HOR1842	IG31424	2	126.2008	156107312	JHI-Hv50k-2016-90347	5.446476	112.9738	59226829	BOPA2_12_10219	3.38372	127.786	212761381	SCRI_RS_87934	3.67421	-0.07539	HOR1842	12.278	2*6
qFW_Hv04_2H_1	HvDRR04	HOR1842	Kharsila	2	121.31161	282127102	SCRI_RS_231897	6.19376	96.76403	55248853	JHI-Hv50k-2016-80337	3.70542	124.024	481962654	JHI-Hv50k-2016-98219	4.12239	-0.06369	HOR1842	19.5662	6*6
qFW_Hv18_2H_1	HvDRR18	HOR383	K10693	2	48	26152710	JHI-Hv50k-2016-73692	10.08659	33.6745	24594197	JHI-Hv50k-2016-72942	5.8686	68.0627	34425590	JHI-Hv50k-2016-76416	4.15637	0.16093	K10693	44.4552	6*6
qFW_Hv19_2H_1	HvDRR19	HOR383	Ancap2	2	99	205588994	SCRI_RS_182959	3.3274	92.34216	102273969	JHI-Hv50k-2016-87465	1.54986	109.45	537192272	JHI-Hv50k-2016-101000	1.78292	-0.07295	HOR383	16.8577	6*6
qFW_Hv22_2H_1	HvDRR22	HOR383	Namhaebori	2	88.557	476887032	SCRI_RS_165669	7.642974	78.96001	156851351	JHI-Hv50k-2016-90462	6.08154	90.5151	508011086	JHI-Hv50k-2016-99117	5.4044	-0.13847	HOR383	32.3674	6*6
qFW_Hv30_2H_1	HvDRR30	IG128216	Georgie	2	53.182	31093852	JHI-Hv50k-2016-75256	4.221	51.24571	29980652	JHI-Hv50k-2016-74920	2.59862	71.7065	47882932	JHI-Hv50k-2016-79228	2.45019	0.04332	Georgie	6.162	2*6
qFW_Hv30_2H_2	HvDRR30	IG128216	Georgie	2	114.588	148697970	JHI-Hv50k-2016-90159	8.64	113.1888	136181076	JHI-Hv50k-2016-89448	6.79911	117.356	384371951	JHI-Hv50k-2016-93210	6.94911	0.066308	Georgie	13.746	2*6
qFW_Hv30_2H_3	HvDRR30	IG128216	Georgie	2	269.585	631516531	JHI-Hv50k-2016-128730	5.67	262.8037	626957890	JHI-Hv50k-2016-126360	2.92774	298.391	649415625	JHI-Hv50k-2016-138465	3.12478	-0.050701	IG128216	8.512	2*6
qFW_Hv31_2H_1	HvDRR31	Lakhan	IG128216	2	169.276	476073146	SCRI_RS_140618	4.395	155.6653	212761381	SCRI_RS_87934	2.8319	175.789	535050261	JHI-Hv50k-2016-100559	2.17569	-0.06679	Lakhan	12.72	6*6
qFW_Hv31_2H_2	HvDRR31	Lakhan	IG128216	2	329	639487015	JHI-Hv50k-2016-133019	3.633073	320.6992	631502759	JHI-Hv50k-2016-128758	2.13101	355.965	662076785	JHI-Hv50k-2016-147100	2.12854	0.05945	IG128216	10.37	6*6
qFW_Hv32_2H_1	HvDRR32	IG128216	K10877	2	81.785	97439643	JHI-Hv50k-2016-86758	3.695783	76.74438	66096126	JHI-Hv50k-2016-81642	2.04269	139.395	592727990	JHI-Hv50k-2016-110405	1.52332	0.09792	K10877	21.26	6*6
qFW_Hv09_3H_1	HvDRR09	Sissy	W23829/803911	3	129.36	508174091	JHI-Hv50k-2016-193139	3.643979	112.4289	467998958	JHI-Hv50k-2016-186692	1.54089	135.051	519406515	JHI-Hv50k-2016-194935	1.53119	-0.04707	Sissy	15.4487	2*2
qFW_Hv10_3H_1	HvDRR10	Sanalta	W23829/803911	3	43	23353607	JHI-Hv50k-2016-161118	5.193653	38.21747	21691873	SCRI_RS_121895	3.08648	63.3614	349363408	SCRI_RS_137552	3.14652	-0.07034	Sanalta	23.5656	2*2
qFW_Hv30_3H_1	HvDRR30	IG128216	Georgie	3	84	316292293	SCRI_RS_151545	4.231	66.69177	57599818	SCRI_RS_178915	2.28663	107.24	457872870	JHI-Hv50k-2016-185368	2.51529	-0.044413	IG128216	6.177	2*6
qFW_Hv32_3H_1	HvDRR32	IG128216	K10877	3	172	567161897	BOPA2_12_30081	3.77549	165.8604	563162661	JHI-Hv50k-2016-205183	1.99678	186.206	581686910	JHI-Hv50k-2016-209853	1.24187	0.10186	K10877	21.83	6*6
qFW_Hv30_4H_1	HvDRR30	IG128216	Georgie	4	219	595534582	JHI-Hv50k-2016-268942	8.237	216.9086	594451852	JHI-Hv50k-2016-268709	6.1773	226.019	599077668	JHI-Hv50k-2016-270573	6.46418	-0.063982	IG128216	13	2*6
qFW_Hv33_4H_1	HvDRR33	Georgie	Lakhan	4	234.7699	595534582	JHI-Hv50k-2016-268942	5.874999	222.3424	586892488	JHI-Hv50k-2016-265457	3.53817	239.014	603899989	JHI-Hv50k-2016-272728	5.3536	0.11068	Lakhan	28.9988	6*6
qFW_Hv02_5H_1	HvDRR02	HOR1842	IG31424	5	114.3342677	438366771	JHI-Hv50k-2016-308617	4.942423	98.9094	401876382	BOPA2_12_31034	3.0648	120.51	443942451	JHI-Hv50k-2016-309096	2.51236	-0.0705	HOR1842	11.042	2*6
qFW_Hv13_5H_1	HvDRR13	SprattArcher	HOR8160	5	56	48340396	JHI-Hv50k-2016-290535	6.121574	44.96227	18327455	JHI-Hv50k-2016-284499	2.02032	84.4199	433386581	JHI-Hv50k-2016-308110	2.39855	0.0714	HOR8160	33.9377	2*2
qFW_Hv27_5H_1	HvDRR27	Unumli-Arpa	SprattArcher	5	47	17554327	JHI-Hv50k-2016-284195	2.5624028	33.49561	9453080	JHI-Hv50k-2016-281309	0.876	95.1487	441356776	JHI-Hv50k-2016-308899	0.74999	0.07737	SprattArcher	11.9165	2*2
qFW_Hv30_5H_1	HvDRR30	IG128216	Georgie	5	202	527185413	JHI-Hv50k-2016-335543	5.629	191.6365	525238666	BOPA2_12_21471	4.09151	213.393	532053779	JHI-Hv50k-2016-337805	3.46578	0.052044	Georgie	8.443	2*6
qFW_Hv35_6H_1	HvDRR35	Lakhan	CM67	6	109	389737553	JHI-Hv50k-2016-402641	3.845472	85.44063	127953699	BOPA2_12_31007	2.28232	121.822	411105600	SCRI_RS_217259	2.16039	0.08169	CM67	18.8071	6*6
qFW_Hv02_7H_1	HvDRR02	HOR1842	IG31424	7	135.6822	451067950	JHI-Hv50k-2016-487422	3.90767	108.6003	88064116	JHI-Hv50k-2016-471347	2.29719	147.839	500720080	JHI-Hv50k-2016-489798	2.35517	-0.06115	HOR1842	8.571	2*6

Supplementary Table S5. Consensus quantitative trait loci (QTLs) associated with flag leaf length and width in the HvDRR population. The consensus interval of QTL/ cluster of QTLs detected in single population analysis were summarized as consensus QTLs. The range of phenotypic variance explained by QTL (PEV) in single sub-population are indicated for consensus QTLs. The consensus QTLs that coincided with flag leaf size associated loci detected in previous genetic mapping studies are reported in black font colour and QTLs co-localized with previously detected QTLs for grain size, flowering time and plant height in HvDRR population are mentioned in grey font colour.

Chr	Consensus interval (Mb)	QTL name for consensus region	Row type of parental inbreds	HvDRR populations with QTLs detected in single population analysis	Associated flag leaf size character	PEV (%)	Colocalization with previously reported QTLs based on physical position	Candidate genes	Potential polymorphic candidate gene in consensus interval	Number of genes in the interval	Comment
1	348.962-420.546	*qHvDRR-FLS-1*	6*6	HvDRR19	FLL	17		*Ckx9, Avp1*		605	
1	477.753-481.730	*qHvDRR-FLS-2*	2*6, 6*6	HvDRR02, HvDRR04, HvDRR16, HvDRR41	FLL, FLW	3-15	(Shrestha et al., 2022), (Cosenza et al., 2024)	*Tcp5*	*Tcp5*	80	
2	29.981-33.267	*qHvDRR-FLS-3*	2*2, 2*6, 6*6	HvDRR18, HvDRR26, HvDRR30, HvDRR39	FLL, FLW	6-44	(Cosenza et al., 2024)			56	QTL in HvDRR18 sub-population harbors *Ppd-H1*
2	59.226-105.155	*qHvDRR-FLS-4*	2*6	HvDRR02	FLL	7-12	(Shrestha et al., 2022), (Cosenza et al., 2024)			708	
2	55.249-97.734	*qHvDRR-FLS-5*	6*6	HvDRR04	FLL	14				429	
2	329.832-384.372	*qHvDRR-FLS-6*	2*6, 6*6	HvDRR04, HvDRR19, HvDRR20, HvDRR22, HvDRR30, HvDRR31, HvDRR32, HvDRR44	FLL, FLW	12-40				212	
2	585.633-593.688	*qHvDRR-FLS-7*	2*2, 2*6, 6*6	HvDRR04, HvDRR10, HvDRR11, HvDRR31, HvDRR33	FLL	5-13	(Cosenza et al., 2024)	*Nrp1*	*Nrp1*	99	
2	626.957-628.669	*qHvDRR-FLS-8*	2*2, 2*6, 6*6	HvDRR02, HvDRR03, HvDRR14, HvDRR16, HvDRR23, HvDRR30, HvDRR31, HvDRR33, HvDRR39, HvDRR40, HvDRR47	FLL, FLW	8-32	(Cosenza et al., 2024)	*Ibh1*	*Ibh1*	81	
2	631.503-662.077	*qHvDRR-FLS-9*	6*6	HvDRR31	FLW	10	(Shrestha et al., 2022), (Cosenza et al., 2024)	*HvAp2*		773	
3	39.932-349.363	*qHvDRR-FLS-10*	2*2, 2*6, 6*6	HvDRR10, HvDRR44, HvDRR48	FLL, FLW	6-23	(Vafadar Shamasbi et al., 2017), (Shrestha et al., 2022), , (Cosenza et al., 2024)	*HvCkx1, HvCkx2*		1420	
3	316.292-457.449	*qHvDRR-FLS-11*	2*6, 6*6	HvDRR21, HvDRR30	FLL, FLW	6-21	(Vafadar Shamasbi et al., 2017), (Cosenza et al., 2024)			1052	
3	485.185-519.407	*qHvDRR-FLS-12*	2*2	HvDRR09	FLL, FLW	15-17	(Shrestha et al., 2022), (Cosenza et al., 2024)	*Tcp5*		391	
3	547.809-563.919	*qHvDRR-FLS-13*	2*2	HvDRR08	FLL	18	(Shrestha et al., 2022), (Cosenza et al., 2024)	*GA20OX1*		322	
3	563.163-581.687	*qHvDRR-FLS-14*	6*6	HvDRR32, HvDRR39	FLL, FLW	7-21	(Du et al., 2019), (Shrestha et al., 2022), (Cosenza et al., 2024)			365	
4	20.251-29.921	*qHvDRR-FLS-15*	6*6	HvDRR40	FLL	11	(Du et al., 2019), (Cosenza et al., 2024)	*HvBlh6, HvGrf5*		133	
4	535.994-567.085	*qHvDRR-FLS-16*	6*6	HvDRR04	FLL	5	(Cosenza et al., 2024)	*Nal7, HvBlh6*		359	
4	594.452-595.133	*qHvDRR-FLS-17*	2*6, 6*6	HvDRR30, HvDRR33, HvDRR43	FLL, FLW	13-28	(Shrestha et al., 2022), (Cosenza et al., 2024)			9	QTL in HvDRR33 sub-population harbors *VRN-H2*
5	401.876-433.387	*qHvDRR-FLS-18*	2*2, 2*6	HvDRR02, HvDRR13, HvDRR27	FLW	11-33	(Cosenza et al., 2024)			266	
5	527.056-530.328	*qHvDRR-FLS-19*	2*2, 2*6, 6*6	HvDRR02, HvDRR04, HvDRR28, HvDRR29, HvDRR30, HvDRR44, HvDRR46	FLL, FLW	7-46	(Xue et al., 2008), (Shrestha et al., 2022), (Cosenza et al., 2024)	*HvVrn-H1, Aglg1*	*HvVrn-H1, Aglg1*	92	
5	543.847-550.651	*qHvDRR-FLS-20*	2*2, 6*6	HvDRR10	FLL	22	(Xue et al., 2008)			182	
6	24.625-38.664	*qHvDRR-FLS-21*	2*6	HvDRR33	FLL	14	(Shrestha et al., 2022), (Cosenza et al., 2024)			234	
6	127.954-392.825	*qHvDRR-FLS-22*	2*2, 6*6	HvDRR10, HvDRR14, HvDRR35, HvDRR42	FLL, FLW	15-22	(Shrestha et al., 2022), (Cosenza et al., 2024)			1032	
6	548.284-557.402	*qHvDRR-FLS-23*	2*2	HvDRR10	FLL	14	(Shrestha et al., 2022), (Cosenza et al., 2024)			225	
7	123.258-498.857	*qHvDRR-FLS-24*	2*6, 6*6	HvDRR02, HvDRR29, HvDRR31, HvDRR44	FLL, FLW	8-13	(Liu et al., 2015), (Shrestha et al., 2022), (Cosenza et al., 2024)			1051	

Supplementary Table S6. Candidate genes present in the consensus intervals. The detailed candidate gene mining was only performed for consensus interval with a physical size of less than 10 Mb and a percent of the explained phenotypic variance of more than 10 %. Sequence polymorphism data obtained from the whole-genome sequencing project of 23 parental inbreds was used to create indels (indel below 50 bp) and predicted structural variants (indels above 50 bp, duplication and inversions) in the coding and regulatory region and SNP annotation data (Weisweiler et al., 2022). The genes present in the consensus interval that revealed allelic differences between the contrasting groups of parental genotypes at a given QTL locus were retained as candidate genes. FLL: flag leaf length; FLW: flag leaf width.

Gene	description	Indel	Structural variation	SNP substitution	QTL	Trait	Chromosome
HORVU.MOREX.r3.1HG0077240	Protein FLLOWERING LOCUS T	5utr/ intron		Deleterious	*qHvDRR-FLS-2*	FLL, FLW	1
HORVU.MOREX.r3.1HG0077250	R ligase/cyclic nucleotide phosphodiesterase family protein	5utr		Tolerated/ Deleterious	*qHvDRR-FLS-2*	FLL, FLW	1
HORVU.MOREX.r3.1HG0077260	Hemoglobin	5utr/ exon	5utr	Tolerated	*qHvDRR-FLS-2*	FLL, FLW	1
HORVU.MOREX.r3.1HG0077270	Gamma-glutamyl hydrolase	intron/ 5utr/ exon	5utr/ exon	Tolerated/ Deleterious	*qHvDRR-FLS-2*	FLL, FLW	1
HORVU.MOREX.r3.1HG0077280	Trehalose-6-phosphate synthase 6	5utr	5utr	Tolerated/ Deleterious	*qHvDRR-FLS-2*	FLL, FLW	1
HORVU.MOREX.r3.1HG0077290	Ribonuclease P protein subunit p29	intron/ 5utr	5utr	Tolerated/ Deleterious	*qHvDRR-FLS-2*	FLL, FLW	1
HORVU.MOREX.r3.1HG0077310	transcription repressor	5utr	5utr	Tolerated	*qHvDRR-FLS-2*	FLL, FLW	1
HORVU.MOREX.r3.1HG0077340	Ras-like protein	5utr/ exon/ intron	5utr		*qHvDRR-FLS-2*	FLL, FLW	1
HORVU.MOREX.r3.1HG0077350	Calcium-binding protein	5utr		Tolerated/ Deleterious	*qHvDRR-FLS-2*	FLL, FLW	1
HORVU.MOREX.r3.1HG0077370	GRF zinc finger family protein, expressed	5utr	5utr	Tolerated/ Deleterious	*qHvDRR-FLS-2*	FLL, FLW	1
HORVU.MOREX.r3.1HG0077390	SNF2 domain-containing protein / helicase domain-containing protein / zinc fing	5utr	5utr		*qHvDRR-FLS-2*	FLL, FLW	1
HORVU.MOREX.r3.1HG0077400	Tyrosine N-monooxygese	5utr	5utr	Tolerated/ Deleterious	*qHvDRR-FLS-2*	FLL, FLW	1
HORVU.MOREX.r3.1HG0077410	28 kDa heat-and acid-stable phosphoprotein, putative	intron/ 5utr			*qHvDRR-FLS-2*	FLL, FLW	1
HORVU.MOREX.r3.1HG0077420	Elongation factor Tu	5utr/ exon/ intron	5utr		*qHvDRR-FLS-2*	FLL, FLW	1
HORVU.MOREX.r3.1HG0077430	Vascular plant one zinc finger transcription factor protein	5utr/ exon/ intron		Tolerated	*qHvDRR-FLS-2*	FLL, FLW	1
HORVU.MOREX.r3.1HG0077440	O-methyltransferase-like protein	5utr	5utr	Tolerated	*qHvDRR-FLS-2*	FLL, FLW	1
HORVU.MOREX.r3.1HG0077470	O-methyltransferase-like protein	5utr		Tolerated/ Deleterious	*qHvDRR-FLS-2*	FLL, FLW	1
HORVU.MOREX.r3.1HG0077480	O-methyltransferase-like protein	exon/ 5utr		Tolerated	*qHvDRR-FLS-2*	FLL, FLW	1
HORVU.MOREX.r3.1HG0077490	O-methyltransferase			Tolerated/ Deleterious	*qHvDRR-FLS-2*	FLL, FLW	1
HORVU.MOREX.r3.1HG0077500	O-methyltransferase-like protein	5utr/ intron/ exon	5utr/ intron	Tolerated	*qHvDRR-FLS-2*	FLL, FLW	1
HORVU.MOREX.r3.1HG0077510	Auxin response factor	5utr/ intron/ exon	intron	Tolerated/ Deleterious	*qHvDRR-FLS-2*	FLL, FLW	1
HORVU.MOREX.r3.1HG0077550	Gibberellin 2-oxidase	5utr/ intron/ exon		Tolerated/ Deleterious	*qHvDRR-FLS-2*	FLL, FLW	1
HORVU.MOREX.r3.1HG0077560	Trihelix transcription factor	5utr	5utr	Tolerated	*qHvDRR-FLS-2*	FLL, FLW	1
HORVU.MOREX.r3.1HG0077570	Interactor of constitutive active ROPs protein, putative	5utr/ exon		Tolerated/ Deleterious	*qHvDRR-FLS-2*	FLL, FLW	1
HORVU.MOREX.r3.1HG0077580	Vascular endothelial growth factor A	5utr		Tolerated/ Deleterious	*qHvDRR-FLS-2*	FLL, FLW	1
HORVU.MOREX.r3.1HG0077610	Dof zinc finger protein	5utr		Tolerated	*qHvDRR-FLS-2*	FLL, FLW	1
HORVU.MOREX.r3.1HG0077620	arginine N-methyltransferase, putative (DUF688)	5utr/ exon		Tolerated	*qHvDRR-FLS-2*	FLL, FLW	1
HORVU.MOREX.r3.1HG0077640	Tubby-like F-box protein	5utr	5utr	Tolerated	*qHvDRR-FLS-2*	FLL, FLW	1
HORVU.MOREX.r3.1HG0077650	Non-specific serine/threonine protein kinase	5utr		Tolerated	*qHvDRR-FLS-2*	FLL, FLW	1
HORVU.MOREX.r3.1HG0077680	Proline iminopeptidase	intron/ exon/ 5utr		Deleterious	*qHvDRR-FLS-2*	FLL, FLW	1
HORVU.MOREX.r3.1HG0077700	Rac-like GTP binding protein	5utr			*qHvDRR-FLS-2*	FLL, FLW	1
HORVU.MOREX.r3.1HG0077710	Glycosyltransferase	5utr/ intron	5utr	Tolerated/ Deleterious	*qHvDRR-FLS-2*	FLL, FLW	1
HORVU.MOREX.r3.1HG0077720	magnesium transporter NIPA (DUF803)	5utr/ exon/ intron	intron/ 5utr		*qHvDRR-FLS-2*	FLL, FLW	1
HORVU.MOREX.r3.1HG0077730	Cleavage stimulation factor subunit 2	5utr		Tolerated	*qHvDRR-FLS-2*	FLL, FLW	1
HORVU.MOREX.r3.1HG0077770	Mitochondrial import inner membrane translocase subunit TIM50	5utr/ intron/ exon	5utr	Tolerated/ Deleterious	*qHvDRR-FLS-2*	FLL, FLW	1
HORVU.MOREX.r3.1HG0077790	Calcium-transporting ATPase	5utr	5utr	Tolerated/ Deleterious	*qHvDRR-FLS-2*	FLL, FLW	1
HORVU.MOREX.r3.1HG0077830	TCP family transcription factor containing protein	5utr/ intron		Tolerated	*qHvDRR-FLS-2*	FLL, FLW	1
HORVU.MOREX.r3.1HG0077840	Glucan endo-1,3-beta-glucosidase 1	5utr/ intron/ exon			*qHvDRR-FLS-2*	FLL, FLW	1
HORVU.MOREX.r3.1HG0077860	D mismatch repair protein Msh6-1	5utr		Tolerated/ Deleterious	*qHvDRR-FLS-2*	FLL, FLW	1
HORVU.MOREX.r3.1HG0077880	BAG family molecular chaperone regulator 7	5utr/ exon	5utr		*qHvDRR-FLS-2*	FLL, FLW	1
HORVU.MOREX.r3.1HG0077930	Lysine--tr ligase	intron/ 5utr	intron	Tolerated	*qHvDRR-FLS-2*	FLL, FLW	1
HORVU.MOREX.r3.1HG0077940	sequence-specific D binding transcription factor ATNDX	5utr	5utr	Tolerated	*qHvDRR-FLS-2*	FLL, FLW	1
HORVU.MOREX.r3.1HG0077950	BSD domain containing protein	intron/ 5utr/ exon	intron/ 5utr	Tolerated/ Deleterious	*qHvDRR-FLS-2*	FLL, FLW	1
HORVU.MOREX.r3.1HG0077960	Cellulose synthase	intron/ 5utr/ exon			*qHvDRR-FLS-2*	FLL, FLW	1
HORVU.MOREX.r3.1HG0077980	Protein kinase, putative	intron/ 5utr/ exon	intron	Tolerated/ Deleterious	*qHvDRR-FLS-2*	FLL, FLW	1
HORVU.MOREX.r3.1HG0078000	Transmembrane protein 56	intron/ exon/ 5utr			*qHvDRR-FLS-2*	FLL, FLW	1
HORVU.MOREX.r3.1HG0078010	Translation initiation factor IF-2	5utr/ intron		Tolerated	*qHvDRR-FLS-2*	FLL, FLW	1
HORVU.MOREX.r3.1HG0078020	Carboxypeptidase	intron/ 5utr/ exon	5utr/ exon	Tolerated/ Deleterious	*qHvDRR-FLS-2*	FLL, FLW	1
HORVU.MOREX.r3.1HG0078100	F-box family protein	5utr		Tolerated/ Deleterious	*qHvDRR-FLS-2*	FLL, FLW	1
HORVU.MOREX.r3.1HG0078110	2-oxoglutarate (2OG) and Fe(II)-dependent oxygese superfamily protein	5utr	5utr	Tolerated/ Deleterious	*qHvDRR-FLS-2*	FLL, FLW	1
HORVU.MOREX.r3.1HG0078150	Serine/threonine-protein kinase			Deleterious	*qHvDRR-FLS-2*	FLL, FLW	1
HORVU.MOREX.r3.1HG0078160	S-adenosyl-L-methionine-dependent methyltransferases superfamily protein	intron/ 5utr/ exon	5utr/ intron	Tolerated/ Deleterious	*qHvDRR-FLS-2*	FLL, FLW	1
HORVU.MOREX.r3.1HG0078170	Colon cancer-associated protein Mic1-like containing protein, expressed	intron/ 5utr	intron	Tolerated	*qHvDRR-FLS-2*	FLL, FLW	1
HORVU.MOREX.r3.1HG0078180	DH dehydrogese [ubiquinone] 1 alpha subcomplex assembly factor 8	5utr	5utr	Deleterious	*qHvDRR-FLS-2*	FLL, FLW	1
HORVU.MOREX.r3.1HG0078200	Protein kinase	intron/ 5utr/ exon		Tolerated	*qHvDRR-FLS-2*	FLL, FLW	1
HORVU.MOREX.r3.1HG0078230	Phosphate transporter	exon/ 5utr/ intron			*qHvDRR-FLS-2*	FLL, FLW	1
HORVU.MOREX.r3.1HG0078260	Protein PAT1-1-like protein	intron		Deleterious	*qHvDRR-FLS-2*	FLL, FLW	1
HORVU.MOREX.r3.1HG0078270	Lipoyl synthase			Tolerated	*qHvDRR-FLS-2*	FLL, FLW	1
HORVU.MOREX.r3.1HG0078330	Thioredoxin-like protein 4A			Tolerated/ Deleterious	*qHvDRR-FLS-2*	FLL, FLW	1
HORVU.MOREX.r3.1HG0078350	Basic-leucine zipper (BZIP) transcription factor family	5utr/ intron	5utr	Tolerated/ Deleterious	*qHvDRR-FLS-2*	FLL, FLW	1
HORVU.MOREX.r3.1HG0078370	breast cancer associated RING 1	exon/ 5utr/ intron	5utr	Tolerated	*qHvDRR-FLS-2*	FLL, FLW	1
HORVU.MOREX.r3.1HG0078400	Tyrosine decarboxylase	5utr		Tolerated/ Deleterious	*qHvDRR-FLS-2*	FLL, FLW	1
HORVU.MOREX.r3.1HG0078410	Collagen alpha-1(VI) chain			Tolerated	*qHvDRR-FLS-2*	FLL, FLW	1
HORVU.MOREX.r3.1HG0078420	F-box protein	5utr		Tolerated	*qHvDRR-FLS-2*	FLL, FLW	1
HORVU.MOREX.r3.1HG0078450	Ubiquitin carboxyl-termil hydrolase	5utr/ intron	5utr	Tolerated	*qHvDRR-FLS-2*	FLL, FLW	1
HORVU.MOREX.r3.1HG0078480	Protein FAR1-RELATED SEQUENCE 3	exon/ intron		Tolerated/ Deleterious	*qHvDRR-FLS-2*	FLL, FLW	1
HORVU.MOREX.r3.1HG0078500	Ethylene-responsive transcription factor	5utr	5utr	Tolerated/ Deleterious	*qHvDRR-FLS-2*	FLL, FLW	1
HORVU.MOREX.r3.1HG0078510	Coilin	intron/ 5utr/ exon	exon/ intron/ 5utr	Tolerated/ Deleterious	*qHvDRR-FLS-2*	FLL, FLW	1
HORVU.MOREX.r3.1HG0078520	Protein FAR1-RELATED SEQUENCE 5	5utr/ exon/ intron	5utr	Tolerated/ Deleterious	*qHvDRR-FLS-2*	FLL, FLW	1
HORVU.MOREX.r3.1HG0078550	Protein FAR1-RELATED SEQUENCE 3	5utr/ intron	5utr	Tolerated	*qHvDRR-FLS-2*	FLL, FLW	1
HORVU.MOREX.r3.1HG0078570	LURP-one-like protein	5utr		Tolerated	*qHvDRR-FLS-2*	FLL, FLW	1
HORVU.MOREX.r3.1HG0078580	glycerol-3-phosphatase 1	5utr		Tolerated/ Deleterious	*qHvDRR-FLS-2*	FLL, FLW	1
HORVU.MOREX.r3.1HG0078590	Poly [ADP-ribose] polymerase	exon/ intron		Deleterious	*qHvDRR-FLS-2*	FLL, FLW	1
HORVU.MOREX.r3.2HG0109310	lectin-receptor kinase	exon/ intron		Tolerated/ Deleterious	*qHvDRR-FLS-3*	FLL, FLW	2
HORVU.MOREX.r3.2HG0109330	U-box domain-containing protein kinase family protein	5utr	5utr	Deleterious	*qHvDRR-FLS-3*	FLL, FLW	2
HORVU.MOREX.r3.2HG0109340	Wound-induced protein 1, putative, expressed			Tolerated	*qHvDRR-FLS-3*	FLL, FLW	2
HORVU.MOREX.r3.2HG0109350	Wound-induced protein 1, putative, expressed	5utr		Tolerated	*qHvDRR-FLS-3*	FLL, FLW	2
HORVU.MOREX.r3.2HG0109400	D-alanine--D-alanine ligase	5utr/ intron	5utr	Tolerated/ Deleterious	*qHvDRR-FLS-3*	FLL, FLW	2
HORVU.MOREX.r3.2HG0109410	Protein COBRA, putative	5utr	5utr	Tolerated/ Deleterious	*qHvDRR-FLS-3*	FLL, FLW	2
HORVU.MOREX.r3.2HG0109420	Pectinesterase	5utr	5utr	Tolerated	*qHvDRR-FLS-3*	FLL, FLW	2
HORVU.MOREX.r3.2HG0109430	ACT domain-containing protein	5utr/ intron	5utr	Tolerated/ Deleterious	*qHvDRR-FLS-3*	FLL, FLW	2
HORVU.MOREX.r3.2HG0109440	F-box family protein			Tolerated/ Deleterious	*qHvDRR-FLS-3*	FLL, FLW	2
HORVU.MOREX.r3.2HG0109520	Macrolide export ATP-binding/permease protein MacB	5utr		Tolerated/ Deleterious	*qHvDRR-FLS-3*	FLL, FLW	2
HORVU.MOREX.r3.2HG0109530	Protein phosphatase 2C-like	5utr/ intron	5utr	Tolerated/ Deleterious	*qHvDRR-FLS-3*	FLL, FLW	2
HORVU.MOREX.r3.2HG0109660	RING/U-box-like protein	exon/ 5utr/ intron		Tolerated/ Deleterious	*qHvDRR-FLS-3*	FLL, FLW	2
HORVU.MOREX.r3.2HG0109680	DUF3511 domain protein, putative (DUF3511)			Tolerated/ Deleterious	*qHvDRR-FLS-3*	FLL, FLW	2
HORVU.MOREX.r3.2HG0109700	Hexosyltransferase	intron/ 5utr/ exon	intron/ 5utr	Tolerated/ Deleterious	*qHvDRR-FLS-3*	FLL, FLW	2
HORVU.MOREX.r3.2HG0109710	Alanine--tR ligase	5utr			*qHvDRR-FLS-3*	FLL, FLW	2
HORVU.MOREX.r3.2HG0109720	BRCT domain-containing protein	exon/ intron/ 5utr	5utr	Tolerated/ Deleterious	*qHvDRR-FLS-3*	FLL, FLW	2
HORVU.MOREX.r3.2HG0109760	Tyrosine N-monooxygese	5utr	5utr	Tolerated/ Deleterious	*qHvDRR-FLS-3*	FLL, FLW	2
HORVU.MOREX.r3.2HG0109790	ABRE binding factor 4	5utr			*qHvDRR-FLS-3*	FLL, FLW	2
HORVU.MOREX.r3.2HG0109800	DJ	5utr/ exon		Tolerated	*qHvDRR-FLS-3*	FLL, FLW	2
HORVU.MOREX.r3.2HG0109850	Protein kinase	5utr/ intron/ exon	intron	Tolerated	*qHvDRR-FLS-3*	FLL, FLW	2
HORVU.MOREX.r3.2HG0109900	Protein FAR1-RELATED SEQUENCE 5			Tolerated/ Deleterious	*qHvDRR-FLS-3*	FLL, FLW	2
HORVU.MOREX.r3.2HG0109910	Ubiquitin-like-specific protease ESD4	5utr		Tolerated/ Deleterious	*qHvDRR-FLS-3*	FLL, FLW	2
HORVU.MOREX.r3.2HG0109930	BED zinc finger,hAT family dimerization domain	5utr	5utr	Tolerated/ Deleterious	*qHvDRR-FLS-3*	FLL, FLW	2
HORVU.MOREX.r3.2HG0109970	Lon protease homolog	intron/ 5utr		Tolerated	*qHvDRR-FLS-3*	FLL, FLW	2

HORVU.MOREX.r3.2HG0109980	Dipeptidyl-peptidase, putative	5utr/ intron		Tolerated/ Deleterious	*qHvDRR-FLS-3*	FLL, FLW	2
HORVU.MOREX.r3.2HG0109990	GRF zinc finger family protein	5utr	5utr	Tolerated/ Deleterious	*qHvDRR-FLS-3*	FLL, FLW	2
HORVU.MOREX.r3.2HG0110000	Nicotiamine synthase	5utr		Tolerated	*qHvDRR-FLS-3*	FLL, FLW	2
HORVU.MOREX.r3.2HG0110020	F-box protein family-like	5utr	intron/ 5utr	Tolerated/ Deleterious	*qHvDRR-FLS-3*	FLL, FLW	2
HORVU.MOREX.r3.2HG0110040	F-box protein family-like	exon/ 5utr	5utr	Tolerated/ Deleterious	*qHvDRR-FLS-3*	FLL, FLW	2
HORVU.MOREX.r3.2HG0110060	Aldehyde dehydrogese	5utr/ intron/ exon			*qHvDRR-FLS-3*	FLL, FLW	2
HORVU.MOREX.r3.2HG0110070	Disease resistance protein (TIR-NBS-LRR class) family	5utr/ intron	5utr/ exon/ intron	Deleterious	*qHvDRR-FLS-3*	FLL, FLW	2
HORVU.MOREX.r3.2HG0110110	Ran GTPase activating protein 2	5utr/ intron/ exon	intron	Tolerated/ Deleterious	*qHvDRR-FLS-3*	FLL, FLW	2
HORVU.MOREX.r3.2HG0110130	Transcription factor protein	5utr	5utr	Tolerated	*qHvDRR-FLS-3*	FLL, FLW	2
HORVU.MOREX.r3.2HG0110140	Poly(A) polymerase	5utr/ exon/ intron	intron	Tolerated/ Deleterious	*qHvDRR-FLS-3*	FLL, FLW	2
HORVU.MOREX.r3.2HG0110160	Zinc finger protein	5utr/ intron/ exon		Tolerated/ Deleterious	*qHvDRR-FLS-3*	FLL, FLW	2
HORVU.MOREX.r3.2HG0110170	Factor of D methylation 1	5utr/ intron/ exon	5utr	Tolerated/ Deleterious	*qHvDRR-FLS-3*	FLL, FLW	2
HORVU.MOREX.r3.2HG0110190	DELLA protein	intron/ 5utr	5utr/ intron	Tolerated	*qHvDRR-FLS-3*	FLL, FLW	2
HORVU.MOREX.r3.2HG0110200	Disease resistance protein (TIR-NBS-LRR class) family	5utr		Tolerated/ Deleterious	*qHvDRR-FLS-3*	FLL, FLW	2
HORVU.MOREX.r3.2HG0110300	U3 small nucleolar R-associated protein 18-like protein			Tolerated/ Deleterious	*qHvDRR-FLS-3*	FLL, FLW	2
HORVU.MOREX.r3.2HG0110340	R-directed D polymerase (reverse transcriptase)-related family protein			Tolerated/ Deleterious	*qHvDRR-FLS-3*	FLL, FLW	2
HORVU.MOREX.r3.2HG0110380	HAT family dimerisation domain containing protein, expressed	5utr	5utr	Tolerated	*qHvDRR-FLS-3*	FLL, FLW	2
HORVU.MOREX.r3.2HG0110400	F-box family protein	5utr		Tolerated/ Deleterious	*qHvDRR-FLS-3*	FLL, FLW	2
HORVU.MOREX.r3.2HG0110410	Mycothiol acetyltransferase	5utr		Tolerated/ Deleterious	*qHvDRR-FLS-3*	FLL, FLW	2
HORVU.MOREX.r3.2HG0110420	Importin subunit alpha	5utr	5utr	Tolerated/ Deleterious	*qHvDRR-FLS-3*	FLL, FLW	2
HORVU.MOREX.r3.2HG0110490	MYB transcription factor	5utr	5utr	Tolerated/ Deleterious	*qHvDRR-FLS-3*	FLL, FLW	2
HORVU.MOREX.r3.2HG0110520	RAPT-1	5utr	5utr	Tolerated/ Deleterious	*qHvDRR-FLS-3*	FLL, FLW	2
HORVU.MOREX.r3.2HG0110530	Hexosyltransferase	5utr		Tolerated	*qHvDRR-FLS-3*	FLL, FLW	2
HORVU.MOREX.r3.2HG0110550	Transducin family protein / WD-40 repeat family protein			Deleterious	*qHvDRR-FLS-3*	FLL, FLW	2
HORVU.MOREX.r3.2HG0110560	Pentatricopeptide repeat-containing protein, putative	5utr		Tolerated	*qHvDRR-FLS-3*	FLL, FLW	2
HORVU.MOREX.r3.2HG0110570	BTB/POZ and MATH domain-containing protein 4	5utr		Tolerated/ Deleterious	*qHvDRR-FLS-3*	FLL, FLW	2
HORVU.MOREX.r3.2HG0110580	Ras-responsive element-binding protein 1	5utr		Tolerated/ Deleterious	*qHvDRR-FLS-3*	FLL, FLW	2
HORVU.MOREX.r3.2HG0110600	GDSL esterase/lipase			Tolerated/ Deleterious	*qHvDRR-FLS-3*	FLL, FLW	2
HORVU.MOREX.r3.2HG0110610	BTB/POZ/MATH-domain protein	5utr	5utr	Tolerated/ Deleterious	*qHvDRR-FLS-3*	FLL, FLW	2
HORVU.MOREX.r3.2HG0110640	transcription factor-like protein	exon/ intron/ 5utr	5utr	Tolerated	*qHvDRR-FLS-3*	FLL, FLW	2
HORVU.MOREX.r3.2HG0110650	Peptidyl-prolyl cis-trans isomerase	exon			*qHvDRR-FLS-3*	FLL, FLW	2
HORVU.MOREX.r3.2HG0187130	RING/U-box superfamily protein	5utr/ intron	5utr/ intron	Tolerated	*qHvDRR-FLS-7*	FLL	2
HORVU.MOREX.r3.2HG0187140	Seryl-tR synthetase	5utr		Tolerated	*qHvDRR-FLS-7*	FLL	2
HORVU.MOREX.r3.2HG0187170	S-adenosyl-L-methionine-dependent methyltransferases superfamily protein	5utr		Tolerated	*qHvDRR-FLS-7*	FLL	2
HORVU.MOREX.r3.2HG0187210	Laminin subunit gamma-1	5utr		Tolerated/ Deleterious	*qHvDRR-FLS-7*	FLL	2
HORVU.MOREX.r3.2HG0187360	IQ domain-containing protein	exon/ 5utr			*qHvDRR-FLS-7*	FLL	2
HORVU.MOREX.r3.2HG0187430	Transmembrane emp24 domain-containing protein	intron		Tolerated	*qHvDRR-FLS-7*	FLL	2
HORVU.MOREX.r3.2HG0187440	S-adenosyl-L-methionine-dependent methyltransferases superfamily protein	5utr/ intron		Tolerated/ Deleterious	*qHvDRR-FLS-7*	FLL	2
HORVU.MOREX.r3.2HG0187450	Rhomboid-like protein	5utr	5utr	Tolerated	*qHvDRR-FLS-7*	FLL	2
HORVU.MOREX.r3.2HG0187460	Homeobox-leucine zipper protein	5utr/ intron	intron	Tolerated/ Deleterious	*qHvDRR-FLS-7*	FLL	2
HORVU.MOREX.r3.2HG0187470	Replication factor C subunit	5utr	5utr		*qHvDRR-FLS-7*	FLL	2
HORVU.MOREX.r3.2HG0187500	ATP-dependent D helicase PIF1	5utr		Tolerated/ Deleterious	*qHvDRR-FLS-7*	FLL	2
HORVU.MOREX.r3.2HG0187530	E3 ubiquitin-protein ligase	5utr/ intron		Tolerated	*qHvDRR-FLS-7*	FLL	2
HORVU.MOREX.r3.2HG0187540	D topoisomerase 4 subunit B (DUF810)	intron		Tolerated/ Deleterious	*qHvDRR-FLS-7*	FLL	2
HORVU.MOREX.r3.2HG0187550	Heat stress transcription factor	5utr	5utr	Tolerated/ Deleterious	*qHvDRR-FLS-7*	FLL	2
HORVU.MOREX.r3.2HG0187560	ORMDL family protein-like	5utr/ exon/ intron	5utr		*qHvDRR-FLS-7*	FLL	2
HORVU.MOREX.r3.2HG0187570	Dof zinc finger protein	exon/ 5utr/ intron	5utr	Tolerated	*qHvDRR-FLS-7*	FLL	2
HORVU.MOREX.r3.2HG0187590	Cortactin-binding protein 2	exon/ 5utr		Tolerated	*qHvDRR-FLS-7*	FLL	2
HORVU.MOREX.r3.2HG0187610	WD-repeat protein, putative	5utr/ intron/ exon		Tolerated/ Deleterious	*qHvDRR-FLS-7*	FLL	2
HORVU.MOREX.r3.2HG0187620	3-hexulose-6-phosphate isomerase	5utr	5utr	Tolerated	*qHvDRR-FLS-7*	FLL	2
HORVU.MOREX.r3.2HG0187630	Aluminum-activated malate transporter-like	5utr/ intron		Tolerated	*qHvDRR-FLS-7*	FLL	2
HORVU.MOREX.r3.2HG0187640	Gamma-tubulin complex component	5utr/ intron		Tolerated	*qHvDRR-FLS-7*	FLL	2
HORVU.MOREX.r3.2HG0187650	Serine/threonine-protein phosphatase 7 long form-like protein	5utr/ exon	5utr	Tolerated/ Deleterious	*qHvDRR-FLS-7*	FLL	2
HORVU.MOREX.r3.2HG0187660	Mitochondrial import inner membrane translocase subunit tim23	5utr	5utr	Tolerated/ Deleterious	*qHvDRR-FLS-7*	FLL	2
HORVU.MOREX.r3.2HG0187680	Glutathione S-transferase			Tolerated/ Deleterious	*qHvDRR-FLS-7*	FLL	2
HORVU.MOREX.r3.2HG0187690	MYB transcription factor-like	5utr/ exon/ intron	intron/ 5utr	Tolerated	*qHvDRR-FLS-7*	FLL	2
HORVU.MOREX.r3.2HG0187760	Argoute	intron	exon/ intron	Tolerated/ Deleterious	*qHvDRR-FLS-7*	FLL	2
HORVU.MOREX.r3.2HG0187780	Zinc finger protein, putative	5utr/ intron/ exon		Tolerated	*qHvDRR-FLS-7*	FLL	2
HORVU.MOREX.r3.2HG0187800	D/R helicase protein	5utr/ intron		Tolerated	*qHvDRR-FLS-7*	FLL	2
HORVU.MOREX.r3.2HG0187810	ArfGap/RecO-like zinc finger domain-containing protein			Tolerated/ Deleterious	*qHvDRR-FLS-7*	FLL	2
HORVU.MOREX.r3.2HG0187820	zinc finger MYM-type-like protein	5utr		Tolerated/ Deleterious	*qHvDRR-FLS-7*	FLL	2
HORVU.MOREX.r3.2HG0187830	zinc finger MYM-type-like protein	5utr		Tolerated/ Deleterious	*qHvDRR-FLS-7*	FLL	2
HORVU.MOREX.r3.2HG0187850	F-box only protein 43	5utr/ intron	5utr	Tolerated	*qHvDRR-FLS-7*	FLL	2
HORVU.MOREX.r3.2HG0187860	basic helix-loop-helix (bHLH) D-binding superfamily protein			Tolerated/ Deleterious	*qHvDRR-FLS-7*	FLL	2
HORVU.MOREX.r3.2HG0187870	Amino acid transporter, putative	5utr	5utr	Tolerated	*qHvDRR-FLS-7*	FLL	2
HORVU.MOREX.r3.2HG0187880	Syntaxin-binding protein 5	5utr/ exon/ intron	intron	Tolerated/ Deleterious	*qHvDRR-FLS-7*	FLL	2
HORVU.MOREX.r3.2HG0187890	High mobility group protein	5utr	5utr	Tolerated	*qHvDRR-FLS-7*	FLL	2
HORVU.MOREX.r3.2HG0187900	Ser/Thr-rich protein T10 in DGCR region	intron/ 5utr	5utr	Tolerated/ Deleterious	*qHvDRR-FLS-7*	FLL	2
HORVU.MOREX.r3.2HG0187910	RWP-RK domain containing protein	5utr/ intron	5utr	Tolerated	*qHvDRR-FLS-7*	FLL	2
HORVU.MOREX.r3.2HG0187920	RWP-RK domain containing protein	5utr/ exon/ intron	intron	Tolerated	*qHvDRR-FLS-7*	FLL	2
HORVU.MOREX.r3.2HG0187930	kinase family protein	5utr/ intron/ exon	5utr	Tolerated/ Deleterious	*qHvDRR-FLS-7*	FLL	2
HORVU.MOREX.r3.2HG0187940	Niemann-Pick C1 protein	5utr/ intron	5utr	Tolerated/ Deleterious	*qHvDRR-FLS-7*	FLL	2
HORVU.MOREX.r3.2HG0187970	Cyclin	5utr/ exon/ intron	5utr/ intron		*qHvDRR-FLS-7*	FLL	2
HORVU.MOREX.r3.2HG0187980	Transmembrane protein 184C	5utr/ intron/ exon	5utr		*qHvDRR-FLS-7*	FLL	2
HORVU.MOREX.r3.2HG0187990	O-fucosyltransferase family protein	5utr/ intron/ exon		Tolerated/ Deleterious	*qHvDRR-FLS-7*	FLL	2
HORVU.MOREX.r3.2HG0188000	Pectin lyase-like superfamily protein	intron/ 5utr	5utr	Tolerated/ Deleterious	*qHvDRR-FLS-7*	FLL	2
HORVU.MOREX.r3.2HG0188010	Pectin lyase-like superfamily protein	5utr/ intron/ exon	5utr	Tolerated/ Deleterious	*qHvDRR-FLS-7*	FLL	2
HORVU.MOREX.r3.2HG0188020	DUF630 family protein, putative (DUF630 and DUF632)	5utr/ exon/ intron	5utr	Tolerated/ Deleterious	*qHvDRR-FLS-7*	FLL	2
HORVU.MOREX.r3.2HG0188030	FBD-associated F-box protein	5utr	5utr	Tolerated/ Deleterious	*qHvDRR-FLS-7*	FLL	2
HORVU.MOREX.r3.2HG0188040	DUF241 domain protein (DUF241)	5utr		Tolerated/ Deleterious	*qHvDRR-FLS-7*	FLL	2
HORVU.MOREX.r3.2HG0188050	Lysine/histidine transporter	5utr/ intron/ exon	5utr	Tolerated/ Deleterious	*qHvDRR-FLS-7*	FLL	2
HORVU.MOREX.r3.2HG0188060	S-acyltransferase	5utr/ intron	5utr	Tolerated	*qHvDRR-FLS-7*	FLL	2
HORVU.MOREX.r3.2HG0188070	L-ascorbate oxidase-like protein			Tolerated/ Deleterious	*qHvDRR-FLS-7*	FLL	2
HORVU.MOREX.r3.2HG0188080	GDSL esterase/lipase	intron/ 5utr/ exon	intron/ 5utr	Tolerated/ Deleterious	*qHvDRR-FLS-7*	FLL	2
HORVU.MOREX.r3.2HG0188090	GDSL esterase/lipase	5utr/ intron	intron/ exon/ 5utr	Tolerated/ Deleterious	*qHvDRR-FLS-7*	FLL	2
HORVU.MOREX.r3.2HG0188110	tR pseudouridine synthase Pus10, putative	5utr/ intron/ exon		Tolerated	*qHvDRR-FLS-7*	FLL	2
HORVU.MOREX.r3.2HG0188120	Sucrose synthase			Tolerated/ Deleterious	*qHvDRR-FLS-7*	FLL	2
HORVU.MOREX.r3.2HG0188130	Coiled-coil domain-containing protein 124	5utr	5utr		*qHvDRR-FLS-7*	FLL	2
HORVU.MOREX.r3.2HG0188160	Prolyl endopeptidase	5utr/ exon/ intron	intron	Tolerated/ Deleterious	*qHvDRR-FLS-7*	FLL	2
HORVU.MOREX.r3.2HG0188170	Mechanosensitive ion channel	5utr/ intron	5utr	Tolerated/ Deleterious	*qHvDRR-FLS-7*	FLL	2
HORVU.MOREX.r3.2HG0188190	tR sulfurtransferase	5utr		Tolerated	*qHvDRR-FLS-7*	FLL	2
HORVU.MOREX.r3.2HG0188200	Calcium-dependent protein kinase	5utr/ intron/ exon	5utr/ intron	Tolerated/ Deleterious	*qHvDRR-FLS-7*	FLL	2
HORVU.MOREX.r3.2HG0188210	Alpha-L-fucosidase 1	5utr/ intron/ exon	intron	Tolerated/ Deleterious	*qHvDRR-FLS-7*	FLL	2
HORVU.MOREX.r3.2HG0188220	Lysine-specific histone demethylase 1-like protein			Tolerated/ Deleterious	*qHvDRR-FLS-7*	FLL	2
HORVU.MOREX.r3.2HG0188230	Thioredoxin, putative	5utr		Tolerated/ Deleterious	*qHvDRR-FLS-7*	FLL	2
HORVU.MOREX.r3.2HG0188270	Protein kinase	exon/ 5utr/ intron	5utr	Tolerated/ Deleterious	*qHvDRR-FLS-7*	FLL	2
HORVU.MOREX.r3.2HG0188290	Aquaporin	5utr			*qHvDRR-FLS-7*	FLL	2
HORVU.MOREX.r3.2HG0188300	CsAtPR5	5utr/ intron/ exon	exon/ 5utr/ intron	Tolerated/ Deleterious	*qHvDRR-FLS-7*	FLL	2
HORVU.MOREX.r3.2HG0188310	CsAtPR5	intron		Tolerated/ Deleterious	*qHvDRR-FLS-7*	FLL	2
HORVU.MOREX.r3.2HG0188320	Branched-chain-amino-acid aminotransferase	5utr/ intron/ exon	5utr	Tolerated/ Deleterious	*qHvDRR-FLS-7*	FLL	2
HORVU.MOREX.r3.2HG0188370	Phosphatidylinositol N-acetylglucosaminlytransferase subunit P-like protein	5utr/ exon/ intron	intron	Tolerated/ Deleterious	*qHvDRR-FLS-7*	FLL	2
HORVU.MOREX.r3.2HG0188380	Rop guanine nucleotide exchange factor, putative	5utr		Tolerated	*qHvDRR-FLS-7*	FLL	2
HORVU.MOREX.r3.2HG0188410	Subtilisin-like protease	5utr	exon	Tolerated/ Deleterious	*qHvDRR-FLS-7*	FLL	2
HORVU.MOREX.r3.2HG0188420	Subtilisin-like protease	5utr		Tolerated/ Deleterious	*qHvDRR-FLS-7*	FLL	2
HORVU.MOREX.r3.2HG0188430	Subtilisin-like protease	5utr	5utr	Tolerated/ Deleterious	*qHvDRR-FLS-7*	FLL	2
HORVU.MOREX.r3.2HG0188440	XH/XS domain-containing family protein	5utr/ intron/ exon		Tolerated/ Deleterious	*qHvDRR-FLS-7*	FLL	2
HORVU.MOREX.r3.2HG0188500	CsAtPR5	5utr/ exon		Tolerated/ Deleterious	*qHvDRR-FLS-7*	FLL	2

HORVU.MOREX.r3.2HG0188520	protein kinase family protein	5utr	exon	Tolerated/ Deleterious	*qHvDRR-FLS-7*	FLL	2
HORVU.MOREX.r3.2HG0188580	CsAtPR5	5utr		Tolerated/ Deleterious	*qHvDRR-FLS-7*	FLL	2
HORVU.MOREX.r3.2HG0188620	F-box family protein	intron/ 5utr	5utr	Tolerated	*qHvDRR-FLS-7*	FLL	2
HORVU.MOREX.r3.2HG0188630	Subtilisin-like protease	5utr	5utr	Tolerated/ Deleterious	*qHvDRR-FLS-7*	FLL	2
HORVU.MOREX.r3.2HG0188640	NHL domain protein	5utr			*qHvDRR-FLS-7*	FLL	2
HORVU.MOREX.r3.2HG0188650	C (No Apical Meristem) domain transcriptiol regulator superfamily protein	5utr		Tolerated/ Deleterious	*qHvDRR-FLS-7*	FLL	2
HORVU.MOREX.r3.2HG0188660	disease resistance protein (TIR-NBS-LRR class) family	intron/ 5utr		Tolerated/ Deleterious	*qHvDRR-FLS-7*	FLL	2
HORVU.MOREX.r3.2HG0188670	Acyl-coenzyme A thioesterase 8	intron/ 5utr	5utr	Tolerated/ Deleterious	*qHvDRR-FLS-7*	FLL	2
HORVU.MOREX.r3.2HG0188700	Cactin	5utr	5utr	Tolerated/ Deleterious	*qHvDRR-FLS-7*	FLL	2
HORVU.MOREX.r3.2HG0188710	Basic helix-loop-helix (BHLH) D-binding superfamily protein	5utr/ intron	5utr/ intron	Tolerated	*qHvDRR-FLS-7*	FLL	2
HORVU.MOREX.r3.2HG0188750	Haloacid dehalogese-like hydrolase superfamily protein	5utr		Tolerated	*qHvDRR-FLS-7*	FLL	2
HORVU.MOREX.r3.2HG0188760	Glycosyltransferases	5utr		Tolerated/ Deleterious	*qHvDRR-FLS-7*	FLL	2
HORVU.MOREX.r3.2HG0188770	C domain protein	5utr		Tolerated/ Deleterious	*qHvDRR-FLS-7*	FLL	2
HORVU.MOREX.r3.2HG0188780	Glycosyltransferase	5utr	5utr	Tolerated/ Deleterious	*qHvDRR-FLS-7*	FLL	2
HORVU.MOREX.r3.2HG0188790	Glycosyltransferase	5utr	5utr	Tolerated/ Deleterious	*qHvDRR-FLS-7*	FLL	2
HORVU.MOREX.r3.2HG0188800	Glycosyltransferase	5utr		Tolerated/ Deleterious	*qHvDRR-FLS-7*	FLL	2
HORVU.MOREX.r3.2HG0188810	Glycosyltransferase	5utr	5utr	Tolerated/ Deleterious	*qHvDRR-FLS-7*	FLL	2
HORVU.MOREX.r3.2HG0188820	Glycosyltransferase	5utr		Tolerated/ Deleterious	*qHvDRR-FLS-7*	FLL	2
HORVU.MOREX.r3.2HG0200740	Zinc finger matrin-type protein 2	intron			*qHvDRR-FLS-8*	FLL, FLW	2
HORVU.MOREX.r3.2HG0200760	Translation initiation factor IF-2	5utr		Tolerated/ Deleterious	*qHvDRR-FLS-8*	FLL, FLW	2
HORVU.MOREX.r3.2HG0200770	Serine/threonine-protein phosphatase 7 long form-like protein	5utr	5utr	Tolerated/ Deleterious	*qHvDRR-FLS-8*	FLL, FLW	2
HORVU.MOREX.r3.2HG0200780	Agmatine coumaroyltransferase-2	5utr/ exon	exon/ 5utr	Tolerated	*qHvDRR-FLS-8*	FLL, FLW	2
HORVU.MOREX.r3.2HG0200920	Agmatine coumaroyltransferase-2	5utr		Tolerated	*qHvDRR-FLS-8*	FLL, FLW	2
HORVU.MOREX.r3.2HG0200970	Auxin response factor			Tolerated/ Deleterious	*qHvDRR-FLS-8*	FLL, FLW	2
HORVU.MOREX.r3.2HG0200990	TLD domain-containing protein	5utr/ intron/ exon	5utr	Tolerated/ Deleterious	*qHvDRR-FLS-8*	FLL, FLW	2
HORVU.MOREX.r3.2HG0201030	O-acyltransferase (WSD1-like) family protein	5utr/ exon		Tolerated/ Deleterious	*qHvDRR-FLS-8*	FLL, FLW	2
HORVU.MOREX.r3.2HG0201070	Protein ROOT HAIR DEFECTIVE 3 homolog 1	5utr/ exon	5utr	Tolerated/ Deleterious	*qHvDRR-FLS-8*	FLL, FLW	2
HORVU.MOREX.r3.2HG0201080	WUSCHEL-related homeobox	5utr/ intron/ exon	5utr	Tolerated/ Deleterious	*qHvDRR-FLS-8*	FLL, FLW	2
HORVU.MOREX.r3.2HG0201100	U11/U12 small nuclear ribonucleoprotein 25 kDa	5utr/ intron	5utr	Tolerated	*qHvDRR-FLS-8*	FLL, FLW	2
HORVU.MOREX.r3.2HG0201120	Zinc finger CCCH domain-containing protein 30			Tolerated/ Deleterious	*qHvDRR-FLS-8*	FLL, FLW	2
HORVU.MOREX.r3.2HG0201150	IQ domain-containing protein	5utr/ intron/ exon		Tolerated/ Deleterious	*qHvDRR-FLS-8*	FLL, FLW	2
HORVU.MOREX.r3.2HG0201180	Regulator of chromosome condensation (RCC1) family protein	5utr/ intron	5utr/ intron	Tolerated/ Deleterious	*qHvDRR-FLS-8*	FLL, FLW	2
HORVU.MOREX.r3.2HG0201190	Oxidative stress 3, putative isoform 2	5utr/ intron/ exon	5utr/ intron/ exon	Tolerated/ Deleterious	*qHvDRR-FLS-8*	FLL, FLW	2
HORVU.MOREX.r3.2HG0201200	Endoribonuclease YbeY	5utr/ exon	5utr	Tolerated/ Deleterious	*qHvDRR-FLS-8*	FLL, FLW	2
HORVU.MOREX.r3.2HG0201220	Callose synthase-like protein	5utr	5utr	Tolerated/ Deleterious	*qHvDRR-FLS-8*	FLL, FLW	2
HORVU.MOREX.r3.2HG0201230	V-type proton ATPase subunit a	intron/ 5utr/ exon	5utr	Tolerated/ Deleterious	*qHvDRR-FLS-8*	FLL, FLW	2
HORVU.MOREX.r3.2HG0201250	GTP cyclohydrolase 1	5utr/ intron/ exon	5utr	Tolerated	*qHvDRR-FLS-8*	FLL, FLW	2
HORVU.MOREX.r3.2HG0201260	Pol polyprotein		5utr	Deleterious	*qHvDRR-FLS-8*	FLL, FLW	2
HORVU.MOREX.r3.2HG0201270	C (No Apical Meristem) domain transcriptiol regulator superfamily protein	5utr			*qHvDRR-FLS-8*	FLL, FLW	2
HORVU.MOREX.r3.2HG0201330	Cysteine/Histidine-rich C1 domain family protein	5utr	exon/ intron/ 5utr	Tolerated/ Deleterious	*qHvDRR-FLS-8*	FLL, FLW	2
HORVU.MOREX.r3.2HG0201340	Cysteine/Histidine-rich C1 domain family protein	5utr	5utr/ exon	Tolerated/ Deleterious	*qHvDRR-FLS-8*	FLL, FLW	2
HORVU.MOREX.r3.2HG0201350	Ethylene-responsive transcription factor	5utr	5utr	Tolerated	*qHvDRR-FLS-8*	FLL, FLW	2
HORVU.MOREX.r3.2HG0201360	Flavanone 3-hydroxylase	intron/ 5utr		Tolerated/ Deleterious	*qHvDRR-FLS-8*	FLL, FLW	2
HORVU.MOREX.r3.2HG0201390	Adenosylhomocysteise	5utr/ intron/ exon		Tolerated/ Deleterious	*qHvDRR-FLS-8*	FLL, FLW	2
HORVU.MOREX.r3.2HG0201400	Serine hydroxymethyltransferase	exon/ intron/ 5utr	5utr		*qHvDRR-FLS-8*	FLL, FLW	2
HORVU.MOREX.r3.2HG0201420	Protein kinase	exon/ intron	intron	Tolerated/ Deleterious	*qHvDRR-FLS-8*	FLL, FLW	2
HORVU.MOREX.r3.2HG0201440	Auxin responsive SAUR protein	5utr		Tolerated/ Deleterious	*qHvDRR-FLS-8*	FLL, FLW	2
HORVU.MOREX.r3.2HG0201480	Auxin responsive SAUR protein	5utr	5utr	Tolerated/ Deleterious	*qHvDRR-FLS-8*	FLL, FLW	2
HORVU.MOREX.r3.2HG0201490	Auxin responsive SAUR protein	5utr	5utr	Tolerated/ Deleterious	*qHvDRR-FLS-8*	FLL, FLW	2
HORVU.MOREX.r3.2HG0201500	SAUR-like auxin-responsive protein family	5utr		Tolerated/ Deleterious	*qHvDRR-FLS-8*	FLL, FLW	2
HORVU.MOREX.r3.2HG0201510	Auxin responsive SAUR protein	5utr		Tolerated	*qHvDRR-FLS-8*	FLL, FLW	2
HORVU.MOREX.r3.2HG0201520	SAUR-like auxin-responsive protein family	5utr	5utr	Tolerated/ Deleterious	*qHvDRR-FLS-8*	FLL, FLW	2
HORVU.MOREX.r3.2HG0201540	SAUR-like auxin-responsive protein family	5utr		Tolerated	*qHvDRR-FLS-8*	FLL, FLW	2
HORVU.MOREX.r3.2HG0201580	SAUR-like auxin-responsive protein family	5utr	5utr	Tolerated	*qHvDRR-FLS-8*	FLL, FLW	2
HORVU.MOREX.r3.2HG0201590	SAUR-like auxin-responsive protein family	5utr	5utr	Deleterious	*qHvDRR-FLS-8*	FLL, FLW	2
HORVU.MOREX.r3.2HG0201610	Auxin responsive SAUR protein	5utr	5utr	Tolerated	*qHvDRR-FLS-8*	FLL, FLW	2
HORVU.MOREX.r3.2HG0201630	SAUR-like auxin-responsive protein family	5utr	5utr	Tolerated	*qHvDRR-FLS-8*	FLL, FLW	2
HORVU.MOREX.r3.2HG0201640	Histone H2A	5utr	exon	Tolerated/ Deleterious	*qHvDRR-FLS-8*	FLL, FLW	2
HORVU.MOREX.r3.2HG0201650	D topoisomerase 1	5utr	5utr	Tolerated/ Deleterious	*qHvDRR-FLS-8*	FLL, FLW	2
HORVU.MOREX.r3.2HG0201690	LINE-1 reverse transcriptase-like protein			Tolerated/ Deleterious	*qHvDRR-FLS-8*	FLL, FLW	2
HORVU.MOREX.r3.2HG0201700	Transcription factor	5utr/ exon/ intron	exon/ 5utr	Tolerated/ Deleterious	*qHvDRR-FLS-8*	FLL, FLW	2
HORVU.MOREX.r3.2HG0201710	Calcium-binding EF-hand family protein	5utr	5utr	Tolerated	*qHvDRR-FLS-8*	FLL, FLW	2
HORVU.MOREX.r3.2HG0201730	Ribosomal R large subunit methyltransferase E	5utr/ intron	intron/ 5utr	Tolerated	*qHvDRR-FLS-8*	FLL, FLW	2
HORVU.MOREX.r3.2HG0201770	Ribosomal protein S4	exon/ intron/ 5utr	5utr		*qHvDRR-FLS-8*	FLL, FLW	2
HORVU.MOREX.r3.2HG0201780	BSD domain containing protein	5utr	5utr	Tolerated	*qHvDRR-FLS-8*	FLL, FLW	2
HORVU.MOREX.r3.2HG0201790	Eukaryotic translation initiation factor 3 subunit F	5utr	5utr		*qHvDRR-FLS-8*	FLL, FLW	2
HORVU.MOREX.r3.2HG0201810	Molybdate transporter 2	5utr/ exon	5utr	Tolerated/ Deleterious	*qHvDRR-FLS-8*	FLL, FLW	2
HORVU.MOREX.r3.2HG0201820	Cyclin-related family protein	5utr/ intron		Tolerated/ Deleterious	*qHvDRR-FLS-8*	FLL, FLW	2
HORVU.MOREX.r3.2HG0201830	Pentatricopeptide repeat-containing protein	5utr	5utr	Tolerated/ Deleterious	*qHvDRR-FLS-8*	FLL, FLW	2
HORVU.MOREX.r3.2HG0201840	Protein UXT-like protein	exon/ intron	exon		*qHvDRR-FLS-8*	FLL, FLW	2
HORVU.MOREX.r3.2HG0201850	Transmembrane 9 superfamily member			Tolerated	*qHvDRR-FLS-8*	FLL, FLW	2
HORVU.MOREX.r3.2HG0201860	Molybdopterin biosynthesis protein CNX1	exon/ 5utr/ intron	5utr	Tolerated/ Deleterious	*qHvDRR-FLS-8*	FLL, FLW	2
HORVU.MOREX.r3.2HG0201870	D topoisomerase 1	5utr/ intron/ exon	5utr	Tolerated/ Deleterious	*qHvDRR-FLS-8*	FLL, FLW	2
HORVU.MOREX.r3.2HG0201880	WRKY transcription factor	intron/ 5utr/ exon	5utr/ intron	Tolerated/ Deleterious	*qHvDRR-FLS-8*	FLL, FLW	2
HORVU.MOREX.r3.2HG0201890	Basic leucine zipper and W2 domain-containing protein 2	5utr/ exon/ intron	5utr	Tolerated	*qHvDRR-FLS-8*	FLL, FLW	2
HORVU.MOREX.r3.2HG0201910	Myosin-H heavy chain	intron/ exon/ 5utr		Deleterious	*qHvDRR-FLS-8*	FLL, FLW	2
HORVU.MOREX.r3.2HG0201920	Inositol-pentakisphosphate 2-kinase			Tolerated	*qHvDRR-FLS-8*	FLL, FLW	2
HORVU.MOREX.r3.2HG0201930	Heavy metal transport/detoxification superfamily protein			Tolerated/ Deleterious	*qHvDRR-FLS-8*	FLL, FLW	2
HORVU.MOREX.r3.2HG0201940	Alpha/beta-Hydrolases superfamily protein, putative	5utr	5utr	Tolerated/ Deleterious	*qHvDRR-FLS-8*	FLL, FLW	2
HORVU.MOREX.r3.2HG0201990	TTF-type zinc finger protein with HAT dimerization domain-containing protein	5utr	exon/ 5utr		*qHvDRR-FLS-8*	FLL, FLW	2
HORVU.MOREX.r3.2HG0202040	CsAtPR5	5utr	exon/ 5utr/ intron	Tolerated/ Deleterious	*qHvDRR-FLS-8*	FLL, FLW	2
HORVU.MOREX.r3.2HG0202050	CsAtPR5	5utr			*qHvDRR-FLS-8*	FLL, FLW	2
HORVU.MOREX.r3.2HG0202060	Protein kinase	5utr/ intron/ exon	intron	Tolerated	*qHvDRR-FLS-8*	FLL, FLW	2
HORVU.MOREX.r3.2HG0202070	Chaperone protein DJ	intron			*qHvDRR-FLS-8*	FLL, FLW	2
HORVU.MOREX.r3.2HG0202090	Xyloglucan endotransglucosylase/hydrolase	5utr/ exon	exon		*qHvDRR-FLS-8*	FLL, FLW	2
HORVU.MOREX.r3.2HG0202100	Xyloglucan endotransglucosylase/hydrolase	5utr	5utr		*qHvDRR-FLS-8*	FLL, FLW	2
HORVU.MOREX.r3.2HG0202110	Alpha-1,4-glucan-protein synthase [UDP-forming]	5utr	5utr	Tolerated	*qHvDRR-FLS-8*	FLL, FLW	2
HORVU.MOREX.r3.2HG0202120	Alpha-1,4-glucan-protein synthase	5utr		Tolerated	*qHvDRR-FLS-8*	FLL, FLW	2
HORVU.MOREX.r3.2HG0202130	Werner Syndrome-like exonuclease			Tolerated	*qHvDRR-FLS-8*	FLL, FLW	2
HORVU.MOREX.r3.2HG0202140	tR pseudouridine synthase A	5utr		Deleterious	*qHvDRR-FLS-8*	FLL, FLW	2
HORVU.MOREX.r3.2HG0202150	Protein kinase-like	5utr/ exon/ intron		Tolerated	*qHvDRR-FLS-8*	FLL, FLW	2
HORVU.MOREX.r3.2HG0202180	Transcription factor, putative	5utr	5utr	Tolerated	*qHvDRR-FLS-8*	FLL, FLW	2
HORVU.MOREX.r3.4HG0337900	global transcription factor group B1	5utr	5utr	Tolerated, Deleterious	*qHvDRR-FLS-15*	FLL	4
HORVU.MOREX.r3.4HG0337910	Transposase	5utr		Tolerated, Deleterious	*qHvDRR-FLS-15*	FLL	4
HORVU.MOREX.r3.4HG0337920	Alpha/beta-Hydrolases superfamily protein	5utr		Tolerated	*qHvDRR-FLS-15*	FLL	4
HORVU.MOREX.r3.4HG0337930	14 kDa proline-rich protein DC2.15			Tolerated	*qHvDRR-FLS-15*	FLL	4
HORVU.MOREX.r3.4HG0337940	Ethylene-responsive transcription factor	5utr		Tolerated, Deleterious	*qHvDRR-FLS-15*	FLL	4
HORVU.MOREX.r3.4HG0337950	65-kDa microtubule-associated-like protein			Tolerated	*qHvDRR-FLS-15*	FLL	4
HORVU.MOREX.r3.4HG0337960	Dihydroxyacetone kinase family protein	5utr		Tolerated	*qHvDRR-FLS-15*	FLL	4
HORVU.MOREX.r3.4HG0337970	Transcription factor Inducer of CBF expression 1			Tolerated	*qHvDRR-FLS-15*	FLL	4
HORVU.MOREX.r3.4HG0338010	Amino acid transporter family protein, putative, expressed	5utr	5utr	Tolerated	*qHvDRR-FLS-15*	FLL	4
HORVU.MOREX.r3.4HG0338020	Alpha/beta-Hydrolases superfamily protein	exon		Tolerated	*qHvDRR-FLS-15*	FLL	4
HORVU.MOREX.r3.4HG0338040	Protein kinase, putative, expressed	5utr, intron	5utr	Tolerated, Deleterious	*qHvDRR-FLS-15*	FLL	4
HORVU.MOREX.r3.4HG0338060	Phytochrome	5utr, intron, exon	5utr	Tolerated, Deleterious	*qHvDRR-FLS-15*	FLL	4
HORVU.MOREX.r3.4HG0338070	Kinase family protein	exon, intron, 5utr		Tolerated	*qHvDRR-FLS-15*	FLL	4
HORVU.MOREX.r3.4HG0338080	Peptide transporter	5utr, exon	5utr	Tolerated	*qHvDRR-FLS-15*	FLL	4
HORVU.MOREX.r3.4HG0338090	MYB transcription factor	5utr		Tolerated, Deleterious	*qHvDRR-FLS-15*	FLL	4

HORVU.MOREX.r3.4HG0338150	Engulfment and cell motility protein 2			Tolerated, Deleterious	*qHvDRR-FLS-15*	FLL	4
HORVU.MOREX.r3.4HG0338160	Translational activator GCN1	intron		Tolerated, Deleterious	*qHvDRR-FLS-15*	FLL	4
HORVU.MOREX.r3.4HG0338170	vacuolar protein sorting-associated protein (DUF946)			Tolerated, Deleterious	*qHvDRR-FLS-15*	FLL	4
HORVU.MOREX.r3.4HG0338190	actin cross-linking protein, putative (DUF569)	5utr		Tolerated	*qHvDRR-FLS-15*	FLL	4
HORVU.MOREX.r3.4HG0338200	RNA-directed DNA polymerase (Reverse transcriptase)	5utr		Tolerated, Deleterious	*qHvDRR-FLS-15*	FLL	4
HORVU.MOREX.r3.4HG0338230	SWI/SNF complex subunit SWI3D			Tolerated, Deleterious	*qHvDRR-FLS-15*	FLL	4
HORVU.MOREX.r3.4HG0338250	Kinase, putative			Tolerated, Deleterious	*qHvDRR-FLS-15*	FLL	4
HORVU.MOREX.r3.4HG0338270	ATP-dependent DNA helicase DDM1			Tolerated	*qHvDRR-FLS-15*	FLL	4
HORVU.MOREX.r3.4HG0338290	Glucan endo-1,3-beta-glucosidase			Tolerated	*qHvDRR-FLS-15*	FLL	4
HORVU.MOREX.r3.4HG0338300	Adenylyl cyclase-associated protein			Tolerated, Deleterious	*qHvDRR-FLS-15*	FLL	4
HORVU.MOREX.r3.4HG0338310	tetratricopeptide repeat (TPR)-containing protein			Tolerated	*qHvDRR-FLS-15*	FLL	4
HORVU.MOREX.r3.4HG0338340	GRAS transcription factor			Tolerated, Deleterious	*qHvDRR-FLS-15*	FLL	4
HORVU.MOREX.r3.4HG0338360	late embryogenesis abundant protein			Tolerated	*qHvDRR-FLS-15*	FLL	4
HORVU.MOREX.r3.4HG0338380	ATP-dependent DNA helicase pif1			Tolerated, Deleterious	*qHvDRR-FLS-15*	FLL	4
HORVU.MOREX.r3.4HG0338400	Histone H2B		5utr		*qHvDRR-FLS-15*	FLL	4
HORVU.MOREX.r3.4HG0338440	auxin response factor 2			Tolerated, Deleterious	*qHvDRR-FLS-15*	FLL	4
HORVU.MOREX.r3.4HG0338450	Pentatricopeptide repeat-containing protein	5utr		Tolerated, Deleterious	*qHvDRR-FLS-15*	FLL	4
HORVU.MOREX.r3.4HG0338460	Carbohydrate kinase-like			Tolerated	*qHvDRR-FLS-15*	FLL	4
HORVU.MOREX.r3.4HG0338470	Serine/threonine protein phosphatase 7 long form isogeny			Tolerated, Deleterious	*qHvDRR-FLS-15*	FLL	4
HORVU.MOREX.r3.4HG0338480	FAR1-related sequence 10			Tolerated, Deleterious	*qHvDRR-FLS-15*	FLL	4
HORVU.MOREX.r3.4HG0338500	BTB/POZ domain-containing protein			Tolerated	*qHvDRR-FLS-15*	FLL	4
HORVU.MOREX.r3.4HG0338520	Glycosyltransferase			Tolerated, Deleterious	*qHvDRR-FLS-15*	FLL	4
HORVU.MOREX.r3.4HG0338530	Alanine--tRNA ligase			Tolerated, Deleterious	*qHvDRR-FLS-15*	FLL	4
HORVU.MOREX.r3.4HG0338540	CUGBP Elav-like family member 1			Tolerated, Deleterious	*qHvDRR-FLS-15*	FLL	4
HORVU.MOREX.r3.4HG0338560	Kinase, putative			Tolerated, Deleterious	*qHvDRR-FLS-15*	FLL	4
HORVU.MOREX.r3.4HG0338590	Sec14p-like phosphatidylinositol transfer family protein	exon		Tolerated, Deleterious	*qHvDRR-FLS-15*	FLL	4
HORVU.MOREX.r3.4HG0338600	Sec14p-like phosphatidylinositol transfer family protein	intron, 5utr, exon	intron	Tolerated, Deleterious	*qHvDRR-FLS-15*	FLL	4
HORVU.MOREX.r3.4HG0338620	Erythronate-4-phosphate dehydrogenase family protein	5utr	5utr	Tolerated	*qHvDRR-FLS-15*	FLL	4
HORVU.MOREX.r3.4HG0338630	Sec14p-like phosphatidylinositol transfer family protein	intron, 5utr	5utr, exon	Tolerated	*qHvDRR-FLS-15*	FLL	4
HORVU.MOREX.r3.4HG0338640	Anthocyanin 5-aromatic acyltransferase	5utr		Tolerated, Deleterious	*qHvDRR-FLS-15*	FLL	4
HORVU.MOREX.r3.4HG0338650	Benzyl alcohol O-benzoyltransferase	5utr		Tolerated	*qHvDRR-FLS-15*	FLL	4
HORVU.MOREX.r3.4HG0338660	Benzyl alcohol O-benzoyltransferase			Tolerated, Deleterious	*qHvDRR-FLS-15*	FLL	4
HORVU.MOREX.r3.4HG0338670	marker for oxidative stress response protein			Tolerated, Deleterious	*qHvDRR-FLS-15*	FLL	4
HORVU.MOREX.r3.4HG0338710	zinc finger MYM-type-like protein	5utr		Tolerated, Deleterious	*qHvDRR-FLS-15*	FLL	4
HORVU.MOREX.r3.4HG0338720	Receptor kinase	5utr, exon, intron		Tolerated	*qHvDRR-FLS-15*	FLL	4
HORVU.MOREX.r3.4HG0338730	Maf-like protein, expressed	intron, exon	5utr	Tolerated, Deleterious	*qHvDRR-FLS-15*	FLL	4
HORVU.MOREX.r3.4HG0338750	Pre-mRNA polyadenylation factor Fip1	intron		Tolerated, Deleterious	*qHvDRR-FLS-15*	FLL	4
HORVU.MOREX.r3.4HG0338760	Lariat debranching enzyme	5utr, exon, intron	exon	Tolerated, Deleterious	*qHvDRR-FLS-15*	FLL	4
HORVU.MOREX.r3.4HG0338770	basic helix-loop-helix (bHLH) DNA-binding superfamily protein	5utr, exon		Tolerated	*qHvDRR-FLS-15*	FLL	4
HORVU.MOREX.r3.4HG0338790	WD repeat-containing protein	intron, 5utr	intron		*qHvDRR-FLS-15*	FLL	4
HORVU.MOREX.r3.4HG0338800	Tubulin alpha chain	5utr, intron, exon	intron	Tolerated	*qHvDRR-FLS-15*	FLL	4
HORVU.MOREX.r3.4HG0338810	Inositol-tetrakisphosphate 1-kinase	intron, 5utr		Tolerated	*qHvDRR-FLS-15*	FLL	4
HORVU.MOREX.r3.4HG0338820	ERD (Early-responsive to dehydration stress) family protein	exon, 5utr, intron			*qHvDRR-FLS-15*	FLL	4
HORVU.MOREX.r3.4HG0338850	myb-like protein X			Tolerated, Deleterious	*qHvDRR-FLS-15*	FLL	4
HORVU.MOREX.r3.4HG0338860	Sulfite exporter TauE/SafE family protein	5utr, intron, exon	5utr		*qHvDRR-FLS-15*	FLL	4
HORVU.MOREX.r3.4HG0338890	Centrosomal protein of 57 kDa			Deleterious	*qHvDRR-FLS-15*	FLL	4
HORVU.MOREX.r3.4HG0338900	AMSH-like ubiquitin thioesterase 1	5utr, exon	5utr	Tolerated	*qHvDRR-FLS-15*	FLL	4
HORVU.MOREX.r3.4HG0338910	GDP-mannose transporter	intron, 5utr		Tolerated	*qHvDRR-FLS-15*	FLL	4
HORVU.MOREX.r3.4HG0338950	Alanine--glyoxylate aminotransferase 2, mitochondrial	5utr		Deleterious	*qHvDRR-FLS-15*	FLL	4
HORVU.MOREX.r3.4HG0338960	Epidermal patterning factor-like protein	5utr		Tolerated	*qHvDRR-FLS-15*	FLL	4
HORVU.MOREX.r3.4HG0338980	Alpha/beta-hydrolase superfamily protein	intron, 5utr		Tolerated	*qHvDRR-FLS-15*	FLL	4
HORVU.MOREX.r3.4HG0338990	E3 ubiquitin-protein ligase FANCL	5utr		Tolerated	*qHvDRR-FLS-15*	FLL	4
HORVU.MOREX.r3.4HG0339090	Pol polyprotein			Tolerated, Deleterious	*qHvDRR-FLS-15*	FLL	4
HORVU.MOREX.r3.4HG0339120	homeobox-1	5utr, intron, exon		Deleterious	*qHvDRR-FLS-15*	FLL	4
HORVU.MOREX.r3.4HG0339140	Holliday junction ATP-dependent DNA helicase RuvA	5utr	5utr	Tolerated	*qHvDRR-FLS-15*	FLL	4
HORVU.MOREX.r3.4HG0339160	1-aminocyclopropane-1-carboxylate synthase 1	5utr		Tolerated	*qHvDRR-FLS-15*	FLL	4
HORVU.MOREX.r3.4HG0339180	F-box-like protein			Tolerated	*qHvDRR-FLS-15*	FLL	4
HORVU.MOREX.r3.4HG0339190	GTPase obg	5utr		Tolerated	*qHvDRR-FLS-15*	FLL	4
HORVU.MOREX.r3.4HG0339220	Pentatricopeptide repeat-containing protein			Tolerated, Deleterious	*qHvDRR-FLS-15*	FLL	4
HORVU.MOREX.r3.4HG0339230	F-box protein			Tolerated, Deleterious	*qHvDRR-FLS-15*	FLL	4
HORVU.MOREX.r3.4HG0339240	BED zinc finger,hAT family dimerization domain			Tolerated, Deleterious	*qHvDRR-FLS-15*	FLL	4
HORVU.MOREX.r3.4HG0339280	DNA binding protein			Tolerated	*qHvDRR-FLS-15*	FLL	4
HORVU.MOREX.r3.4HG0339290	ATP dependent RNA helicase			Tolerated, Deleterious	*qHvDRR-FLS-15*	FLL	4
HORVU.MOREX.r3.4HG0339300	Basic helix-loop-helix transcription factor	5utr		Tolerated	*qHvDRR-FLS-15*	FLL	4
HORVU.MOREX.r3.4HG0339340	ethylene-dependent gravitropism-deficient and yellow-green-like 2			Tolerated, Deleterious	*qHvDRR-FLS-15*	FLL	4
HORVU.MOREX.r3.4HG0339350	transmembrane protein	5utr		Tolerated, Deleterious	*qHvDRR-FLS-15*	FLL	4
HORVU.MOREX.r3.4HG0339390	Ribosomal RNA small subunit methyltransferase E	5utr		Tolerated, Deleterious	*qHvDRR-FLS-15*	FLL	4
HORVU.MOREX.r3.4HG0339420	RNA recognition motif (RRM)-containing protein			Tolerated, Deleterious	*qHvDRR-FLS-15*	FLL	4
HORVU.MOREX.r3.4HG0339430	Growth-regulating factor	5utr, intron		Tolerated, Deleterious	*qHvDRR-FLS-15*	FLL	4
HORVU.MOREX.r3.4HG0339440	Gag polyprotein			Tolerated, Deleterious	*qHvDRR-FLS-15*	FLL	4
HORVU.MOREX.r3.4HG0339550	Subtilisin-like protease	5utr, intron		Tolerated, Deleterious	*qHvDRR-FLS-15*	FLL	4
HORVU.MOREX.r3.4HG0339560	B3 domain-containing protein	5utr		Tolerated	*qHvDRR-FLS-15*	FLL	4
HORVU.MOREX.r3.4HG0339570	ACT domain containing protein, expressed	5utr, intron		Tolerated, Deleterious	*qHvDRR-FLS-15*	FLL	4
HORVU.MOREX.r3.4HG0339580	BSD domain containing protein			Tolerated, Deleterious	*qHvDRR-FLS-15*	FLL	4
HORVU.MOREX.r3.4HG0339590	Ribosomal RNA small subunit methyltransferase F			Tolerated, Deleterious	*qHvDRR-FLS-15*	FLL	4
HORVU.MOREX.r3.4HG0339600	Lecithin-cholesterol acyltransferase-like 1			Tolerated	*qHvDRR-FLS-15*	FLL	4
HORVU.MOREX.r3.4HG0339610	Serine carboxypeptidase family protein, expressed			Tolerated	*qHvDRR-FLS-15*	FLL	4
HORVU.MOREX.r3.4HG0339620	Serine carboxypeptidase family protein, expressed			Tolerated, Deleterious	*qHvDRR-FLS-15*	FLL	4
HORVU.MOREX.r3.4HG0339640	Calcium-transporting ATPase			Tolerated	*qHvDRR-FLS-15*	FLL	4
HORVU.MOREX.r3.4HG0339720	Leishmanolysin-like peptidase			Tolerated	*qHvDRR-FLS-15*	FLL	4
HORVU.MOREX.r3.4HG0339730	Cathepsin B-like cysteine protease	5utr		Tolerated, Deleterious	*qHvDRR-FLS-15*	FLL	4
HORVU.MOREX.r3.4HG0339740	Cathepsin B-like cysteine protease	intron		Tolerated	*qHvDRR-FLS-15*	FLL	4
HORVU.MOREX.r3.4HG0339750	Cathepsin B-like cysteine protease	5utr, intron		Tolerated	*qHvDRR-FLS-15*	FLL	4
HORVU.MOREX.r3.4HG0339760	Glycosyltransferase		5utr	Tolerated, Deleterious	*qHvDRR-FLS-15*	FLL	4
HORVU.MOREX.r3.4HG0339780	Glycosyltransferase		5utr	Tolerated, Deleterious	*qHvDRR-FLS-15*	FLL	4
HORVU.MOREX.r3.4HG0339790	4-hydroxy-3-methylbut-2-enyl diphosphate reductase	5utr			*qHvDRR-FLS-15*	FLL	4
HORVU.MOREX.r3.4HG0339800	DNA double-strand break repair rad50 ATPase		5utr		*qHvDRR-FLS-15*	FLL	4
HORVU.MOREX.r3.4HG0339810	Homeobox protein bel1-like protein	intron		Tolerated, Deleterious	*qHvDRR-FLS-15*	FLL	4
HORVU.MOREX.r3.4HG0339820	Sugar transporter family protein	5utr, exon	5utr	Tolerated	*qHvDRR-FLS-15*	FLL	4
HORVU.MOREX.r3.4HG0339860	Pathogenesis-related protein 1	5utr	5utr	Tolerated	*qHvDRR-FLS-15*	FLL	4
HORVU.MOREX.r3.4HG0339880	Zinc finger BED domain-containing protein DAYSLEEPER	intron, 5utr		Tolerated, Deleterious	*qHvDRR-FLS-15*	FLL	4
HORVU.MOREX.r3.4HG0339890	Pollen Ole e 1 allergen and extensin family protein, putative	intron, 5utr		Tolerated, Deleterious	*qHvDRR-FLS-15*	FLL	4
HORVU.MOREX.r3.4HG0339900	Zinc finger BED domain-containing protein DAYSLEEPER	intron, 5utr	5utr	Tolerated	*qHvDRR-FLS-15*	FLL	4
HORVU.MOREX.r3.4HG0339920	GRF1-interacting factor-like protein	exon, 5utr, intron		Deleterious	*qHvDRR-FLS-15*	FLL	4
HORVU.MOREX.r3.4HG0339930	Endoplasmic reticulum oxidoreductin-1	intron	5utr		*qHvDRR-FLS-15*	FLL	4
HORVU.MOREX.r3.4HG0339940	protein kinase family protein			Tolerated, Deleterious	*qHvDRR-FLS-15*	FLL	4
HORVU.MOREX.r3.4HG0339950	Dehydrin	5utr, exon	exon	Tolerated, Deleterious	*qHvDRR-FLS-15*	FLL	4
HORVU.MOREX.r3.4HG0339960	serine-type endopeptidase inhibitor			Tolerated	*qHvDRR-FLS-15*	FLL	4
HORVU.MOREX.r3.4HG0339970	serine-type endopeptidase inhibitor			Tolerated	*qHvDRR-FLS-15*	FLL	4
HORVU.MOREX.r3.4HG0339980	Outer membrane protein class 4			Tolerated	*qHvDRR-FLS-15*	FLL	4
HORVU.MOREX.r3.4HG0340000	CAI-1 autoinducer sensor kinase/phosphatase cqsS isoform 1			Tolerated	*qHvDRR-FLS-15*	FLL	4
HORVU.MOREX.r3.4HG0340020	Myb/SANT-like DNA-binding domain protein			Tolerated, Deleterious	*qHvDRR-FLS-15*	FLL	4
HORVU.MOREX.r3.4HG0340030	beta-fructofuranosidase 5			Tolerated	*qHvDRR-FLS-15*	FLL	4
HORVU.MOREX.r3.4HG0340040	BnaCnng07380D protein		5utr	Tolerated	*qHvDRR-FLS-15*	FLL	4
HORVU.MOREX.r3.4HG0340050	Filament-like plant protein			Tolerated, Deleterious	*qHvDRR-FLS-15*	FLL	4
HORVU.MOREX.r3.4HG0340070	Mitochondrial carrier protein, expressed	5utr		Tolerated	*qHvDRR-FLS-15*	FLL	4
HORVU.MOREX.r3.4HG0340080	ACT domain-containing protein ACR4			Tolerated, Deleterious	*qHvDRR-FLS-15*	FLL	4

HORVU.MOREX.r3.4HG0340090	GATA transcription factor		5utr	Tolerated	*qHvDRR-FLS-15*	FLL	4
HORVU.MOREX.r3.4HG0340100	XH/XS domain-containing family protein			Tolerated, Deleterious	*qHvDRR-FLS-15*	FLL	4
HORVU.MOREX.r3.4HG0340140	F-box family protein	5utr	5utr	Tolerated, Deleterious	*qHvDRR-FLS-15*	FLL	4
HORVU.MOREX.r3.4HG0340150	F-box family protein	5utr		Tolerated, Deleterious	*qHvDRR-FLS-15*	FLL	4
HORVU.MOREX.r3.4HG0340180	Transducin/WD-like repeat-protein			Tolerated	*qHvDRR-FLS-15*	FLL	4
HORVU.MOREX.r3.4HG0340210	Pentatricopeptide repeat-containing protein			Tolerated, Deleterious	*qHvDRR-FLS-15*	FLL	4
HORVU.MOREX.r3.4HG0340220	Eukaryotic translation initiation factor 3 subunit G	5utr, intron		Tolerated, Deleterious	*qHvDRR-FLS-15*	FLL	4
HORVU.MOREX.r3.4HG0340230	Alba DNA/RNA-binding protein	5utr, intron			*qHvDRR-FLS-15*	FLL	4
HORVU.MOREX.r3.4HG0340240	Leucine-rich repeat receptor-like protein kinase family			Tolerated, Deleterious	*qHvDRR-FLS-15*	FLL	4
HORVU.MOREX.r3.4HG0340250	Cell wall invertase	5utr, exon	5utr	Tolerated, Deleterious	*qHvDRR-FLS-15*	FLL	4
HORVU.MOREX.r3.4HG0340300	transmembrane protein, putative (DUF247)	5utr	5utr		*qHvDRR-FLS-15*	FLL	4
HORVU.MOREX.r3.4HG0340330	Protein ZINC INDUCED FACILITATOR-LIKE 1	5utr, intron, exon	exon	Tolerated, Deleterious	*qHvDRR-FLS-15*	FLL	4
HORVU.MOREX.r3.4HG0340350	Glycerol-3-phosphate acyltransferase	5utr		Tolerated, Deleterious	*qHvDRR-FLS-15*	FLL	4
HORVU.MOREX.r3.4HG0340360	Pentatricopeptide repeat-containing protein	5utr		Tolerated, Deleterious	*qHvDRR-FLS-15*	FLL	4
HORVU.MOREX.r3.4HG0340370	Endoglucanase			Tolerated	*qHvDRR-FLS-15*	FLL	4
HORVU.MOREX.r3.4HG0412430	Sugar transporter, putative	5utr	5utr		*qHvDRR-FLS-17*	FLL, FLW	4
HORVU.MOREX.r3.4HG0412450	E2 ubiquitin-conjugating-like enzyme	5utr			*qHvDRR-FLS-17*	FLL, FLW	4
HORVU.MOREX.r3.4HG0412460	MADS-box transcription factor	5utr/ intron/ exon	intron	Tolerated/ Deleterious	*qHvDRR-FLS-17*	FLL, FLW	4
HORVU.MOREX.r3.4HG0412480	Glutathione S-transferase T3	5utr		Tolerated/ Deleterious	*qHvDRR-FLS-17*	FLL, FLW	4
HORVU.MOREX.r3.4HG0412490	2-oxoglutarate (2OG) and Fe(II)-dependent oxygese superfamily protein	exon		Tolerated/ Deleterious	*qHvDRR-FLS-17*	FLL, FLW	4
HORVU.MOREX.r3.4HG0412500	ArfGap/RecO-like zinc finger domain-containing protein	intron		Tolerated	*qHvDRR-FLS-17*	FLL, FLW	4
HORVU.MOREX.r3.4HG0412540	GRF zinc finger family protein	5utr	5utr	Tolerated/ Deleterious	*qHvDRR-FLS-17*	FLL, FLW	4
HORVU.MOREX.r3.4HG0412550	Amino acid dehydrogese family protein	5utr		Deleterious	*qHvDRR-FLS-17*	FLL, FLW	4
HORVU.MOREX.r3.4HG0412560	Basic helix-loop-helix transcription factor	5utr	5utr	Tolerated	*qHvDRR-FLS-17*	FLL, FLW	4
HORVU.MOREX.r3.4HG0412570	kinase family protein	exon/ 5utr/ intron	5utr	Tolerated/ Deleterious	*qHvDRR-FLS-17*	FLL, FLW	4
HORVU.MOREX.r3.4HG0412600	Endoribonuclease Dicer-like protein 3	5utr/ intron		Tolerated/ Deleterious	*qHvDRR-FLS-17*	FLL, FLW	4
HORVU.MOREX.r3.5HG0510630	Receptor-like protein kinase	5utr	5utr	Tolerated/ Deleterious	*qHvDRR-FLS-19*	FLL, FLW	5
HORVU.MOREX.r3.5HG0510640	Beta-glucosidase	5utr/ intron/ exon	intron/ 5utr	Tolerated/ Deleterious	*qHvDRR-FLS-19*	FLL, FLW	5
HORVU.MOREX.r3.5HG0510650	Beta-glucosidase	5utr/ intron/ exon	5utr/ exon	Tolerated/ Deleterious	*qHvDRR-FLS-19*	FLL, FLW	5
HORVU.MOREX.r3.5HG0510670	D topoisomerase	5utr	5utr	Tolerated/ Deleterious	*qHvDRR-FLS-19*	FLL, FLW	5
HORVU.MOREX.r3.5HG0510690	B3 domain-containing protein	5utr		Tolerated/ Deleterious	*qHvDRR-FLS-19*	FLL, FLW	5
HORVU.MOREX.r3.5HG0510700	Beta-glucosidase	5utr/ exon/ intron	intron/ 5utr/ exon	Tolerated/ Deleterious	*qHvDRR-FLS-19*	FLL, FLW	5
HORVU.MOREX.r3.5HG0510720	R-directed D polymerase (Reverse transcriptase)	5utr		Tolerated/ Deleterious	*qHvDRR-FLS-19*	FLL, FLW	5
HORVU.MOREX.r3.5HG0510760	Protein kinase	5utr/ intron/ exon	5utr	Tolerated/ Deleterious	*qHvDRR-FLS-19*	FLL, FLW	5
HORVU.MOREX.r3.5HG0510770	Protein-lysine N-methyltransferase			Tolerated/ Deleterious	*qHvDRR-FLS-19*	FLL, FLW	5
HORVU.MOREX.r3.5HG0510780	Universal stress protein family protein			Tolerated	*qHvDRR-FLS-19*	FLL, FLW	5
HORVU.MOREX.r3.5HG0510820	Universal stress protein family protein	intron/ 5utr	5utr	Tolerated	*qHvDRR-FLS-19*	FLL, FLW	5
HORVU.MOREX.r3.5HG0510830	Tetratricopeptide repeat protein	5utr	5utr	Tolerated/ Deleterious	*qHvDRR-FLS-19*	FLL, FLW	5
HORVU.MOREX.r3.5HG0510840	U3 small nucleolar R-associated protein 18-like protein	5utr	5utr	Tolerated/ Deleterious	*qHvDRR-FLS-19*	FLL, FLW	5
HORVU.MOREX.r3.5HG0510850	LURP-one-like protein	5utr/ intron		Tolerated/ Deleterious	*qHvDRR-FLS-19*	FLL, FLW	5
HORVU.MOREX.r3.5HG0510860	Kinesin-like protein	5utr/ intron/ exon	5utr	Tolerated/ Deleterious	*qHvDRR-FLS-19*	FLL, FLW	5
HORVU.MOREX.r3.5HG0510870	Strictosidine synthase	intron/ exon/ 5utr	intron/ 5utr	Tolerated/ Deleterious	*qHvDRR-FLS-19*	FLL, FLW	5
HORVU.MOREX.r3.5HG0510920	Transcriptiol adapter ADA2	5utr/ intron		Tolerated	*qHvDRR-FLS-19*	FLL, FLW	5
HORVU.MOREX.r3.5HG0510930	ATPase alpha subunit	5utr	5utr/ intron	Tolerated/ Deleterious	*qHvDRR-FLS-19*	FLL, FLW	5
HORVU.MOREX.r3.5HG0510940	HMG-Y-related protein A	exon/ 5utr	5utr	Tolerated	*qHvDRR-FLS-19*	FLL, FLW	5
HORVU.MOREX.r3.5HG0510950	Glucan endo-1,3-beta-glucosidase-like protein	5utr/ intron	5utr	Tolerated/ Deleterious	*qHvDRR-FLS-19*	FLL, FLW	5
HORVU.MOREX.r3.5HG0510960	CDO504	5utr/ intron	5utr	Tolerated	*qHvDRR-FLS-19*	FLL, FLW	5
HORVU.MOREX.r3.5HG0510970	Glucan endo-1,3-beta-glucosidase 1			Tolerated	*qHvDRR-FLS-19*	FLL, FLW	5
HORVU.MOREX.r3.5HG0510980	Protein TORDO 1			Tolerated/ Deleterious	*qHvDRR-FLS-19*	FLL, FLW	5
HORVU.MOREX.r3.5HG0510990	oligopeptide transporter	5utr	5utr	Tolerated/ Deleterious	*qHvDRR-FLS-19*	FLL, FLW	5
HORVU.MOREX.r3.5HG0511070	Peroxisome proliferator-activated receptor gamma coactivator 1-alpha	5utr		Tolerated	*qHvDRR-FLS-19*	FLL, FLW	5
HORVU.MOREX.r3.5HG0511090	Phytochrome	exon/ 5utr	5utr	Tolerated	*qHvDRR-FLS-19*	FLL, FLW	5
HORVU.MOREX.r3.5HG0511100	D topoisomerase 6 subunit A			Tolerated/ Deleterious	*qHvDRR-FLS-19*	FLL, FLW	5
HORVU.MOREX.r3.5HG0511110	Potassium channel	5utr		Deleterious	*qHvDRR-FLS-19*	FLL, FLW	5
HORVU.MOREX.r3.5HG0511130	Chaperone DJ-domain containing protein	5utr/ intron		Tolerated	*qHvDRR-FLS-19*	FLL, FLW	5
HORVU.MOREX.r3.5HG0511140	Cysteine protease	5utr/ intron	5utr	Tolerated	*qHvDRR-FLS-19*	FLL, FLW	5
HORVU.MOREX.r3.5HG0511150	Potassium channel	5utr	5utr	Deleterious	*qHvDRR-FLS-19*	FLL, FLW	5
HORVU.MOREX.r3.5HG0511200	Transposase			Tolerated/ Deleterious	*qHvDRR-FLS-19*	FLL, FLW	5
HORVU.MOREX.r3.5HG0511210	MADS box transcription factor	intron/ 5utr/ exon	5utr	Tolerated/ Deleterious	*qHvDRR-FLS-19*	FLL, FLW	5
HORVU.MOREX.r3.5HG0511250	MADS-box transcription factor	intron/ 5utr/ exon		Tolerated/ Deleterious	*qHvDRR-FLS-19*	FLL, FLW	5
HORVU.MOREX.r3.5HG0511290	protein kinase family protein	5utr	5utr	Tolerated/ Deleterious	*qHvDRR-FLS-19*	FLL, FLW	5
HORVU.MOREX.r3.5HG0511330	COBRA-like protein	5utr/ exon/ intron		Tolerated/ Deleterious	*qHvDRR-FLS-19*	FLL, FLW	5
HORVU.MOREX.r3.5HG0511400	COBRA protein	5utr	5utr	Tolerated/ Deleterious	*qHvDRR-FLS-19*	FLL, FLW	5
HORVU.MOREX.r3.5HG0511420	Mitochondrial carrier family protein	intron/ 5utr	intron	Tolerated	*qHvDRR-FLS-19*	FLL, FLW	5
HORVU.MOREX.r3.5HG0511430	WD repeat-containing protein	5utr/ intron	5utr/ intron/ exon	Tolerated/ Deleterious	*qHvDRR-FLS-19*	FLL, FLW	5
HORVU.MOREX.r3.5HG0511440	kinase family protein	5utr/ intron	5utr	Tolerated/ Deleterious	*qHvDRR-FLS-19*	FLL, FLW	5
HORVU.MOREX.r3.5HG0511450	ABC transporter B family protein	exon/ intron		Tolerated	*qHvDRR-FLS-19*	FLL, FLW	5
HORVU.MOREX.r3.5HG0511460	ABC transporter B family protein	intron		Tolerated/ Deleterious	*qHvDRR-FLS-19*	FLL, FLW	5
HORVU.MOREX.r3.5HG0511470	Haloacid dehalogese-like hydrolase (HAD) superfamily protein	5utr/ exon/ intron	5utr	Tolerated/ Deleterious	*qHvDRR-FLS-19*	FLL, FLW	5
HORVU.MOREX.r3.5HG0511490	Receptor-like kinase	5utr/ intron/ exon	5utr	Tolerated/ Deleterious	*qHvDRR-FLS-19*	FLL, FLW	5
HORVU.MOREX.r3.5HG0511500	Glucan endo-1,3-beta-glucosidase 3	5utr/ intron/ exon		Tolerated	*qHvDRR-FLS-19*	FLL, FLW	5
HORVU.MOREX.r3.5HG0511510	Transmembrane protein adipocyte-associated 1	5utr/ intron	5utr	Tolerated	*qHvDRR-FLS-19*	FLL, FLW	5
HORVU.MOREX.r3.5HG0511520	R polymerase-associated protein LEO1	intron/ 5utr/ exon	intron	Tolerated/ Deleterious	*qHvDRR-FLS-19*	FLL, FLW	5
HORVU.MOREX.r3.5HG0511590	Mitotic-spindle organizing protein 1B	5utr		Tolerated/ Deleterious	*qHvDRR-FLS-19*	FLL, FLW	5
HORVU.MOREX.r3.5HG0511600	Dentin sialophosphoprotein-like protein, putative	5utr/ intron	5utr	Tolerated/ Deleterious	*qHvDRR-FLS-19*	FLL, FLW	5
HORVU.MOREX.r3.5HG0511630	UDP-glycosyltransferase	5utr	5utr	Tolerated/ Deleterious	*qHvDRR-FLS-19*	FLL, FLW	5
HORVU.MOREX.r3.5HG0511640	UDP-glycosyltransferase	intron/ 5utr	5utr/ intron	Tolerated/ Deleterious	*qHvDRR-FLS-19*	FLL, FLW	5
HORVU.MOREX.r3.5HG0511660	UDP-glycosyltransferase	5utr	5utr	Tolerated/ Deleterious	*qHvDRR-FLS-19*	FLL, FLW	5
HORVU.MOREX.r3.5HG0511670	UDP-glycosyltransferase	5utr/ exon		Tolerated/ Deleterious	*qHvDRR-FLS-19*	FLL, FLW	5
HORVU.MOREX.r3.5HG0511680	UDP-glycosyltransferase	5utr	5utr	Tolerated/ Deleterious	*qHvDRR-FLS-19*	FLL, FLW	5
HORVU.MOREX.r3.5HG0511690	carboxyl-termil peptidase, putative (DUF239)	5utr/ exon		Tolerated/ Deleterious	*qHvDRR-FLS-19*	FLL, FLW	5
HORVU.MOREX.r3.5HG0511700	UDP-glycosyltransferase	5utr		Tolerated/ Deleterious	*qHvDRR-FLS-19*	FLL, FLW	5
HORVU.MOREX.r3.5HG0511710	UDP-glycosyltransferase	5utr/ intron/ exon	exon/ 5utr	Tolerated/ Deleterious	*qHvDRR-FLS-19*	FLL, FLW	5
HORVU.MOREX.r3.5HG0511720	UDP-glycosyltransferase			Tolerated/ Deleterious	*qHvDRR-FLS-19*	FLL, FLW	5
HORVU.MOREX.r3.5HG0511730	Phosphate translocator-related family protein	5utr		Tolerated/ Deleterious	*qHvDRR-FLS-19*	FLL, FLW	5
HORVU.MOREX.r3.5HG0511740	UDP-glycosyltransferase			Tolerated	*qHvDRR-FLS-19*	FLL, FLW	5
HORVU.MOREX.r3.5HG0511750	UDP-glycosyltransferase			Tolerated	*qHvDRR-FLS-19*	FLL, FLW	5
HORVU.MOREX.r3.5HG0511770	UDP-glucose 6-dehydrogese	5utr			*qHvDRR-FLS-19*	FLL, FLW	5
HORVU.MOREX.r3.5HG0511780	C (No Apical Meristem) domain transcriptiol regulator superfamily protein	5utr		Deleterious	*qHvDRR-FLS-19*	FLL, FLW	5
HORVU.MOREX.r3.5HG0511790	WRKY transcription factor	5utr/ intron/ exon	intron	Tolerated	*qHvDRR-FLS-19*	FLL, FLW	5
HORVU.MOREX.r3.5HG0511800	Alpha-1,4 glucan phosphorylase	intron/ 5utr		Tolerated/ Deleterious	*qHvDRR-FLS-19*	FLL, FLW	5
HORVU.MOREX.r3.5HG0511820	Cyclic nucleotide-gated channel	intron/ 5utr			*qHvDRR-FLS-19*	FLL, FLW	5
HORVU.MOREX.r3.5HG0511830	Ankyrin repeat family protein	5utr/ intron/ exon		Tolerated	*qHvDRR-FLS-19*	FLL, FLW	5
HORVU.MOREX.r3.5HG0511860	Blue copper protein	5utr		Tolerated	*qHvDRR-FLS-19*	FLL, FLW	5
HORVU.MOREX.r3.5HG0511890	Serine/threonine phosphatase-like protein	intron/ exon		Tolerated/ Deleterious	*qHvDRR-FLS-19*	FLL, FLW	5
HORVU.MOREX.r3.5HG0511920	Blue copper protein	5utr	5utr	Tolerated/ Deleterious	*qHvDRR-FLS-19*	FLL, FLW	5
HORVU.MOREX.r3.5HG0511930	Ring finger protein, putative	5utr	5utr		*qHvDRR-FLS-19*	FLL, FLW	5
HORVU.MOREX.r3.5HG0511950	Kinesin-like protein	5utr/ intron	5utr	Tolerated/ Deleterious	*qHvDRR-FLS-19*	FLL, FLW	5
HORVU.MOREX.r3.5HG0511960	Disease resistance protein RPM1	intron/ 5utr	5utr	Tolerated/ Deleterious	*qHvDRR-FLS-19*	FLL, FLW	5
HORVU.MOREX.r3.5HG0511970	Disease resistance protein (TIR-NBS-LRR class) family	5utr/ intron	5utr		*qHvDRR-FLS-19*	FLL, FLW	5
HORVU.MOREX.r3.5HG0511980	Leucine-rich repeat (LRR) family protein			Deleterious	*qHvDRR-FLS-19*	FLL, FLW	5
HORVU.MOREX.r3.5HG0511990	cell cycle checkpoint control protein family	5utr		Tolerated/ Deleterious	*qHvDRR-FLS-19*	FLL, FLW	5
HORVU.MOREX.r3.5HG0512000	Disease resistance protein	5utr/ exon/ intron	5utr	Tolerated/ Deleterious	*qHvDRR-FLS-19*	FLL, FLW	5
HORVU.MOREX.r3.5HG0512090	Protein FAR1-RELATED SEQUENCE 5	5utr	5utr/ exon	Tolerated	*qHvDRR-FLS-19*	FLL, FLW	5
HORVU.MOREX.r3.5HG0512150	Protein kinase family protein, putative, expressed	5utr/ intron		Tolerated/ Deleterious	*qHvDRR-FLS-19*	FLL, FLW	5
HORVU.MOREX.r3.5HG0517500	Ubiquitin-conjugating enzyme (E2)	5utr			*qHvDRR-FLS-20*	FLL	5
HORVU.MOREX.r3.5HG0517520	Purine permease-like protein			Tolerated/ Deleterious	*qHvDRR-FLS-20*	FLL	5

HORVU.MOREX.r3.5HG0517590	Peptidase M50 family protein	intron/ exon/ 5utr	intron	Tolerated	*qHvDRR-FLS-20*	FLL	5
HORVU.MOREX.r3.5HG0517600	BTB-POZ and MATH domain protein			Tolerated	*qHvDRR-FLS-20*	FLL	5
HORVU.MOREX.r3.5HG0517610	Holliday junction ATP-dependent D helicase RuvB	intron/ exon/ 5utr			*qHvDRR-FLS-20*	FLL	5
HORVU.MOREX.r3.5HG0517630	Zinc finger A20 and AN1 domain stress-associated protein	exon/ 5utr/ intron	5utr	Tolerated/ Deleterious	*qHvDRR-FLS-20*	FLL	5
HORVU.MOREX.r3.5HG0517640	Glucan endo-1,3-beta-glucosidase, putative	5utr		Tolerated	*qHvDRR-FLS-20*	FLL	5
HORVU.MOREX.r3.5HG0517650	egg cell-secreted-like protein (DUF1278)	5utr	5utr	Tolerated/ Deleterious	*qHvDRR-FLS-20*	FLL	5
HORVU.MOREX.r3.5HG0517660	Blue copper protein			Tolerated/ Deleterious	*qHvDRR-FLS-20*	FLL	5
HORVU.MOREX.r3.5HG0517670	Sec14p-like phosphatidylinositol transfer family protein	5utr			*qHvDRR-FLS-20*	FLL	5
HORVU.MOREX.r3.5HG0517710	Blue copper protein	5utr		Tolerated	*qHvDRR-FLS-20*	FLL	5
HORVU.MOREX.r3.5HG0517730	Blue copper protein			Tolerated/ Deleterious	*qHvDRR-FLS-20*	FLL	5
HORVU.MOREX.r3.5HG0517740	Peroxidase	5utr	5utr	Tolerated/ Deleterious	*qHvDRR-FLS-20*	FLL	5
HORVU.MOREX.r3.5HG0517760	Zinc finger A20 and AN1 domain-containing stress-associated protein	5utr	5utr	Tolerated/ Deleterious	*qHvDRR-FLS-20*	FLL	5
HORVU.MOREX.r3.5HG0517770	Blue copper protein	5utr		Tolerated/ Deleterious	*qHvDRR-FLS-20*	FLL	5
HORVU.MOREX.r3.5HG0517790	Evolutiorily conserved C-termil region 2	5utr		Tolerated/ Deleterious	*qHvDRR-FLS-20*	FLL	5
HORVU.MOREX.r3.5HG0517800	evolutiorily conserved C-termil region 2	5utr		Tolerated/ Deleterious	*qHvDRR-FLS-20*	FLL	5
HORVU.MOREX.r3.5HG0517840	Eukaryotic translation initiation factor 3 subunit D			Deleterious	*qHvDRR-FLS-20*	FLL	5
HORVU.MOREX.r3.5HG0517850	F-box family protein			Tolerated/ Deleterious	*qHvDRR-FLS-20*	FLL	5
HORVU.MOREX.r3.5HG0517890	F-box domain containing protein, expressed			Tolerated/ Deleterious	*qHvDRR-FLS-20*	FLL	5
HORVU.MOREX.r3.5HG0517910	kinase family protein	intron/ 5utr	intron	Tolerated/ Deleterious	*qHvDRR-FLS-20*	FLL	5
HORVU.MOREX.r3.5HG0517920	Serine/threonine-protein kinase	5utr		Tolerated/ Deleterious	*qHvDRR-FLS-20*	FLL	5
HORVU.MOREX.r3.5HG0517940	Type I inositol-1,4,5-trisphosphate 5-phosphatase CVP2	5utr/ exon/ intron		Tolerated/ Deleterious	*qHvDRR-FLS-20*	FLL	5
HORVU.MOREX.r3.5HG0517950	Globulin-1	5utr/ intron/ exon	5utr	Tolerated/ Deleterious	*qHvDRR-FLS-20*	FLL	5
HORVU.MOREX.r3.5HG0517960	Proteasome subunit beta type	5utr/ intron	5utr	Tolerated/ Deleterious	*qHvDRR-FLS-20*	FLL	5
HORVU.MOREX.r3.5HG0517990	Ripening related protein family			Tolerated/ Deleterious	*qHvDRR-FLS-20*	FLL	5
HORVU.MOREX.r3.5HG0518000	Glutathione S-transferase	5utr/ intron	exon	Tolerated/ Deleterious	*qHvDRR-FLS-20*	FLL	5
HORVU.MOREX.r3.5HG0518010	Lipid transfer protein	5utr	5utr	Tolerated/ Deleterious	*qHvDRR-FLS-20*	FLL	5
HORVU.MOREX.r3.5HG0518020	Lipid transfer protein	5utr		Tolerated/ Deleterious	*qHvDRR-FLS-20*	FLL	5
HORVU.MOREX.r3.5HG0518030	Lipid transfer protein	5utr		Tolerated/ Deleterious	*qHvDRR-FLS-20*	FLL	5
HORVU.MOREX.r3.5HG0518040	Lipid transfer protein	5utr/ intron/ exon	5utr	Tolerated/ Deleterious	*qHvDRR-FLS-20*	FLL	5
HORVU.MOREX.r3.5HG0518060	Glycosyltransferase	5utr	5utr	Tolerated/ Deleterious	*qHvDRR-FLS-20*	FLL	5
HORVU.MOREX.r3.5HG0518070	Glycosyltransferase	5utr	5utr	Tolerated/ Deleterious	*qHvDRR-FLS-20*	FLL	5
HORVU.MOREX.r3.5HG0518090	Acetyl-coenzyme A carboxylase carboxyl transferase subunit beta			Tolerated/ Deleterious	*qHvDRR-FLS-20*	FLL	5
HORVU.MOREX.r3.5HG0518100	Serine/threonine protein phosphatase 7 long form isogeny			Tolerated/ Deleterious	*qHvDRR-FLS-20*	FLL	5
HORVU.MOREX.r3.5HG0518110	Protease inhibitor/seed storage/lipid transfer family protein	5utr	5utr	Tolerated	*qHvDRR-FLS-20*	FLL	5
HORVU.MOREX.r3.5HG0518120	RAPT-1			Deleterious	*qHvDRR-FLS-20*	FLL	5
HORVU.MOREX.r3.5HG0518130	Acetyltransferase, GT family protein, expressed	5utr		Tolerated/ Deleterious	*qHvDRR-FLS-20*	FLL	5
HORVU.MOREX.r3.5HG0518140	Acetyltransferase, GT family protein, expressed	5utr/ exon	5utr	Tolerated/ Deleterious	*qHvDRR-FLS-20*	FLL	5
HORVU.MOREX.r3.5HG0518150	Glutamate dehydrogese	5utr	5utr	Tolerated/ Deleterious	*qHvDRR-FLS-20*	FLL	5
HORVU.MOREX.r3.5HG0518190	Cyclin delta-3, putative	5utr	intron	Tolerated/ Deleterious	*qHvDRR-FLS-20*	FLL	5
HORVU.MOREX.r3.5HG0518200	Receptor lectin kinase			Tolerated/ Deleterious	*qHvDRR-FLS-20*	FLL	5
HORVU.MOREX.r3.5HG0518210	Receptor lectin kinase	5utr	5utr	Tolerated/ Deleterious	*qHvDRR-FLS-20*	FLL	5
HORVU.MOREX.r3.5HG0518220	B3 domain-containing protein	5utr/ exon/ intron		Tolerated/ Deleterious	*qHvDRR-FLS-20*	FLL	5
HORVU.MOREX.r3.5HG0518240	5'-3' exoribonuclease, putative, expressed	intron/ 5utr		Tolerated/ Deleterious	*qHvDRR-FLS-20*	FLL	5
HORVU.MOREX.r3.5HG0518250	Protein FRIGIDA			Tolerated/ Deleterious	*qHvDRR-FLS-20*	FLL	5
HORVU.MOREX.r3.5HG0518270	BTB/POZ domain containing protein			Tolerated/ Deleterious	*qHvDRR-FLS-20*	FLL	5
HORVU.MOREX.r3.5HG0518280	BTB/POZ domain containing protein	5utr	5utr	Tolerated	*qHvDRR-FLS-20*	FLL	5
HORVU.MOREX.r3.5HG0518330	Protein phosphatase 2C family protein	5utr	5utr	Tolerated/ Deleterious	*qHvDRR-FLS-20*	FLL	5
HORVU.MOREX.r3.5HG0518340	Myosin heavy chain-related protein, putative	5utr	5utr	Tolerated/ Deleterious	*qHvDRR-FLS-20*	FLL	5
HORVU.MOREX.r3.5HG0518350	BTB/POZ domain containing protein, expressed	5utr		Tolerated/ Deleterious	*qHvDRR-FLS-20*	FLL	5
HORVU.MOREX.r3.5HG0518360	BTB/POZ domain containing protein	5utr		Tolerated/ Deleterious	*qHvDRR-FLS-20*	FLL	5
HORVU.MOREX.r3.5HG0518370	BTB/POZ domain containing protein			Tolerated/ Deleterious	*qHvDRR-FLS-20*	FLL	5
HORVU.MOREX.r3.5HG0518380	BTB/POZ domain containing protein, expressed	5utr	5utr	Tolerated/ Deleterious	*qHvDRR-FLS-20*	FLL	5
HORVU.MOREX.r3.5HG0518390	BTB/POZ domain containing protein	5utr	5utr	Tolerated/ Deleterious	*qHvDRR-FLS-20*	FLL	5
HORVU.MOREX.r3.5HG0518410	BTB/POZ domain containing protein, expressed			Tolerated/ Deleterious	*qHvDRR-FLS-20*	FLL	5
HORVU.MOREX.r3.5HG0518430	ATP-dependent zinc metalloprotease FtsH 1			Tolerated/ Deleterious	*qHvDRR-FLS-20*	FLL	5
HORVU.MOREX.r3.5HG0518450	BTB/POZ domain containing protein, expressed	5utr	5utr	Tolerated	*qHvDRR-FLS-20*	FLL	5
HORVU.MOREX.r3.5HG0518460	BTB/POZ domain containing protein, expressed	5utr		Tolerated/ Deleterious	*qHvDRR-FLS-20*	FLL	5
HORVU.MOREX.r3.5HG0518500	BTB/POZ domain containing protein			Tolerated/ Deleterious	*qHvDRR-FLS-20*	FLL	5
HORVU.MOREX.r3.5HG0518510	Folate/biopterin transporter family protein, expressed	exon/ 5utr/ intron		Tolerated/ Deleterious	*qHvDRR-FLS-20*	FLL	5
HORVU.MOREX.r3.5HG0518530	Queuine tR-ribosyltransferase activity protein			Tolerated	*qHvDRR-FLS-20*	FLL	5
HORVU.MOREX.r3.5HG0518540	P-loop containing nucleoside triphosphate hydrolases superfamily protein	5utr		Tolerated/ Deleterious	*qHvDRR-FLS-20*	FLL	5
HORVU.MOREX.r3.5HG0518550	Pentatricopeptide repeat-containing protein	5utr	5utr	Tolerated/ Deleterious	*qHvDRR-FLS-20*	FLL	5
HORVU.MOREX.r3.5HG0518560	Leucine-rich repeat protein kinase family protein	5utr		Tolerated	*qHvDRR-FLS-20*	FLL	5
HORVU.MOREX.r3.5HG0518570	Pentatricopeptide repeat-containing protein	5utr		Tolerated/ Deleterious	*qHvDRR-FLS-20*	FLL	5
HORVU.MOREX.r3.5HG0518610	Histone H2A			Tolerated/ Deleterious	*qHvDRR-FLS-20*	FLL	5
HORVU.MOREX.r3.5HG0518640	Methionine S-methyltransferase	intron		Tolerated/ Deleterious	*qHvDRR-FLS-20*	FLL	5
HORVU.MOREX.r3.5HG0518660	Glycosyltransferase		5utr	Tolerated/ Deleterious	*qHvDRR-FLS-20*	FLL	5
HORVU.MOREX.r3.5HG0518700	Werner syndrome-like exonuclease	5utr	5utr	Tolerated/ Deleterious	*qHvDRR-FLS-20*	FLL	5
HORVU.MOREX.r3.5HG0518730	Zinc finger CCCH domain-containing protein 4	5utr		Tolerated/ Deleterious	*qHvDRR-FLS-20*	FLL	5
HORVU.MOREX.r3.5HG0518770	Ubiquitin carboxyl-termil hydrolase			Tolerated/ Deleterious	*qHvDRR-FLS-20*	FLL	5
HORVU.MOREX.r3.5HG0518810	Alpha/beta-Hydrolases superfamily protein, putative	5utr		Tolerated/ Deleterious	*qHvDRR-FLS-20*	FLL	5
HORVU.MOREX.r3.5HG0518840	Transcription initiation factor IIA subunit 1	5utr		Tolerated/ Deleterious	*qHvDRR-FLS-20*	FLL	5
HORVU.MOREX.r3.5HG0518870	Embryo defective 2735	5utr		Tolerated/ Deleterious	*qHvDRR-FLS-20*	FLL	5
HORVU.MOREX.r3.5HG0518880	B3 domain protein (DUF313)	5utr	5utr	Tolerated/ Deleterious	*qHvDRR-FLS-20*	FLL	5
HORVU.MOREX.r3.5HG0518890	R-directed D polymerase (reverse transcriptase)-related family protein	5utr		Tolerated/ Deleterious	*qHvDRR-FLS-20*	FLL	5
HORVU.MOREX.r3.5HG0518900	F-box domain containing protein	5utr	5utr	Tolerated/ Deleterious	*qHvDRR-FLS-20*	FLL	5
HORVU.MOREX.r3.5HG0518920	Kinesin-like protein	intron/ 5utr	5utr	Tolerated/ Deleterious	*qHvDRR-FLS-20*	FLL	5
HORVU.MOREX.r3.5HG0518960	PITH domain-containing protein 1	5utr		Tolerated/ Deleterious	*qHvDRR-FLS-20*	FLL	5
HORVU.MOREX.r3.5HG0518970	Bax inhibitor-1 family protein	5utr		Tolerated/ Deleterious	*qHvDRR-FLS-20*	FLL	5
HORVU.MOREX.r3.5HG0518980	Bax inhibitor-1 family protein	5utr	5utr		*qHvDRR-FLS-20*	FLL	5
HORVU.MOREX.r3.5HG0519000	Heat shock transcription factor	5utr/ exon/ intron		Tolerated	*qHvDRR-FLS-20*	FLL	5
HORVU.MOREX.r3.5HG0519010	Transmembrane protein 97, Putative			Tolerated	*qHvDRR-FLS-20*	FLL	5
HORVU.MOREX.r3.5HG0519020	F-box domain containing protein	intron/ 5utr/ exon		Tolerated/ Deleterious	*qHvDRR-FLS-20*	FLL	5
HORVU.MOREX.r3.5HG0519030	Transmembrane protein 97	5utr		Tolerated/ Deleterious	*qHvDRR-FLS-20*	FLL	5
HORVU.MOREX.r3.5HG0519040	Serine/arginine repetitive matrix protein 2, putative isoform 1	5utr		Tolerated	*qHvDRR-FLS-20*	FLL	5
HORVU.MOREX.r3.5HG0519050	B3 domain-containing protein	5utr/ intron	5utr	Tolerated/ Deleterious	*qHvDRR-FLS-20*	FLL	5
HORVU.MOREX.r3.5HG0519060	B3 domain-containing protein			Tolerated/ Deleterious	*qHvDRR-FLS-20*	FLL	5
HORVU.MOREX.r3.5HG0519070	Stem-specific protein TSJT1	5utr		Tolerated/ Deleterious	*qHvDRR-FLS-20*	FLL	5
HORVU.MOREX.r3.5HG0519080	Werner Syndrome-like exonuclease		5utr	Tolerated/ Deleterious	*qHvDRR-FLS-20*	FLL	5
HORVU.MOREX.r3.5HG0519110	Histone-lysine N-methyltransferase SUVR5	5utr	5utr	Tolerated/ Deleterious	*qHvDRR-FLS-20*	FLL	5
HORVU.MOREX.r3.5HG0519120	CASP-like protein	5utr/ exon/ intron		Tolerated/ Deleterious	*qHvDRR-FLS-20*	FLL	5
HORVU.MOREX.r3.5HG0519140	Protein EMSY	5utr/ exon/ intron	5utr	Tolerated	*qHvDRR-FLS-20*	FLL	5
HORVU.MOREX.r3.5HG0519200	DUF506 family protein	exon		Tolerated	*qHvDRR-FLS-20*	FLL	5
HORVU.MOREX.r3.5HG0519210	Werner Syndrome-like exonuclease	5utr		Tolerated/ Deleterious	*qHvDRR-FLS-20*	FLL	5
HORVU.MOREX.r3.5HG0519220	B3 domain-containing protein	5utr		Tolerated/ Deleterious	*qHvDRR-FLS-20*	FLL	5
HORVU.MOREX.r3.5HG0519230	U3 small nucleolar R-associated protein 18-like protein	exon/ 5utr	intron	Tolerated/ Deleterious	*qHvDRR-FLS-20*	FLL	5
HORVU.MOREX.r3.5HG0519240	PHD finger-containing protein			Tolerated/ Deleterious	*qHvDRR-FLS-20*	FLL	5
HORVU.MOREX.r3.5HG0519250	RING/U-box superfamily protein, putative	5utr	5utr	Tolerated/ Deleterious	*qHvDRR-FLS-20*	FLL	5
HORVU.MOREX.r3.5HG0519270	Pathogenesis-related protein 1			Tolerated	*qHvDRR-FLS-20*	FLL	5
HORVU.MOREX.r3.5HG0519330	Pathogenesis-related protein 1	5utr			*qHvDRR-FLS-20*	FLL	5
HORVU.MOREX.r3.5HG0519340	Pathogenesis-related protein 1	5utr			*qHvDRR-FLS-20*	FLL	5
HORVU.MOREX.r3.5HG0519350	Receptor protein kinase, putative			Tolerated/ Deleterious	*qHvDRR-FLS-20*	FLL	5
HORVU.MOREX.r3.5HG0519390	HAT dimerisation domain-containing protein-like			Tolerated/ Deleterious	*qHvDRR-FLS-20*	FLL	5
HORVU.MOREX.r3.5HG0519400	Mannitol transporter, putative, expressed	5utr/ exon/ intron	5utr	Tolerated/ Deleterious	*qHvDRR-FLS-20*	FLL	5
HORVU.MOREX.r3.5HG0519410	Guanylate-binding family protein, putative, expressed	5utr/ exon/ intron	intron/ 5utr	Tolerated/ Deleterious	*qHvDRR-FLS-20*	FLL	5
HORVU.MOREX.r3.5HG0519420	Basic-leucine zipper (BZIP) transcription factor family	5utr	5utr	Tolerated	*qHvDRR-FLS-20*	FLL	5
HORVU.MOREX.r3.5HG0519470	BTB/POZ domain containing protein	5utr		Tolerated/ Deleterious	*qHvDRR-FLS-20*	FLL	5

HORVU.MOREX.r3.5HG0519480	Disease resistance protein			Tolerated/ Deleterious	*qHvDRR-FLS-20*	FLL	5
HORVU.MOREX.r3.5HG0519490	Tryptophan synthase alpha chain	5utr		Deleterious	*qHvDRR-FLS-20*	FLL	5
HORVU.MOREX.r3.5HG0519500	Tryptophan synthase alpha chain	5utr	5utr	Tolerated/ Deleterious	*qHvDRR-FLS-20*	FLL	5
HORVU.MOREX.r3.5HG0519510	Pseudouridine synthase	5utr	5utr	Tolerated/ Deleterious	*qHvDRR-FLS-20*	FLL	5
HORVU.MOREX.r3.5HG0519530	Tryptophan synthase alpha chain	exon/ 5utr/ intron		Tolerated/ Deleterious	*qHvDRR-FLS-20*	FLL	5
HORVU.MOREX.r3.5HG0519550	Endo-1,4-beta-xylase	5utr		Tolerated/ Deleterious	*qHvDRR-FLS-20*	FLL	5
HORVU.MOREX.r3.5HG0519560	cytochrome p450 78a9			Deleterious	*qHvDRR-FLS-20*	FLL	5
HORVU.MOREX.r3.5HG0519580	Endo-1,4-beta-xylase	5utr		Tolerated/ Deleterious	*qHvDRR-FLS-20*	FLL	5
HORVU.MOREX.r3.5HG0519630	Endo-1,4-beta-xylase	5utr	5utr	Tolerated/ Deleterious	*qHvDRR-FLS-20*	FLL	5
HORVU.MOREX.r3.5HG0519660	Basic helix-loop-helix transcription factor	5utr/ intron			*qHvDRR-FLS-20*	FLL	5
HORVU.MOREX.r3.5HG0519680	rR-processing protein efg1	intron/ 5utr/ exon	intron	Deleterious	*qHvDRR-FLS-20*	FLL	5
HORVU.MOREX.r3.5HG0519690	Auxin-responsive protein	5utr	5utr	Deleterious	*qHvDRR-FLS-20*	FLL	5
HORVU.MOREX.r3.5HG0519710	Leucine-rich repeat receptor-like protein kinase family protein	5utr	5utr	Tolerated/ Deleterious	*qHvDRR-FLS-20*	FLL	5
HORVU.MOREX.r3.5HG0519720	Lysine--tR ligase	intron/ 5utr		Tolerated	*qHvDRR-FLS-20*	FLL	5
HORVU.MOREX.r3.5HG0519730	D-binding protein SMUBP-2	intron		Tolerated/ Deleterious	*qHvDRR-FLS-20*	FLL	5
HORVU.MOREX.r3.5HG0519740	Purple acid phosphatase	5utr		Tolerated/ Deleterious	*qHvDRR-FLS-20*	FLL	5
HORVU.MOREX.r3.5HG0519750	Sucrose synthase	5utr/ intron		Tolerated/ Deleterious	*qHvDRR-FLS-20*	FLL	5
HORVU.MOREX.r3.5HG0519760	Eukaryotic translation initiation factor 3 subunit B			Tolerated/ Deleterious	*qHvDRR-FLS-20*	FLL	5
HORVU.MOREX.r3.5HG0519810	Diphosphomevalote decarboxylase	intron/ 5utr		Tolerated/ Deleterious	*qHvDRR-FLS-20*	FLL	5
HORVU.MOREX.r3.5HG0519820	E3 ubiquitin protein ligase DRIP2	exon/ 5utr/ intron	5utr	Tolerated	*qHvDRR-FLS-20*	FLL	5
HORVU.MOREX.r3.5HG0519890	Cytosine-specific methyltransferase			Tolerated/ Deleterious	*qHvDRR-FLS-20*	FLL	5
HORVU.MOREX.r3.5HG0519900	PRA1 family protein			Tolerated	*qHvDRR-FLS-20*	FLL	5
HORVU.MOREX.r3.5HG0519910	Expansin	5utr		Tolerated/ Deleterious	*qHvDRR-FLS-20*	FLL	5
HORVU.MOREX.r3.5HG0519920	WRKY transcription factor, putative	5utr/ intron/ exon		Tolerated	*qHvDRR-FLS-20*	FLL	5
HORVU.MOREX.r3.5HG0519940	Histone H1	5utr/ exon		Tolerated/ Deleterious	*qHvDRR-FLS-20*	FLL	5
HORVU.MOREX.r3.5HG0519970	Histone H1	5utr			*qHvDRR-FLS-20*	FLL	5
HORVU.MOREX.r3.5HG0520010	rR N-glycosidase	5utr	5utr	Tolerated/ Deleterious	*qHvDRR-FLS-20*	FLL	5
HORVU.MOREX.r3.5HG0520030	Ovomucoid	5utr			*qHvDRR-FLS-20*	FLL	5
HORVU.MOREX.r3.5HG0520060	2-oxoglutarate (2OG) and Fe(II)-dependent oxygese superfamily protein			Tolerated/ Deleterious	*qHvDRR-FLS-20*	FLL	5
HORVU.MOREX.r3.5HG0520080	kinase-like	5utr		Tolerated/ Deleterious	*qHvDRR-FLS-20*	FLL	5
HORVU.MOREX.r3.5HG0520090	Myosin-binding protein 1	exon/ 5utr/ intron		Tolerated	*qHvDRR-FLS-20*	FLL	5
HORVU.MOREX.r3.5HG0520100	TPX2 (Targeting protein for Xklp2) family protein	intron/ 5utr/ exon			*qHvDRR-FLS-20*	FLL	5
HORVU.MOREX.r3.5HG0520110	Histone H1	5utr/ intron/ exon	5utr	Tolerated/ Deleterious	*qHvDRR-FLS-20*	FLL	5
HORVU.MOREX.r3.5HG0520120	Receptor-like protein kinase	intron/ 5utr/ exon	5utr	Tolerated/ Deleterious	*qHvDRR-FLS-20*	FLL	5
HORVU.MOREX.r3.5HG0520130	Receptor-like protein kinase	5utr/ intron	5utr	Tolerated/ Deleterious	*qHvDRR-FLS-20*	FLL	5
HORVU.MOREX.r3.5HG0520190	Pleiotropic drug resistance ABC transporter	intron/ 5utr/ exon	intron/ exon/ 5utr	Tolerated/ Deleterious	*qHvDRR-FLS-20*	FLL	5
HORVU.MOREX.r3.5HG0520200	Succite dehydrogese assembly factor 2, mitochondrial	5utr/ exon/ intron	5utr	Tolerated	*qHvDRR-FLS-20*	FLL	5
HORVU.MOREX.r3.5HG0520210	Aminopeptidase	5utr		Deleterious	*qHvDRR-FLS-20*	FLL	5
HORVU.MOREX.r3.5HG0520220	DUF674 family protein			Tolerated/ Deleterious	*qHvDRR-FLS-20*	FLL	5
HORVU.MOREX.r3.5HG0520230	RING/U-box superfamily protein			Tolerated/ Deleterious	*qHvDRR-FLS-20*	FLL	5
HORVU.MOREX.r3.5HG0520240	Protein REVERSION-TO-ETHYLENE SENSITIVITY1	5utr/ exon/ intron	intron	Tolerated/ Deleterious	*qHvDRR-FLS-20*	FLL	5
HORVU.MOREX.r3.5HG0520250	BAH-PHD domain-containing protein	5utr/ intron/ exon			*qHvDRR-FLS-20*	FLL	5
HORVU.MOREX.r3.5HG0520260	GTPase obg	exon		Tolerated/ Deleterious	*qHvDRR-FLS-20*	FLL	5
HORVU.MOREX.r3.5HG0520270	carboxyl-termil peptidase, putative (DUF239)	5utr/ intron	exon	Tolerated/ Deleterious	*qHvDRR-FLS-20*	FLL	5
HORVU.MOREX.r3.5HG0520280	Heat shock protein 70 (Hsp 70) family protein	5utr		Deleterious	*qHvDRR-FLS-20*	FLL	5
HORVU.MOREX.r3.5HG0520330	WD repeat-containing protein 1	intron	intron	Tolerated/ Deleterious	*qHvDRR-FLS-20*	FLL	5
HORVU.MOREX.r3.5HG0520340	krueppel-like factor	5utr		Tolerated/ Deleterious	*qHvDRR-FLS-20*	FLL	5
HORVU.MOREX.r3.5HG0520360	Transposase	5utr	intron		*qHvDRR-FLS-20*	FLL	5
HORVU.MOREX.r3.5HG0520380	Centrosomal protein	5utr/ intron/ exon	5utr	Tolerated/ Deleterious	*qHvDRR-FLS-20*	FLL	5
HORVU.MOREX.r3.5HG0520390	Nodulin-like / Major Facilitator Superfamily protein	5utr		Tolerated/ Deleterious	*qHvDRR-FLS-20*	FLL	5
HORVU.MOREX.r3.5HG0520500	WD repeat-containing protein 1	5utr	5utr	Tolerated/ Deleterious	*qHvDRR-FLS-20*	FLL	5
HORVU.MOREX.r3.5HG0520510	Sec14p-like phosphatidylinositol transfer family protein			Tolerated/ Deleterious	*qHvDRR-FLS-20*	FLL	5
HORVU.MOREX.r3.5HG0520520	OTU domain-containing protein			Tolerated	*qHvDRR-FLS-20*	FLL	5
HORVU.MOREX.r3.5HG0520540	Cactin	intron/ 5utr/ exon	5utr	Tolerated/ Deleterious	*qHvDRR-FLS-20*	FLL	5
HORVU.MOREX.r3.5HG0520550	Argoute protein	intron/ 5utr/ exon	5utr	Tolerated/ Deleterious	*qHvDRR-FLS-20*	FLL	5
HORVU.MOREX.r3.5HG0520560	Small multi-drug export protein	exon/ 5utr/ intron	5utr/ intron	Tolerated/ Deleterious	*qHvDRR-FLS-20*	FLL	5
HORVU.MOREX.r3.5HG0520570	R-directed D polymerase (Reverse transcriptase)-related family protein	5utr	intron	Tolerated	*qHvDRR-FLS-20*	FLL	5
HORVU.MOREX.r3.5HG0520630	GRF zinc finger family protein, expressed			Tolerated/ Deleterious	*qHvDRR-FLS-20*	FLL	5
HORVU.MOREX.r3.5HG0520680	Transcription factor GTE6	exon/ 5utr	intron/ 5utr	Tolerated/ Deleterious	*qHvDRR-FLS-20*	FLL	5
HORVU.MOREX.r3.5HG0520690	essential meiotic endonuclease 1B	5utr/ intron		Tolerated/ Deleterious	*qHvDRR-FLS-20*	FLL	5
HORVU.MOREX.r3.5HG0520730	Thioredoxin family protein	intron/ 5utr			*qHvDRR-FLS-20*	FLL	5
HORVU.MOREX.r3.5HG0520740	Forkhead-associated (FHA) domain-containing protein	exon/ intron		Tolerated/ Deleterious	*qHvDRR-FLS-20*	FLL	5
HORVU.MOREX.r3.6HG0627980	Phosphate transporter PHO1-like protein	5utr/ exon	5utr	Tolerated	*qHvDRR-FLS-23*	FLL	6
HORVU.MOREX.r3.6HG0628010	Beta-toxin Cn4	5utr		Tolerated	*qHvDRR-FLS-23*	FLL	6
HORVU.MOREX.r3.6HG0628030	FAR1-related sequence 3			Tolerated	*qHvDRR-FLS-23*	FLL	6
HORVU.MOREX.r3.6HG0628040	Transducin/WD40 repeat-like superfamily protein	5utr		Tolerated/ Deleterious	*qHvDRR-FLS-23*	FLL	6
HORVU.MOREX.r3.6HG0628050	Cytosine-specific methyltransferase			Tolerated/ Deleterious	*qHvDRR-FLS-23*	FLL	6
HORVU.MOREX.r3.6HG0628070	Cticosapeptide/Phox/Bem1p (PB1) domain-containing protein-like			Tolerated/ Deleterious	*qHvDRR-FLS-23*	FLL	6
HORVU.MOREX.r3.6HG0628090	Cinmoyl CoA reductase	intron		Tolerated/ Deleterious	*qHvDRR-FLS-23*	FLL	6
HORVU.MOREX.r3.6HG0628110	CRT-binding factor			Tolerated/ Deleterious	*qHvDRR-FLS-23*	FLL	6
HORVU.MOREX.r3.6HG0628120	Cinmoyl CoA reductase			Tolerated/ Deleterious	*qHvDRR-FLS-23*	FLL	6
HORVU.MOREX.r3.6HG0628130	Cinmoyl CoA reductase			Tolerated/ Deleterious	*qHvDRR-FLS-23*	FLL	6
HORVU.MOREX.r3.6HG0628180	Ethylene-responsive transcription factor	5utr		Tolerated/ Deleterious	*qHvDRR-FLS-23*	FLL	6
HORVU.MOREX.r3.6HG0628210	F-box protein PP2	5utr		Tolerated/ Deleterious	*qHvDRR-FLS-23*	FLL	6
HORVU.MOREX.r3.6HG0628240	Translation initiation factor eIF-2B subunit epsilon			Tolerated/ Deleterious	*qHvDRR-FLS-23*	FLL	6
HORVU.MOREX.r3.6HG0628250	Cinmoyl CoA reductase			Tolerated/ Deleterious	*qHvDRR-FLS-23*	FLL	6
HORVU.MOREX.r3.6HG0628260	Germin-like protein 1-1			Tolerated/ Deleterious	*qHvDRR-FLS-23*	FLL	6
HORVU.MOREX.r3.6HG0628330	Werner syndrome-like exonuclease	5utr		Tolerated	*qHvDRR-FLS-23*	FLL	6
HORVU.MOREX.r3.6HG0628340	U-box domain-containing family protein			Tolerated/ Deleterious	*qHvDRR-FLS-23*	FLL	6
HORVU.MOREX.r3.6HG0628360	Bidirectiol sugar transporter SWEET			Deleterious	*qHvDRR-FLS-23*	FLL	6
HORVU.MOREX.r3.6HG0628390	Bidirectiol sugar transporter SWEET			Tolerated/ Deleterious	*qHvDRR-FLS-23*	FLL	6
HORVU.MOREX.r3.6HG0628400	U-box domain-containing family protein			Tolerated/ Deleterious	*qHvDRR-FLS-23*	FLL	6
HORVU.MOREX.r3.6HG0628410	Germin-like protein 1-1			Tolerated	*qHvDRR-FLS-23*	FLL	6
HORVU.MOREX.r3.6HG0628430	F-box protein PP2			Tolerated	*qHvDRR-FLS-23*	FLL	6
HORVU.MOREX.r3.6HG0628440	Protein kinase family protein, putative, expressed			Tolerated/ Deleterious	*qHvDRR-FLS-23*	FLL	6
HORVU.MOREX.r3.6HG0628480	Protein kinase, putative	intron		Tolerated/ Deleterious	*qHvDRR-FLS-23*	FLL	6
HORVU.MOREX.r3.6HG0628490	F-box protein PP2	5utr		Tolerated	*qHvDRR-FLS-23*	FLL	6
HORVU.MOREX.r3.6HG0628500	Myb/SANT-like D-binding domain protein			Tolerated/ Deleterious	*qHvDRR-FLS-23*	FLL	6
HORVU.MOREX.r3.6HG0628530	pre-mR cleavage complex 2 Pcf11-like protein	5utr			*qHvDRR-FLS-23*	FLL	6
HORVU.MOREX.r3.6HG0628540	tR dimethylallyltransferase			Tolerated/ Deleterious	*qHvDRR-FLS-23*	FLL	6
HORVU.MOREX.r3.6HG0628580	3-ketoacyl-CoA synthase			Tolerated/ Deleterious	*qHvDRR-FLS-23*	FLL	6
HORVU.MOREX.r3.6HG0628590	Glutathione reductase			Tolerated/ Deleterious	*qHvDRR-FLS-23*	FLL	6
HORVU.MOREX.r3.6HG0628610	F-box protein PP2	5utr		Tolerated/ Deleterious	*qHvDRR-FLS-23*	FLL	6
HORVU.MOREX.r3.6HG0628630	F-box protein PP2			Tolerated/ Deleterious	*qHvDRR-FLS-23*	FLL	6
HORVU.MOREX.r3.6HG0628660	PPPDE thiol peptidase family protein, putative			Tolerated	*qHvDRR-FLS-23*	FLL	6
HORVU.MOREX.r3.6HG0628670	R-directed D polymerase (reverse transcriptase)-related family protein	5utr		Tolerated/ Deleterious	*qHvDRR-FLS-23*	FLL	6
HORVU.MOREX.r3.6HG0628680	Fatty acid hydroxylase superfamily protein	5utr		Tolerated/ Deleterious	*qHvDRR-FLS-23*	FLL	6
HORVU.MOREX.r3.6HG0628700	myosin heavy chain, embryonic smooth protein	5utr			*qHvDRR-FLS-23*	FLL	6
HORVU.MOREX.r3.6HG0628710	Leucine-rich repeat receptor-like protein kinase family protein			Tolerated/ Deleterious	*qHvDRR-FLS-23*	FLL	6
HORVU.MOREX.r3.6HG0628740	Clavesin-2	5utr		Tolerated/ Deleterious	*qHvDRR-FLS-23*	FLL	6
HORVU.MOREX.r3.6HG0628760	Receptor-kinase, putative			Tolerated/ Deleterious	*qHvDRR-FLS-23*	FLL	6
HORVU.MOREX.r3.6HG0628790	Myb-like transcription factor family protein			Tolerated/ Deleterious	*qHvDRR-FLS-23*	FLL	6
HORVU.MOREX.r3.6HG0628800	fanconi anemia group F protein (FANCF)			Tolerated/ Deleterious	*qHvDRR-FLS-23*	FLL	6
HORVU.MOREX.r3.6HG0628820	myosin family protein with Dil	5utr		Deleterious	*qHvDRR-FLS-23*	FLL	6
HORVU.MOREX.r3.6HG0628830	Nicotimide-nucleotide adenylyltransferase			Tolerated/ Deleterious	*qHvDRR-FLS-23*	FLL	6
HORVU.MOREX.r3.6HG0628860	tR-2-methylthio-N(6)-dimethylallyladenosine synthase			Tolerated/ Deleterious	*qHvDRR-FLS-23*	FLL	6
HORVU.MOREX.r3.6HG0628870	Calcium-dependent lipid-binding (CaLB domain) family protein			Tolerated/ Deleterious	*qHvDRR-FLS-23*	FLL	6

HORVU.MOREX.r3.6HG0628890	Nicotiamine synthase	5utr			*qHvDRR-FLS-23*	FLL	6
HORVU.MOREX.r3.6HG0628900	R-binding family protein			Tolerated/ Deleterious	*qHvDRR-FLS-23*	FLL	6
HORVU.MOREX.r3.6HG0628910	Synechocystis YCF37			Tolerated	*qHvDRR-FLS-23*	FLL	6
HORVU.MOREX.r3.6HG0628920	Maltose/maltodextrin import ATP-binding protein MalK			Tolerated	*qHvDRR-FLS-23*	FLL	6
HORVU.MOREX.r3.6HG0628930	Alcohol dehydrogese			Tolerated/ Deleterious	*qHvDRR-FLS-23*	FLL	6
HORVU.MOREX.r3.6HG0628940	Diphthamide biosynthesis protein			Tolerated	*qHvDRR-FLS-23*	FLL	6
HORVU.MOREX.r3.6HG0628960	Receptor-like kinase	5utr		Tolerated/ Deleterious	*qHvDRR-FLS-23*	FLL	6
HORVU.MOREX.r3.6HG0629000	C2 calcium/lipid-binding and GRAM domain protein			Tolerated/ Deleterious	*qHvDRR-FLS-23*	FLL	6
HORVU.MOREX.r3.6HG0629060	Phosphoglycolate phosphatase, putative			Tolerated/ Deleterious	*qHvDRR-FLS-23*	FLL	6
HORVU.MOREX.r3.6HG0629070	GDSL esterase/lipase			Tolerated/ Deleterious	*qHvDRR-FLS-23*	FLL	6
HORVU.MOREX.r3.6HG0629090	transmembrane protein, putative (DUF679)	5utr		Tolerated/ Deleterious	*qHvDRR-FLS-23*	FLL	6
HORVU.MOREX.r3.6HG0629110	transmembrane protein, putative (DUF679)			Tolerated/ Deleterious	*qHvDRR-FLS-23*	FLL	6
HORVU.MOREX.r3.6HG0629120	transmembrane protein, putative (DUF679)	5utr		Tolerated/ Deleterious	*qHvDRR-FLS-23*	FLL	6
HORVU.MOREX.r3.6HG0629140	CLIP-associating protein-like	intron		Tolerated/ Deleterious	*qHvDRR-FLS-23*	FLL	6
HORVU.MOREX.r3.6HG0629150	ATPase expression protein 1, mitochondrial	5utr	5utr/ intron		*qHvDRR-FLS-23*	FLL	6
HORVU.MOREX.r3.6HG0629160	Disease resistance protein RPM1	5utr		Tolerated/ Deleterious	*qHvDRR-FLS-23*	FLL	6
HORVU.MOREX.r3.6HG0629170	Disease resistance protein RPM1		intron	Tolerated/ Deleterious	*qHvDRR-FLS-23*	FLL	6
HORVU.MOREX.r3.6HG0629180	Disease resistance protein RPM1	intron		Tolerated/ Deleterious	*qHvDRR-FLS-23*	FLL	6
HORVU.MOREX.r3.6HG0629220	methyl-coenzyme M reductase II subunit gamma, putative (DUF3741)	exon		Tolerated/ Deleterious	*qHvDRR-FLS-23*	FLL	6
HORVU.MOREX.r3.6HG0629230	F-box family protein	5utr		Tolerated/ Deleterious	*qHvDRR-FLS-23*	FLL	6
HORVU.MOREX.r3.6HG0629240	O-methyltransferase			Tolerated	*qHvDRR-FLS-23*	FLL	6
HORVU.MOREX.r3.6HG0629260	Glutathione S-transferase			Tolerated/ Deleterious	*qHvDRR-FLS-23*	FLL	6
HORVU.MOREX.r3.6HG0629270	Glutathione S-transferase	intron/ 5utr		Tolerated/ Deleterious	*qHvDRR-FLS-23*	FLL	6
HORVU.MOREX.r3.6HG0629290	Alpha/beta-Hydrolases superfamily protein, putative			Tolerated/ Deleterious	*qHvDRR-FLS-23*	FLL	6
HORVU.MOREX.r3.6HG0629320	Kinesin-like protein			Tolerated/ Deleterious	*qHvDRR-FLS-23*	FLL	6
HORVU.MOREX.r3.6HG0629330	ABC1-like kinase	5utr		Tolerated	*qHvDRR-FLS-23*	FLL	6
HORVU.MOREX.r3.6HG0629340	ATP synthase CF0 B subunit subunit I	5utr		Tolerated/ Deleterious	*qHvDRR-FLS-23*	FLL	6
HORVU.MOREX.r3.6HG0629350	DH dehydrogese [ubiquinone] 1 alpha subcomplex subunit 9, mitochondrial			Tolerated	*qHvDRR-FLS-23*	FLL	6
HORVU.MOREX.r3.6HG0629380	HVA22-like protein	5utr/ intron	5utr/ intron	Tolerated/ Deleterious	*qHvDRR-FLS-23*	FLL	6
HORVU.MOREX.r3.6HG0629410	Lysine-rich arabinogalactan protein 17	5utr		Tolerated/ Deleterious	*qHvDRR-FLS-23*	FLL	6
HORVU.MOREX.r3.6HG0629440	Serine/threonine-protein kinase			Tolerated/ Deleterious	*qHvDRR-FLS-23*	FLL	6
HORVU.MOREX.r3.6HG0629450	Disease resistance protein RPM1			Tolerated/ Deleterious	*qHvDRR-FLS-23*	FLL	6
HORVU.MOREX.r3.6HG0629460	Chorismate synthase			Deleterious	*qHvDRR-FLS-23*	FLL	6
HORVU.MOREX.r3.6HG0629470	Serine/threonine-protein kinase			Tolerated/ Deleterious	*qHvDRR-FLS-23*	FLL	6
HORVU.MOREX.r3.6HG0629480	Serine/threonine-protein kinase			Tolerated/ Deleterious	*qHvDRR-FLS-23*	FLL	6
HORVU.MOREX.r3.6HG0629490	Serine/threonine-protein kinase			Tolerated/ Deleterious	*qHvDRR-FLS-23*	FLL	6
HORVU.MOREX.r3.6HG0629510	Acetyl-coenzyme A synthetase	5utr		Tolerated/ Deleterious	*qHvDRR-FLS-23*	FLL	6
HORVU.MOREX.r3.6HG0629520	Ethylene-responsive transcription factor	5utr		Tolerated	*qHvDRR-FLS-23*	FLL	6
HORVU.MOREX.r3.6HG0629530	Myb/SANT-like D-binding domain protein	5utr		Tolerated/ Deleterious	*qHvDRR-FLS-23*	FLL	6
HORVU.MOREX.r3.6HG0629540	Myb/SANT-like domain-containing protein	5utr		Tolerated/ Deleterious	*qHvDRR-FLS-23*	FLL	6
HORVU.MOREX.r3.6HG0629550	receptor kinase 1			Tolerated/ Deleterious	*qHvDRR-FLS-23*	FLL	6
HORVU.MOREX.r3.6HG0629580	Myosin	5utr/ intron	5utr	Tolerated/ Deleterious	*qHvDRR-FLS-23*	FLL	6
HORVU.MOREX.r3.6HG0629600	Myb-like D-binding protein, putative		5utr	Tolerated/ Deleterious	*qHvDRR-FLS-23*	FLL	6
HORVU.MOREX.r3.6HG0629650	Ripening-related protein			Tolerated	*qHvDRR-FLS-23*	FLL	6
HORVU.MOREX.r3.6HG0629660	Ripening-related protein	5utr		Tolerated/ Deleterious	*qHvDRR-FLS-23*	FLL	6
HORVU.MOREX.r3.6HG0629670	Ripening-related protein			Tolerated/ Deleterious	*qHvDRR-FLS-23*	FLL	6
HORVU.MOREX.r3.6HG0629680	NBS-LRR resistance-like protein	5utr		Tolerated/ Deleterious	*qHvDRR-FLS-23*	FLL	6
HORVU.MOREX.r3.6HG0629700	Protein PLASTID MOVEMENT IMPAIRED 1			Tolerated/ Deleterious	*qHvDRR-FLS-23*	FLL	6
HORVU.MOREX.r3.6HG0629710	Actin-related protein 2/3 complex subunit			Deleterious	*qHvDRR-FLS-23*	FLL	6
HORVU.MOREX.r3.6HG0629730	Inosine-5'-monophosphate dehydrogese			Tolerated	*qHvDRR-FLS-23*	FLL	6
HORVU.MOREX.r3.6HG0629740	Serine/threonine-protein phosphatase 7 long form-like protein			Tolerated/ Deleterious	*qHvDRR-FLS-23*	FLL	6
HORVU.MOREX.r3.6HG0629760	Dihydrolipoamide acetyltransferase component of pyruvate dehydrogese complex			Tolerated/ Deleterious	*qHvDRR-FLS-23*	FLL	6
HORVU.MOREX.r3.6HG0629770	Telomere binding protein	exon/ 5utr		Tolerated/ Deleterious	*qHvDRR-FLS-23*	FLL	6
HORVU.MOREX.r3.6HG0629790	3-ketoacyl-CoA thiolase-like protein			Deleterious	*qHvDRR-FLS-23*	FLL	6
HORVU.MOREX.r3.6HG0629810	Auxin-responsive protein	5utr	5utr	Tolerated/ Deleterious	*qHvDRR-FLS-23*	FLL	6
HORVU.MOREX.r3.6HG0629830	Riboflavin biosynthesis protein RibD			Tolerated	*qHvDRR-FLS-23*	FLL	6
HORVU.MOREX.r3.6HG0629840	C domain protein	5utr	5utr	Tolerated	*qHvDRR-FLS-23*	FLL	6
HORVU.MOREX.r3.6HG0629860	Methyltransferase family protein			Tolerated/ Deleterious	*qHvDRR-FLS-23*	FLL	6
HORVU.MOREX.r3.6HG0629870	Pentatricopeptide repeat-containing protein			Tolerated/ Deleterious	*qHvDRR-FLS-23*	FLL	6
HORVU.MOREX.r3.6HG0629880	Heavy metal transport/detoxification superfamily protein			Tolerated	*qHvDRR-FLS-23*	FLL	6
HORVU.MOREX.r3.6HG0629910	Heavy metal-associated protein	5utr/ exon		Tolerated/ Deleterious	*qHvDRR-FLS-23*	FLL	6
HORVU.MOREX.r3.6HG0629930	Ankyrin repeat domain-containing protein 20A4		exon	Tolerated	*qHvDRR-FLS-23*	FLL	6
HORVU.MOREX.r3.6HG0629950	Disease resistance protein (TIR-NBS-LRR class) family	5utr		Tolerated/ Deleterious	*qHvDRR-FLS-23*	FLL	6
HORVU.MOREX.r3.6HG0629960	S-acyltransferase	5utr/ intron		Tolerated/ Deleterious	*qHvDRR-FLS-23*	FLL	6
HORVU.MOREX.r3.6HG0629970	D mismatch repair protein Msh6-1	5utr	5utr	Tolerated/ Deleterious	*qHvDRR-FLS-23*	FLL	6
HORVU.MOREX.r3.6HG0629990	Pentatricopeptide repeat-containing protein	5utr	5utr	Tolerated/ Deleterious	*qHvDRR-FLS-23*	FLL	6
HORVU.MOREX.r3.6HG0630000	Thioredoxin			Tolerated/ Deleterious	*qHvDRR-FLS-23*	FLL	6
HORVU.MOREX.r3.6HG0630010	Pumilio-like protein	5utr/ exon		Tolerated/ Deleterious	*qHvDRR-FLS-23*	FLL	6
HORVU.MOREX.r3.6HG0630020	2-phosphoglycerate kinase	5utr	5utr	Tolerated	*qHvDRR-FLS-23*	FLL	6
HORVU.MOREX.r3.6HG0630040	C2 domain-containing protein	intron/ 5utr	5utr	Deleterious	*qHvDRR-FLS-23*	FLL	6
HORVU.MOREX.r3.6HG0630050	OTU domain-containing protein	5utr/ intron/ exon			*qHvDRR-FLS-23*	FLL	6
HORVU.MOREX.r3.6HG0630070	Protein kinase	5utr/ intron		Tolerated	*qHvDRR-FLS-23*	FLL	6
HORVU.MOREX.r3.6HG0630080	stress response NST1-like protein	5utr	5utr	Tolerated	*qHvDRR-FLS-23*	FLL	6
HORVU.MOREX.r3.6HG0630100	ABC transporter G family member	exon/ 5utr/ intron	5utr	Tolerated	*qHvDRR-FLS-23*	FLL	6
HORVU.MOREX.r3.6HG0630110	DNL-type zinc finger protein	5utr		Tolerated/ Deleterious	*qHvDRR-FLS-23*	FLL	6
HORVU.MOREX.r3.6HG0630120	Ankyrin repeat family protein			Tolerated/ Deleterious	*qHvDRR-FLS-23*	FLL	6
HORVU.MOREX.r3.6HG0630150	Ankyrin repeat-containing protein			Tolerated/ Deleterious	*qHvDRR-FLS-23*	FLL	6
HORVU.MOREX.r3.6HG0630200	Protein FAR1-RELATED SEQUENCE 3	5utr/ exon		Tolerated/ Deleterious	*qHvDRR-FLS-23*	FLL	6
HORVU.MOREX.r3.6HG0630210	Ankyrin repeat family protein	5utr	5utr	Tolerated/ Deleterious	*qHvDRR-FLS-23*	FLL	6
HORVU.MOREX.r3.6HG0630240	no-apical-meristem-associated carboxy-termil domain protein			Tolerated	*qHvDRR-FLS-23*	FLL	6
HORVU.MOREX.r3.6HG0630250	kinase family protein	5utr	5utr	Tolerated/ Deleterious	*qHvDRR-FLS-23*	FLL	6
HORVU.MOREX.r3.6HG0630260	Serine/threonine-protein phosphatase	5utr/ intron/ exon		Deleterious	*qHvDRR-FLS-23*	FLL	6
HORVU.MOREX.r3.6HG0630270	F-box family protein	5utr	5utr	Tolerated/ Deleterious	*qHvDRR-FLS-23*	FLL	6
HORVU.MOREX.r3.6HG0630280	F-box/RNI-like/FBD-like domains-containing protein	5utr/ intron/ exon		Tolerated/ Deleterious	*qHvDRR-FLS-23*	FLL	6
HORVU.MOREX.r3.6HG0630340	F-box/RNI-like/FBD-like domains-containing protein	exon/ 5utr	5utr	Tolerated/ Deleterious	*qHvDRR-FLS-23*	FLL	6
HORVU.MOREX.r3.6HG0630350	Ring finger protein, putative			Tolerated/ Deleterious	*qHvDRR-FLS-23*	FLL	6
HORVU.MOREX.r3.6HG0630360	Protein KINESIN LIGHT CHAIN-RELATED 3			Tolerated/ Deleterious	*qHvDRR-FLS-23*	FLL	6
HORVU.MOREX.r3.6HG0630390	F-box family protein			Tolerated/ Deleterious	*qHvDRR-FLS-23*	FLL	6
HORVU.MOREX.r3.6HG0630410	LOB domain protein-like			Tolerated	*qHvDRR-FLS-23*	FLL	6
HORVU.MOREX.r3.6HG0630420	Myosin type-2 heavy chain 2	5utr		Tolerated/ Deleterious	*qHvDRR-FLS-23*	FLL	6
HORVU.MOREX.r3.6HG0630450	Nicotiamine synthase			Tolerated/ Deleterious	*qHvDRR-FLS-23*	FLL	6
HORVU.MOREX.r3.6HG0630480	Ribonuclease 3			Tolerated/ Deleterious	*qHvDRR-FLS-23*	FLL	6
HORVU.MOREX.r3.6HG0630490	F-box family protein	5utr		Tolerated/ Deleterious	*qHvDRR-FLS-23*	FLL	6
HORVU.MOREX.r3.6HG0630500	Deoxyhypusine hydroxylase			Tolerated	*qHvDRR-FLS-23*	FLL	6
HORVU.MOREX.r3.6HG0630520	AT hook motif D-binding family protein			Tolerated	*qHvDRR-FLS-23*	FLL	6
HORVU.MOREX.r3.6HG0630540	protein kinase family protein			Tolerated/ Deleterious	*qHvDRR-FLS-23*	FLL	6
HORVU.MOREX.r3.6HG0630550	T-complex protein 1 subunit zeta	5utr	intron/ 5utr	Tolerated/ Deleterious	*qHvDRR-FLS-23*	FLL	6
HORVU.MOREX.r3.6HG0630560	Ethylene receptor			Tolerated	*qHvDRR-FLS-23*	FLL	6
HORVU.MOREX.r3.6HG0630570	Ribonuclease H-like superfamily protein	5utr	intron	Tolerated/ Deleterious	*qHvDRR-FLS-23*	FLL	6
HORVU.MOREX.r3.6HG0630580	Zinc finger family protein	5utr	5utr	Deleterious	*qHvDRR-FLS-23*	FLL	6
HORVU.MOREX.r3.6HG0630590	Receptor-like kinase	5utr	5utr	Tolerated/ Deleterious	*qHvDRR-FLS-23*	FLL	6
HORVU.MOREX.r3.6HG0630600	RING/U-box superfamily protein, putative	intron/ 5utr	5utr	Tolerated	*qHvDRR-FLS-23*	FLL	6
HORVU.MOREX.r3.6HG0630610	SHC-transforming protein 2	5utr		Deleterious	*qHvDRR-FLS-23*	FLL	6
HORVU.MOREX.r3.6HG0630620	Disease resistance protein RGA2	5utr	exon	Tolerated/ Deleterious	*qHvDRR-FLS-23*	FLL	6
HORVU.MOREX.r3.6HG0630630	NB-ARC domain-containing disease resistance protein	5utr		Tolerated/ Deleterious	*qHvDRR-FLS-23*	FLL	6
HORVU.MOREX.r3.6HG0630640	Aconitate hydratase	5utr		Tolerated/ Deleterious	*qHvDRR-FLS-23*	FLL	6
HORVU.MOREX.r3.6HG0630650	Protein DETOXIFICATION			Tolerated/ Deleterious	*qHvDRR-FLS-23*	FLL	6

HORVU.MOREX.r3.6HG0630660	Protein DETOXIFICATION	5utr		Tolerated	*qHvDRR-FLS-23*	FLL	6
HORVU.MOREX.r3.6HG0630670	rR 2'-O-methyltransferase fibrillarin 2	intron/ exon			*qHvDRR-FLS-23*	FLL	6
HORVU.MOREX.r3.6HG0630680	F-box family protein	exon/ 5utr	exon/ 5utr	Tolerated/ Deleterious	*qHvDRR-FLS-23*	FLL	6
HORVU.MOREX.r3.6HG0630710	Leucine-rich repeat receptor-like protein kinase family protein	5utr		Tolerated/ Deleterious	*qHvDRR-FLS-23*	FLL	6
HORVU.MOREX.r3.6HG0630750	Leucine-rich repeat receptor-like protein kinase family protein	5utr		Tolerated/ Deleterious	*qHvDRR-FLS-23*	FLL	6
HORVU.MOREX.r3.6HG0630760	Leucine-rich repeat receptor-like protein kinase family protein	5utr	exon/ 5utr	Tolerated	*qHvDRR-FLS-23*	FLL	6
HORVU.MOREX.r3.6HG0630790	Leucine-rich repeat receptor-like protein kinase family protein			Tolerated/ Deleterious	*qHvDRR-FLS-23*	FLL	6
HORVU.MOREX.r3.6HG0630800	NBS-LRR disease resistance protein, putative	5utr/ intron/ exon	5utr/ intron	Tolerated/ Deleterious	*qHvDRR-FLS-23*	FLL	6
HORVU.MOREX.r3.6HG0630880	Leucine-rich repeat receptor-like protein kinase family protein	5utr	5utr	Tolerated/ Deleterious	*qHvDRR-FLS-23*	FLL	6
HORVU.MOREX.r3.6HG0630890	Mannosyl-oligosaccharide glucosidase	5utr	5utr	Tolerated/ Deleterious	*qHvDRR-FLS-23*	FLL	6
HORVU.MOREX.r3.6HG0630900	transmembrane protein, putative (DUF594)	exon/ 5utr/ intron	5utr	Tolerated/ Deleterious	*qHvDRR-FLS-23*	FLL	6
HORVU.MOREX.r3.6HG0630920	NBS-LRR disease resistance protein-like	intron		Tolerated/ Deleterious	*qHvDRR-FLS-23*	FLL	6
HORVU.MOREX.r3.6HG0630950	pleiotropic drug resistance 13	5utr		Tolerated/ Deleterious	*qHvDRR-FLS-23*	FLL	6
HORVU.MOREX.r3.6HG0631040	Mesoderm induction early response protein 1, putative isoform 1	intron/ 5utr/ exon	intron	Tolerated/ Deleterious	*qHvDRR-FLS-23*	FLL	6
HORVU.MOREX.r3.6HG0631050	Histone H2A	exon/ 5utr		Tolerated	*qHvDRR-FLS-23*	FLL	6
HORVU.MOREX.r3.6HG0631070	F-box family protein	5utr	5utr	Tolerated/ Deleterious	*qHvDRR-FLS-23*	FLL	6
HORVU.MOREX.r3.6HG0631080	Hydroxyproline-rich glycoprotein-like	5utr/ exon	5utr	Tolerated	*qHvDRR-FLS-23*	FLL	6
HORVU.MOREX.r3.6HG0631090	(+)/H(+) antiporter NhaB	intron/ exon		Tolerated	*qHvDRR-FLS-23*	FLL	6
HORVU.MOREX.r3.6HG0631110	Myb/SANT-like D-binding domain protein	5utr	5utr	Tolerated/ Deleterious	*qHvDRR-FLS-23*	FLL	6
HORVU.MOREX.r3.6HG0631130	High-affinity branched-chain amino acid transport system permease protein LivH	5utr	5utr	Tolerated	*qHvDRR-FLS-23*	FLL	6
HORVU.MOREX.r3.6HG0631190	Ubiquitin carboxyl-termil hydrolase			Tolerated	*qHvDRR-FLS-23*	FLL	6
HORVU.MOREX.r3.6HG0631210	R-binding protein Nova	intron/ 5utr/ exon	intron/ 5utr	Tolerated	*qHvDRR-FLS-23*	FLL	6
HORVU.MOREX.r3.6HG0631250	Serine/threonine protein phosphatase 7 long form isogeny	5utr	5utr	Tolerated/ Deleterious	*qHvDRR-FLS-23*	FLL	6
HORVU.MOREX.r3.6HG0631280	Serine/threonine-protein kinase	5utr		Tolerated/ Deleterious	*qHvDRR-FLS-23*	FLL	6
HORVU.MOREX.r3.6HG0631290	Disease resistance protein (TIR-NBS-LRR class) family	5utr/ exon/ intron	intron	Tolerated/ Deleterious	*qHvDRR-FLS-23*	FLL	6
HORVU.MOREX.r3.6HG0631310	Disease resistance protein RPM1	5utr		Tolerated/ Deleterious	*qHvDRR-FLS-23*	FLL	6
HORVU.MOREX.r3.6HG0631330	FBD-associated F-box protein			Tolerated/ Deleterious	*qHvDRR-FLS-23*	FLL	6
HORVU.MOREX.r3.6HG0631340	Oligoribonuclease	intron/ exon		Tolerated/ Deleterious	*qHvDRR-FLS-23*	FLL	6
HORVU.MOREX.r3.6HG0631350	Subtilisin-like protease	5utr		Tolerated/ Deleterious	*qHvDRR-FLS-23*	FLL	6
HORVU.MOREX.r3.6HG0631360	Disease resistance protein RPM1	5utr/ intron/ exon	exon	Tolerated/ Deleterious	*qHvDRR-FLS-23*	FLL	6
HORVU.MOREX.r3.6HG0631370	Pathogenesis-related protein PR-4			Tolerated	*qHvDRR-FLS-23*	FLL	6
HORVU.MOREX.r3.6HG0631390	Disease resistance protein RPM1	5utr/ intron/ exon	5utr	Tolerated/ Deleterious	*qHvDRR-FLS-23*	FLL	6
HORVU.MOREX.r3.6HG0631400	Disease resistance protein RPM1	5utr/ intron	5utr	Tolerated/ Deleterious	*qHvDRR-FLS-23*	FLL	6
HORVU.MOREX.r3.6HG0631410	Pol polyprotein			Tolerated/ Deleterious	*qHvDRR-FLS-23*	FLL	6
HORVU.MOREX.r3.6HG0631420	Remorin	5utr		Tolerated/ Deleterious	*qHvDRR-FLS-23*	FLL	6
HORVU.MOREX.r3.6HG0631440	Janus kinase and microtubule-interacting protein 3			Tolerated	*qHvDRR-FLS-23*	FLL	6
HORVU.MOREX.r3.6HG0631450	AT hook motif D-binding family protein, putative	exon		Tolerated	*qHvDRR-FLS-23*	FLL	6
HORVU.MOREX.r3.6HG0631490	Zinc finger family protein	5utr		Tolerated/ Deleterious	*qHvDRR-FLS-23*	FLL	6
HORVU.MOREX.r3.6HG0631520	Werner Syndrome-like exonuclease	5utr		Deleterious	*qHvDRR-FLS-23*	FLL	6
HORVU.MOREX.r3.6HG0631530	LINE-1 reverse transcriptase		5utr	Tolerated/ Deleterious	*qHvDRR-FLS-23*	FLL	6
HORVU.MOREX.r3.6HG0631560	Serine/threonine-protein phosphatase	intron/ 5utr	intron/ 5utr	Tolerated/ Deleterious	*qHvDRR-FLS-23*	FLL	6
HORVU.MOREX.r3.6HG0631570	Succite--CoA ligase [ADP-forming] subunit beta	5utr/ exon	5utr	Tolerated/ Deleterious	*qHvDRR-FLS-23*	FLL	6
HORVU.MOREX.r3.6HG0631580	Protein SMG8	5utr/ exon	5utr	Tolerated/ Deleterious	*qHvDRR-FLS-23*	FLL	6
HORVU.MOREX.r3.6HG0631600	Rop guanine nucleotide exchange factor, putative	5utr			*qHvDRR-FLS-23*	FLL	6
HORVU.MOREX.r3.6HG0631630	Smad/FHA domain protein	intron/ 5utr		Tolerated/ Deleterious	*qHvDRR-FLS-23*	FLL	6
HORVU.MOREX.r3.6HG0631640	O-methyltransferase	5utr/ intron		Tolerated/ Deleterious	*qHvDRR-FLS-23*	FLL	6
HORVU.MOREX.r3.6HG0631650	RING/U-box superfamily protein	5utr			*qHvDRR-FLS-23*	FLL	6
HORVU.MOREX.r3.6HG0631660	RING/U-box superfamily protein	5utr	5utr	Tolerated	*qHvDRR-FLS-23*	FLL	6
HORVU.MOREX.r3.6HG0631680	Lysine-specific histone demethylase 1-3-like protein	5utr		Tolerated/ Deleterious	*qHvDRR-FLS-23*	FLL	6
HORVU.MOREX.r3.6HG0631700	Aquaporin			Tolerated/ Deleterious	*qHvDRR-FLS-23*	FLL	6
HORVU.MOREX.r3.6HG0631710	Aquaporin	5utr	5utr	Deleterious	*qHvDRR-FLS-23*	FLL	6
HORVU.MOREX.r3.6HG0631730	Peptidyl-prolyl cis-trans isomerase	5utr		Tolerated/ Deleterious	*qHvDRR-FLS-23*	FLL	6
HORVU.MOREX.r3.6HG0631760	Sigl peptide peptidase-like protein	intron/ 5utr/ exon	intron/ 5utr	Tolerated/ Deleterious	*qHvDRR-FLS-23*	FLL	6
HORVU.MOREX.r3.6HG0631770	Acyl-CoA-binding domain-containing protein 4	intron		Tolerated	*qHvDRR-FLS-23*	FLL	6

Supplementary Table S7. The barley orthologs of genes associated with development in other plant species.

Generic name	Gene	Species	Citation	Barley ortholog	Generic name	Chromosc	Start (bp)	End (bp)	Annotation
AtAvp1	At1g15690	Arabidopsis	(Zhang et al. 2009; Schilling et al. 2017)	HORVU.MOREX.r3.1HG0062900.1	*HvAvp1*	1H	416,798,216	416,803,167	Pyrophosphate-energized vacuolar membrane proton pump
AtTcp5	At5g60970	Arabidopsis	(Zhang et al. 2021)	HORVU.MOREX.r3.1HG0077830.1	*HvTcp5*	1H	479,576,955	479,579,301	TCP family transcription factor containing protein
Ckx9	Os05g0374200	Rice		HORVU.MOREX.r3.1HG0059670.1	*HvCkx9*	1H	397,171,105	397,173,059	Cytokinin oxidase/dehydrogenase
AtPrr3	AT5G60100	Arabidopsis	(Digel et al., 2016)	HORVU.MOREX.r3.2HG0107710.1	*Ppd-H1*	2H	25,876,427	25,880,400	Pseudo-response regulator
Nrp1	Os07g0471900	Rice	(Chen et al. 2021)	HORVU.MOREX.r3.2HG0187860.1	*Nrp1*	2H	589,035,123	589,038,128	basic helix-loop-helix (bHLH) DNA-binding superfamily protein
Nal1	Os04g0615000	Rice	(Qi et al., 2008)	HORVU.MOREX.r3.2HG0190650	*blf13*	2H	599,603,404	599,608,773	Trypsin family protein
Oslbh1	Os04g0660100	Rice	(Zhang et al., 2009)	HORVU.MOREX.r3.2HG0202180	*lbh1*	2H	628645529	628646836	Transcription factor, putative
AtAp2	AT4G36920	Arabidopsis	(Jofuku et al., 1994; Modrusan et al., 1994; Ohto et al., 2005)	HORVU.MOREX.r3.2HG0204770.1	*HvAp2*	2H	635,314,602	635,318,153	AP2-like ethylene-responsive transcription factor
AtCkx3	AT5G56970	Arabidopsis	(Bilyeu et al., 2001; Werner et al., 2001)	HORVU.MOREX.r3.3HG0236930.1	*HvCkx1*	3H	48,332,444	48,334,763	Cytokinin oxidase/dehydrogenase
AtCkx3	AT5G56970	Arabidopsis	(Bilyeu et al., 2001; Werner et al., 2001)	HORVU.MOREX.r3.3HG0244570.1	*HvCkx2*	3H	99,555,698	99,558,842	Cytokinin oxidase/dehydrogenase
AtTcp5	At5g60970	Arabidopsis	(Yu et al. 2021)	HORVU.MOREX.r3.3HG0290910.1	*HvTcp5*	3H	498,350,130	498,352,650	TCP family transcription factor containing protein
AtGA20OX1	At4g25420	Arabidopsis	(Rieu et al. 2008)	HORVU.MOREX.r3.3HG0306160.1	*HvGA20OX1*	3H	561,164,973	561,168,444	Gibberellin 20 oxidase
OsBlh6	Os03g0165300	Rice	(Hirano et al. 2013)	HORVU.MOREX.r3.4HG0334360.1	*HvBlh6*	4H	8,722,968	8,726,333	Homeobox protein BEL1 like
AtGRF5	At3g13960	Arabidopsis	(Vercruyssen et al. 2015; Horiguchi et al. 2005)	HORVU.MOREX.r3.4HG0339430.2	*HvGrf5*	4H	26,194,138	26,198,105	Growth-regulating factor
OsBlh6	Os03g0165300	Rice	(Hirano et al. 2013)	HORVU.MOREX.r3.4HG0339810.1	*HvBlh6*	4H	27,555,371	27,565,963	Homeobox protein bel1-like protein
Nal7	Os03g0162000	Rice	(Fujino et al. 2008)	HORVU.MOREX.r3.4HG0402190.1	*Nal7*	4H	559,703,961	559,706,589	Flavin-containing monooxygenase
OsBlh6	Os03g0165300	Rice	(Hirano et al., 2013)	HORVU.MOREX.r3.4HG0402730.1	*HvBlh6*	4H	561,849,331	561,852,756	Homeobox protein BEL1 like
			(Dubcovsky et al., 2005)	HORVU.MOREX.r3.4HG0415230.1	*Vrn-H2*	4H	601,535,222	601,544,088	basic helix-loop-helix (bHLH) DNA-binding superfamily protein
Atldd	AT1G68130, AT1G25250, AT2G01940	Arabidopsis	(Jöst et al., 2016)	HORVU.MOREX.r3.5HG0485730.1	*Blf1*	5H	456,055,817	456,059,003	Zinc finger family protein
AtAp1	AT1G69120.1	Arabidopsis	(Greenup et al., 2010)	HORVU.MOREX.r3.5HG0511210.1	*Vrn-H1*	5H	528,147,816	528,157,990	MADS box transcription factor
AtGA20OX2	At5g51810	Arabidopsis	(Rieu et al. 2008)	HORVU.MOREX.r3.5HG0536610.1	*HvGA20OX2*	5H	583,942,988	583,944,186	Gibberellin 20 oxidase
Nrp1	Os07g0471900	Rice	(Chen et al. 2021)	HORVU.MOREX.r3.6HG0603090.1	*Nrp1*	6H	430,796,647	430,799,341	basic helix-loop-helix (bHLH) DNA-binding superfamily protein
AtGrf5	At3g13960	Arabidopsis	(Vercruyssen et al. 2015; Horiguchi et al. 2005)	HORVU.MOREX.r3.6HG0620090.1	*HvGrf5*	6H	526,609,451	526,611,446	Growth-regulating factor
AtFT	AT1G65480	Arabidopsis	(Yan et al., 2006)	HORVU.MOREX.r3.7HG0653910.1	*Vrn-H3*	7H	42,284,165	42,285,781	Flowering locus T
AtAvp1	At1g15690	Arabidopsis	(Zhang et al. 2009; Schilling et al. 2017)	HORVU.MOREX.r3.7HG0745070.1	*HvAvp1*	7H	615,331,039	615,336,002	Pyrophosphate-energized vacuolar membrane proton pump

Supplementary Table S8.The allele of the *Ppd-H1* gene among the parental inbreds. The table summarizes the presence of photoperiod sensitive and reduced photoperiod sensitive allele at SNP22 in the CCT-domain of *Ppd-H1* gene in barley for the parental inbreds of those sub-populations where a QTL was detected for flag leaf length (FLL) and width (FLW) at this locus. The nomenclature of the *Ppd-H1* allele was adapted from Cosenza et al. (2024). The flowering time QTLs detected by Cosenza et al. (2024) were used to compare the association of effect of late or early *Ppd-H1* flowering time (FT) allele with FLL and FLW.

Population	Parent 1 (P1)	Parent 2 (P2)	SNP22 P1	SNP22 P2	QTL at *Ppd-H1* for FT	Late FT allele	Larger FLL allele	Additive effect (cm)
HvDRR18	HOR383	K10693	Early allele	Late allele	Yes	K10693	K10693	0.16 (FLW)
HvDRR26	Unumli-Arpa	Sanalta	Early allele	Late allele	Yes	Sanalta	Unumli-Arpa	0.63 (FLL)
HvDRR30	IG128216	Georgie	Early allele	Late allele	Yes	Georgie	Georgie	0.04 (FLW)
HvDRR39	HOR12830	ItuNative	Early allele	Late allele	Yes	ItuNative	HOR12830	0.53 (FLL)

Supplementary Table S9.The allele of the *Vrn-H2* gene among the parental inbreds. The table summarizes the presence/absence variation (PAV) for the parental inbreds of those sub-populations where a QTL was detected for flag leaf length (FLL) and width (FLW) at *Vrn-H2* locus. PAV of *Vrn-H2* for parental inbreds was performed in accordance to Cosenza et al. (2024). The flowering time QTLs detected by Cosenza et al. (2024) were used to compare the association of the effect of late or early *Vrn-H2* flowering time (FT) allele with FLL.

Population	Parent 1 (P1)	Parent 2 (P2)	PAV P1	PAV P2	QTL at *Vrn-H2* for FT	Late FT allele	Larger FLL allele	Additive effect (cm)
HvDRR30	IG128216	Georgie	*ZCCT-a:ZCCT-b:ZCCT-c*	*ZCCT-b*	Yes	IG128216	IG128216	0.06 (FLW)
HvDRR33	Lakhan	Georgie	Null	*ZCCT-b*	No	Georgie	Lakhan	0.11 (FLW)
HvDRR43	Kombyne	Namhebori	*ZCCT-a:ZCCT-b:ZCCT-c*	*ZCCT-a:ZCCT-b*	Yes	Kombyne	Namhaebori	0.94 (FLL)

Supplementary Table S10. List of high confidence, functionally annotated genes inside the new reduced interval of QTL *qHvDRR-FLS-8*. Sequence polymorphism data obtained from the whole-genome sequencing project of 23 parental inbreds was used to create indels (indel below 50 bp) and predicted structural variants (indels above 50 bp, duplication and inversions) in the coding and regulatory region and SNP annotation data (Weisweiler et al., 2022). FLL: flag leaf length

Gene	description	Indel	Structural variation	SNP substitution	Population	Trait	Chromosome	Comment
HORVU.MOREX.r3.2HG0201440	Auxin responsive SAUR protein		Tolerated	Tolerated	HvDRR14	FLL	2	
HORVU.MOREX.r3.2HG0201480	Auxin responsive SAUR protein	5utr	Tolerated/ Deleterious	Tolerated/ Deleterious	HvDRR14	FLL	2	
HORVU.MOREX.r3.2HG0201490	Auxin responsive SAUR protein	5utr	Tolerated/ Deleterious	Tolerated/ Deleterious	HvDRR14	FLL	2	
HORVU.MOREX.r3.2HG0201500	SAUR-like auxin-responsive protein family	5utr	Tolerated/ Deleterious	Tolerated/ Deleterious	HvDRR14	FLL	2	
HORVU.MOREX.r3.2HG0201510	Auxin responsive SAUR protein	5utr	Tolerated	Tolerated	HvDRR14	FLL	2	
HORVU.MOREX.r3.2HG0201520	SAUR-like auxin-responsive protein family	5utr	Tolerated/ Deleterious	Tolerated/ Deleterious	HvDRR14	FLL	2	
HORVU.MOREX.r3.2HG0201540	SAUR-like auxin-responsive protein family	5utr	Tolerated	Tolerated	HvDRR14	FLL	2	
HORVU.MOREX.r3.2HG0201580	SAUR-like auxin-responsive protein family	5utr/ exon	Tolerated	Tolerated	HvDRR14	FLL	2	
HORVU.MOREX.r3.2HG0201590	SAUR-like auxin-responsive protein family	5utr	Deleterious	Deleterious	HvDRR14	FLL	2	
HORVU.MOREX.r3.2HG0201610	Auxin responsive SAUR protein	5utr	Tolerated	Tolerated	HvDRR14	FLL	2	
HORVU.MOREX.r3.2HG0201630	SAUR-like auxin-responsive protein family	5utr	Tolerated	Tolerated	HvDRR14	FLL	2	
HORVU.MOREX.r3.2HG0201640	Histone H2A	5utr	Tolerated/ Deleterious	Tolerated/ Deleterious	HvDRR14	FLL	2	
HORVU.MOREX.r3.2HG0201650	DNA topoisomerase 1	5utr	Tolerated/ Deleterious	Tolerated/ Deleterious	HvDRR14	FLL	2	
HORVU.MOREX.r3.2HG0201690	LINE-1 reverse transcriptase-like protein		Tolerated/ Deleterious	Tolerated/ Deleterious	HvDRR14	FLL	2	
HORVU.MOREX.r3.2HG0201700	Transcription factor	5utr/ exon/ intron	Tolerated/ Deleterious	Tolerated/ Deleterious	HvDRR14	FLL	2	
HORVU.MOREX.r3.2HG0201710	Calcium-binding EF-hand family protein	5utr	Tolerated	Tolerated	HvDRR14	FLL	2	
HORVU.MOREX.r3.2HG0201730	Ribosomal RNA large subunit methyltransferase E	intron/ 5utr	Tolerated	Tolerated	HvDRR14	FLL	2	
HORVU.MOREX.r3.2HG0201770	Ribosomal protein S4	intron/ exon/ 5utr			HvDRR14	FLL	2	
HORVU.MOREX.r3.2HG0201780	BSD domain containing protein	5utr	Tolerated	Tolerated	HvDRR14	FLL	2	
HORVU.MOREX.r3.2HG0201790	Eukaryotic translation initiation factor 3 subunit F	5utr			HvDRR14	FLL	2	
HORVU.MOREX.r3.2HG0201810	Molybdate transporter 2	5utr/ exon	Tolerated/ Deleterious	Tolerated/ Deleterious	HvDRR14	FLL	2	
HORVU.MOREX.r3.2HG0201820	Cyclin-related family protein	5utr/ intron	Tolerated/ Deleterious	Tolerated/ Deleterious	HvDRR14	FLL	2	
HORVU.MOREX.r3.2HG0201830	Pentatricopeptide repeat-containing protein	5utr	Tolerated/ Deleterious	Tolerated/ Deleterious	HvDRR14	FLL	2	
HORVU.MOREX.r3.2HG0201840	Protein UXT-like protein	intron/ exon			HvDRR14	FLL	2	
HORVU.MOREX.r3.2HG0201850	Transmembrane 9 superfamily member		Tolerated	Tolerated	HvDRR14	FLL	2	
HORVU.MOREX.r3.2HG0201860	Molybdopterin biosynthesis protein CNX1	5utr/ intron/ exon	Tolerated/ Deleterious	Tolerated/ Deleterious	HvDRR14	FLL	2	
HORVU.MOREX.r3.2HG0201870	DNA topoisomerase 1	5utr/ exon/ intron	Tolerated/ Deleterious	Tolerated/ Deleterious	HvDRR14	FLL	2	
HORVU.MOREX.r3.2HG0201880	WRKY transcription factor	5utr/ intron/ exon	Tolerated/ Deleterious	Tolerated/ Deleterious	HvDRR14	FLL	2	
HORVU.MOREX.r3.2HG0201890	Basic leucine zipper and W2 domain-containing protein 2	5utr/ intron/ exon	Tolerated	Tolerated	HvDRR14	FLL	2	
HORVU.MOREX.r3.2HG0201910	Myosin-H heavy chain	intron/ exon/ 5utr	Deleterious	Deleterious	HvDRR14	FLL	2	
HORVU.MOREX.r3.2HG0201920	Inositol-pentakisphosphate 2-kinase		Tolerated	Tolerated	HvDRR14	FLL	2	
HORVU.MOREX.r3.2HG0201930	Heavy metal transport/detoxification superfamily protein		Tolerated/ Deleterious	Tolerated/ Deleterious	HvDRR14	FLL	2	
HORVU.MOREX.r3.2HG0201940	Alpha/beta-Hydrolases superfamily protein/ putative	5utr	Tolerated/ Deleterious	Tolerated/ Deleterious	HvDRR14	FLL	2	
HORVU.MOREX.r3.2HG0201990	TTF-type zinc finger protein with HAT dimerization domain-containing protein	5utr			HvDRR14	FLL	2	
HORVU.MOREX.r3.2HG0202020	CsAtPR5				HvDRR14	FLL	2	Not polymorphic
HORVU.MOREX.r3.2HG0202040	CsAtPR5	5utr	Tolerated/ Deleterious	Tolerated/ Deleterious	HvDRR14	FLL	2	
HORVU.MOREX.r3.2HG0202050	CsAtPR5	5utr			HvDRR14	FLL	2	
HORVU.MOREX.r3.2HG0202060	Protein kinase	exon/ 5utr/ intron	Tolerated	Tolerated	HvDRR14	FLL	2	
HORVU.MOREX.r3.2HG0202070	Chaperone protein DnaJ	intron			HvDRR14	FLL	2	
HORVU.MOREX.r3.2HG0202090	Xyloglucan endotransglucosylase/hydrolase	5utr/ exon			HvDRR14	FLL	2	
HORVU.MOREX.r3.2HG0202100	Xyloglucan endotransglucosylase/hydrolase	5utr			HvDRR14	FLL	2	
HORVU.MOREX.r3.2HG0202110	Alpha-1/4-glucan-protein synthase [UDP-forming]	5utr	Tolerated	Tolerated	HvDRR14	FLL	2	
HORVU.MOREX.r3.2HG0202120	Alpha-1/4-glucan-protein synthase	5utr	Tolerated	Tolerated	HvDRR14	FLL	2	
HORVU.MOREX.r3.2HG0202130	Werner Syndrome-like exonuclease		Tolerated	Tolerated	HvDRR14	FLL	2	
HORVU.MOREX.r3.2HG0202140	tRNA pseudouridine synthase A	5utr	Deleterious	Deleterious	HvDRR14	FLL	2	
HORVU.MOREX.r3.2HG0202150	Protein kinase-like	5utr/ exon/ intron	Tolerated	Tolerated	HvDRR14	FLL	2	
HORVU.MOREX.r3.2HG0202180	Transcription factor/ putative	5utr	Tolerated	Tolerated	HvDRR14	FLL	2	
HORVU.MOREX.r3.2HG0202200	trehalose-phosphatase/synthase 7	5utr	Tolerated	Tolerated	HvDRR14	FLL	2	
HORVU.MOREX.r3.2HG0202220	Protein pelota homolog	intron/ 5utr/ exon	Tolerated	Tolerated	HvDRR14	FLL	2	
HORVU.MOREX.r3.2HG0202230	Ubiquinone/menaquinone biosynthesis C-methyltransferase UbiE				HvDRR14	FLL	2	Not polymorphic
HORVU.MOREX.r3.2HG0202250	Kelch repeat-containing protein	5utr/ exon/ intron	Tolerated	Tolerated	HvDRR14	FLL	2	

HORVU.MOREX.r3.2HG0202270	DUF1365 family protein	5utr	Tolerated/ Deleterious	Tolerated/ Deleterious	HvDRR14	FLL	2
HORVU.MOREX.r3.2HG0202280	Amino acid permease		Tolerated	Tolerated	HvDRR14	FLL	2
HORVU.MOREX.r3.2HG0202290	Sec14p-like phosphatidylinositol transfer family protein	5utr/ exon/ intron	Tolerated	Tolerated	HvDRR14	FLL	2
HORVU.MOREX.r3.2HG0202310	BTB/POZ/MATH-domain protein	5utr	Tolerated/ Deleterious	Tolerated/ Deleterious	HvDRR14	FLL	2
HORVU.MOREX.r3.2HG0202320	Protein phosphatase 2C	5utr/ intron/ exon	Tolerated	Tolerated	HvDRR14	FLL	2
HORVU.MOREX.r3.2HG0202340	Bifunctional lysine-specific demethylase and histidyl-hydroxylase NO66	intron/ 5utr	Tolerated	Tolerated	HvDRR14	FLL	2
HORVU.MOREX.r3.2HG0202350	Glutamine synthetase		Deleterious	Deleterious	HvDRR14	FLL	2
HORVU.MOREX.r3.2HG0202360	xyloglucan endotransglucosylase/hydrolase 5	5utr	Tolerated	Tolerated	HvDRR14	FLL	2
HORVU.MOREX.r3.2HG0202390	Receptor-like protein kinase	intron/ 5utr	Tolerated	Tolerated	HvDRR14	FLL	2
HORVU.MOREX.r3.2HG0202400	Ribosomal RNA processing protein 1-like protein	5utr	Tolerated/ Deleterious	Tolerated/ Deleterious	HvDRR14	FLL	2
HORVU.MOREX.r3.2HG0202420	RING/U-box superfamily protein		Tolerated	Tolerated	HvDRR14	FLL	2
HORVU.MOREX.r3.2HG0202440	Dehydration responsive element binding transcription factor	5utr	Tolerated/ Deleterious	Tolerated/ Deleterious	HvDRR14	FLL	2
HORVU.MOREX.r3.2HG0202450	Ribulose bisphosphate carboxylase/oxygenase activase	5utr/ intron/ exon	Tolerated/ Deleterious	Tolerated/ Deleterious	HvDRR14	FLL	2
HORVU.MOREX.r3.2HG0202460	C2 domain-containing protein	5utr/ intron/ exon	Tolerated/ Deleterious	Tolerated/ Deleterious	HvDRR14	FLL	2
HORVU.MOREX.r3.2HG0202470	D-aminoacid aminotransferase-like PLP-dependent enzymes superfamily protein	5utr/ exon	Tolerated/ Deleterious	Tolerated/ Deleterious	HvDRR14	FLL	2
HORVU.MOREX.r3.2HG0202480	SsrA-binding	5utr/ intron/ exon	Tolerated/ Deleterious	Tolerated/ Deleterious	HvDRR14	FLL	2
HORVU.MOREX.r3.2HG0202490	ATP synthase		Deleterious	Deleterious	HvDRR14	FLL	2
HORVU.MOREX.r3.2HG0202500	Transcriptional adapter 1	5utr	Tolerated/ Deleterious	Tolerated/ Deleterious	HvDRR14	FLL	2
HORVU.MOREX.r3.2HG0202520	Aldose 1-epimerase family protein	5utr/ intron/ exon	Tolerated/ Deleterious	Tolerated/ Deleterious	HvDRR14	FLL	2
HORVU.MOREX.r3.2HG0202540	Transmembrane protein/ putative	5utr	Tolerated	Tolerated	HvDRR14	FLL	2
HORVU.MOREX.r3.2HG0202550	Lipase	5utr	Tolerated	Tolerated	HvDRR14	FLL	2
HORVU.MOREX.r3.2HG0202590	Farnesyl pyrophosphate synthase	5utr/ exon/ intron	Tolerated/ Deleterious	Tolerated/ Deleterious	HvDRR14	FLL	2
HORVU.MOREX.r3.2HG0202600	Kinase-like	5utr	Tolerated/ Deleterious	Tolerated/ Deleterious	HvDRR14	FLL	2
HORVU.MOREX.r3.2HG0202620	Peroxidase	intron/ 5utr/ exon	Tolerated/ Deleterious	Tolerated/ Deleterious	HvDRR14	FLL	2
HORVU.MOREX.r3.2HG0202640	Universal stress family protein	5utr	Deleterious	Deleterious	HvDRR14	FLL	2
HORVU.MOREX.r3.2HG0202650	Squamosa promoter-binding-like protein	exon/ intron/ 5utr	Tolerated	Tolerated	HvDRR14	FLL	2

List of publications

1. **Gao, Y.**, Stein, M., Oshana, L., Zhao, W., Matsubara, S., & Stich, B. (2024). Exploring natural genetic variation in photosynthesis-related traits of barley in the field. *Journal of Experimental Botany*, *75*(16), 4904-4925.
2. Lapasiya, T.[+], **Gao, Y.**[+], Wu, P. Y., Haweit, A., van Inghelandt, D., Stich, B., & Shrestha, A. (2025). Genetic architecture and cellular basis of flag leaf size variation in barley. *Journal of Experimental Botany*, eraf487.
3. **Gao, Y.**, Wu, P. Y., Matsubara, S., & Stich, B. (2025). The potential of considering photosynthesis parameters in crop yield breeding by genomic prediction. Under review at *Journal of Experimental Botany*.

+ Contributed equally

Acknowledgement

I would like to express my heartfelt gratitude to my supervisors, Benjamin Stich and Shizue Matsubara. Thank you for your patient guidance, insightful feedback, and continuous support throughout my PhD. Benjamin, I still remember what you said on my first day: in Germany a PhD supervisor is sometimes affectionately called a "PhD parent." Whenever I faced difficulties, you were there to help. You answered all my questions no matter how small it is. When I made mistakes during the research, you never complain, but always focused on finding solutions. From you I learned not only how to do rigorous research but also how to conduct myself as a scientist and as a person.

Shizue, it was unfortunate that distance meant most of our meetings were online, but your broad knowledge of biology and your dedication to research have been a constant source of inspiration. Your resilience, conscientiousness, and scientific rigor encouraged me throughout my studies. Although we did not work together in the same institute day-to-day, I learned a lot from you both scientifically and in my approach to doing careful, responsible research.

I would also like to thank the members of the QGGP and IBG-2 groups. I am grateful to Delphine van Inghelandt for teaching me how to arrange the field experiments. I would like to thank Michael Schneider. I still remember how you kindly offered to explain how to use R for statistical analysis when I was struggling at the beginning. Many thanks to Asis Shrestha for all our discussions on physiological aspects. I am also very grateful to Po-Ya; whenever I had questions about statistics, you were always the person I turned to for help. Thanks to Wenxia, Merle, Lilian and Sarah for your help in field experiments. Thanks to Francesco Cosenza, Federico Casale, Marius Weisweiler, Nadia Baig, Maria Schmidt, Christopher Arlt, Marius Kühl, Alessio Maggiorelli, Anjali Walpola Mudalige Dona, Twinkal Lapasiya, Aashu, Kathrin Thelen, Amelie Kok, for all your insightful discussions. Thanks to Stephanie Krey, Konstantin Shek, Florian Esser, George Alskief, and Vesna Lamesic for your help with all the fields arrangements. And thanks all the other former members of the Institute for Quantitative Genetics and Genomics of Plants for creating such a great and pleasant working atmosphere. Regarding IBG-2 group, I am also very grateful to Yuxi, you always encourage me and help me from the beginning till the very end of my PhD. Thanks to Ana for all the discussions about our projects, and also thanks to Genghong for

your kindness offered help when I visited Jülich. I would like to thank Onno Muller for organization of the field trial in Bonn. I would like to thank Urte Schlüter for support with LI-6800. I would like thank to Michael and Huaiyue, for your supports and guidance with the equipment for photosynthesis experiments.

I would also like to thank to the colleagues in JKI, especially to Bernd Hackauf, who offered a good opportunity for me to continue my career. Thanks to Vasantha for your kindly help and thanks to Yeneneh for your thoughtful suggestions to the manuscripts. And thanks to all the other members of the JKI for such a great and pleasant working atmosphere.

I would also like to thank my friend, Binghan Wang. Even though we live far apart and in different time zones, you have always been an important friend of emotional support for me. Our countless conversations about everything under the sun have brought me comfort and strength throughout this journey. I am deeply grateful to Tianyu Lan, who offered me tremendous help in both life and work when I first arrived in Düsseldorf. Without you, my life in Düsseldorf would have been much more difficult. I would also like to thank Zhe Lu, Mingming Cui, Mengyun Zhang, Di He, and Chengmin Yang for your company in Düsseldorf. I would like to thank to my girls, Lin, Yueyin, Sisi, Zilei, Yufei, Lu, I always feel so lucky to have all of you in my life.

I am especially grateful to my husband, Zhenxiang Li, for your continuous support and understanding throughout this journey. Your patience, encouragement, and willingness to stand behind my decisions have been indispensable to the completion of this work.

Most especially, I would like to thank my mother, my father, my sister, and all my family and friends in China. No words can fully express my gratitude for your unconditional love, trust, and support. Even from afar, you have always been my strongest backing. This achievement belongs to you as much as it does to me.